Defining membrane contact sites between chloroplasts, mitochondria and the endoplasmic reticulum in plants

Inaugural-Dissertation

zur Erlangung des Doktorgrades
der Mathematisch-Naturwissenschaftlichen Fakultät
der Heinrich-Heine-Universität Düsseldorf

vorgelegt von

Vanessa Valencia
aus Solingen

Düsseldorf, August 2025

aus dem Institut für Biochemie der Pflanzen
der Heinrich-Heine-Universität Düsseldorf

Gedruckt mit der Genehmigung der
Mathematisch-Naturwissenschaftlichen Fakultät der
Heinrich-Heine-Universität Düsseldorf

Berichterstatter:

1. Prof. Dr. Andreas P. M. Weber

2. Prof. Dr. Matias Zurbriggen

Tag der mündlichen Prüfung: 16.12.2025

Eidesstattliche Erklärung

Ich versichere an Eides Statt, dass die Dissertation von mir selbständig und ohne unzulässige fremde Hilfe unter Beachtung der „Grundsätze zur Sicherung guter wissenschaftlicher Praxis an der Heinrich-Heine-Universität Düsseldorf“ erstellt worden ist. Die Dissertation habe ich in der vorgelegten oder in ähnlicher Form noch bei keiner anderen Institution eingereicht.
Ich habe bisher keine erfolglosen Promotionsversuche unternommen.

Düsseldorf, den 18.08.2025

_____

Vanessa Valencia

SUMMARY

Cellular homeostasis of eukaryotic organisms is governed by optimal intracellular communication between the organelles. One such communication mechanism is the non-vesicular transport mechanism, which physically connects membranous compartments at specific regions, called membrane contact sites. Membrane contact sites facilitate a wide range of transport, signaling, and regulatory processes between cell organelles. Disruption of such contact sites can have drastic effects on the organism. For instance, diseases such as cancer or diabetes in humans are consequences of contact site dysfunction. In plants, the impact and importance of membrane contact sites on cellular homeostasis are less well understood compared to mammals or yeast. While techniques to identify contact sites and unravel their functions in mammals and yeast can be adapted for use in plants, investigating plant contact sites requires innovative and tailored approaches.

The aim of this thesis was to develop methods for identifying novel contact sites in plants and to provide first insights into their characterization. To this end, we established a modular and adjustable bimolecular fluorescence complementation assay for plants (Chapter 1). This method reliably visualized contact sites between the ER and chloroplasts, the ER and mitochondria, mitochondria and chloroplasts, and enabled characterization of intermembrane distances between these organelles. The chloroplasts-ER contact sites were simultaneously visualized with a contact site-candidate protein, TGD4, which co-localized with these regions. Besides its known role in lipid transport from the ER to chloroplasts, TGD4 appears to possess an additional function, which may be regulated by the phosphatase PAH1, a putative interaction partner of the chloroplast-localized TGD4 protein (Chapter 2). In another approach, we established an immunopurification method to rapidly isolate intact chloroplasts or chloroplast envelope fractions. This enabled the identification of proteins that may mediate the attachment of membrane patches to the chloroplast surface (Chapter 3). The physical interaction of membranes and the consequential proximity are employed to establish a bimolecular proximity labeling approach to specifically label contact site-resident proteins in a membrane proximity-dependent manner (Chapter 4). Both, the immunopurification and proximity labeling methods identified a set of candidate proteins involved in cellular processes such as lipid transport or organelle organization, which are commonly regulated by MCSs. These approaches provide unbiased means of identifying putative contact site-resident proteins and offer new avenues for investigating membrane contact sites in plants.

In summary, the methods and foundational work presented in this thesis lay the groundwork for future research on novel plant membrane contact sites.

ZUSAMMENFASSUNG

Das zelluläre Gleichgewicht eukaryotischer Organismen wird durch optimale intrazelluläre Kommunikation zwischen den Organellen bestimmt. Einer von diesen intrazellulären Kommunikationswegen ist der nicht-vesikuläre Transport, der die Membranen von zwei Organellen an bestimmten Regionen, den sogenannten Membrankontaktstellen, physisch miteinander verbindet. Membrankontaktstellen sind für eine Vielzahl von Transport-, Signal-, und Regulationswegen zwischen Organellen verantwortlich. Ein Defekt an solchen Kontaktstellen hat erhebliche Auswirkungen auf den Organismus, so sind bspw. Krankheiten beim Menschen wie Krebs oder Diabetes Folgen einer Fehlfunktion spezifischer Kontaktstellen. Bei Pflanzen hingegen ist die Bedeutung von Membrankontaktstellen für das Zellgleichgewicht noch nicht so gut verstanden wie bei Säugetieren oder Hefen. Methoden zur Identifizierung von Membrankontaktstellen und zur Charakterisierung ihrer Funktion, die bei Säugetieren und Hefen Anwendung finden, können auch in ähnlicher Weise bei Pflanzen angewendet werden, aber die Erforschung solcher pflanzlicher Kontaktstellen erfordert auf langer Sicht weitere innovativere Methoden.

Ziel dieser Arbeit war es, Methoden zur Erforschung von bisher unbekannten Kontaktstellen in Pflanzen zu etablieren und damit erste Kenntnisse zur Charakterisierung dieses Transportmechanismus zu gewinnen. Zu diesem Zweck haben wir einen modularen und anpassbaren bimolekularen Fluoreszenz-Komplementationsassay für Pflanzen entwickelt (Kapitel 1). Diese Methode visualisierte zuverlässig Membrankontaktstellen zwischen dem ER und Chloroplasten, dem ER und Mitochondrien sowie Mitochondrien und Chloroplasten und ermöglichte die Charakterisierung des Intermembran-Abstandes zwischen den interagierenden Membranen in einer Membrankontaktstelle. Die Membrankontaktstellen zwischen dem ER und Chloroplasten wurden gleichzeitig mit dem TGD4 Protein, welches wahrscheinlich in solchen Kontaktstellen zu finden ist, visualisiert und zeigten, dass sich dieses Protein überwiegend an solchen Kontaktstellen befindet. Wir haben das TGD4 Protein in seiner Funktion und Rolle in dieser Membrankontaktstelle weiter charakterisiert (Kapitel 2). Dabei zeigte sich, dass TGD4 neben dem Lipidtransport aus dem ER zu den Chloroplasten eine weitere Funktion besitzt. Diese scheint durch die Phosphatase PAH1 reguliert zu werden, die ein möglicher Interaktionspartner für TGD4 darstellt. In einem anderen Ansatz haben wir eine Immun-Aufreinigungsmethode entwickelt, um intakte Chloroplasten oder deren Hüllmembranen schnell zu isolieren. Dies ermöglicht die Identifizierung von Proteinen, die die Interaktion von Membranregionen an die Chloroplasten-Oberfläche vermitteln (Kapitel 3). Die physikalische Interaktion von Membranen in solchen Kontaktstellen und die daraus

resultierende Nähe werden außerdem genutzt, um einen bimolekularen Proximity-Labeling Ansatz zu etablieren, mit dem Kandidaten-Proteine aus solchen Membrankontaktstellen spezifisch markiert werden können (Kapitel 4). Beide Methoden, die Immun-Aufreinigungsmethode und das bimolekulare Proximity-Labeling, führten zu der Identifizierung von mehreren Kandidaten-Proteinen, welche eine Rolle in Lipidtransport oder der Struktur der Organellen spielen - bekannte Funktionen von Membrankontaktstellen. Diese Methoden werden langfristig dazu beitragen putative Kandidaten zu identifizieren.

Zusammenfassend lässt sich sagen, dass die in dieser Arbeit vorgestellten etablierten Methoden und grundlegenden Arbeiten die Forschung neuartiger pflanzlicher Membrankontaktstellen vorantreiben werden.

TABLE OF CONTENTS

PREFACE AND OUTLINE

Over the last decades, membrane contact sites have received increasing attention, leading to a growing body of knowledge and a deeper understanding of their importance for eukaryotic organisms. The first membrane contact sites were observed by transmission electron microscopy in 1956 by Bernhard and Rouiller, who described them as dense regions between two membranes. These regions are shaped and maintained by specific proteins and serve a variety of essential cellular functions. Most of our current understanding of membrane contact sites originates from research on yeast and mammalian cells. In contrast, knowledge of plant membrane contact sites remains limited – a gap this thesis aims to address.

This thesis consists of four chapters that describe the development and application of tools to investigate MCSs *in planta*, and applies some of these tools to characterize a specific membrane contact site in more detail. My own contribution to the work is stated on the first page of each chapter. In chapter 1, a bimolecular fluorescence complementation using split-GFP gives an overview of present membrane contact sites in plant cells. This method forms the basis of subsequent chapters, where it is further employed to localize a candidate protein to specific membrane contact sites. In chapter 2, the work continues with a functional and molecular characterization of this particular membrane contact site and the proteins involved in its formation and function. Chapter 3 and 4 introduce two methods for identifying putative candidate proteins of membrane contact sites. First, an epitope-based immunopurification approach is described, enabling the rapid isolation of intact organelles and their membrane, including attached interacting membrane regions (Chapter 3). Secondly, a targeted proximity labeling strategy is developed, using a split variant of a biotin ligase. This enables the biotinylation of proximal unknown proteins, residing in a membrane contact site, and allowing for their subsequent identification (Chapter 4).

COMPARTMENTALIZATION IN EUKARYOTES

Eukaryotes contain subcellular compartments that enable the spatial separation of distinct metabolic and cellular processes. Specific sets of proteins localize to different compartments to maintain cellular homeostasis, perform metabolic functions, and regulate cellular activity.

Eukaryogenesis represents a major evolutionary event in the history of life. Approximately 2 – 3 billion years ago, an endosymbiotic event between an α-proteobacterium and a prokaryotic host gave rise to the formation of the first eukaryotic common ancestor (Dacks and Doolittle, 2001). This ancestor contained a nucleus, mitochondria, and another intracellular structure. Although our understanding of the evolutionary transition towards cellular complexity remains incomplete, several models have been proposed to explain the acquisition of such compartments. These models are broadly classified as outside-in- or inside-out models. The former suggests that mitochondria were acquired first via a phagocytosis-like mechanism, followed by the development of the nuclear compartment, or vice versa. The latter model proposes that cellular protrusions extended towards the bacterium, establishing a mutual relationship and metabolic dependency first (Koumandou et al., 2013; Baum and Baum, 2014; Butterfield, 2015). The acquisition of plastids occurred approximately one billion years later by primary, secondary or tertiary endosymbiosis of the eukaryotic host cell with cyanobacteria or photoautotrophic eukaryotes (Douglas, 1998; Martin et al., 2002; Gould et al., 2008).

THE ENDOPLASMIC RETICULUM

The largest compartment of the cell is the endoplasmic reticulum (ER). The ER is structurally as well as functionally diverse. It is essential for the synthesis and folding of especially secreted and integral membrane proteins (Jan et al., 2014). Messenger RNAs form complexes with ribosomes and are recruited to the ER membrane, where translation occurs in a co-translational manner (Pobre-Piza and Hendershot, 2021). These ribosome-studded regions define the rough ER, which typically forms a network close to the nucleus (Voeltz et al., 2002). The smooth ER forms a tubular network throughout the cell and exhibits diverse functions depending on the cell type such as detoxification of hydrophobic molecules in liver cells or calcium release and uptake in muscle cells (Palade, 1956; Voeltz et al., 2002). The ER is also the major site for lipid biogenesis (Fagone and Jackowski, 2009) and key reservoir for calcium storage and signaling (Endo, 1977; Orci et al., 2009). Moreover, the tubular ER network forms physical connections to other organelles to

facilitate lipid trafficking and calcium signaling (Orci et al., 2009; Michel and Kornmann, 2012).

THE MITOCHONDRIA

Mitochondria are semi-autonomous organelles that originated from the intake of an α-proteobacterium by an ancestral cell. This event led to a mutual relationship marked by metabolic interdependence (Chandel, 2021). Today, the mitochondrial genomes encode only a small fraction (~ 1%) of the mitochondrial proteins. The vast majority are nuclear encoded and must be imported into the organelle via specialized protein import machineries, such as the translocase of the outer membrane (TOM) and the translocase of the inner membrane (TIM) (Schatz and Dobberstein, 1996). Mitochondria play a central role in a cell's energy metabolism by producing ATP via oxidative phosphorylation, which occurs across the inner mitochondrial membrane. This process is tightly coupled to the tricarboxylic acid (TCA) cycle, also known as the Krebs cycle, which generates high-energy electron carriers (NADH and $FADH_2$) that feed into the electron transport chain to drive ATP synthesis (Krebs and Johnson, 1980). Mitochondria are typically shaped in an oval form and the inner membrane form cristae that are extrusions towards the mitochondrial matrix, extending the surface of the inner mitochondrial membrane and thereby enhancing oxidative phosphorylation efficiency (Freya and Mannellab, 2000). In addition, mitochondria are involved in calcium signaling (Baughman et al., 2011) and lipid biogenesis (Daum and Vance, 1997; Flis and Daum, 2013). In plants, mitochondria play a crucial role for photorespiration, which is a process to remove the toxic product of the oxygenation reaction by Ribulose-1,5-bisphosphate carboxylase/oxygenase, and involves the conversion of glycine to serine in the mitochondria (Bauwe et al., 2010).

THE CHLOROPLASTS

Chloroplasts are another type of semi-autonomous organelles. Similar to mitochondria, their genomes are highly reduced, with most proteins encoded in the nucleus and imported post-translationally (Martin et al., 2002; Jarvis, 2008). This import is mediated by the translocase of the outer (TOC) and inner (TIC) chloroplast membrane (Flügge, 1990). Chloroplasts contain an additional internal membrane system, the thylakoids, which house the photosynthetic apparatus. This enables photosynthetic eukaryotes to capture solar energy and convert it into chemical energy equivalents (Staehelin, 2003; Kirchhoff, 2019). Through the Calvin Benson Bassham cycle (Calvin, 1956), these energy equivalents are used to fix atmospheric carbon dioxide into organic carbon compounds that serve as

precursors for biosynthetic pathways, including the synthesis of sugars, amino acids, fatty acids and lipids (Weber and Linka, 2011; Mehrshahi et al., 2014; Hölzl and Dörmann, 2019).

INTRACELLULAR COMMUNICATION BETWEEN COMPARTMENTS

Compartmentalization in eukaryotic cells enables the spatial organization of metabolic pathways. In order to maintain cellular homeostasis, support growth, and ensure optimal responses to environmental cues, eukaryotic cells must preserve the integrity of their internal compartments and coordinate the transport of substrates and metabolic intermediates. Consequently, they employ diverse transport mechanisms (Figure 1) (Mogre et al., 2020).

The movement of small particles through diffusion results in uncoordinated motion over time and space as these particles follow their concentration gradient. While important in biological systems, such as for the transport of CO_2 or O_2 across membranes, more directed modes of transportation are often favorable (Vale, 2003; Mogre et al., 2020). In the cytosol, circulation introduces an advective component to this movement. However, this still is limited in both its rate and directionality. In eukaryotic cells a motor-driven mechanism evolved. ATP hydrolysis provides energy for motor proteins transporting cargo across the cell using the cytoskeleton (Vale, 2003; Ross et al., 2008). Such cargo includes vesicles (Šamaj et al., 2006; Racine et al., 2007), organelles like mitochondria (Nan et al., 2008; Schwarz, 2013) or RNA molecules (Steward and Banker, 1992; Hirokawa, 2006). Vesicles can transport proteins and lipids to their target membrane. However, experimental evidence also points to a non-vesicular transport mechanism. For instance, lipid trafficking is not entirely blocked by disrupting the vesicular trafficking (Vance et al., 1991; Kok et al., 1998). Consistent with the proposed inside-out model, membrane contact sites (MCSs) have been identified as direct physical connections between membranes. These structures play crucial roles in metabolite exchange and maintaining cellular homeostasis (Area-Gomez et al., 2012; Giorgi et al., 2015; Grossmann et al., 2019; Wilson et al., 2024).

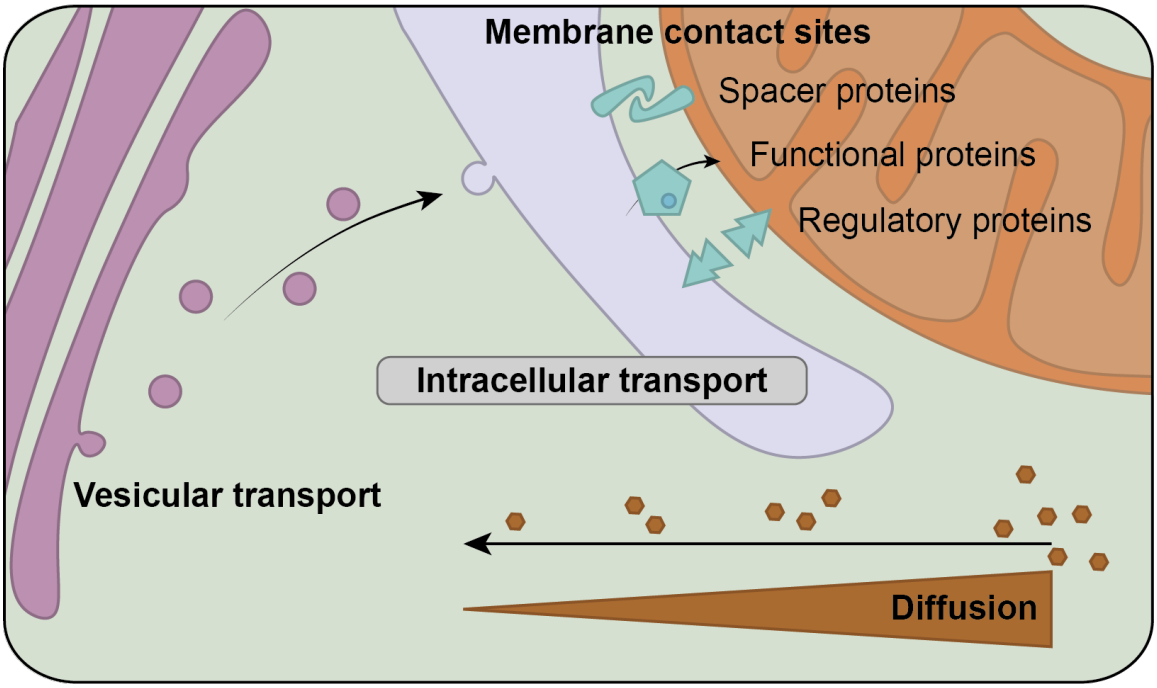

Figure 1: Schematic overview of the intracellular transport mechanisms. Diffusion is the passive motion of particles through a medium along its concentration gradient. Vesicular transport represents the bulk transport of proteins or lipids. Membrane contact sites are regions in which membranes interact by direct contact. This is facilitated by spacer proteins and functional proteins allow for transport of intermediates or molecules. Regulatory proteins supervise the contact site *(Mogre et al., 2020; Reinisch and Prinz, 2021)*.

THE THIRD TRANSPORT MECHANISM: MEMBRANE CONTACT SITE

MCSs are regions of close proximity between interacting membranes. These regions are characterized by their distinct protein skeleton, functional diversity, lack of membrane fusion and unique lipidome and proteome.

The protein skeleton of MCSs is built by diverse proteins, which can be divided into (1) spacer proteins, (2) regulatory proteins, and (3) functional proteins. Spacer proteins include proteins that mediate the interaction between different membranes while, at the same time, maintaining a defined intermembrane distance to preserve membrane identity (Saravanan et al., 2009; Wang et al., 2014; Fernández-Busnadiego et al., 2015). In mammalian cells, for instance, synaptotagmins (SYTs) contribute to the formation of ER-PM MCSs. Electro tomography has revealed that these MCSs exhibit an intermembrane distance of approximately 20 nm, consistent with the length of the cytosolic domain of SYTs (Fernández-Busnadiego et al., 2015). Depending on the specific proteins involved, MCS intermembrane space can vary from 10 to 80 nm (Wang et al., 2015; Giacomello and Pellegrini, 2016; Cardoen et al., 2024). In addition to protein-protein interactions, lipid-protein interaction also contributes to MCS formation. For instance, oxysterol-binding protein-related proteins 5 and 8 interact with phosphatidylinositol-(3,4)-diphosphate at ER-PM contact sites (Santos et al., 2020).

Regulatory proteins coordinate the presence and activity of MCSs by controlling their size and number, and by restricting or recruiting specific proteins to the MCS (Raiborg et al., 2015; Selitrennik and Lev, 2016; Bean et al., 2018). For example, Vacuolar Protein Sorting 13 is a characterized protein within multiple MCSs of yeast. Its recruitment to different MCSs is regulated by numerous adaptor proteins (Bean et al., 2018). The size of MCSs can be dynamically regulated in response to environmental or developmental cues. For example, upon ionic stress induced by salt, ER-PM MCSs that depend on the interaction between phosphoinositide and SYT1 expand (Lee et al., 2019).

Functional proteins define the diverse roles of MCSs in maintaining cellular homeostasis and mediating responses to developmental or environmental cues. MCSs enable the transport of intermediates and metabolites such as lipids between organelles. For example, ceramide transport between the ER and Golgi in mammalian cells (Kok et al., 1998; Liu et al., 2017), or sterol transport between the ER and mitochondria or vacuole (Murley et al., 2015; Tong et al., 2018) are facilitated by MCSs. Lipid transport across the aqueous cytosol at MCS is typically mediated by lipid transport proteins (Tong et al., 2018; Mavuduru et al., 2024). Other examples include the transfer of products from β-oxidation at peroxisome-mitochondrion MCSs (Shai et al., 2018), and calcium signaling. In mammalian cells, the ER-PM MCSs mediated by STIM1-ORAI (Stiber et al., 2008; Zhou et al., 2010) and E-SYT-NIR2 (Chang et al., 2013) are well characterized examples that regulate calcium flux. The E-SYT-dependent calcium signaling is regulated by phosphoinositide. Phosphoinositide levels across the cell govern multiple signaling mechanisms, and these levels are maintained in part through MCSs (Balla et al., 2009; Dickson and Hille, 2019). In addition, MCSs influence organelle morphology and dynamics. At ER-mitochondria MCSs, they participate in mitochondrial fission and fusion processes, potentially playing both regulatory as well as mechanical roles (Yamaoka et al., 2011; Hu et al., 2017; White et al., 2020). Specific MCSs at the ER membrane also regulate autophagy - the degradation of cellular components, including organelles marked for breakdown (Mao et al., 2013; Nascimbeni et al., 2017). Under stress conditions, the cell respond by dynamically up- or downregulating MCSs. Excess lipids, such as diacylglycerol or fatty acids, can cause lipotoxicity. In response, cells form lipid droplets from ER membrane regions via MCS-mediated processes (Hariri et al., 2018, 2019; Krawczyk et al., 2022). During prolonged stress, particularly ER stress, the cell is programmed to undergo cell death (apoptosis), during which, the tumor suppressor p53 accumulates at ER-mitochondria MCSs in mammalian cells (Giorgi et al., 2015).

In summary, MCSs are multifunctional hubs essential for cellular homeostasis and development. Their dysfunction can have severe physiological consequences. Impaired organelle communication at mammalian MCSs has been implicated in a range of diseases,

including Alzheimer's disease (Area-Gomez et al., 2012), Parkinson's disease (Grossmann et al., 2019), cancer or diabetes (Koga et al., 2008; Santos et al., 2020).

Table 1: Recently characterized MCS. Co-IP, co-immunopurification; TEM, transmission electron microscopy; FRET, Förster resonance energy transfer; MERBiT, mitochondria-ER contact reporter applying NanoBit (Shiiba et al., 2025); PI(4)P, phosphatidylinositol-4-phosphate

Membrane - membrane	Proteins involved	Organism	Methods	Function	Reference
PM - ER	NIR2, VAPA	mammalian cells	co-IP, co-localization	lipid transport	Polianskyte-Prause et al., (2025)
LD - mitochondria	E-SYT, VAPB	mammalian cells	proximity proteomics, FRET	fatty acid transport	Bezawork-Geleta et al., (2025)
endosome - peroxisome	PxdA, DipA, AbcdA	yeast	co-localization	peroxisome movement	Driscoll et al., (2025)
ER - mitochondria	PDZD8, FKBP8	mammalian cells	co-localization, proximity labeling	mitochondrial dynamics	Nakamura et al., (2025)
	RMDN3, PTPIP51	mammalian cells	MERBiT, lipid transfer assay, growth assay	lipid radical transfer as stress response	Shiiba et al., (2025)
Mitochondria - ER - PM	Num1, Mdm36, Scs2	yeast	Localization, growth assay	Mitochondrial dynamics and PI(4)P metabolism	Casler et al., (2024)

Research on MCSs has gained increasing attention over the last decades, and some characterized MCSs of the recent years are summarized in Table 1. Pan and colleagues (2024) compiled a database (https://cellknowledge.com.cn/mcsdb/index.html) of all known MCSs and associated proteins, which includes a total of 7,010 proteins across 11 species. Among these, only 17 proteins are from *Arabidopsis thaliana*, highlighting a significant knowledge gap regarding MCSs in plants.

MEMBRANE CONTACT SITES OF PLANTS

Pan and colleagues (2024) summarized 17 proteins associated with 4 different MCSs in plants (Table 2).

Table 2: Arabidopsis thaliana MCSs summarized by **Pan et al., (2024)** *and recently characterized MCSs.* FRET-FLIM, Förster resonance energy transfer-fluorescence lifetime imaging; co-IP, co-immunopurification; BiFC, bimolecular fluorescence complementation; Y2H, yeast two hybrid

Membrane - membrane	Proteins involved	Methods	Function	Reference
PM - ER	VAP27, NET3C	FRET-FLIM, co-IP	tethering	Wang et al., (2014)
	SYT1	localization, lipid transfer assay	Lipid homeostasis	Qian et al., (2022), Ruiz-Lopez et al., (2021)
	MSL10, VAP27	FRET-FLIM, BiFC		Codjoe et al., (2022)
LD - PM	SLDP1, SLDP2, LIPA	FRET-FLIM, Y2H	Lipid transport	Krawczyk et al., (2022)
ER - autophagosome	VAP27, ORP2A, ATG8E	localization	autophagy	Ye et al., (2022)
ER - mitochondria	VAP27, TRB1, TRB2	localization, co-IP	mitophagy	Li et al., (2022)
	MIRO2	localization	mitochondrial dynamics	White et al., (2020)
ER - chloroplasts	VAP27-1, VAP27-3, ORP2A	Y2H, co-localization	lipid homeostasis	Renna et al., (2024)
Chloroplasts - mitochondria	TPT, PGAM, Enolase, PYK, VDAC	BiFC, split *Renilla* luciferase assay		Zhang et al., (2020)

SYT1 and VAP27 are plant homologs of mammalian synaptotagmins and vesicle associated proteins, respectively, which have been extensively characterized in mammalian cells. Homology-based studies enabled the functional characterization of the Arabidopsis homologs, revealing multiple roles in different MCSs similar to their counterparts in mammals and yeast (Herdman & Moss, 2016 (SYTs); Murphy & Levine, 2016 (VAPs)). SYT1 localizes to ER-PM MCSs, where it responds to abiotic (e.g., mechanical) or biotic stresses or contributes to lipid homeostasis (Pérez-Sancho et al.,

2015; Ruiz-Lopez et al., 2021). VAP27, on the other hand, is more versatile. It has been identified at ER-PM MCSs together with NET3C (Wang et al., 2014), at ER-mitochondria MCSs, where it regulates mitophagy together with TRB1/2 (Li et al., 2022), or at ER-autophagosomes MCSs with ORP2A and ATG8E in the context of autophagy (Ye et al., 2022).

While homology-driven research has served as a useful starting point in identifying MCSs components in plants, this approach has limitations, especially, when considering organelles unique to phototrophic organisms, such as the plastid.

PLASTIDS COMMUNICATE WITH THEIR INTRACELLULAR ENVIRONMENT

Plants contain various plastid types that differentiate from an undifferentiated proplastid, which are found in meristems and reproductive tissue. These include etioplasts, leucoplasts, chromoplasts, and chloroplasts (Jarvis and López-Juez, 2013). Etioplasts, found in dark-grown plants, are intermediate plastid types and contain transitional structures such prolamellar body, prothylakoids, and small plastoglobules, which are precursors to chloroplast development (Austin et al., 2006; Solymosi and Schoefs, 2010). Leucoplasts are found in non-photosynthetic tissue and include amyloplasts, proteinoplasts and elaioplasts. Amyloplasts store starch granules and have been reported to contribute to gravitropism in roots. Proteinoplasts play a role in protein storage, and elaioplasts in the storage of lipids and terpenoids (Nakamura et al., 2019; Sadali et al., 2019; Choi et al., 2021). Chromoplasts accumulate carotenoid crystals within plastoglobules and give rise to a colorful function for pollinator attraction (Sadali et al., 2019). Chloroplasts, the best-studied plastids, develop under light and form the thylakoid membranes that house the photosynthetic apparatus (Waters and Langdale, 2009). Upon senescence, that transition into gerontoplasts that ultimately get degraded to recycle nitrogen and nutrients (Choi et al., 2021).

Chloroplasts are the site of a plethora of diverse metabolic pathways, including photosynthesis. Photosynthesis fixes atmospheric carbon through light-dependent- and light-independent reactions. The light-dependent reactions take place in the thylakoid membranes, where solar energy is converted into chemical energy in the form of NADPH and ATP. The light-independent reaction, also known as the carbon fixation reaction or Calvin Bassham Benson cycle, occur in the stroma and fix atmospheric CO_2 to ribulose-1,5-bisphosphate (Calvin, 1956). Ribulose 1,5-bisphosphate carboxylase-oxygenase (RubisCO) catalyzes the first step of the carbon fixation reactions. Besides its carboxylation activity, it can also catalyze the incorporation of molecular oxygen. The latter generates, amongst 3-phosphoglycerate (3-PGA) from the carboxylation reaction,

phosphoglycolate (2PG) via its oxygenase activity, which is a toxic molecule and is converted to 3-PGA in the photorespiratory cycle. This conversion requires multiple steps across three different organelles, namely chloroplast, mitochondrion and peroxisome, and leads to the loss of energy, nitrogen in form of ammonium, and previously fixed carbon. Briefly, 2-PG is converted to glycolate in the chloroplasts and transported into the peroxisomes, where it is subsequently oxidized to glycine. This is shuttled to the mitochondria, where it is metabolized to serine leading to the loss of ammonia and CO_2. Serine is returned to the peroxisomes and ultimately converted to glycerate, which re-enters the chloroplasts, where it is phosphorylated in the final step to 3-PGA, and used for carbon fixation (Bauwe et al., 2010). This requires multiple transport steps to direct the metabolites and supply the reactions with auxiliary compounds such as further substrates or energy derivatives. Two characterized transporters involved in these transport mechanisms are the Plastidic Glycolate Glycerate transporter 1 (Pick et al., 2013) and the Bile Acid Sodium Symporter 6 (South et al., 2017), which transport glycolate from the chloroplast. Such transport steps of photorespiration might be directed by MCSs between the involved organelles.

Products from carbon fixation reactions serve as precursors for various biosynthetic pathways, such as amino acid, sugar, starch and lipid synthesis. The majority of chloroplast membranes are composed of galactolipids, which differs from the phospholipids usually found in other membranes. Galactolipids consists of a diacylglycerol (DAG) backbone with a galactosyl headgroup and are synthesized via two pathways – the prokaryotic and eukaryotic pathway (Figure 2).

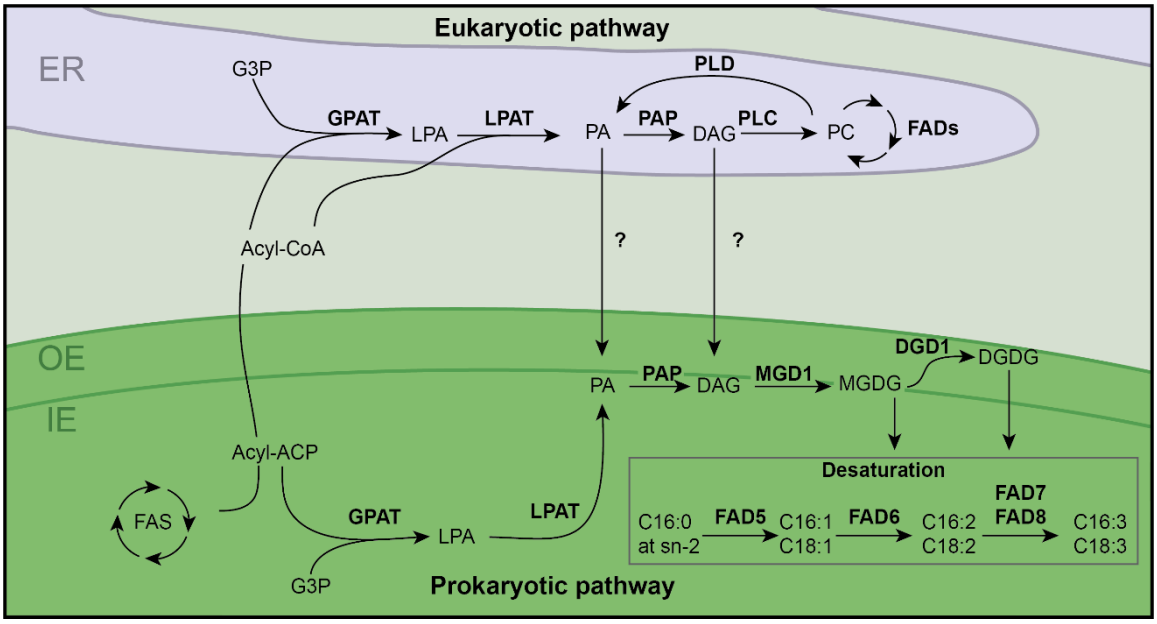

Figure 2: Schematic overview of galactolipid biosynthesis pathways in plants. Fatty acids are synthesized in the chloroplast stroma, generating C16:0, C18:0, or C18:1 acyl-ACP. In the eukaryotic pathway, these precursors get converted to respective acyl-CoA, which are transported to the ER. At the ER, the acyl-chains are added to a G3P backbone by GPAT and LPAT to form PA. PA is dephosphorylated by PAP to DAG, which is further converted to PC by PLC. Acyl-groups of PCs can be further desaturated by FADs. PLD converts PC to PA. A lipid precursor, presumably PA or DAG is transported to the chloroplast for galactolipid biosynthesis, starting by DAG as substrate for MGD1 to form MGDG, which is further converted to DGDG by DGD1, adding a second galactosyl-group. In the prokaryotic pathway, the acyl-groups of the acyl-ACP are added to the G3P by the plastidic GPAT and LPAT, forming PA. PA is then dephosphorylated by a plastidic PAP initiating the prokaryotic galactolipid biosynthesis pathway. SQDG is formed by SLS utilizing MGDG. This step is not depicted in this overview. MGDG, DGDG and SQDG undergo further desaturation by FAD5, which specifically desaturases C16:0 acyl-groups at the *sn-2* position, FAD6, FAD7, and the temperature-sensitive FAD8, forming PUFA. Question marks indicate the to date unresolved transport mechanisms. Abbreviations: ACP, acyl carrier protein; CoA, coenzyme A; DAG, diacylglycerol; DGDG, digalactosyl diacylglycerol; ER, endoplasmic reticulum; FAD, fatty acid desaturase; FAS fatty acid synthase; G3P, glycerol-3-phosphate; GPAT, glycerol-3-phosphate acyltransferase; IE, inner envelope; LPA, lysophosphatidic acid; MGD1, monogalactosyl diacylglycerol synthase 1; MGDG, monogalactosyl diacylglycerol; OE, outer envelope; PA, phosphatidic acid; PAP, phosphatidic acid phosphatase; PC, phosphatidylcholine; PLC, phospholipase C; PLD, phospholipase D; PUFA, polyunsaturated fatty acid

Lipid biosynthesis starts with the fatty acid synthesis in the chloroplast. For the eukaryotic pathway, fatty acids are exported as acyl-Coenzyme A to the ER. There, usually C16 or C18 acyl-groups are linked to the *sn-1* position from glycerol-3-phosphate by a glycerol-3-phosphate acyltransferase. The 1-acylglycerol-3-phosphate acyltransferase specifically adds a C18 acyl-group to the *sn-2* position generating phosphatidic acid (PA) (Frentzen et al., 1983). PA is further converted to DAG, and subsequently to phosphatidylcholine (PC). Desaturation of fatty acids in the PC pool of the ER is mediated by fatty acid desaturase (FAD) 2 and FAD3. The lipid precursors – likely PA or DAG – are transferred back into the chloroplast for galactolipid biosynthesis (Karki et al., 2019). The transport from the ER to the chloroplast is hypothesized to be facilitated by MCSs, with trigalactosyldiacylglycerol (TGD) proteins contributing to the transport mechanisms. However, the nature of the

transported lipid precursor and the precise transport mechanism remain unresolved. In the chloroplast, the lipid precursor is converted to DAG, which is used by either monogalactosyl diacylglycerol synthase 1 (MGD1) to synthesize monogalactosyl diacylglycerol (MGDG) or by sulfolipid synthase (SLS) to generate sulfoquinovosyl diacylglycerol (SQDG). MGDG is subsequently transformed into digalactosyl diacylglycerol (DGDG) by digalactosyl diacylglycerol synthase 1 (DGD1) (Froehlich et al., 2001; Dubots et al., 2010). Unlike the eukaryotic pathway, which requires lipid transport across multiple membranes, the prokaryotic pathway is entirely confined to the chloroplast. Within the chloroplasts, acyl-groups from acyl-acyl carrier protein are transferred to the glycerol-3-phosphate, with a C16 acyl-group specifically added at the *sn-2* position. The resulting PA is then converted to DAG, which serves as a substrate for the synthesis of MGDG, DGDG, and SQDG by MGD1, DGD1 and SLS, respectively (Hurlock et al., 2014; LaBrant et al., 2018). The acyl-chains of these three galactolipids can undergo further desaturation, catalyzed by FAD5, FAD6, FAD7 and FAD8. FAD5 introduces the first double bond specifically at C16 chains at the *sn-2* position. FAD6 catalyzes the second desaturation step, while FAD7 and the temperature-sensitive FAD8 are responsible for the third desaturation step (Hölzl and Dörmann, 2019; Xiao et al., 2022). The origin of galactolipids – whether from the eukaryotic or prokaryotic pathway – can be distinguished based on their acyl-chain composition. Galactolipids derived from the eukaryotic pathway typically contain a C18 acyl-chain at the *sn-2* position and lack desaturated C16 acyl-chains, whereas those from the prokaryotic pathway carry a C16 acyl-chain at the *sn-2* position, which can be desaturated by FAD5. This biochemical distinction is also reflected in plant taxonomy. So-called 16:3 plants, such as Arabidopsis and spinach, utilize both pathways for galactolipid biosynthesis. In contrast, 18:3 plants, including monocots and legumes, rely solely on the eukaryotic pathway (Heinz and Roughan, 1983). In addition to their structural roles in membranes, galactolipids also serve as substrates in the jasmonic acid biosynthesis. A lipase removes an 18:3 or 16:3 acyl-group from a galactolipid. The generated polyunsaturated fatty acid is further converted to OPDA within the chloroplast, subsequently transported to the peroxisome, where it is further processed into jasmonic acid. Jasmonic acid functions as a plant hormone involved in developmental process and in response to biotic and abiotic stress, such as tissue wounding (Chaturvedi et al., 2008).

The metabolic and signaling pathways linking the chloroplasts to other compartments suggest the existence of complex transport mechanisms and unique MCSs. A major indication for MCSs at the chloroplast was provided by Andersson et al., (2007), who identified plastid associated membranes (PLAMs) from the ER remaining attached to

chloroplasts after their isolation. The strength of this attachment is comparable to that of protein – protein interactions, suggesting a physical contact rather than a loose association. The presence of PLAMs (Andersson et al., 2007), together with the detection of galactolipids in mitochondria under phosphate starvation (Jouhet et al., 2004), supports the existence of functional MCSs at chloroplasts. Further evidence comes from the recent discovery that ER-chloroplasts MCSs at non-mobile chloroplasts are photosensitive, leading to various responses such as calcium release upon photostimulation (Maynard and Griffing, 2024). Nonetheless, functionally characterized MCSs at chloroplasts are scarce to date.

Few proteins in MCSs of chloroplasts are identified and characterized. Cytosolic enzymes involved in glycolysis, namely phosphoglycerate mutase, enolase, and pyruvate kinase, were shown to link mitochondria and chloroplasts by interacting with the voltage dependent anion channel and triose phosphate translocator proteins. However, its functional role is not known yet (Zhang et al., 2020). The aminophospholipid ATPase 10 (ALA10), a phospholipid flippase at the ER, has been characterized to play a role in lipid homeostasis by forming MCSs with either the chloroplast or the plasma membrane, presumably facilitating the distribution of PC across different leaflets from two membranes (Botella et al., 2016). Another MCS involves the chloroplast protein TGD4, which plays a role in the lipid trafficking from the ER to the chloroplast (Xu et al., 2008; Fan et al., 2015). However, the specific lipid species transported, and the protein partners involved in tethering the membranes remain unidentified.

AIM OF THE THESIS

While MCSs are well studied in mammalian and yeast systems, fundamental research on MCSs in plants remains limited. The presence of the plastid as an additional compartment in plant cells introduces the possibility of unique MCSs and complex regulatory mechanisms. The aim of this thesis is to investigate MCSs between the ER, mitochondria and chloroplasts in plant cells. This is enabled by establishing a proximity-dependent bimolecular fluorescence complementation to visualize MCSs between two defined organelles (Chapter 1). Based on this, the chloroplast-localized TGD4 protein is confirmed as an MCSs component and further characterized for its role in lipid trafficking (Chapter 2). Taking advantage of observed PLAMs, a new strategy for a rapid chloroplast purification was attempted to investigate the bases of putative chloroplast-associated MCSs (Chapter 3). Characterization of novel MCSs in plants is addressed by establishing a proximity-dependent split-TurboID for specific proximity labeling of MCS-associated proteins (Chapter 4).

REFRENCES

Andersson, M.X., Goksör, M., and Sandelius, A.S., (2007). Optical manipulation reveals strong attracting forces at membrane contact sites between endoplasmic reticulum and chloroplasts. Journal of Biological Chemistry. 2007:**282**(2):1170–1174. https://doi.org/10.1074/jbc.M608124200

Area-Gomez, E., Del Carmen Lara Castillo, M., Tambini, M.D., Guardia-Laguarta, C., De Groof, A.J.C., Madra, M., Ikenouchi, J., Umeda, M., Bird, T.D., Sturley, S.L., et al., (2012). Upregulated function of mitochondria-associated ER membranes in Alzheimer disease. EMBO Journal. 2012:**31**(21):4106–4123. https://doi.org/10.1038/emboj.2012.202

Austin, J.R., Frost, E., Vidi, P.A., Kessler, F., and Staehelin, L.A., (2006). Plastoglobules are lipoprotein subcompartments of the chloroplast that are permanently coupled to thylakoid membranes and contain biosynthetic enzymes. Plant Cell. 2006:**18**(7):1693–1703. https://doi.org/10.1105/tpc.105.039859

Balla, T., Szentpetery, Z., and Kim, Y.J., (2009). Phosphoinositide Signaling: New Tools and Insights. Physiology. 2009:**24**(4):231–244. https://doi.org/10.1152/physiol.00014.2009

Baughman, J.M., Perocchi, F., Girgis, H.S., Plovanich, M., Belcher-Timme, C.A., Sancak, Y., Bao, X.R., Strittmatter, L., Goldberger, O., Bogorad, R.L., et al., (2011). Integrative genomics identifies MCU as an essential component of the mitochondrial calcium uniporter. Nature. 2011:**476**(7360):341–345. https://doi.org/10.1038/nature10234

Baum, D.A., and Baum, B., (2014). An inside-out origin for the eukaryotic cell. BMC Biol. 2014:**12**(1):1–22. https://doi.org/10.1186/s12915-014-0076-2

Bauwe, H., Hagemann, M., and Fernie, A.R., (2010). Photorespiration: players, partners and origin. Trends Plant Sci. 2010:**15**(6):330–336. https://doi.org/10.1016/j.tplants.2010.03.006

Bean, B.D.M., Dziurdzik, S.K., Kolehmainen, K.L., Fowler, C.M.S., Kwong, W.K., Grad, L.I., Davey, M., Schluter, C., and Conibear, E., (2018). Competitive organelle-specific adaptors recruit Vps13 to membrane contact sites. Journal of Cell Biology. 2018:**217**(10):3593–3607. https://doi.org/10.1083/JCB.201804111

Bezawork-Geleta, A., Devereux, C.J., Keenan, S.N., Lou, J., Cho, E., Nie, S., De Souza, D.P., Narayana, V.K., Siddall, N.A., Rodrigues, C.H.M., et al., (2025). Proximity proteomics reveals a mechanism of fatty acid transfer at lipid droplet-mitochondria- endoplasmic reticulum contact sites. Nature Communications. 2025:**16**(1). https://doi.org/10.1038/s41467-025-57405-5

Botella, C., Sautron, E., Boudiere, L., Michaud, M., Dubots, E., Yamaryo-Botté, Y., Albrieux, C., Marechal, E., Block, M.A., and Jouhet, J., (2016). ALA10, a phospholipid flippase, controls FAD2/FAD3 desaturation of phosphatidylcholine in the ER and affects chloroplast lipid composition in Arabidopsis thaliana. Plant Physiol. 2016:**170**(3):1300–1314. https://doi.org/10.1104/pp.15.01557

Butterfield, N.J., (2015). Early evolution of the Eukaryota. Palaeontology. 2015:**58**(1):5–17. https://doi.org/10.1111/pala.12139

Calvin, M., (1956). The photosynthetic carbon cycle. Journal of the Chemical Society (Resumed). 1956:1895. https://doi.org/10.1039/jr9560001895

Cardoen, B., Vandevoorde, K.R., Gao, G., Ortiz-Silva, M., Alan, P., Liu, W., Tiliakou, E., Wayne Vogl, A., Hamarneh, G., and Nabi, I.R., (2024). Membrane contact site detection (MCS-DETECT) reveals dual control of rough mitochondria–ER contacts. Journal of Cell Biology. 2024:**223**(1). https://doi.org/10.1083/jcb.202206109

Casler, J.C., Harper, C.S., White, A.J., Anderson, H.L., and Lackner, L.L., (2024). Mitochondria-ER-PM contacts regulate mitochondrial division and PI(4)P distribution. J Cell Biol. 2024:**223**(9). https://doi.org/10.1083/jcb.202308144

Chandel, N.S., (2021). Mitochondria. Cold Spring Harb Perspect Biol. 2021:**13**(3):1–23. https://doi.org/10.1101/cshperspect.a040543

Chang, C.L., Hsieh, T.S., Yang, T.T., Rothberg, K.G., Azizoglu, D.B., Volk, E., Liao, J.C., and Liou, J., (2013). Feedback regulation of receptor-induced ca2+ signaling mediated by e-syt1 and nir2 at endoplasmic reticulum-plasma membrane junctions. Cell Rep. 2013:**5**(3):813–825. https://doi.org/10.1016/j.celrep.2013.09.038

Chaturvedi, R., Krothapalli, K., Makandar, R., Nandi, A., Sparks, A.A., Roth, M.R., Welti, R., and Shah, J., (2008). Plastid ω3-fatty acid desaturase-dependent accumulation of a systemic acquired resistance inducing activity in petiole exudates of Arabidopsis thaliana is independent of jasmonic acid. Plant Journal. 2008:**54**(1):106–117. https://doi.org/10.1111/j.1365-313X.2007.03400.x

Choi, H., Yi, T., and Ha, S.H., (2021). Diversity of Plastid Types and Their Interconversions. Front Plant Sci. 2021:**12**(June):1–14. https://doi.org/10.3389/fpls.2021.692024

Codjoe, J.M., Richardson, R.A., McLoughlin, F., Vierstra, R.D., and Haswell, E.S., (2022). Unbiased proteomic and forward genetic screens reveal that mechanosensitive ion channel MSL10 functions at ER-plasma membrane contact sites in Arabidopsis thaliana. Elife. 2022:**11**(6):777–782. https://doi.org/10.7554/eLife.80501

Dacks, J.B., and Doolittle, W.F., (2001). Reconstructing/Deconstructing the Earliest Eukaryotes. Cell. 2001:**107**(4):419–425. https://doi.org/10.1016/s0092-8674(01)00584-0

Daum, G., and Vance, J.E., (1997). Import of lipids into mitochondria. Prog Lipid Res. 1997:**36**(2–3):103–130. https://doi.org/10.1016/S0163-7827(97)00006-4

Dickson, E.J., and Hille, B., (2019). Understanding phosphoinositides: Rare, dynamic, and essential membrane phospholipids. Biochemical Journal. 2019:**476**(1):1–23. https://doi.org/10.1042/BCJ20180022

Douglas, S.E., (1998). Plastid evolution: Origins, diversity, trends. Curr Opin Genet Dev. 1998:**8**(6):655–661. https://doi.org/10.1016/S0959-437X(98)80033-6

Driscoll, B., Fountain, M.B., Gates, I.N., Abdollahi, R., Langley, A.M., Owens, M.B., Christensen, J.R., and Salogiannis, J., (2025). Acyl-coA binding protein AcbdA regulates peroxisome hitchhiking on early endosomes. 2025. https://doi.org/10.1101/2025.04.17.649231

Dubots, E., Audry, M., Yamaryo, Y., Bastien, O., Ohta, H., Breton, C., Maréchal, E., and Block, M.A., (2010). Activation of the chloroplast monogalactosyldiacylglycerol synthase MGD1 by phosphatidic acid and phosphatidylglycerol. Journal of Biological Chemistry. 2010:**285**(9):6003–6011. https://doi.org/10.1074/jbc.M109.071928

Endo, M., (1977). Calcium release from the sarcoplasmic reticulum. Physiol Rev. 1977:**57**(1):71–108. https://doi.org/10.1152/physrev.1977.57.1.71

Fagone, P., and Jackowski, S., (2009). Membrane phospholipid synthesis and endoplasmic reticulum function. J Lipid Res. 2009:**50**(SUPPL.):S311–S316. https://doi.org/10.1194/jlr.R800049-JLR200

Fan, J., Zhai, Z., Yan, C., and Xu, C., (2015). Arabidopsis TRIGALACTOSYLDIACYLGLYCEROL5 interacts with TGD1, TGD2, and TGD4 to facilitate lipid transfer from the endoplasmic reticulum to plastids. Plant Cell. 2015:**27**(10):2941–2955. https://doi.org/10.1105/tpc.15.00394

Fernández-Busnadiego, R., Saheki, Y., and De Camilli, P., (2015). Three-dimensional architecture of extended synaptotagmin-mediated endoplasmic reticulum–plasma membrane contact sites. Proceedings of the National Academy of Sciences. 2015:**112**(16):E2004–E2013. https://doi.org/10.1073/pnas.1503191112

Flis, V. V., and Daum, G., (2013). Lipid transport between the endoplasmic reticulum and mitochondria. Cold Spring Harb Perspect Biol. 2013:**5**(6). https://doi.org/10.1101/cshperspect.a013235

Flügge, U.I., (1990). Import of proteins into chloroplasts. J Cell Sci. 1990:**96**(3):351–354. https://doi.org/10.1242/jcs.96.3.351

Frentzen, M., Heinz, E., McKeon, T.A., and Stumpf, P.K., (1983). Specificities and Selectivities of Glycerol-3-Phosphate Acyltransferase and Monoacylglycerol-3-Phosphate Acyltransferase from Pea and Spinach Chloroplasts. Eur J Biochem. 1983:**129**(3):629–636. https://doi.org/10.1111/j.1432-1033.1983.tb07096.x

Freya, T.G., and Mannellab, C.A., (2000). The internal structure of mitochondria. Trends Biochem Sci. 2000:**25**(7):319–324. https://doi.org/10.1016/S0968-0004(00)01609-1

Froehlich, J.E., Benning, C., and Dörmann, P., (2001). The Digalactosyldiacylglycerol (DGDG) Synthase DGD1 Is Inserted into the Outer Envelope Membrane of Chloroplasts in a Manner Independent of the General Import Pathway and Does Not Depend on Direct Interaction with Monogalactosyldiacylglycerol Synthase for DGDG Biosynthesis. Journal of Biological Chemistry. 2001:**276**(34):31806–31812. https://doi.org/10.1074/jbc.M104652200

Giacomello, M., and Pellegrini, L., (2016). The coming of age of the mitochondria-ER contact: A matter of thickness. Cell Death Differ. 2016:**23**(9):1417–1427. https://doi.org/10.1038/cdd.2016.52

Giorgi, C., Bonora, M., Sorrentino, G., Missiroli, S., Poletti, F., Suski, J.M., Ramirez, F.G., Rizzuto, R., Virgilio, F. Di, Zito, E., et al., (2015). P53 at the endoplasmic reticulum regulates apoptosis in a Ca2+-dependent manner. Proc Natl Acad Sci U S A. 2015:**112**(6):1779–1784. https://doi.org/10.1073/pnas.1410723112

Gould, S.B., Waller, R.F., and McFadden, G.I., (2008). Plastid evolution. Annu Rev Plant Biol. 2008:**59**:491–517. https://doi.org/10.1146/annurev.arplant.59.032607.092915

Grossmann, D., Berenguer-Escuder, C., Bellet, M.E., Scheibner, D., Bohler, J., Massart, F., Rapaport, D., Skupin, A., Fouquier D'Hérouël, A., Sharma, M., et al., (2019). Mutations in RHOT1 Disrupt Endoplasmic Reticulum-Mitochondria Contact Sites Interfering with Calcium Homeostasis and Mitochondrial Dynamics in Parkinson's Disease. Antioxid Redox Signal. 2019:**31**(16):1213–1234. https://doi.org/10.1089/ars.2018.7718

Hariri, H., Rogers, S., Ugrankar, R., Liu, Y.L., Feathers, J.R., and Henne, W.M., (2018). Lipid droplet biogenesis is spatially coordinated at ER –vacuole contacts under nutritional stress. EMBO Rep. 2018:**19**(1):57–72. https://doi.org/10.15252/embr.201744815

Hariri, H., Speer, N., Bowerman, J., Rogers, S., Fu, G., Reetz, E., Datta, S., Feathers, J.R., Ugrankar, R., Nicastro, D., et al., (2019). Mdm1 maintains endoplasmic reticulum homeostasis by spatially regulating lipid droplet biogenesis. Journal of Cell Biology. 2019:**218**(4):1319–1334. https://doi.org/10.1083/jcb.201808119

Heinz, E., and Roughan, P.G., (1983). Similarities and Differences in Lipid Metabolism of Chloroplasts Isolated from 18:3 and 16:3 Plants. Plant Physiol. 1983:**72**(2):273–279. https://doi.org/10.1104/pp.72.2.273

Herdman, C., and Moss, T., (2016). Extended-Synaptotagmins (E-Syts); The extended story. Pharmacol Res. 2016:**107**:48–56. https://doi.org/10.1016/j.phrs.2016.01.034

Hirokawa, N., (2006). mRNA transport in dendrites: RNA granules, motors, and tracks. J Neurosci. 2006:**26**(27):7139–7142. https://doi.org/10.1523/JNEUROSCI.1821-06.2006

Hölzl, G., and Dörmann, P., (2019). Chloroplast Lipids and Their Biosynthesis. Annu Rev Plant Biol. 2019:**70**:51–81. https://doi.org/10.1146/annurev-arplant-050718-100202

Hu, C., Huang, Y., and Li, L., (2017). Drp1-dependent mitochondrial fission plays critical roles in physiological and pathological progresses in mammals. Int J Mol Sci. 2017:**18**(1). https://doi.org/10.3390/ijms18010144

Hurlock, A.K., Roston, R.L., Wang, K., and Benning, C., (2014). Lipid trafficking in plant cells. Traffic. 2014:**15**(9):915–932. https://doi.org/10.1111/tra.12187

Jan, C.H., Williams, C.C., and Weissman, J.S., (2014). Principles of ER cotranslational translocation revealed by proximity-specific ribosome profiling. Science (1979). 2014:**346**(6210). https://doi.org/10.1126/science.1257521

Jarvis, P., (2008). Targeting of nucleus-encoded proteins to chloroplasts in plants. New Phytologist. 2008:**179**(2):257–285. https://doi.org/10.1111/j.1469-8137.2008.02452.x

Jarvis, P., and López-Juez, E., (2013). Biogenesis and homeostasis of chloroplasts and other plastids. Nat Rev Mol Cell Biol. 2013:**14**(12):787–802. https://doi.org/10.1038/nrm3702

Jouhet, J., Maréchal, E., Baldan, B., Bligny, R., Joyard, J., and Block, M.A., (2004). Phosphate deprivation induces transfer of DGDG galactolipid from chloroplast to mitochondria. Journal of Cell Biology. 2004:**167**(5):863–874. https://doi.org/10.1083/jcb.200407022

Karki, N., Johnson, B.S., and Bates, P.D., (2019). Metabolically distinct pools of phosphatidylcholine are involved in trafficking of fatty acids out of and into the chloroplast for membrane production. Plant Cell. 2019:tpc.00121.2019. https://doi.org/10.1105/tpc.19.00121

Kirchhoff, H., (2019). Chloroplast ultrastructure in plants. New Phytologist. 2019:**223**(2):565–574. https://doi.org/10.1111/nph.15730

Koga, Y., Ishikawa, S., Nakamura, T., Masuda, T., Nagai, Y., Takamori, H., Hirota, M., Kanemitsu, K., Baba, Y., and Baba, H., (2008). Oxysterol binding protein-related protein-5 is related to invasion and poor prognosis in pancreatic cancer. Cancer Sci. 2008:**99**(12):2387–2394. https://doi.org/10.1111/j.1349-7006.2008.00987.x

Kok, J.W., Babia, T., Klappe, K., Egea, G., and Hoekstra, D., (1998). Ceramide transport from endoplasmic reticulum to Golgi apparatus is not vesicle-mediated.

Koumandou, V.L., Wickstead, B., Ginger, M.L., Van Der Giezen, M., Dacks, J.B., and Field, M.C., (2013). Molecular paleontology and complexity in the last eukaryotic common ancestor. Crit Rev Biochem Mol Biol. 2013:**48**(4):373–396. https://doi.org/10.3109/10409238.2013.821444

Krawczyk, H.E., Sun, S., Doner, N.M., Yan, Q., Lim, M.S.S., Scholz, P., Niemeyer, P.W., Schmitt, K., Valerius, O., Pleskot, R., et al., (2022). SEED LIPID DROPLET PROTEIN1, SEED LIPID DROPLET PROTEIN2, and LIPID DROPLET PLASMA MEMBRANE ADAPTOR mediate lipid droplet–plasma membrane tethering. Plant Cell. 2022. https://doi.org/10.1093/plcell/koac095

Krebs, H.A., and Johnson, W.A., (1980). The role of citric acid in intermediate metabolism in animal tissues. FEBS Lett. 1980:**117**:K2–K10. https://doi.org/10.1016/0014-5793(80)80564-3

LaBrant, E., Barnes, A.C., and Roston, R.L., (2018). Lipid transport required to make lipids of photosynthetic membranes. Photosynth Res. 2018:**138**(3):345–360. https://doi.org/10.1007/s11120-018-0545-5

Lee, E., Vanneste, S., Pérez-Sancho, J., Benitez-Fuente, F., Strelau, M., Macho, A.P., Botella, M.A., Friml, J., and Rosado, A., (2019). Ionic stress enhances ER–PM connectivity via phosphoinositide-associated SYT1 contact site expansion in Arabidopsis. Proc Natl Acad Sci U S A. 2019:**116**(4):1420–1429. https://doi.org/10.1073/pnas.1818099116

Li, C., Duckney, P., Zhang, T., Fu, Y., Li, X., Kroon, J., De Jaeger, G., Cheng, Y., Hussey, P.J., and Wang, P., (2022). TraB family proteins are components of ER-mitochondrial contact sites and regulate ER-mitochondrial interactions and mitophagy. Nat Commun. 2022:**13**(1):5658. https://doi.org/10.1038/s41467-022-33402-w

Liu, L.K., Choudhary, V., Toulmay, A., and Prinz, W.A., (2017). An inducible ER-Golgi tether facilitates ceramide transport to alleviate lipotoxicity. Journal of Cell Biology. 2017:**216**(1):131–147. https://doi.org/10.1083/jcb.201606059

Mao, K., Wang, K., Liu, X., and Klionsky, D.J., (2013). The scaffold protein Atg11 recruits fission machinery to drive selective mitochondria degradation by autophagy. Dev Cell. 2013:**26**(1):9–18. https://doi.org/10.1016/j.devcel.2013.05.024

Martin, W., Rujan, T., Richly, E., Hansen, A., Cornelsen, S., Lins, T., Leister, D., Stoebe, B., Hasegawa, M., and Penny, D., (2002). Evolutionary analysis of Arabidopsis, cyanobacterial, and chloroplast genomes reveals plastid phylogeny and thousands of cyanobacterial genes in the nucleus. Proceedings of the National

Academy of Sciences. 2002:**99**(19):12246–12251. https://doi.org/10.1073/pnas.182432999

Mavuduru, V.A., Vadupu, L., Ghosh, K.K., Chakrabortty, S., Gulyás, B., Padmanabhan, P., and Ball, W.B., (2024). Mitochondrial phospholipid transport: Role of contact sites and lipid transport proteins. Prog Lipid Res. 2024:**94**:101268. https://doi.org/10.1016/j.plipres.2024.101268

Maynard, S.N., and Griffing, L.R., (2024). The photosensitive endoplasmic reticulum-chloroplast contact site. J Microsc. 2024. https://doi.org/10.1111/jmi.13377

Mehrshahi, P., Johnny, C., and DellaPenna, D., (2014). Redefining the metabolic continuity of chloroplasts and ER. Trends Plant Sci. 2014:**19**(8):501–507. https://doi.org/10.1016/j.tplants.2014.02.013

Michel, A.H., and Kornmann, B., (2012). The ERMES complex and ER-mitochondria connections. Biochem Soc Trans. 2012:**40**(2):445–450. https://doi.org/10.1042/BST20110758

Mogre, S.S., Brown, A.I., and Koslover, E.F., (2020). Getting around the cell: physical transport in the intracellular world. Phys Biol. 2020:**17**(6):061003. https://doi.org/10.1088/1478-3975/aba5e5

Murley, A., Sarsam, R.D., Toulmay, A., Yamada, J., Prinz, W.A., and Nunnari, J., (2015). Ltc1 is an ER-localized sterol transporter and a component of ER-mitochondria and ER-vacuole contacts. Journal of Cell Biology. 2015:**209**(4):539–548. https://doi.org/10.1083/jcb.201502033

Murphy, S.E., and Levine, T.P., (2016). VAP, a Versatile Access Point for the Endoplasmic Reticulum: Review and analysis of FFAT-like motifs in the VAPome. Biochim Biophys Acta Mol Cell Biol Lipids. 2016:**1861**(8):952–961. https://doi.org/10.1016/j.bbalip.2016.02.009

Nakamura, K., Aoyama-Ishiwatari, S., Nagao, T., Paaran, M., Obara, C.J., Sakurai-Saito, Y., Johnston, J., Du, Y., Suga, S., Tsuboi, M., et al., (2025). Mitochondrial complexity is regulated at ER-mitochondria contact sites via PDZD8-FKBP8 tethering. Nat Commun. 2025:**16**(1):3401. https://doi.org/10.1038/s41467-025-58538-3

Nakamura, M., Nishimura, T., and Morita, M.T., (2019). Gravity sensing and signal conversion in plant gravitropism. J Exp Bot. 2019:**70**(14):3495–3506. https://doi.org/10.1093/jxb/erz158

Nan, X., Sims, P.A., and Xie, X.S., (2008). Organelle tracking in a living cell with microsecond time resolution and nanometer spatial precision. ChemPhysChem. 2008:**9**(5):707–712. https://doi.org/10.1002/cphc.200700839

Nascimbeni, A.C., Codogno, P., and Morel, E., (2017). Phosphatidylinositol-3-phosphate in the regulation of autophagy membrane dynamics. FEBS Journal. 2017:**284**(9):1267–1278. https://doi.org/10.1111/febs.13987

Orci, L., Ravazzola, M., Le Coadic, M., Shen, W., Demaurex, N., and Cosson, P., (2009). STIM1-induced precortical and cortical subdomains of the endoplasmic reticulum. Proceedings of the National Academy of Sciences. 2009:**106**(46):19358–19362. https://doi.org/10.1073/pnas.0911280106

Palade, G.E., (1956). The endoplasmic reticulum. J Biophys Biochem Cytol. 1956:**2**(4, Suppl):85–98. https://doi.org/10.1083/jcb.2.4.85

Pan, X., Ren, L., Yang, Y., Xu, Y., Ning, L., Zhang, Y., Luo, H., Zou, Q., and Zhang, Y., (2024). MCSdb, a database of proteins residing in membrane contact sites. Sci Data. 2024:**11**(1). https://doi.org/10.1038/s41597-024-03104-7

Pérez-Sancho, J., Vanneste, S., Lee, E., McFarlane, H.E., del Valle, A.E., Valpuesta, V., Friml, J., Botella, M.A., and Rosado, A., (2015). The arabidopsis synaptotagmin1 is enriched in endoplasmic reticulum-plasma membrane contact sites and confers cellular resistance to mechanical stresses. Plant Physiol. 2015:**168**(1):132–143. https://doi.org/10.1104/pp.15.00260

Pick, T.R., Bräutigam, A., Schulz, M.A., Obata, T., Fernie, A.R., and Weber, A.P.M., (2013). PLGG1, a plastidic glycolate glycerate transporter, is required for photorespiration and defines a unique class of metabolite transporters. Proc Natl Acad Sci U S A. 2013:**110**(8):3185–3190. https://doi.org/10.1073/pnas.1215142110

Pobre-Piza, K.F.R., and Hendershot, L.M., (2021). Protein folding: Protein folding in the endoplasmic reticulum. Encyclopedia of Biological Chemistry: Third Edition. 2021:**3**:127–139. https://doi.org/10.1016/B978-0-12-819460-7.00070-0

Polianskyte-Prause, Z., Arora, A., Taskinen, J.H., Chaurasiya, V., Keskitalo, S., Tuhkala, A., Hilska, I., Varjosalo, M., and Olkkonen, V.M., (2025). The role of Nir2, a lipid-transfer protein, in regulating endothelial cell functions. Biochim Biophys Acta Mol Cell Res. 2025:**1872**(3):119926. https://doi.org/10.1016/j.bbamcr.2025.119926

Qian, T., Li, C., Liu, F., Xu, K., Wan, C., Liu, Y., and Yu, H., (2022). Arabidopsis synaptotagmin 1 mediates lipid transport in a lipid composition-dependent manner. Traffic. 2022:**23**(6):346–356. https://doi.org/10.1111/tra.12844

Racine, V., Sachse, M., Salamero, J., Fraisier, V., Trubuil, A., and Sibarita, J.B., (2007). Visualization and quantification of vesicle trafficking on a three-dimensional cytoskeleton network in living cells. J Microsc. 2007:**225**(3):214–228. https://doi.org/10.1111/j.1365-2818.2007.01723.x

Raiborg, C., Wenzel, E.M., Pedersen, N.M., Olsvik, H., Schink, K.O., Schultz, S.W., Vietri, M., Nisi, V., Bucci, C., Brech, A., et al., (2015). Repeated ER-endosome

contacts promote endosome translocation and neurite outgrowth. Nature. 2015:**520**(7546):234–238. https://doi.org/10.1038/nature14359

Reinisch, K.M., and Prinz, W.A., (2021). Mechanisms of nonvesicular lipid transport. Journal of Cell Biology. 2021:**220**(3):1–11. https://doi.org/10.1083/JCB.202012058

Renna, L., Stefano, G., Puggioni, M.P., Kim, S.J., Lavell, A., Froehlich, J.E., Burkart, G., Mancuso, S., Benning, C., and Brandizzi, F., (2024). ER-associated VAP27-1 and VAP27-3 proteins functionally link the lipid-binding ORP2A at the ER-chloroplast contact sites. Nat Commun. 2024:**15**(1). https://doi.org/10.1038/s41467-024-50425-7

Ross, J.L., Ali, M.Y., and Warshaw, D.M., (2008). Cargo transport: molecular motors navigate a complex cytoskeleton. Curr Opin Cell Biol. 2008:**20**(1):41–47. https://doi.org/10.1016/j.ceb.2007.11.006

Ruiz-Lopez, N., Pérez-Sancho, J., del Valle, A.E., Haslam, R.P., Vanneste, S., Catalá, R., Perea-Resa, C., van Damme, D., García-Hernández, S., Albert, A., et al., (2021). Synaptotagmins at the endoplasmic reticulum–plasma membrane contact sites maintain diacylglycerol homeostasis during abiotic stress. Plant Cell. 2021:**33**(7):2431–2453. https://doi.org/10.1093/plcell/koab122

Sadali, N.M., Sowden, R.G., Ling, Q., and Jarvis, R.P., (2019). Differentiation of chromoplasts and other plastids in plants. Plant Cell Rep. 2019:**38**(7):803–818. https://doi.org/10.1007/s00299-019-02420-2

Šamaj, J., Müller, J., Beck, M., Böhm, N., and Menzel, D., (2006). Vesicular trafficking, cytoskeleton and signalling in root hairs and pollen tubes. Trends Plant Sci. 2006:**11**(12):594–600. https://doi.org/10.1016/j.tplants.2006.10.002

Santos, N.C., Girik, V., and Nunes-Hasler, P., (2020). ORP5 and ORP8: Sterol sensors and phospholipid transfer proteins at membrane contact sites? Biomolecules. 2020:**10**(6):1–17. https://doi.org/10.3390/biom10060928

Saravanan, R.S., Slabaugh, E., Singh, V.R., Lapidus, L.J., Haas, T., and Brandizzi, F., (2009). The targeting of the oxysterol-binding protein ORP3a to the endoplasmic reticulum relies on the plant VAP33 homolog PVA12. Plant Journal. 2009:**58**(5):817–830. https://doi.org/10.1111/j.1365-313X.2009.03815.x

Schatz, G., and Dobberstein, B., (1996). Common Principles of Protein Translocation Across Membranes. Science (1979). 1996:**271**(5255):1519–1526. https://doi.org/10.1126/science.271.5255.1519

Schwarz, T.L., (2013). Mitochondrial trafficking in neurons. Cold Spring Harb Perspect Biol. 2013:**5**(6). https://doi.org/10.1101/cshperspect.a011304

Selitrennik, M., and Lev, S., (2016). The role of phosphatidylinositol-transfer proteins at membrane contact sites. Biochem Soc Trans. 2016:**44**(2):419–424. https://doi.org/10.1042/BST20150182

Shai, N., Yifrach, E., Van Roermund, C.W.T., Cohen, N., Bibi, C., IJlst, L., Cavellini, L., Meurisse, J., Schuster, R., Zada, L., et al., (2018). Systematic mapping of contact sites reveals tethers and a function for the peroxisome-mitochondria contact. Nat Commun. 2018:**9**(1). https://doi.org/10.1038/s41467-018-03957-8

Shiiba, I., Ito, N., Oshio, H., Ishikawa, Y., Nagao, T., Shimura, H., Oh, K.W., Takasaki, E., Yamaguchi, F., Konagaya, R., et al., (2025). ER-mitochondria contacts mediate lipid radical transfer via RMDN3/PTPIP51 phosphorylation to reduce mitochondrial oxidative stress. Nature Communications. 2025:**16**(1). https://doi.org/10.1038/s41467-025-56666-4

Solymosi, K., and Schoefs, B., (2010). Etioplast and etio-chloroplast formation under natural conditions: The dark side of chlorophyll biosynthesis in angiosperms. Photosynth Res. 2010:**105**(2):143–166. https://doi.org/10.1007/s11120-010-9568-2

South, P.F., Walker, B.J., Cavanagh, A.P., Rolland, V., Badger, M., and Ort, D.R., (2017). Bile acid sodium symporter BASS6 can transport glycolate and is involved in photorespiratory metabolism in Arabidopsis thaliana. Plant Cell. 2017:**29**(4):808–823. https://doi.org/10.1105/tpc.16.00775

Staehelin, L.A., (2003). Chloroplast structure: From chlorophyll granules to supra-molecular architecture of thylakoid membranes. Photosynth Res. 2003:**76**(1–3):185–196. https://doi.org/10.1023/A:1024994525586

Steward, O., and Banker, G.A., (1992). Getting the message from the gene to the synapse: sorting and intracellular transport of RNA in neurons. Trends Neurosci. 1992:**15**(5):180–186. https://doi.org/10.1016/0166-2236(92)90170-D

Stiber, J., Hawkins, A., Zhang, Z.S., Wang, S., Burch, J., Graham, V., Ward, C.C., Seth, M., Finch, E., Malouf, N., et al., (2008). STIM1 signalling controls store-operated calcium entry required for development and contractile function in skeletal muscle. Nat Cell Biol. 2008:**10**(6):688–697. https://doi.org/10.1038/ncb1731

Tong, J., Manik, M.K., and Im, Y.J., (2018). Structural basis of sterol recognition and nonvesicular transport by lipid transfer proteins anchored at membrane contact sites. Proc Natl Acad Sci U S A. 2018:**115**(5):E856–E865. https://doi.org/10.1073/pnas.1719709115

Vale, R.D., (2003). The Molecular Motor Toolbox for Intracellular Transport. Cell. 2003:**112**(4):467–480. https://doi.org/10.1016/S0092-8674(03)00111-9

Vance, J.E., Aasman, E.J., and Szarka, R., (1991). Brefeldin a does not inhibit the movement of phosphatidylethanolamine from its sites of synthesis to the cell surface.

Journal of Biological Chemistry. 1991:**266**(13):8241–8247. https://doi.org/10.1016/s0021-9258(18)92968-6

Voeltz, G.K., Rolls, M.M., and Rapoport, T.A., (2002). Structural organization of the endoplasmic reticulum. EMBO Rep. 2002:**3**(10):944–950. https://doi.org/10.1093/embo-reports/kvf202

Wang, P., Hawkins, T.J., Richardson, C., Cummins, I., Deeks, M.J., Sparkes, I., Hawes, C., and Hussey, P.J., (2014). The plant cytoskeleton, NET3C, and VAP27 mediate the link between the plasma membrane and endoplasmic reticulum. Current Biology. 2014:**24**(12):1397–1405. https://doi.org/10.1016/j.cub.2014.05.003

Wang, P.T.C., Garcin, P.O., Fu, M., Masoudi, M., St-Pierre, P., Panté, N., and Nabi, I.R., (2015). Distinct mechanisms controlling rough and smooth endoplasmic reticulum contacts with mitochondria. J Cell Sci. 2015:**128**(15):2759–2765. https://doi.org/10.1242/jcs.171132

Waters, M.T., and Langdale, J.A., (2009). The making of a chloroplast. EMBO Journal. 2009:**28**(19):2861–2873. https://doi.org/10.1038/emboj.2009.264

Weber, A.P.M., and Linka, N., (2011). Connecting the plastid: Transporters of the plastid envelope and their role in linking plastidial with cytosolic metabolism. Annu Rev Plant Biol. 2011:**62**:53–77. https://doi.org/10.1146/annurev-arplant-042110-103903

White, R.R., Lin, C., Leaves, I., Castro, I.G., Metz, J., Bateman, B.C., Botchway, S.W., Ward, A.D., Ashwin, P., and Sparkes, I., (2020). Miro2 tethers the ER to mitochondria to promote mitochondrial fusion in tobacco leaf epidermal cells. Commun Biol. 2020:**3**(1):1–8. https://doi.org/10.1038/s42003-020-0872-x

Wilson, E.L., Yu, Y., Leal, N.S., Woodward, J.A., Patikas, N., Morris, J.L., Field, S.F., Plumbly, W., Paupe, V., Chowdhury, S.R., et al., (2024). Genome-wide CRISPR/Cas9 screen shows that loss of GET4 increases mitochondria-endoplasmic reticulum contact sites and is neuroprotective. Cell Death Dis. 2024:**15**. https://doi.org/10.1038/s41419-024-06568-y

Xiao, R., Zou, Y., Guo, X., Li, H., and Lu, H., (2022). Fatty acid desaturases (FADs) modulate multiple lipid metabolism pathways to improve plant resistance. Mol Biol Rep. 2022:**49**(10):9997–10011. https://doi.org/10.1007/s11033-022-07568-x

Xu, C., Fan, J., Cornish, A.J., and Benning, C., (2008). Lipid trafficking between the endoplasmic reticulum and the plastid in Arabidopsis requires the extraplastidic TGD4 protein. Plant Cell. 2008:**20**(8):2190–2204. https://doi.org/10.1105/tpc.108.061176

Yamaoka, S., Nakajima, M., Fujimoto, M., and Tsutsumi, N., (2011). MIRO1 influences the morphology and intracellular distribution of mitochondria during embryonic cell division in Arabidopsis. Plant Cell Rep. 2011:**30**(2):239–244. https://doi.org/10.1007/s00299-010-0926-5

Ye, H., Gao, J., Liang, Z., Lin, Y., Yu, Q., Huang, S., and Jiang, L., (2022). Arabidopsis ORP2A mediates ER-autophagosomal membrane contact sites and regulates PI3P in plant autophagy. 2022. https://doi.org/10.1073/pnas

Zhang, Y., Sampathkumar, A., Kerber, S.M.-L., Swart, C., Hille, C., Seerangan, K., Graf, A., Sweetlove, L., and Fernie, A.R., (2020). A moonlighting role for enzymes of glycolysis in the co-localization of mitochondria and chloroplasts. Nat Commun. 2020:**11**(1). https://doi.org/10.1038/s41467-020-18234-w

Zhou, Y., Meraner, P., Kwon, H.T., Machnes, D., Oh-Hora, M., Zimmer, J., Huang, Y., Stura, A., Rao, A., and Hogan, P.G., (2010). STIM1 gates the store-operated calcium channel ORAI1 in vitro. Nat Struct Mol Biol. 2010:**17**(1):112–117. https://doi.org/10.1038/nsmb.1724

Chapter I:

Proximity-dependent bimolecular fluorescence complementation visualizes membrane contact sites in plants

Vanessa Valencia[1], Franziska Kuhnert[1]†, Andreas P.M. Weber[1]

[1] Institute of Plant Biochemistry, SFB1208, Heinrich Heine University, Universitätsstrasse 1, 40225 Düsseldorf, Germany

† Plant Energy Biology, University of Western Australia; Crawley, 6009, Australia

Author contribution: VV designed the experiments, performed cloning, transient expressions, and confocal microscopy; FK and APMW designed the research and supervised the experiments

ABSTRACT

Bimolecular fluorescence complementation (BiFC) is widely used to verify interactions *in vivo.* Membrane-membrane interactions allowing communication between organelles, referred to as membrane contact sites (MCSs), have received increasing attention over the recent years due to their important but diverse roles in cellular metabolism. Most research to date has been conducted in mammalian cells or yeast, leading to the hypothesis that all organelles form MCSs with other membranous compartments. This hypothesis provided the initial clues for the existence of MCSs in plants. In phototrophic organisms, the presence of plastids suggests the existence of additional and unique types of MCSs. In this study, a modular BiFC approach was established that verified the presence of MCSs between the endoplasmic reticulum, mitochondria and chloroplasts. Beyond the simple visualization, the BiFC system allows differentiation between distinct types of MCSs through a careful implementation of diverse spacer modules. Hereby, MCSs at the endoplasmic reticulum revealed a wider gap size between the two interacting organelles compared to other visualized MCSs. Thus, this modular toolkit enables the precise modular engineering to effectively visualize specific membrane contact sites *in planta*.

INTRODUCTION

Cellular processes are determined by the coordinated function of numerous proteins organized in multi-protein complexes. Identifying and localizing such protein-protein interactions (PPIs) *in vivo* is crucial for understanding cellular function across diverse organisms. Bimolecular fluorescence complementation (BiFC) has become a popular technique over recent years for reliably detecting these interactions. The principle of BiFC relies on non-fluorescent fragments of a fluorescent protein (FP) that reassembles to a functional unit when brought into proximity. This reassembly leads to a fluorescent signal, enabling the detection of PPI *in vivo*. BiFC has been successfully used to reliably detect and verify PPIs in a range of organisms, such as mammalian cells (Hu et al., 2002), *Caenorhabditis elegans* (Hiatt et al., 2008), and yeast (Sung and Huh, 2007). Various FPs including green FP (GFP) (Barnard et al., 2008), yellow FP (YFP) (Citovsky et al., 2006), mCherry (Fan et al., 2008), or mVenus (Sung and Huh, 2007) have been broadly used in different studies for BiFC assays. Further development of this technique explored the possibility to use a multicolor (Tamura et al., 2021) or a trimolecular approach (Foglieni et al., 2017; Koraïchi et al., 2018), allowing for the study of more complex interactions.

Cabantous and colleagues developed a BiFC version based on the superfolder GFP (sfGFP) (Pédelacq et al., 2006) to improve protein solubility and sensitivity of the assay. The truncated and self-assembling fragments – named sfGFP1-10 OPT (hereafter referred to as GFP1-10) and sfGFP11 M3 (hereafter referred to as GFP11) – are employed in this study. GFP1-10 contains the first ten beta-strands of the GFP protein, while the GFP11 represents the eleventh beta-strand, and their separation disrupts the fluorophore (Cabantous et al., 2005). Consequently, the two separate fragments do not exhibit fluorescence. Upon reassembly into the complete β-barrel structure of the GFP protein, the fluorophore is reconstituted, enabling a fluorescent signal. The reassembly of the GFP fragments is irreversible making this system unsuitable for monitoring the dynamics of interactions (Pédelacq et al., 2006; Horstman et al., 2014; Cieri et al., 2018). Depending on the biological question, the irreversible nature of BiFC can be advantageous. For instance, highly transient interactions can be stabilized and readily visualized. In contrast, techniques such as dimerization-dependent FP (Alford et al., 2012; Ding et al., 2015) or fluorescence/bioluminescence resonance energy transfer (Demarco et al., 2006; Denay et al., 2019; Hertlein et al., 2020) are more suitable approaches for studying temporal dynamics, but might fail to detect highly transient interactions. A major limitation of BiFC is its relatively high probability of false positive results, which necessitates stringent controls. Generally, the negative control should show no detectable fluorescent signal upon simultaneous expression of the two fragments. Ideally, in studies investigating potential

PPIs, an unrelated or truncated version of one of the proteins can be fused to one of the FP fragments as control (Horstman et al., 2014).

Membrane contact sites (MCSs) are areas of close proximity between interacting membranes. The proximity of these membranes in such an MCS is usually around 10 – 40 nm (Scorrano et al., 2019; Voeltz et al., 2024), and can be exploited to identify unknown MCSs. With the presence of the plastid as an additional organelle, it is reasonable to hypothesize that unique and complex MCSs exist in plants and other photosynthetically active organisms. Indeed, MCSs in plants have been found at chloroplast membranes such as plastid associated membranes (PLAMs) (Andersson et al., 2007a). Such interactions between plant membranes are likely mediated by proteins, which remain largely unidentified to date. The implementation of a proximity-dependent but PPI-independent BiFC approach might shed further light on plant MCSs. For establishing the proximity-dependency in this BiFC, unbiased proteins are used as anchors. These anchors are membrane proteins with well characterized topology and localization, allowing reliable targeting of the FP fragments to specific organellar membranes. At an MCS, where two organelles are in close contact, reassembly of the GFP leads to the production of a fluorescent signal. This approach enables the identification of putative MCSs *in planta*.

In this chapter, modular cloning using the Golden Gate cloning method is employed to establish a flexible system for studying MCSs *in planta.* This method, based on the Modular Cloning system described by Engler and colleagues (2014), simplifies the cloning process and enables the rapid assembly of transcriptional units and their integration into multigene constructs. Transcriptional units can be customized by varying promoters, self-assembling GFP fragments, genes used as anchors or candidates, spacers and linkers, and terminators. In this study, we established anchors for the endoplasmic reticulum (ER), chloroplast and mitochondrion. These anchors were utilized in the proximity-dependent BiFC approach, in which the GFP fragments are fused to the cytosolic side of the membrane anchors, to visualize putative novel MCSs in plants. Thus, this modular system provides an efficient platform to design, build and test hypotheses regarding PPIs and to discover novel MCSs using the molecularly adjustable BiFC presented here.

MATERIALS AND METHODS

PLASMID CONSTRUCTION

The membrane proteins outer envelope membrane protein 7 (OEP7; At3g52420), translocase of outer membrane 20 kDa subunit 2 (TOM20; At1g27390) and ent-kaurenoic acid oxidase 2 (KAO2; At2g32440) were chosen as membrane anchors for chloroplasts, mitochondria and ER, respectively. Furthermore, the translocase of the outer membrane 5 kDa (TOM5; AT5G08040) was established as a positive control. Internal *Bsa*I and *Bbs*I recognition sites were removed during the cloning process. In addition, truncated variants of the membrane proteins containing only the transmembrane domain were created: OEP7 1-141 aa, and TOM20 179-210 aa. Full-length sfGFP from Aequorea victoria was used to generate the two split parts GFP1-10 and GFP11 (Cabantous et al., 2005). Single or double copies of GFP11 were used and referred to as GFP11 and 2xGFP11, respectively. Constructs were designed with a GS linker in form of 'GSSG' or 'SGGS' between the membrane anchor and the GFP part. The expression constructs with the pAGM4723 (Addgene #48015) backbone contained the following gene cassettes: (1) membrane anchor fused to one GFP part under the control of the 35S promoter (Gallie et al., 1987), (2) membrane anchor fused to the corresponding GFP part under the control of the UBQ10 promoter (Grefen et al., 2010), (3) kanamycin resistance cassette driven by the nos promoter (Gynheung, 1986). Expression constructs with pICH86966 (Addgene #48075) backbone contained one transcriptional unit for single expression of gene cassettes. All constructs were assembled via Golden Gate cloning using the MoClo toolkit (Weber et al., 2011; Engler et al., 2014). All final expression constructs and oligonucleotides used in this study are listed in Supplementary Table 1 and Supplementary Table 2.

TRANSIENT EXPRESSION IN *NICOTIANA BENTHAMIANA*

Agrobacterium tumefaciens GV3101 strains containing the final expression constructs were used to infiltrate leaves from 4- to 5-week-old *Nicotiana benthamiana* (tobacco) plants. To this end, the respective strain was grown over night in liquid culture at 30 °C with 200 rpm shaking. Cells were harvested and resuspended in infiltration buffer (10 mM MES-KOH pH 5.7, 10 mM $MgCl_2$, 200 µM Acetosyringone) to an OD_{600} of 0.5. For ER visualization, an *A. tumefaciens* GV3101 strain containing an ER marker, which is a fusion protein of the wall-associated receptor kinase 2 fused to CFP and the ER retention signal HDEL by Nelson et al., (2007) (referred to as WAK2-CFP), was co-infiltrated with the *A. tumefaciens* GV3101 strain containing the expression construct by resuspending and mixing each strain to OD_{600} of 0.4. The infiltration suspensions were infiltrated into the

abaxial side of two tobacco leaves per plant. The plants were further grown for 2 days at 22 °C.

PROTOPLAST ISOLATION

Infiltrated leaves were cut into small pieces and vacuum-infiltrated with isolation buffer (0.4 M Mannitol, 20 mM MES-KOH pH 5.7, 20 mM KCl, 10 mM $CaCl_2$) supplemented with 1.5% (w/v) Cellulase R-10, 0.4% (w/v) Macerozyme R-10, and 0.1% (w/v) BSA. The infiltrated tobacco leaves were subsequently incubated in the digestion solution for 2 h at 30 °C in the dark to extract protoplasts. After isolation, protoplasts were transferred into a fresh 2 mL tube, washed with wash buffer (0.7 M mannitol, 15 mM $MgCl_2$, 4 mM MES-KOH pH 5.7) and used for microscopy. If needed 200 µM MitoTracker Red CMXRos (Thermo Fisher Scientific) was supplemented to the protoplasts 15 min prior to microscopy analyses.

CONFOCAL MICROSCOPY

Fluorescence images were obtained on SP8 confocal microscope (Leica) with the following excitation/emission settings: GFP fluorescence (488 nm/498–550 nm), MitoTracker (561nm/582 –615 nm), and WAK2-CFP marker (458 nm/465-500 nm). Chlorophyll fluorescence (autofluorescence) was observed at 640 to 710 nm. Crosstalk was minimized by using sequential scanning mode. Images were analyzed using Fiji (Schindelin et al., 2012) and Inkscape (version 1.4.1).

RESULTS

DESIGN OF THE SELF-ASSEMBLING SPLIT GFP ASSAY

The self-assembling GFP assay consists of two essential parts - (1) membrane proteins of known topology that target the (outer) membrane of the desired organelle, called membrane anchors, and (2) the GFP fragments. Fundamental work, such as the majority of the cloning procedure, was previously described in the master thesis by Vanessa Valencia (2022). Briefly, the cloning process follows the principle of the MoClo toolkit described by Engler and colleagues (2014). Hereby, the membrane anchors, GFP fragments and optional molecular spacers were established as modules to quickly and efficiently screen for MCSs in plant systems (Figure 1).

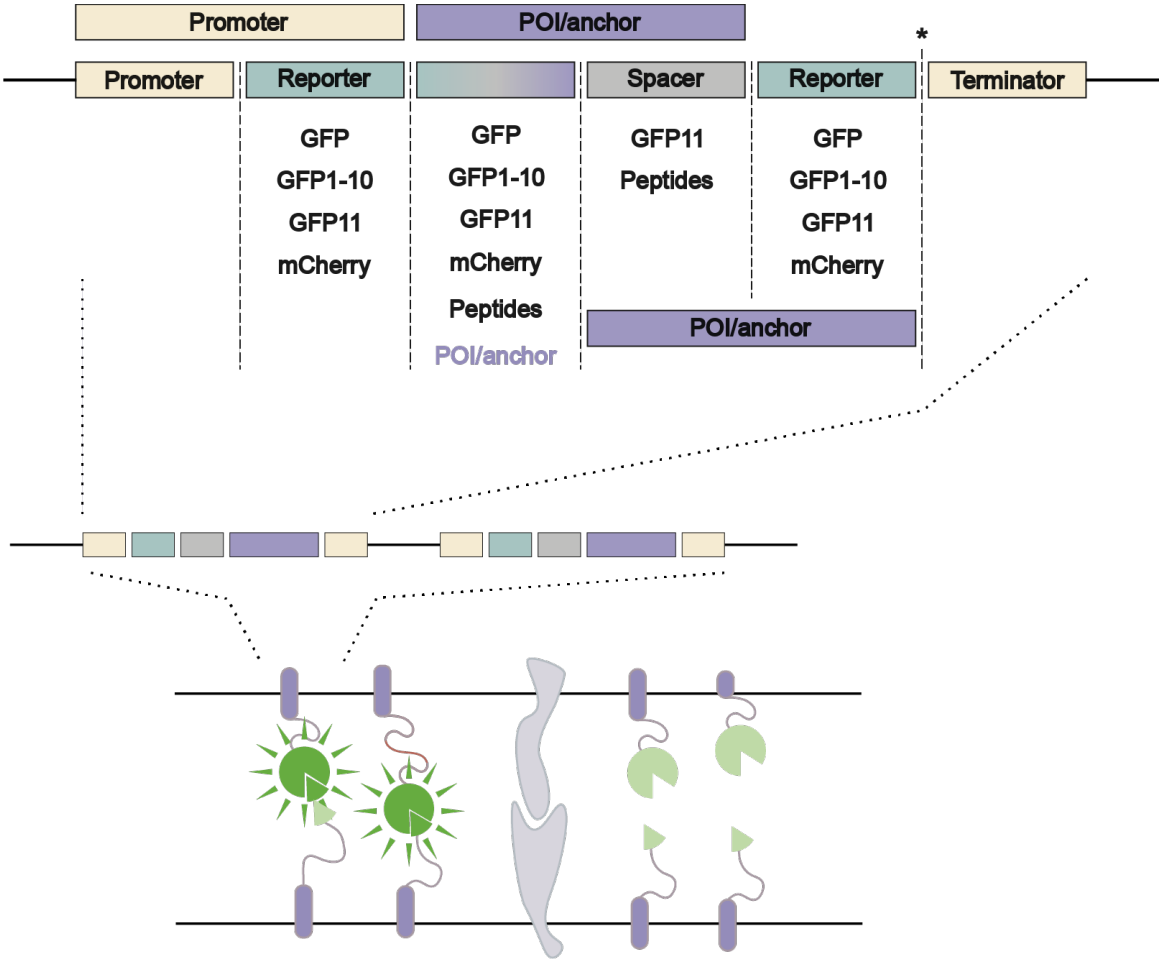

Figure 1: Scheme of the MoClo toolkit with the BiFC assay modules. BiFC modules as well as other reporters (GFP, mCherry) can be modularly fused with protein of interests (POIs) or membrane anchors. This system enables the simultaneous expression of both transcriptional units for BiFC assays testing for multiple types of interactions. Promoter and terminators as well as other plant parts are used from the MoClo toolkit (Engler et al., 2014). The system can be adjusted with spacers to overcome the gap between two interacting membranes at an MCS. At a given proximity, GFP1-10 and GFP11 reconstitute to the full β-barrel structure of the GFP protein, which emits a fluorescent signal.

The *Arabidopsis thaliana* membrane proteins OEP7 (Lee et al., 2001), TOM20 (Werhahn et al., 2003) and KAO2 (Helliwell et al., 2001), localizing to the chloroplast, mitochondrion and the ER, respectively, were chosen as membrane anchors and fused to GFP to verify correct targeting to the outer membrane. OEP7 contains a N-terminal transmembrane domain. Therefore, the GFP, as well as the GFP fragments used in the self-assembling GFP assay, were fused to its C-terminus. The same strategy was applied for the KAO2. TOM20 was fused to the GFP and the GFP fragments at its N-terminus. The use of either N- or C-terminal fusions depending on the topology of the membrane anchor ensured that the reporter system faced the cytosol.

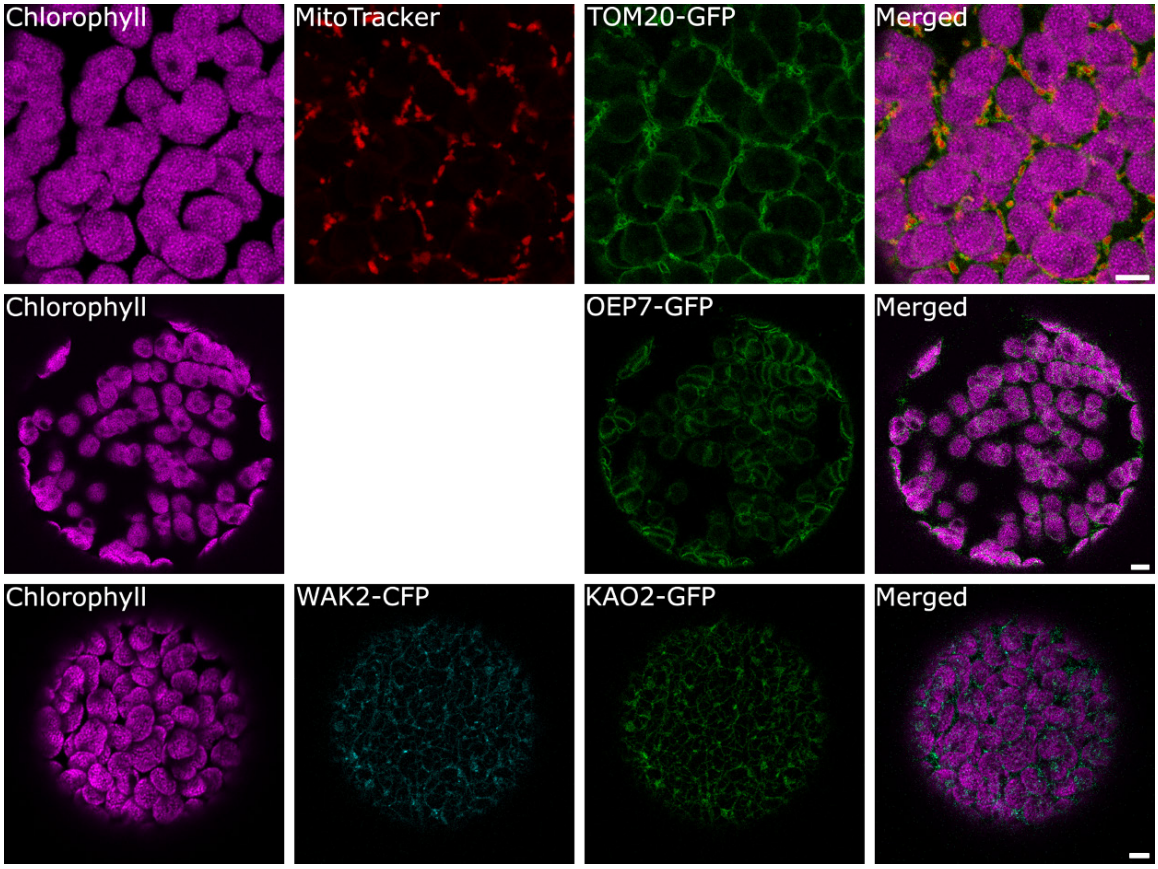

Figure 2: Subcellular localization of membrane anchors fused to GFP at their cytosol-facing termini. Localization of different membrane anchors was analyzed by transient expression in *Nicotiana benthamiana* (tobacco) protoplasts. The fluorescent signal of the GFP-tagged anchors targeting to destined organelles were visualized in green. The MitoTracker Red CMXRos marked mitochondria (red). Chloroplasts were visualized by their chlorophyll autofluorescence (magenta), and the ER marker (*WAK2-CFP;* (Nelson et al., 2007)) visualized the ER. Scale bar = 5 µm.

OEP7-, TOM20-, and KAO2-GFP fusion proteins were transiently expressed in tobacco protoplasts and showed the correct localization to and even distribution at the outer membrane of their respective organelle. As expected, TOM20 localized to the mitochondria, which were stained with MitoTracker Red CMXRos (red). Likewise, OEP7 localized to the chloroplast visualized by the chlorophyll autofluorescence (magenta).

KAO2 evenly distributed at the ER and co-localize with the ER marker (WAK2-CFP; Nelson et al., 2007) (Figure 2).

Subsequently, the functionality of the self-assembling GFP system, consisting of GFP1-10 and GFP11 fragments of the self-assembling GFP, was validated in this expression system. As a proof of principle, the GFP fragments were fused to TOM20 and TOM5, both components of the translocase of the outer membrane (TOM) complex, a protein import machinery of the mitochondria (Werhahn et al., 2003). Hence, the two proteins are known to come into close proximity of each other enabling GFP reassembly.

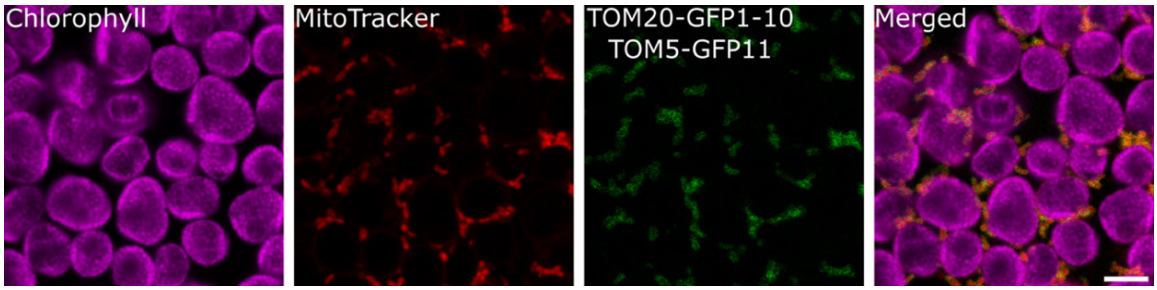

Figure 3: Subcellular localization of the self-assembling GFP fragments within the TOM complex in tobacco protoplasts. The fluorescent signal (green) of TOM20 and TOM5 fused to GFP1-10 and GFP11, respectively, showed localization at the mitochondria visualized by co-localization with the fluorescent signal of the MitoTracker Red CMXRos (red). Scale bar = 5 µm.

The gene cassettes containing the GFP fragments fused to TOM20 and TOM5 were transiently expressed in tobacco, and the reassembly of the GFP fragments was visualized in isolated protoplast. Indeed, GFP fluorescence was observed co-localizing with the MitoTracker Red CMXRos at the mitochondrial membrane (Figure 3). The interaction within the TOM complex provides the proximity required for GFP reassembly and thus serves as a positive control to validate the functionality of the self-assembling GFP assay in tobacco protoplasts.

Additional controls were performed to test the specificity of the GFP fragments. The GFP fragments should not emit a fluorescent signal on their own, but only upon close proximity to each other as demonstrated for the TOM complex (Figure 3). To assess the likelihood for detecting false positive interactions, the GFP fragments were expressed separately: either targeted to organellar membranes without a known interaction partner or with one GFP fragment unfused in the cytosol.

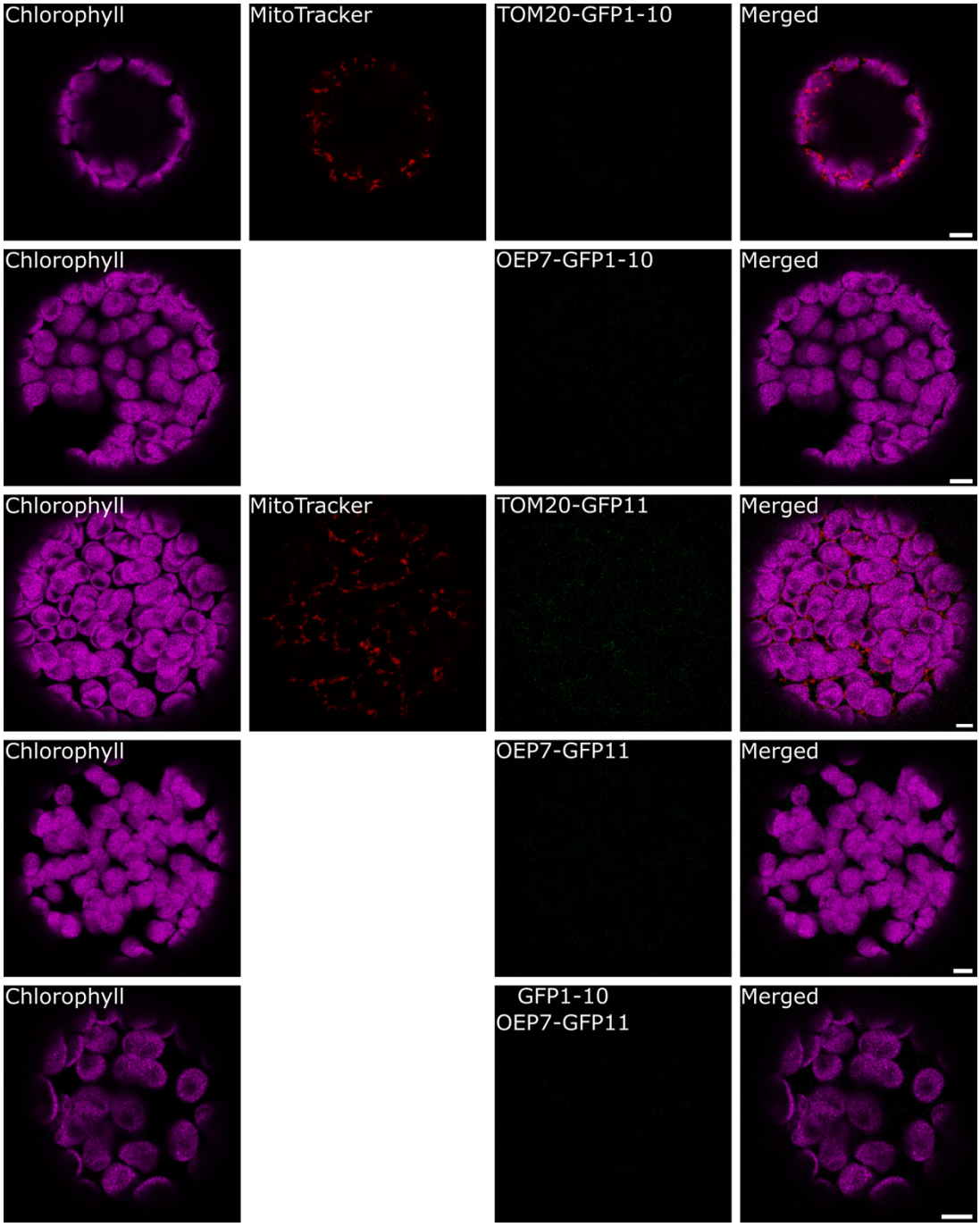

Figure 4: Expression of the split GFP controls in tobacco protoplasts. Both GFP parts, GFP1-10 and GFP11, expressed separately at either the chloroplast or mitochondrial membrane in tobacco protoplasts showed no detectable fluorescence (green). Similarly, cytosolic GFP1-10 together with a membrane-bound GFP11 showed no detectable fluorescent signal. Mitochondria were visualized with the MitoTracker Red CMXRos (red) and chloroplasts were visualized by their chlorophyll autofluorescence (magenta). Scale bar = 5 µm.

As expected, expression of the single GFP fragments (GFP1-10 or GFP11) targeted to different organellar membranes showed no detectable fluorescent signal. Furthermore, co-expression of GFP1-10 in the cytosol with GFP11 targeted to the chloroplast outer envelope did not result in a fluorescent signal, indicating the absence of false positive interactions (Figure 4). These results demonstrate that the system established here

specifically reports *in vivo* interactions, hence making it suitable to visualize MCSs *in planta*.

VISUALIZATION OF ER-MITOCHONDRION CONTACT SITES

Using the established screening assay, the existence of MCSs between the ER and mitochondria was assessed. To this end, gene cassettes encoding GFP1-10 and GFP11, targeted to the ER and mitochondria, respectively, were transiently co-expressed in tobacco leaves. Co-expression of KAO2 and TOM20 fused to either GFP1-10 or GFP11 resulted in no detectable fluorescent signal (Figure 5A). However, replacing the single GFP11 with a tandem repeat (2xGFP11) produced a punctate fluorescent pattern. These puncta co-localized to both the mitochondrial surface (red) and to the ER (cyan) simultaneously, indicating regions of close proximity between these two organelles (Figure 5B). The observed pattern resembles previously described MCSs in yeast, plants and mammalian cells (Cieri et al., 2018; Kakimoto et al., 2018; Yang et al., 2018; Li et al., 2020), suggesting that ER-mitochondria MCSs were successfully visualized. The requirement for a tandem GFP11 may reflect a greater distance between the membranes in these MCSs.

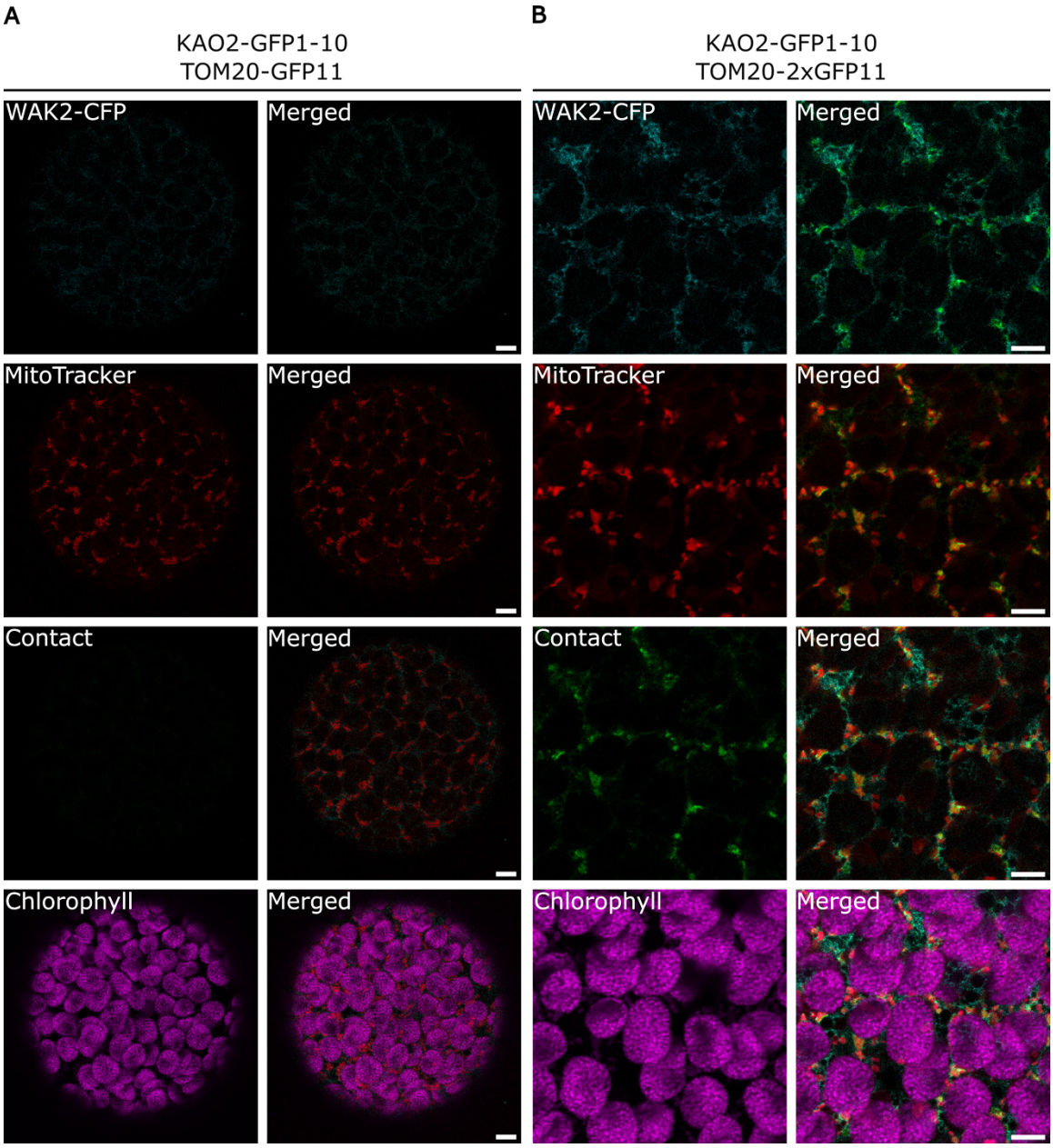

Figure 5: Visualization of ER-mitochondria MCSs in tobacco protoplasts. Gene cassettes containing ER and mitochondrial tethers for the split GFP assay were transiently expressed in tobacco leaves. The copy number of GFP11 affected the reassembly of the GFP, as the combination with the 2xGFP11 showed fluorescent signal in a punctuate pattern, whereas a fluorescent signal was not detectable with a single GFP11. The ER was visualized with the ER marker (cyan). Mitochondria were visualized with the MitoTracker Red CMXRos (red) and chloroplasts were visualized by their chlorophyll autofluorescence (magenta). The detected GFP signal (green) co-localized simultaneously to the ER and mitochondria. Scale bar = 5 µm.

VISUALIZATION OF ER-CHLOROPLAST CONTACT SITES

ER-chloroplast MCSs were visualized using the same approach. Gene cassettes encoding KAO2 and OEP7 fused to GFP1-10 or GFP11, respectively, were co-expressed to target the GFP fragment to the ER and chloroplast membranes. This combination did not yield a detectable fluorescent signal (Figure 6A). However, replacing the single GFP11 with a tandem GFP11 (2xGFP11) resulted in a detectable fluorescent signal, visible as larger

regions on the chloroplast surface (magenta). These signals co-localized with the ER marker (cyan), indicating regions of close proximity between the ER and the chloroplasts (Figure 6B).

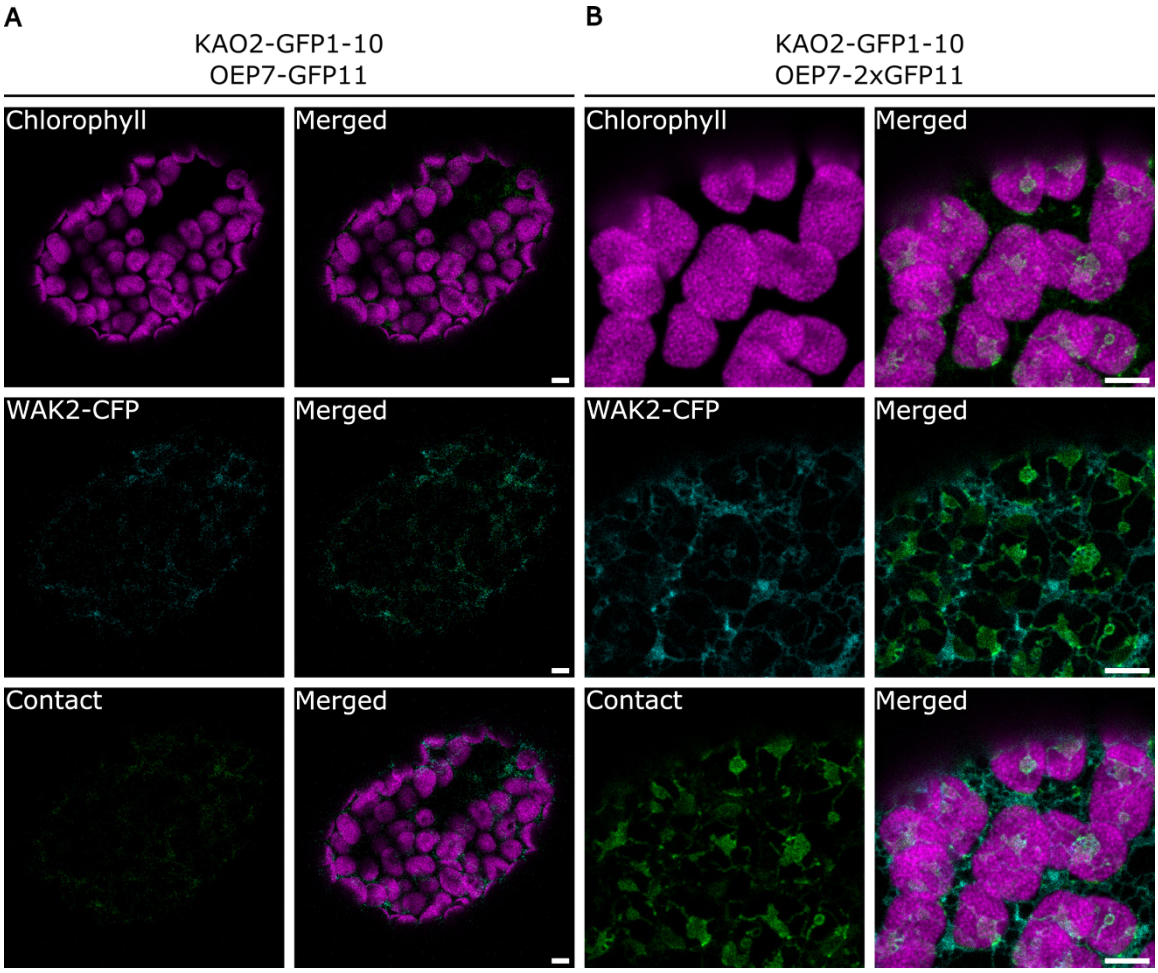

Figure 6: Visualization of ER-chloroplast MCS by the self-assembling GFP assay. Simultaneous transient expression of ER and chloroplast tethers enables visualization of ER-chloroplast MCS as regions between the ER and chloroplast interfaces. A fluorescent signal was only detected by using a tandem GFP11 (2xGFP11). The ER was visualized with the ER marker (cyan). Chloroplasts were visualized by their chlorophyll autofluorescence (magenta). The detected GFP signal (green) co-localized simultaneously to the ER and chloroplast. Scale bar = 5 µm.

MCSs between the ER and chloroplast or mitochondria were only visualized when using a tandem GFP11 (2xGFP11), suggesting that the single copy construct was insufficient presumably due to a larger intermembrane distance at these MCSs. This observation prompted further investigation of chloroplast-mitochondrion MCSs.

VISUALIZATION OF CHLOROPLAST-MITOCHONDRION CONTACT SITES

For visualization of chloroplast-mitochondrion MCSs, gene cassettes encoding TOM20 fused to GFP1-10 and OEP7 fused to either a single or tandem GFP11 were transiently co-expressed in tobacco leaves.

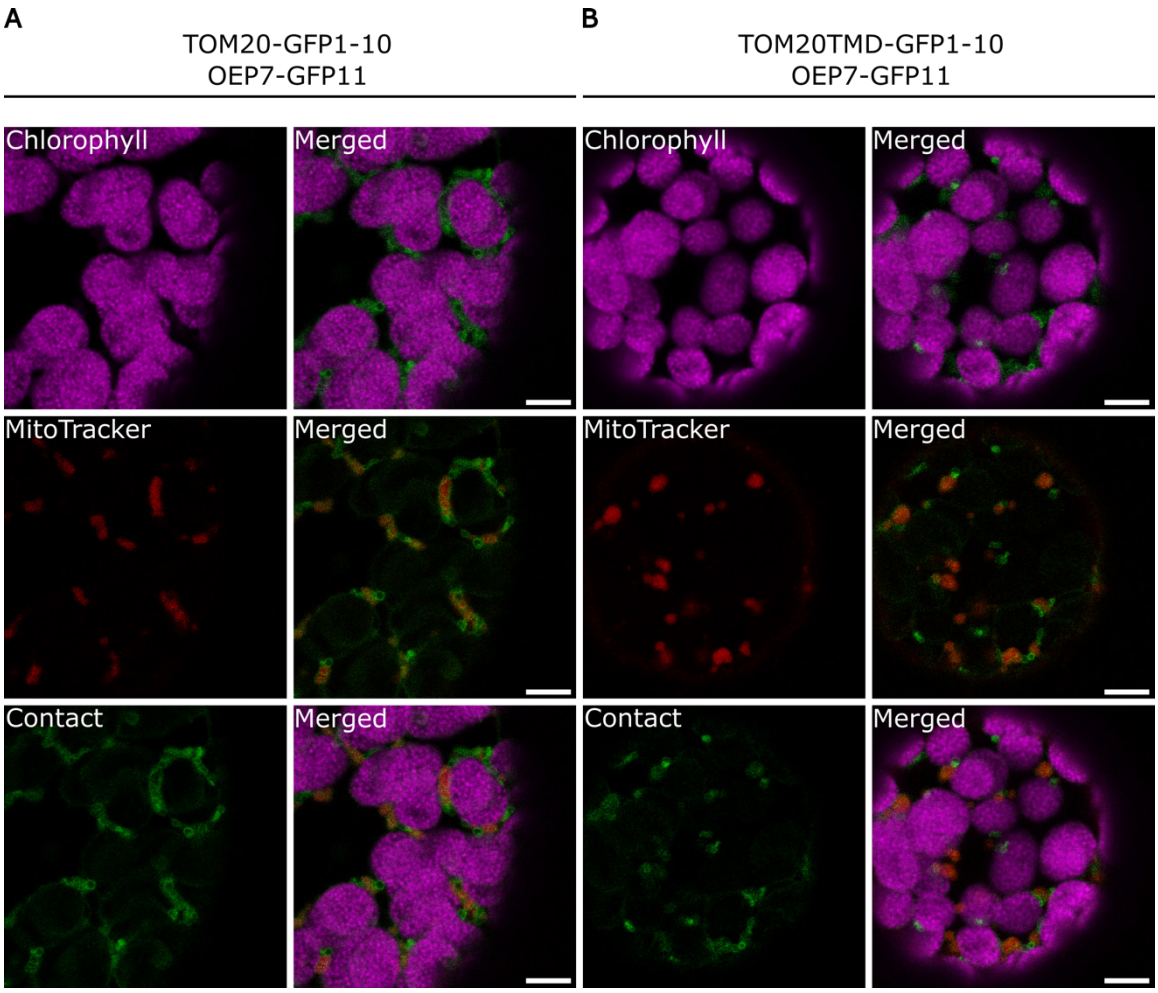

Figure 7: Visualization of mitochondrion-chloroplast MCS in plant cells. Transient expression of GFP fragments targeted to chloroplast and mitochondrion by OEP7 and TOM20 or TOM20TMD, respectively. Only the shortened assay resulted in a more distinct fluorescent pattern between the mitochondrial and plastidial membranes. Mitochondria were visualized with the MitoTracker Red CMXRos (red) and chloroplasts were visualized by their chlorophyll autofluorescence (magenta). The detected GFP signal (green) co-localized simultaneously to the chloroplasts and mitochondria. Scale bar = 5 µm.

In contrast to the ER-derived MCSs, a prominent fluorescent signal surrounding the mitochondria was observed with both the single and tandem GFP11 constructs (Figure 7A, Supplementary Figure 1). To further refine the localization, the cytosolic domain of TOM20 was deleted, retaining only the transmembrane domain (hereafter referred to as TOM20TMD). TOM20TMD was fused to GFP1-10 and simultaneously expressed with the OEP7-GFP11 in tobacco protoplasts. This adjustment led to the visualization of more distinct fluorescent signals at regions between the chloroplast and mitochondrion (Figure 7B).

The established BiFC assay with the self-assembling GFP fragments in the modular Golden Gate toolkit successfully visualized MCSs between the ER and mitochondria, ER and chloroplasts, and chloroplasts and mitochondria. Comparison of the visualized ER-derived (Figure 5, Figure 6) with the chloroplast-mitochondrion MCSs (Figure 7), suggests that ER MCSs exhibit a larger intermembrane distance.

DISCUSSION

MCSs in plants remain largely uncharacterized to date. Early evidence for MCSs in plants came from transmission electron microscopy (Stephenson and Hawes, 1986), and later, optical manipulation studies (Andersson et al., 2007b), gradually drawing attention to their presence and relevance in plant cells. In this study, we further broadened the knowledge about MCSs in plant cells by visualizing membrane proximity using a modular BiFC assay. BiFC utilizes self-assembling GFP fragments (Cabantous et al., 2005) to detect MCSs via a fluorescent signal. Similar approaches by using split FP version have successfully visualized MCSs in yeast and mammalian cells (Cieri et al., 2018; Kakimoto et al., 2018; Yang et al., 2018). Using the established BiFC system, we precisely visualized plant MCSs between the ER and mitochondria, the ER and chloroplasts, and chloroplasts and mitochondria in this study. Notably, the system allowed not only the visualization of MCSs but also differentiation between specific organelle MCSs. This was achieved by selectively implementing different spacer modules, such as one or two GFP11 copies or deleting the cytosolic domain of the membrane anchor.

This study revealed that ER-associated MCSs have wider intermembrane distances compared to those between mitochondria and chloroplasts. In mammalian cells, ER-associated MCSs fall into two categories: (1) narrow regions of 5 to 20 nm between the smooth ER and another organelle, and (2) wider regions at the rough ER, extending up to 80 nm (Wang et al., 2015; Giacomello and Pellegrini, 2016; Ilacqua et al., 2022; Cardoen et al., 2024). Several proteins were proposed to play a role in the formation of these specific MCSs. Those include for instance STIM1-involved MCSs between the ER and the PM with an intermembrane distance of around 15 nm (Orci et al., 2009), or Gp78 MCSs, which specifically occur between the rough ER and mitochondria with an intermembrane space of approximately 50 nm (Wang et al., 2015). Other studies further suggest that MCSs can be dynamically regulated, narrowing or widening in response to cellular processes (Csordás et al., 2006).

In this plant BiFC system, MCSs at the tubular smooth ER could only be visualized using a tandem GFP11, suggesting that the intermembrane distance exceeded the reach of a single copy GFP11, putting these in the range of narrow MCSs. In contrast, mitochondria-chloroplasts MCSs required not only a single GFP11 but also removal of the cytosolic domain of TOM20, further reducing the spacer length. Exact length of the reduction cannot be given, due to protein folding. However, modelling with AlphaFold3 (Abramson et al., 2024) suggests a length of 3 to 5 nm for the deleted cytosolic domain (Supplementary Figure 2). These results suggest that mitochondria and chloroplasts form tighter contacts than the narrow-region MCSs at the ER with these organelles. Although

intermembrane distances at mitochondrial MCS remain poorly characterized, previous work demonstrated direct interaction between mitochondria and chloroplasts via a complex of glycolytic enzymes and membrane proteins from both organelles (Zhang et al., 2020). Furthermore, the tight communication of chloroplasts, mitochondria and peroxisomes during photorespiration (Bauwe et al., 2010; Eisenhut et al., 2019) leads to the hypothesis that MCSs may coordinate energy regulation and metabolite allocation between certain organelles.

The specificity of the BiFC system is highlighted by its sensitivity to small differences in spacer lengths. Given that the GFP11 consists of 21 amino acids and the theoretical contour length of one amino acid ~0.36 nm (Ainavarapu et al., 2007), the additional GFP11 in the tandem GFP11 (2xGFP11) contributes approximately 8 nm of spacer length. This implies that the system can precisely identify and distinguish MCSs, differing by as little as approximately 8 nm in proximity. This showcases possible precise engineering of the BiFC assay to enable visualization of MCSs of specific intermembrane distances. Longer spacers might allow visualization of MCSs with an even wider intermembrane distance at the ER membrane, though this may increase the risk of false positive interactions and require careful spacer optimization. Previous studies have utilized different spacers to adapt to different MCS intermembrane distances in mammalian cells (Cieri et al., 2018). The modular design of this BiFC assay, implemented via the MoClo toolkit, allows for straightforward adjustment with the available spacer and peptide modules to tune the system's sensitivity (Supplementary Table 3, Supplementary Figure 3).

Future studies will involve characterizing the proteome of MCSs. This can be accomplished by utilizing the irreversibility of the GFP reassembly at MCSs. The stabilized MCSs might be isolated by anti-GFP beads to identify candidate proteins involved in MCSs by mass spectrometry. Taking advantage of the modularity of the system, other reporter systems for identifying MCSs and proteins within MCSs can be rapidly implemented, such as proximity labeling techniques using enzymes to label proximal proteins (Branon et al., 2018). These enzymes can be easily fused to various proteins involved in MCSs with the MoClo toolkit to characterize the MCS' proteome.

Moreover, the capacity to generate multi-gene constructs enables the modular design of a more complex BiFC approach. A tripartite self-assembling GFP system (Koraïchi et al., 2018) could be implemented into the MoClo toolkit to detect MCSs involving three organelles, generating a trimolecular fluorescence complementation assay. Multi-organelle complexes, such as those regulating organelle dynamics between the ER, mitochondria and peroxisomes in mammalian (Ilacqua et al., 2022) may also exist in plants and could be detected using this approach. Therefore, the GFP1-9, GFP10, and GFP11

can be implemented as modules into the MoClo toolkit and utilized in three different gene expression cassettes to target to three different organellar membranes. The communication between the chloroplasts, mitochondria and peroxisomes during photorespiration might harbor such tri-partite MCSs, which can be easily investigated by implementing the trimolecular fluorescence complementation assay to the MoClo toolkit in the future. The addition of further membrane anchors, as required for targeting the GFP fragment to the peroxisomes, can be easily achieved. Similarly, membrane anchors for other compartments such as the nucleus, the vacuole, or the plasma membrane can be implemented, and further MCSs between various membranes can be tested by using the modular cloning system. Additionally, the modularity of the system and ability to easily generate multi-gene constructs enables co-expression of BiFC constructs with candidate proteins fused to a different reporter (e.g., mCherry) to verify co-localization to visualized MCSs.

In conclusion, this modular BiFC approach expands upon previous work (Li et al., 2020), and significantly contributes to our understanding of MCSs in plant cells, in particular at the chloroplast interface. Its implementation into the MoClo toolkit (Engler et al., 2014) facilitates precise engineering for an easy and efficient visualization of distinct MCSs through a proximity-dependent self-assembling GFP, offering a versatile tool for characterizing novel membrane interactions.

REFERENCES

Abramson, J., Adler, J., Dunger, J., Evans, R., Green, T., Pritzel, A., Ronneberger, O., Willmore, L., Ballard, A.J., Bambrick, J., et al., (2024). Accurate structure prediction of biomolecular interactions with AlphaFold 3. Nature. 2024:**630**(8016):493–500. https://doi.org/10.1038/s41586-024-07487-w

Ainavarapu, S.R.K., Brujić, J., Huang, H.H., Wiita, A.P., Lu, H., Li, L., Walther, K.A., Carrion-Vazquez, M., Li, H., and Fernandez, J.M., (2007). Contour length and refolding rate of a small protein controlled by engineered disulfide bonds. Biophys J. 2007:**92**(1):225–233. https://doi.org/10.1529/biophysj.106.091561

Alford, S.C., Ding, Y., Simmen, T., and Campbell, R.E., (2012). Dimerization-dependent green and yellow fluorescent proteins. ACS Synth Biol. 2012:**1**(12):569–575. https://doi.org/10.1021/sb300050j

Andersson, M.X., Goksör, M., and Sandelius, A.S., (2007a). Membrane contact sites: Physical attachment between chloroplasts and endoplasmic reticulum revealed by optical manipulation. Plant Signal Behav. 2007:**2**(3):185–187. https://doi.org/10.4161/psb.2.3.3973

Andersson, M.X., Goksör, M., and Sandelius, A.S., (2007b). Optical manipulation reveals strong attracting forces at membrane contact sites between endoplasmic reticulum and chloroplasts. Journal of Biological Chemistry. 2007:**282**(2):1170–1174. https://doi.org/10.1074/jbc.M608124200

Barnard, E., McFerran, N. V., Trudgett, A., Nelson, J., and Timson, D.J., (2008). Development and implementation of split-GFP-based bimolecular fluorescence complementation (BiFC) assays in yeast. In Biochemical Society Transactions, pp. 479–482. https://doi.org/10.1042/BST0360479

Bauwe, H., Hagemann, M., and Fernie, A.R., (2010). Photorespiration: players, partners and origin. Trends Plant Sci. 2010:**15**(6):330–336. https://doi.org/10.1016/j.tplants.2010.03.006

Branon, T.C., Bosch, J.A., Sanchez, A.D., Udeshi, N.D., Svinkina, T., Carr, S.A., Feldman, J.L., Perrimon, N., and Ting, A.Y., (2018). Efficient proximity labeling in living cells and organisms with TurboID. Nat Biotechnol. 2018:**36**(9):880–898. https://doi.org/10.1038/nbt.4201

Cabantous, S., Terwilliger, T.C., and Waldo, G.S., (2005). Protein tagging and detection with engineered self-assembling fragments of green fluorescent protein. Nat Biotechnol. 2005:**23**(1):102–107. https://doi.org/10.1038/nbt1044

Cardoen, B., Vandevoorde, K.R., Gao, G., Ortiz-Silva, M., Alan, P., Liu, W., Tiliakou, E., Wayne Vogl, A., Hamarneh, G., and Nabi, I.R., (2024). Membrane contact site

detection (MCS-DETECT) reveals dual control of rough mitochondria–ER contacts. Journal of Cell Biology. 2024:**223**(1). https://doi.org/10.1083/jcb.202206109

Cieri, D., Vicario, M., Giacomello, M., Vallese, F., Filadi, R., Wagner, T., Pozzan, T., Pizzo, P., Scorrano, L., Brini, M., et al., (2018). SPLICS: A split green fluorescent protein-based contact site sensor for narrow and wide heterotypic organelle juxtaposition. Cell Death Differ. 2018:**25**(6):1131–1145. https://doi.org/10.1038/s41418-017-0033-z

Citovsky, V., Lee, L.Y., Vyas, S., Glick, E., Chen, M.H., Vainstein, A., Gafni, Y., Gelvin, S.B., and Tzfira, T., (2006). Subcellular Localization of Interacting Proteins by Bimolecular Fluorescence Complementation in Planta. J Mol Biol. 2006:**362**(5):1120–1131. https://doi.org/10.1016/j.jmb.2006.08.017

Csordás, G., Renken, C., Várnai, P., Walter, L., Weaver, D., Buttle, K.F., Balla, T., Mannella, C.A., and Hajnóczky, G., (2006). Structural and functional features and significance of the physical linkage between ER and mitochondria. Journal of Cell Biology. 2006:**174**(7):915–921. https://doi.org/10.1083/jcb.200604016

Demarco, I.A., Periasamy, A., Booker, C.F., and Day, R.N., (2006). Monitoring dynamic protein interactions with photoquenching FRET. Nat Methods. 2006:**3**(7):519–524. https://doi.org/10.1038/nmeth889

Denay, G., Schultz, P., Hänsch, S., Weidtkamp-Peters, S., and Simon, R., (2019). Over the rainbow: A practical guide for fluorescent protein selection in plant FRET experiments. Plant Direct. 2019:**3**(12):1–14. https://doi.org/10.1002/pld3.189

Ding, Y., Li, J., Enterina, J.R., Shen, Y., Zhang, I., Tewson, P.H., Mo, G.C.H., Zhang, J., Quinn, A.M., Hughes, T.E., et al., (2015). Ratiometric biosensors based on dimerization-dependent fluorescent protein exchange. Nat Methods. 2015:**12**(3):195–198. https://doi.org/10.1038/nmeth.3261

Eisenhut, M., Roell, M.S., and Weber, A.P.M., (2019). Mechanistic understanding of photorespiration paves the way to a new green revolution. New Phytologist. 2019:**223**(4):1762–1769. https://doi.org/10.1111/nph.15872

Engler, C., Youles, M., Gruetzner, R., Ehnert, T.M., Werner, S., Jones, J.D.G., Patron, N.J., and Marillonnet, S., (2014). A Golden Gate modular cloning toolbox for plants. ACS Synth Biol. 2014:**3**(11):839–843. https://doi.org/10.1021/sb4001504

Fan, J.Y., Cui, Z.Q., Wei, H.P., Zhang, Z.P., Zhou, Y.F., Wang, Y.P., and Zhang, X.E., (2008). Split mCherry as a new red bimolecular fluorescence complementation system for visualizing protein-protein interactions in living cells. Biochem Biophys Res Commun. 2008:**367**(1):47–53. https://doi.org/10.1016/j.bbrc.2007.12.101

Foglieni, C., Papin, S., Salvadè, A., Afroz, T., Pinton, S., Pedrioli, G., Ulrich, G., Polymenidou, M., and Paganetti, P., (2017). Split GFP technologies to structurally

characterize and quantify functional biomolecular interactions of FTD-related proteins. Sci Rep. 2017:**7**(1):1–15. https://doi.org/10.1038/s41598-017-14459-w

Gallie, D.R., Sleat, D.E., Watts, J.W., Tumer, P.C., Michael, T., and Wilson, A., (1987). The 5'-leader sequence of tobacco mosaic virus RNA enhances the expression of foreign gene transcripts in vitro and in vivo.

Giacomello, M., and Pellegrini, L., (2016). The coming of age of the mitochondria-ER contact: A matter of thickness. Cell Death Differ. 2016:**23**(9):1417–1427. https://doi.org/10.1038/cdd.2016.52

Grefen, C., Donald, N., Hashimoto, K., Kudla, J., Schumacher, K., and Blatt, M.R., (2010). A ubiquitin-10 promoter-based vector set for fluorescent protein tagging facilitates temporal stability and native protein distribution in transient and stable expression studies. Plant Journal. 2010:**64**(2):355–365. https://doi.org/10.1111/j.1365-313X.2010.04322.x

Gynheung, A.N., (1986). Development of Plant Promoter Expression Vectors and Their Use for Analysis of Differential Activity of Nopaline Synthase Promoter in Transformed Tobacco Cells'.

Helliwell, C.A., Sullivan, J.A., Mould, R.M., Gray, J.C., Peacock, W.J., and Dennis, E.S., (2001). A plastid envelope location of Arabidopsis ent-kaurene oxidase links the plastid and endoplasmic reticulum steps of the gibberellin biosynthesis pathway. The Plant Journal. 2001:**28**(2):201–208. https://doi.org/10.1046/j.1365-313X.2001.01150.x

Hertlein, V., Flores-Romero, H., Das, K.K., Fischer, S., Heunemann, M., Calleja-Felipe, M., Knafo, S., Hipp, K., Harter, K., Fitzgerald, J.C., et al., (2020). Merlin: A novel BRET-based proximity biosensor for studying mitochondria–ER contact sites. Life Sci Alliance. 2020:**3**(1):1–11. https://doi.org/10.26508/lsa.201900600

Hiatt, S.M., Shyu, Y.J., Duren, H.M., and Hu, C.D., (2008). Bimolecular fluorescence complementation (BiFC) analysis of protein interactions in Caenorhabditis elegans. Methods. 2008:**45**(3):185–191. https://doi.org/10.1016/j.ymeth.2008.06.003

Horstman, A., Tonaco, I.A.N., Boutilier, K., and Immink, R.G.H., (2014). A Cautionary note on the use of split-YFP/BiFC in plant protein-protein interaction studies. Int J Mol Sci. 2014:**15**(6):9628–9643. https://doi.org/10.3390/ijms15069628

Hu, C.-D., Chinenov, Y., and Kerppola, T.K., (2002). Visualization of Interactions among bZIP and Rel Family Proteins in Living Cells Using Bimolecular Fluorescence Complementation.

Ilacqua, N., Anastasia, I., Raimondi, A., Lemieux, P., De Aguiar Vallim, T.Q., Toth, K., Koonin, E. V., and Pellegrini, L., (2022). A three-organelle complex made by

wrappER contacts with peroxisomes and mitochondria responds to liver lipid flux changes. J Cell Sci. 2022:**135**(5). https://doi.org/10.1242/jcs.259091

Kakimoto, Y., Tashiro, S., Kojima, R., Morozumi, Y., Endo, T., and Tamura, Y., (2018). Visualizing multiple inter-organelle contact sites using the organelle-Targeted split-GFP system. Sci Rep. 2018:**8**(1):1–13. https://doi.org/10.1038/s41598-018-24466-0

Koraïchi, F., Gence, R., Bouchenot, C., Grosjean, S., Lajoie-Mazenc, I., Favre, G., and Cabantous, S., (2018). High-content tripartite split-GFP cell-based assays to screen for modulators of small GTPase activation. J Cell Sci. 2018:**131**(1). https://doi.org/10.1242/jcs.210419

Lee, Y.J., Kim, D.H., Kim, Y.-W., and Hwang, I., (2001). Identification of a Signal That Distinguishes between the Chloroplast Outer Envelope Membrane and the Endomembrane System in Vivo. Plant Cell. 2001:**13**(10):2175–2190. https://doi.org/10.1105/tpc.010232

Li, T., Xiao, Z., Li, H., Liu, C., Shen, W., and Gao, C., (2020). A Combinatorial Reporter Set to Visualize the Membrane Contact Sites Between Endoplasmic Reticulum and Other Organelles in Plant Cell. Front Plant Sci. 2020:**11**(August):1–15. https://doi.org/10.3389/fpls.2020.01280

Nelson, B.K., Cai, X., and Nebenführ, A., (2007). A multicolored set of in vivo organelle markers for co-localization studies in Arabidopsis and other plants. Plant Journal. 2007:**51**(6):1126–1136. https://doi.org/10.1111/j.1365-313X.2007.03212.x

Orci, L., Ravazzola, M., Le Coadic, M., Shen, W., Demaurex, N., and Cosson, P., (2009). STIM1-induced precortical and cortical subdomains of the endoplasmic reticulum. Proceedings of the National Academy of Sciences. 2009:**106**(46):19358–19362. https://doi.org/10.1073/pnas.0911280106

Pédelacq, J.D., Cabantous, S., Tran, T., Terwilliger, T.C., and Waldo, G.S., (2006). Engineering and characterization of a superfolder green fluorescent protein. Nat Biotechnol. 2006:**24**(1):79–88. https://doi.org/10.1038/nbt1172

Schindelin, J., Arganda-Carreras, I., Frise, E., Kaynig, V., Longair, M., Pietzsch, T., Preibisch, S., Rueden, C., Saalfeld, S., Schmid, B., et al., (2012). Fiji: An open-source platform for biological-image analysis. Nat Methods. 2012:**9**(7):676–682. https://doi.org/10.1038/nmeth.2019

Scorrano, L., De Matteis, M.A., Emr, S., Giordano, F., Hajnóczky, G., Kornmann, B., Lackner, L.L., Levine, T.P., Pellegrini, L., Reinisch, K., et al., (2019). Coming together to define membrane contact sites. Nat Commun. 2019:**10**(1):1–11. https://doi.org/10.1038/s41467-019-09253-3

Stephenson, J.L.M., and Hawes, C.R., (1986). Stereology and stereometry of endoplasmic reticulum during differentiation in the maize root cap. Protoplasma. 1986:**131**(1):32–46. https://doi.org/10.1007/BF01281685

Sung, M.-K., and Huh, W.-K., (2007). Bimolecular fluorescence complementation analysis system for in vivo detection of protein-protein interaction in Saccharomyces cerevisiae. Yeast. 2007:**24**(9):767–75. https://doi.org/10.1002/yea.1504

Tamura, R., Jiang, F., Xie, J., and Kamiyama, D., (2021). Multiplexed labeling of cellular proteins with split fluorescent protein tags. Commun Biol. 2021:**4**(1):1–8. https://doi.org/10.1038/s42003-021-01780-4

Voeltz, G.K., Sawyer, E.M., Hajnóczky, G., and Prinz, W.A., (2024). Making the connection: How membrane contact sites have changed our view of organelle biology. Cell. 2024:**187**(2):257–270. https://doi.org/10.1016/j.cell.2023.11.040

Wang, P.T.C., Garcin, P.O., Fu, M., Masoudi, M., St-Pierre, P., Panté, N., and Nabi, I.R., (2015). Distinct mechanisms controlling rough and smooth endoplasmic reticulum contacts with mitochondria. J Cell Sci. 2015:**128**(15):2759–2765. https://doi.org/10.1242/jcs.171132

Weber, E., Engler, C., Gruetzner, R., Werner, S., and Marillonnet, S., (2011). A modular cloning system for standardized assembly of multigene constructs. PLoS One. 2011:**6**(2). https://doi.org/10.1371/JOURNAL.PONE.0016765

Werhahn, W., Jänsch, L., and Braun, H.-P., (2003). Identification of novel subunits of the TOM complex from Arabidopsis thaliana. Plant Physiology and Biochemistry. 2003:**41**(5):407–416. https://doi.org/10.1016/S0981-9428(03)00047-0

Yang, Z., Zhao, X., Xu, J., Shang, W., and Tong, C., (2018). A novel fluorescent reporter detects plastic remodeling of mitochondria-ER contact sites. J Cell Sci. 2018:**131**(1). https://doi.org/10.1242/jcs.208686

Zhang, Y., Sampathkumar, A., Kerber, S.M.-L., Swart, C., Hille, C., Seerangan, K., Graf, A., Sweetlove, L., and Fernie, A.R., (2020). A moonlighting role for enzymes of glycolysis in the co-localization of mitochondria and chloroplasts. Nat Commun. 2020:**11**(1). https://doi.org/10.1038/s41467-020-18234-w

SUPPLEMENTARY DATA

Supplementary Table 1: Expression constructs used in this study. Expression constructs listed here were used for verifying the BiFC assay and testing for MCSs. Gene expression was either driven by the 35S promoter (35Ssp) or by the ubiquitin 10 promoter (UBQ10p).

Expression construct	Purpose
35Sp::GFP::TOM20	Verification of mitochondrial targeting
35Sp::OEP7::GFP	Verification of plastidial targeting
35Sp::KAO2::GFP	Verification of ER membrane targeting
35Sp::GFP1-10::TOM5	Negative controls
35Sp::OEP7::Linker37::GFP1-10	
35Sp::GFP11::TOM20	
35Sp::OEP7::GFP11	
35Sp::OEP7::GFP11 + UBQ10p::GFP1-10	
35Sp::GFP11::TOM5 + UBQ10p::GFP1-10::Linker16::TOM20	Positive control
35Sp::KAO2::GFP1-10 + UBQ10p::OEP7::2xGFP11	ER-chloroplast MCSs
35Sp::OEP7::GFP11 + UBQ10p::KAO2::GFP1-10	
35Sp::KAO2::GFP1-10 + UBQ10p::2xGFP11::TOM20	ER-mitochondria MCSs
35Sp::GFP11::TOM20 + UBQ10p::KAO2::GFP1-10	
35Sp::GFP1-10::TOM20 + UBQ10p::OEP7::2xGFP11	Chloroplasts-mitochondria MCSs
35Sp::GFP1-10::TOM20 + UBQ10p::OEP7::GFP11	
35Sp::GFP1-10::TOM20TMD + UBQ10p::OEP7::2xGFP11	

Supplementary Table 2: List of oligonucleotides used in this study. Oligonucleotides were used for cloning purposes of nucleotide sequences into level 0 backbones of the MoClo toolkit (Engler et al., 2014). Four bases at the end or beginning of the oligonucleotide name represents the fusion sites. If amplicons were, prior to level 0 cloning, inserted into the level -1 backbone, the oligonucleotide name used for these amplicons states this as "lvl-1". Due to the nature of the MoClo toolkit, oligonucleotides can be used interchangeable to amplify a gene of interest with the correct fusion sites for the destination level 0 backbone.

Name	Oligonucleotide sequence (5' → 3')
AGGT_TOM5.fwd	ttGAAGACaaAGGTATGGTGAACAACGTTGTCTC
AGGT_TOM5TMD.fwd	ttGAAGACaaAGGTAAATGGGCGGTGAACATG
TOM5_TTCG.rev	ttGAAGACaaAAGCTCAAACTCCCATGAGATCC
AGGT_TOM20.fwd	ttGAAGACaaAGGTATGGAGTTCTCTACCGCC
AGGT_TOM20TMD.fwd	ttGAAGACaaAGGTTTCACTTATGATGTATGCGGT
TOM20_TTCG.rev	ttGAAGACaaAAGCTTATCTGGCAGGAGGTGG
AATG_KAO2.1.fwd	ttGAAGACatAATGACGGAAACGGGTTTG
KAO2.1_TTTC.rev	ttGAAGACaaTTTCATCAATAACCTGAGAAAGATACAC
TTTC_KAO2.2.fwd	ttGAAGACaaGAAACCCTTCGAGTAATTACATTCTC
KAO2.2_GS_TTCG.rev	ttGAAGACaaCGAACCTCCAGATGGCATCGTTCTGGTGAT
KAO2.2_GS_AGGT.rev	ttGAAGACaaACCTGATGATCCTGGCATCGTTCTGGTGAT
AATG_OEP7.1.fwd	ttGAAGACatAATGGGAAAAACTTCGGGA
OEP7.1_GS_TTCG.rev	ttGAAGACaaCGAACCTCCAGACAAACCCTCTTTGGATGTG
OEP7.1TMD_GS_TTCG.rev	ttGAAGACaaCGAACCTCCAGAGTCTTTGGTTGGGTCAGAT
AATG_GFP11 M3.fwd	ttGAAGACaaaATGAGGGATCACATGGTCCTTC
GFP11 M3_AGGT.rev	ttGAAGACaaACCTGATGATCCCGTGATGCCAGCTGCT
AATG_GFP.fwd	ttGAAGACaaaATGTCTAAGGGCGAAGAG
GFP1-10 OPT_GS_AGGT.rev	ttGAAGACaaACCTGATGATCCCTTTTCATTTGGATCTTTTGATAAAA

Continued on the next page

Supplementary table 2 (continued)

Name	Oligonucleotide sequence (5' → 3')
CCAT_GFP11 M3.fwd	ttGAAGACaaCCATGAGGGATCACATGGTCCTTC
GFP11 M3_GS_AATG.rev	ttGAAGACaaCATTGAACCTCCAGACGTGATGCCAGCTGC
CCAT_GFP1-10 OPT.fwd	ttGAAGACaaCCATGTCTAAGGGCGAAGAG
GFP1-10 OPT_GS_AATG.rev	ttGAAGACaaCATTGAACCTCCAGACTTTTCATTTGGATCTTTTGATAAAA
TTCG_GFP.fwd	ttGAAGACaaTTCGATGTCTAAGGGCGAAGAG
GFP_GCTT.rev	ttGAAGACaaAAGCTCACGTGATGCCAGCTGCT
GFP1-10 OPT_GCTT.rev	ttGAAGACaaAAGCTCACTTTTCATTTGGATCTTTTGATAAAA
TTCG_GFP11 M3.fwd	ttGAAGACaaTTCGAGGGATCACATGGTCCTTC
OEP7.1TMD_lvl-1.fwd	ttggtctcaacataatgGGAAAAACTTCGGGAG
OEP7.1TMD_lvl-1.rev	ttggtctcaacaaCGAACCTCCAGAGTCT
GFP_lvl-1.fwd	ttggtctcaacatttcgATGTCTAAGGGCGAAG
GFP_lvl-1.rev	ttggtctcaacaaAAGCTCACGTGATGCCAG
GFP11 M3_lvl-1.fwd	ttGGTCTCaacataatgAGGGATCACATGGTCC
GFP11 M3_lvl-1.rev	ttggtctcaacaaACCTGATGATCCCGTGATGC
GFP_lvl-1.fwd	ttggtctcaacataatgTCTAAGGGCGAAGAGCT
GFP_lvl-1.rev	ttggtctcaacaaACCTGATGATCCCGTGATGC
AATG_Linker 5.fwd	ttgaagacaaaATGGGTTCTGGAGGCGGTGGTAGTGGTGGGGGAGGATCAGGAGGAGGTggaggtttgtcttcaa
Linker 5_AGGT.rev	ttgaagacaaacctccACCTCCTCCTGATCCTCCCCCACCACTACCACCGCCTCCAGAACCCATttgtcttcaa
AGGT_Linker 5.fwd	ttgaagacaaAGGTGGTTCTGGAGGCGGTGGTAGTGGTGGGGGAGGATCAGGAGGAGGTggTTCGttgtcttcaa
Linker 5_TTCG.rev	ttgaagacaaCGAAccACCTCCTCCTGATCCTCCCCCACCACTACCACCGCCTCCAGAACCACCTttgtcttcaa
AGGT_Linker37.fwd	ttGAAGACaaAGGTGGAAGTGGTAGTG

Continued on the next page

Supplementary table 2 (continued)

Linker37_TTCG.rev	ttGAAGACaaCGAAccAGATCCGG
Linker16(part1, pICH41258)_lvl-1.fwd	tttggtctcaacataATGGGTTCTGGAGGCGGTGG TAGTGGTGGGGGAGGATCAGGAGGAGGTG GTTttgtagagaccttt
Linker16(part1, pICH41258)_lvl-1.rev	aaaggtctctacaaAACCACCTCCTCCTGATCCT CCCCCACCACTACCACCGCCTCCAGAACC CATtatgttgagaccaaa
Linker16(part2)_lvl-1.fwd	tttggtctcaacatGGTTCTGGAGGCGGTGGTAGT GGTGGGGGAGGATCAGGAGGAGGTGGATtt gtagagaccttt
Linker16(part2)_lvl-1.rev	aaaggtctctacaaATCCACCTCCTCCTGATCCT CCCCCACCACTACCACCGCCTCCAGAACCa tgttgagaccaaa
Linker16(part3, pICH41258)_lvl-1.fwd	tttggtctcaacatGGATCTGGAGGCGGTGGTAGT GGTGGGGGAGGATCAGGAGGAGGTggAGG Tttgtagagaccttt
Linker16(part3, pICH41258)_lvl-1.rev	aaaggtctctacaaACCTccACCTCCTCCTGATCC TCCCCCACCACTACCACCGCCTCCAGATCC atgttgagaccaaa
Linker16(part1, pAGM1299)_lvl-1.fwd	tttggtctcaacatAGGTGGTTCTGGAGGCGGTG GTAGTGGTGGGGGAGGATCAGGAGGAGGT GGTTttgtagagaccttt
Linker16(part1, pAGM1299)_lvl-1.rev	aaaggtctctacaaAACCACCTCCTCCTGATCCT CCCCCACCACTACCACCGCCTCCAGAACC ACCTatgttgagaccaaa
Linker16(part3, pAGM1299)_lvl-1.fwd	tttggtctcaacatGGATCTGGAGGCGGTGGTAGT GGTGGGGGAGGATCAGGAGGAGGTggTTC Gttgtagagaccttt
Linker16(part3, pAGM1299)_lvl-1.rev	aaaggtctctacaaCGAAccACCTCCTCCTGATCC TCCCCCACCACTACCACCGCCTCCAGATCC atgttgagaccaaa
Linker48(part2)_lvl-1.fwd	tttggtctcaacatGGTTccGGAAGTGGTAGTGAG GCC
Linker48(part2)_lvl-1.rev	aaaggtctctacaaATCCAGATCCGGAACCCTTA GCA
GFP11 M3_TTCG.rev	ttGAAGACaaCGAACCTCCAGACGTGATGCC AGCTGCATT

Continued on the next page

Supplementary table 2 (continued)

AGGT_GFP11 M3.fwd	ttGAAGACaaAGGTAGGGATCACATGGTCCTTCA
AGGT_GFP.fwd	ttGAAGACaaAGGTATGTCTAAGGGCGAAGAG
sfGFP1-10 OPT_GS_TTCG.rev	ttGAAGACaaCGAACCTCCAGACTTTTCATTTGGATCTTTTGATAAAA
2xGFP11_GTTC.rev	ttGAAGACaaGAACCTCCAGACGTGATG
GTTC_2xGFP11.fwd	ttGAAGACaaGTTCGAGGGATCACATGG

Supplementary Table 3: Linker amino acid (AA) sequence implemented in the MoClo toolkit as modules.

Name	AA sequence	AA length
Linker 5	GSGGGGSGGGGSGGG	15
Linker 16	GSGGGGSGGGGSGGGGSGGGGSGGGGSGGGGS	45
Linker 37	GSGSEAAAKEAAAKEAAAKEAAAKALEAEAAAKEAAAKEAAAKEAAAKEAAAKEAAAKGSGSEAAAKEAAAKEAAAKEAAAKGSGSALEAEAAAKEAAAKEAAAKEAAAKGSGS	104
Linker 48	GSGGGGSGGGGSGGGGSGSGSEAAAKEAAAKEAAAKEAAAKALEAEAAAKEAAAKEAAAKEAAAKEAAAKEAAAKGSGSEAAAKEAAAKEAAAKEAAAKGSGSALEAEAAAKEAAAKEAAAKEAAAKGSGGGGSGGGGSGGG	136

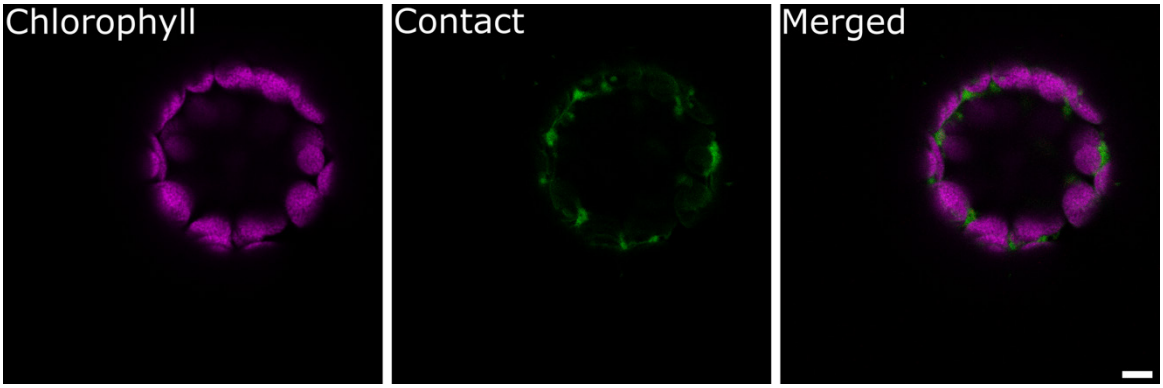

Supplementary Figure 1: Visualization of mitochondrion-chloroplast MCSs in plant cells. Transient expression of GFP fragments, the tandem 2xGFP11 and GFP1-10, targeted to chloroplast and mitochondrion by OEP7 and TOM2, respectively. Prominent GFP fluorescence was detected (green), surrounding the mitochondria. Chloroplasts were visualized by their chlorophyll autofluorescence (magenta). Scale bar = 5 µm

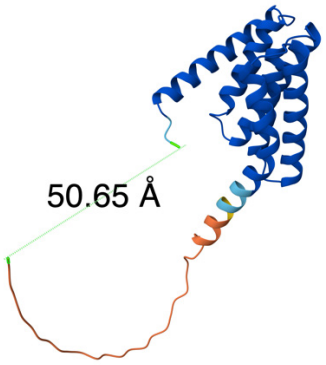

Supplementary Figure 2: Modelling of cytosolic domain of TOM20 (1-178 amino acid) by AlphaFold3 (Abramson et al., 2024). This structure revealed a distance of 5 nm between the two termini of the cytosolic domain. Due to folding and dynamics, the length might not be highly accurate.

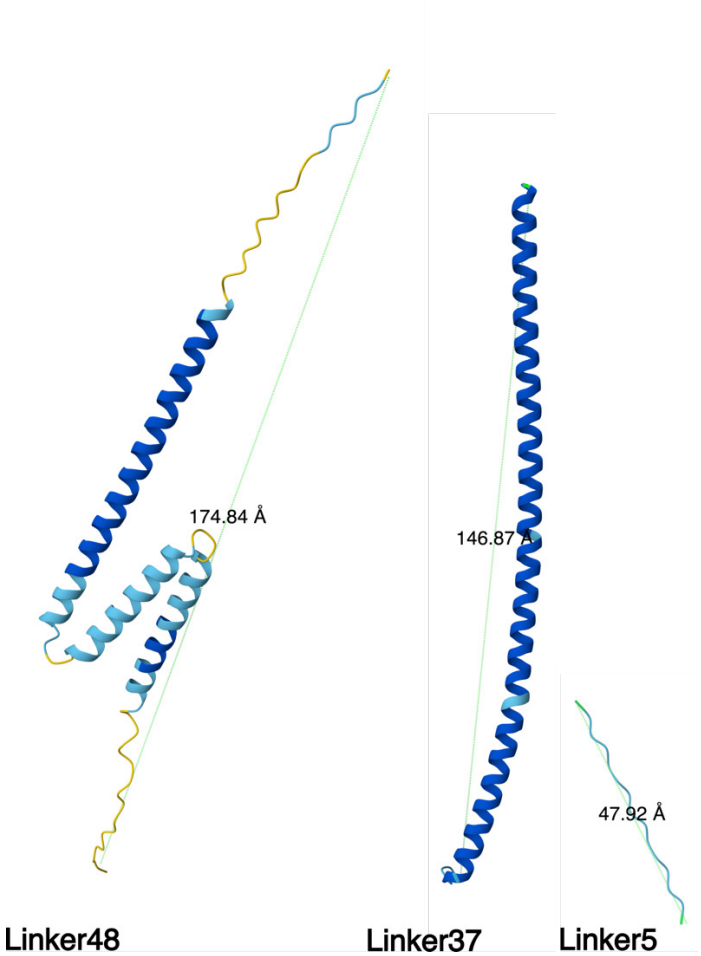

Supplementary Figure 3: Modelling of linker modules with AlphaFold3 (Abramson et al., 2024). Linker 48 showed a theoretical length of approx. 17 nm due to helical structure, but might be longer *in vivo* due the more flexible parts. Linker 37 showed a theoretical length determined by AlphaFold3 of approx. 15 nm. The flexible linker 5 showed a length of approx. 5 nm. AlphaFold3 could only model Linker 16 with low confidence. It is a very flexible linker and hence was not included here.

Chapter II:

The chloroplast outer envelope protein, TriGalactosylDiacylglycerol 4, has a dual function, regulating cellular lipid trafficking with the endoplasmic reticulum

Vanessa Valencia[1], Elisa S. Großmann[1], Anja Stefanski[2], Marten Exterkarte[3], Sergiy Gan[3], Peter Jahns[4], Kai Stühler[2], Franziska Kuhnert[1]†, Andreas P.M. Weber[1]

[1] Institute of Plant Biochemistry, SFB1208, Heinrich Heine University, Universitätsstrasse 1, 40225 Düsseldorf, Germany

[2] Molecular Proteomics Laboratory, Biologisch-Medizinisches Forschungszentrum für Synthetische Lebenswissenschaften, Heinrich Heine University, Universitätsstrasse 1, 40225 Düsseldorf, Germany

[3] Institute of Membrane Biogenesis and Lipidomics, Heinrich Heine University, Universitätsstrasse 1, 40225 Düsseldorf, Germany

[4] Institute of Plant Biochemistry, Heinrich Heine University, Universitätsstrasse 1, 40225 Düsseldorf, Germany

† Plant Energy Biology, University of Western Australia; Crawley, 6009, Australia

Author contribution: VV designed the experiments, performed cloning, plant transformations, confocal microscopy, protein purification, pigment extraction, qRT-PCR, lipid extraction, and analyzed data; ESG assisted with the cloning; AS and KS performed proteomic analyses; ME and SG performed lipid analyses; PJ performed pigment analyses with HPLC; APMW and FK designed the research and supervised experiments

ABSTRACT

Galactolipid biosynthesis is unique to phototrophic organisms and essential for biogenesis and function of chloroplast membranes, especially, for the inner envelope and thylakoid membranes. The galactolipids are produced via two biosynthesis pathways: the prokaryotic and eukaryotic pathway. The latter involves lipid trafficking across multiple membranes and is thought to rely on non-vesicular transport. TriGalactosylDiacylglycerol 4 (TGD4), a chloroplast outer envelope protein, has been proposed as a key player in this process, potentially linking the endoplasmic reticulum (ER) and chloroplasts at membrane contact sites. Here, we provide new insights into the role of TGD4 at ER-chloroplast membrane contact sites and its involvement in lipid trafficking. A CRISPR/Cas9 generated TGD4 mutant, defective in phosphatidic acid binding, revealed a possible additional function of the TGD4 protein. Using proximity labeling and localization studies, we identified PAH1, an ER-localized phosphatase, as potential interaction partner of TGD4. This interaction suggests a regulatory role as additional function by modulating phosphatidic acid import by TGD4, beyond its function as a transporter.

INTRODUCTION

Photosynthetically active membranes are predominantly composed of galactolipids, which constitute up to 75% of their lipid content (Block et al., 1983). This contrasts with most other eukaryotic membranes, where phospholipids predominate (Moreau et al., 1974).

In plants, biosynthesis of galactolipids occurs via two distinct pathways: the prokaryotic pathway, located entirely within the chloroplasts, and the eukaryotic pathway, which additionally involves the endoplasmic reticulum (ER). In the prokaryotic pathway, 16C- and 18C-chained fatty acids are incorporated into the *sn-1* and *sn-2* position of a glycerol-3-phosphate backbone to form phosphatidic acid (PA). PA is subsequently dephosphorylated by PA phosphatase (PAP) to generate diacylglycerol (DAG) (Ongun and Mudd, 1968; Douce, 1974). Identified chloroplast-localized PAPs include lipid phosphate phosphatase (LPP) γ, LPPε1, and LPPε2 (Nakamura et al., 2007; Nguyen and Nakamura, 2023; Cook et al., 2024). Monogalactosyl diacylglycerol synthase 1 (MGD1), localized to the inner envelope, transfers a galactosyl residue from UDP-galactose to DAG to form monogalactosyl diacylglycerol (MGDG). This is further converted into digalactosyl diacylglycerol (DGDG) at the outer envelope by digalactosyl diacylglycerol 1 (DGD1), which adds a second galactosyl residue (Ongun and Mudd, 1968; Douce, 1974; van Besouw and Wintermans, 1978). MGDG and DGDG undergo several desaturation steps catalyzed by fatty acid desaturase (FAD-) 4, FAD5, and FAD6 to form mono-, di-, or trienoic conjugated fatty-acyl chains, respectively.

In the eukaryotic pathway, fatty acids in form of acyl-acyl carrier proteins (acyl-ACPs) are converted to acyl-CoA at the outer envelope, and subsequently transported to the ER. Similar to the prokaryotic pathway, the acyl groups of the acyl-CoA are transferred to glycerol-3-phosphate to form PA. PA is then dephosphorylated by ER-localized PAPs to generate DAG. Possible candidates for PAPs of the ER include the prokaryotic LPPs (LPP1 – 4) and phosphate phosphatase (PAH) 1 and PAH2 (Nakamura et al., 2007, 2009; Paradis et al., 2011; Nguyen and Nakamura, 2023). DAG is subsequently used for synthesis of phosphatidylcholine (PC), a major membrane lipid in eukaryotic organisms, which can be desaturated by FAD2, or FAD3 at the ER. Desaturated acyl-chains can be re-incorporated into the acyl-CoA pool, thereby re-entering PA, DAG, or PC synthesis (van Besouw and Wintermans, 1978; Hurlock et al., 2014; LaBrant et al., 2018). The eukaryotic-derived lipid precursor is used to form MGDG and DGDG in the chloroplasts, similarly to the prokaryotic-derived precursor (van Besouw and Wintermans, 1978; Hurlock et al., 2014). While the precise lipid species exported from the ER to the chloroplast remains unclear, PC, PA, and DAG have been proposed as potential candidates (Frentzen et al., 1983; Wang et al., 2013; Cook et al., 2024). MGDG and DGDG deriving from either the

prokaryotic or the eukaryotic pathway can be distinguished. In the eukaryotic pathway, a 18C acyl-chain is present at the *sn-2* position, due to the specificity of the ER-localized acyltransferase. In contrast, the prokaryotic pathway results in a 16C acyl-chain at this position (Frentzen et al., 1983). Plants that contain both types of lipid species, and therefore synthesize galactolipids via both pathways, are referred to as 16:3 plants. Examples include *Arabidopsis thaliana* (Arabidopsis), tobacco, and spinach. Whereas, monocots and legumes such as *Ricinus communis* or *Zea mays* are classified as 18:3 plants, as they can only synthesize galactolipids with 18C acyl-chain at the *sn-2* position, relying exclusively on the eukaryotic pathway. This restriction can be attributed to the absence of plastidial PAP activity (Frentzen et al., 1983; Mongrand et al., 1998).

Lipid transport within the cell is limited, as lipids are unable to move freely between two membranes across the aqueous cytosol. Transport of lipid precursors from the ER to chloroplasts is thought to occur via mechanisms such as vesicular trafficking, hemi-fusions or membrane contact sites (MCSs) (LaBrant et al., 2018). MCSs are known mediate the transport of lipids, metabolites, and other molecules across different membranes in multiple organisms (Michel and Kornmann, 2012; Chang et al., 2013; Grossmann et al., 2019). Thus, it has been hypothesized that lipid trafficking for galactolipid biosynthesis is facilitated by such MCSs. These MCSs are formed by protein-protein or protein-lipid interactions between adjacent membranes (Eisenberg-Bord et al., 2016).

Advancing our understanding of the molecular mechanisms of lipid trafficking between the ER and chloroplast led to the identification of the TriGalactosylDiacylglycerol (TGD) proteins. Xu and colleagues discovered mutants at different loci that are defective in the eukaryotic pathway of galactolipid biosynthesis (Xu et al., 2003). These mutants exhibit reduced levels of ER-derived galactolipids, while plastid-derived galactolipids were elevated. In addition, they accumulate oligogalactolipids due to the activity of galactosyltransferases such as Sensitive to Freezing 2 (SFR2), and show increased levels of PA and triacylglycerol (TAG) (Xu et al., 2003, 2005; Roston et al., 2014). The accumulation of oligogalactolipids, such as trigalactosyl diacylglycerol (TGDG), in these mutants prompted the naming of the involved genes as *TGD.*

Arabidopsis contains five genes encoding for TGD proteins. TGD1, TGD2, and TGD3 localize to the inner chloroplast envelope. TGD1 is a half pore protein with six transmembrane domains embedded in the inner envelope (Xu et al., 2003). TGD2 contains a transmembrane domain and a PA binding domain (Lu and Benning, 2009). TGD3 exhibits ATPase activity and is located on the stromal side of the inner envelope (Lu et al., 2007). Together they form a multipartite ABC transporter with permease (TGD1), substrate binding (TGD2), and ATPase (TGD3) activity (Roston et al., 2012). The TGD1/2/3 complex, with a size of approximately 500 kDa, most likely consists of a TGD1 homodimer and 8 to

12 TGD2 subunits embedded in the inner envelope, along with a TGD3 homodimer located on the stromal side. This architecture resembles canonical ATP-binding cassette (ABC) transporters, but includes multiple substrate-binding domains that may exhibit cooperative binding activity, similar to those of the OpuA ABC transporter from *Lactococcus lactis* (Biemans-Oldehinkel, 2003; Roston et al., 2012). In contrast to the inner-envelope-localized components, TGD4 and TGD5 are situated at the outer envelope and the intermembrane space, respectively. *TGD4* encodes a β-barrel protein localized in the outer envelope of the chloroplast, where it forms a homodimer via a C-terminal region. Its PA-binding domains face the cytosol, enabling for interaction and binding to ER-derived PA and suggesting a role in mediating lipid trafficking from the ER (Xu et al., 2008; Wang et al., 2012, 2013). Interestingly, PA binding capacity of TGD4 orthologs from 18:3 plants is higher than that of Arabidopsis (a 16:3 plant), highlighting the importance of TGD4 for galactolipid biosynthesis in the eukaryotic pathway (Wang et al., 2013). Knockout mutants, such as *tgd4-2* and *tgd4-3,* show reduced levels of ER-derived galactolipids, further underscoring TGD4's role in this pathway, while also suggesting the existence of additional TGD4-independent mechanisms for lipid trafficking within the eukaryotic pathway (Xu et al., 2008; Nakamura et al., 2009). TGD5 facilitates the lipid trafficking across the aqueous space between the inner and outer envelopes. Although not identified as part of the TGD1/2/3 complex (Roston et al., 2012), TGD5 may transiently bridge the two envelope membranes resembling MCS (Fan et al., 2015).

Although TGD4 has been extensively characterized in previous studies, many questions regarding the transport mechanism of the TGD4-dependent pathway remains to be unresolved to date. The aim of this study was to further elucidate the molecular mechanisms underlying the eukaryotic galactolipid biosynthesis pathway. Here, we show that TGD4 is present at a MCS between the ER and chloroplasts using BiFC. Previous work proposed PA as the imported lipid class. Thus, functional studies were performed using a CRISPR/Cas9-generated Arabidopsis line, *tgd4-4,* which specifically lacks the PA-binding domain of the TGD4 protein. These plants exhibited reduced chlorophyll content, altered levels of light harvesting complexes, and different alterations in galactolipid content compared to the published T-DNA insertion knockout line *tgd4-2*, suggesting an additional role for TGD4. The identification of a new interaction partner via proximity labeling provides novel insights into lipid trafficking between the ER and chloroplasts and highlights the crucial role and possibly dual function of TGD4 in cellular lipid homeostasis.

MATERIALS & METHODS

PLASMID CONSTRUCTION

The coding sequence of *TGD4* (At3g06960) was amplified from Arabidopsis Col-0 cDNA. Intrinsic cutting sites for *Bsa*I and *Bpi*I were removed by Golden Gate cloning. The coding sequence of *PAH1* (At3g09560) was synthesized as gBlock by ThermoFisher Scientific. All constructs were generated using the Golden Gate MoClo system (Engler et al., 2014). Visualization of TGD4 to MCSs was achieved using the self-assembling split green fluorescent protein (GFP) fragments from *Aequorea victoria* (Cabantous et al., 2005) (Chapter1), with one fragment targeted to each membrane and mCherry fused to TGD4. Expression constructs for the co-localization to MCSs were assembled as following: expression cassettes of (1) chloroplast membrane anchor (outer envelope membrane protein 7 from *Arabidopsis thaliana*) fused to a split GFP fragment under the control of the 35S promoter (Gallie et al., 1987), (2) ER membrane anchor (ent-kaurenoic acid oxidase 2 from *Arabidopsis thaliana*) fused to the corresponding split GFP fragment under the control of UBQ10 promoter (Grefen et al., 2010), (3) kanamycin resistance cassette, (4) mCherry from *Discosoma sp.* fused to TGD4 under the control of the MAS promoter (Langridge et al., 1989). Expression constructs for the co-localization study with TGD4 and PAH1 contained a plant kanamycin resistance cassette with the gene expression cassette encoding mVenus (from *Aequorea victoria)* -TGD4 and PAH1-mCherry, separated by the self-cleaving peptide P2A (Lee et al., 2020), under the control of the 35S promoter (Gallie et al., 1987).

TurboID was amplified from the Addgene plasmid #107171 (Branon et al., 2018) compatible for implementation into Level 0 modules by Golden Gate cloning. TurboID was fused to either TGD4 alone or TGD4 and GFP, and constitutively expressed under the control of 35S promoter (Gallie et al., 1987).

Tgd4 mutant plants were generated using CRISPR/Cas9 (Jinek et al., 2012). Four guideRNAs targeting the coding sequence of *TGD4* were chosen using the CRISPR-P webtool (Lei et al., 2014). The final construct contained the following expression cassettes: (1) phosphinothricin resistance, (2) Cas9 under the control of the egg-cell specific EC1.2-promoter (Wang et al., 2015), (3) the four guides under control of the U6-26 promoter in one transcriptional unit using the PTG (Xie et al., 2015), and (4) a GFP under the control of the seed specific At2S3-promoter (Aliaga-Franco et al., 2019). Generated constructs and all oligonucleotides are listed in the Supplementary Table 1 and Supplementary Table 2.

Plant material and growth conditions

Arabidopsis thaliana (Arabidopsis) Col-0 and *Nicotiana benthamiana* (tobacco) plants were used in this study. Tobacco was grown at 22 °C with 10h light/14h dark. Arabidopsis seeds were sterilized by washing twice with 70% ethanol supplemented with 0.1% Triton-X100, and additional two times with 100% ethanol. Sterilized Arabidopsis seeds were germinated on 0.5-strength Murashige and Skoog medium supplemented with 0.8% (w/v) agar. After germination plants were transferred to soil and further grown at ambient CO_2 conditions and 12h light/12h dark cycles with 22 °C/18 °C temperature cycle.

Stable Transformation of *Arabidopsis thaliana*

Agrobacterium tumefaciens GV3101 were transformed with the expression constructs or the CRISPR constructs. Arabidopsis Col-0 plants were transformed via floral dipping after Clough and Bent, (1998). Positive transformants were selected on 0.5-strength Murashige and Skoog medium supplemented with 0.8% (w/v) agar and 50 µg/mL kanamycin or 7.5 µg/mL glufosinate ammonium.

Transient expression in *Nicotiana benthamiana*

Agrobacterium tumefaciens GV3101 strains containing the expression constructs were used to infiltrate leaves from 4- to 5-week-old tobacco plants. The *Agrobacterium tumefaciens* GV3101 strains from a 5 mL overnight culture were resuspended in infiltration buffer (10 mM MES-KOH pH 5.7, 10 mM $MgCl_2$) at an OD_{600} of 0.5. Expression was conducted for 48 hours.

Protoplast isolation

Tobacco protoplasts were isolated two days post infiltration. Leaves were cut into small pieces and vacuum-infiltrated with digestions solution (0.4 M Mannitol, 20 mM MES-KOH pH 5.7, 20 mM KCl, 10 mM $CaCl_2$). The suspension was incubated for 2 h at 30 °C. Protoplasts were collected, sedimented and washed with MMg-0.7 solution (0.7 M mannitol, 15 mM MgCl2, 4 mM MES-KOH pH 5.7; after Lin et al., (2018)).

Confocal microscopy and FRET

Microscopy images were obtained using the SP8 confocal microscope (Leica) with the following excitation/emission wavelengths: GFP fluorescence (488 nm/498–550 nm), MitoTracker (561nm/582 –615 nm), mCherry (587 nm/595–630 nm) and ER-CFP marker

(458 nm/465-500 nm). Chlorophyll fluorescence (autofluorescence) was observed at 640 to 710 nm. Crosstalk was minimized by using sequential scanning mode.

Förster resonance energy transfer – acceptor photo bleaching (FRET-APB) analysis were performed at the Fluoview 3000 (Olympus). Acceptor fluorophore (mCherry) was photo-bleached at the wavelength of 561 nm and subsequent changes in intensity of the donor fluorophore (mVenus) was measured. Following excitation/emission wavelengths were used: mVenus (488 nm/500 – 541 nm, mCherry (561 nm/570 – 630 nm). Efficiency [%] was calculated using measured intensities of mVenus before [I_{pre}] and after [I_{post}] photo-bleaching with the following formula: $((I_{post} - I_{pre})/I_{post}) * 100$. Images were analyzed using Fiji (Schindelin et al., 2012) and InkScape (version 1.4.1).

Quantitative real-time PCR

Total RNA from 5-weeks old plants was extracted using the RNeasy Plant Mini Kit (Qiagen). 1 µg RNA was treated with RNase-free DNase (Promega) and subsequently reverse-transcribed into cDNA using the LunaScript™ RT Super Mix (New England Biolabs). The quantitative real-time PCR was performed using the Luna® Universal qPCR Master Mix (New England Biolabs) and the StepOnePlus™ Real-Time PCR System (Applied Biosystems). Oligonucleotides for the *TGD4* gene, and its T-DNA insertion as well as CRISPR/Cas9 mutation, *PAH1*, *SFR2*, *FAD6*, and *FAD7* genes, and the reference gene *Protein Phosphatase 2A Subunit A3 (PP2A,* At1g13320; Czechowski et al., (2005)) are listed in Supplementary Table 2.

Total protein extraction

Total protein extracts for SDS-PAGE and western blots were prepared as previously described (Tsugama et al., 2011). Briefly, 50 mg ground plant material was resuspended in 150 µL SDS loading buffer (0.1 M EDTA; 0.12 M Tris-HCl, pH 6.8; 4% (w/v) SDS; 10% (v/v) β-mercaptoethanol; 5%(v/v) glycerol; 0.005% (w/v) bromophenol blue) and incubated for 10 min at 95 °C. After centrifugation at 16,000 x g for 1 min, the proteins in the supernatant were separated by SDS-PAGE.

Proximity labeling

Expression constructs containing the coding sequence of *TGD4* fused to the biotin ligase *TurboID* (Branon et al., 2018) were generated using Golden Gate MoClo (Engler et al., 2014). *Agrobacterium tumefaciens* GV3101 were transformed with the expression

constructs to infiltrate tobacco leaves. Infiltrated leaves were treated with 200 µM biotin 48 h after infiltration. Plant material was harvested 6 h post treatment in liquid nitrogen.

PROTEIN PURIFICATION

Biotinylated proteins were purified after Shi et al., (2023) and Zhang et al., (2019). Briefly, the harvested plant material was grinded in liquid nitrogen with mortar and pestle. Total protein was extracted from 5 g ground plant material with 10 mL of RIPA buffer (25 mM Tris-HCl pH 7.6; 150 mM NaCl; 1.0% NP-40; 1.0% deoxycholate; 0.1% SDS) supplemented with cOmplete protease inhibitor cocktail (Roche). The suspension was vortexed and cooled for 15 min, centrifuged for 30 min at 4,300 x g, and the supernatant was collected. Free biotin was removed using PD10 desalting columns according to the manufacturer's instructions. The flow-through, containing the biotinylated proteins, was incubated with magnetic streptavidin-beads for 1 h at 4 °C. Afterwards, the beads were captured using a magnetic stand and washed with NP40-free RIPA buffer. Washed beads were either stored in SDS loading buffer or NP40-free RIPA buffer and used for SDS-PAGE or proteomics, respectively.

SDS-PAGE & IMMUNOBLOT

Proteins were resolved on a 10% mini-gel (Bio-Rad) for 30 min at 180 V. Subsequently, the proteins were transferred onto Nitrocellulose membrane via semi-dry blotting. Membranes were blocked with 5% (w/v) non-fat milk powder prepared in 1 x tris-buffered saline (TBS) supplemented with 1% (v/v) Tween-20 (TBS-T) buffer for 1 h. The membranes were washed two times with 1 x TBS, and probed with the streptavidin-antibody (Thermo Fisher Scientific; 1:1,000 dilution) for 1 h at room temperature or overnight at 4 °C. Following antibody incubation, the membranes were washed three times with TBS-T and developed using Immobilon Western Chemiluminescent HRP Substrates (Millipore). For primary antibodies, anti-RbcL (1:7,500), anti-Lhcb1 (1:2,000), anti-PsaG (1:1,000), and anti-PsbP (1:5,000) antibodies (Agrisera) were used. The anti-rabbit horse radish peroxidase (Millipore; 1:2,000) were used as secondary antibody. Both antibodies were each incubated 1 h at room temperature or overnight at 4 °C, with two washing steps of each 10 min with TBS in-between the antibody incubation steps.

PIGMENT EXTRACTION & HPLC

Plant material from 5-weeks old plants was harvested in liquid nitrogen. Pigments were extracted from 20 mg ground plant material using 1 mL 100% acetone. The suspension

was centrifuged for 5 min at 4 °C, supernatant collected and filtered through a membrane filter (pore size 0.2 µm). The filtrate was directly used for pigment analysis via high-performance liquid chromatography (HPLC) (Farber et al., 1997).

PROTEOMICS

Protein samples were loaded on a SDS polyacrylamide gel, concentrated in the stacking gel, silver stained according to MS-compatible protocol, reduced, alkylated and digested with trypsin. Peptides were extracted from the gel with 0.1% trifluoroacetic acid and subjected to liquid chromatography. For the LC-MS acquisition an Orbitrap Fusion Lumos Tribrid Mass Spectrometer (Thermo Fisher Scientific) coupled to an Ultimate 3000 Rapid Separation liquid chromatography system (Thermo Fisher Scientific, Idstein, Germany) equipped with an Aurora Ultimate C18 column (75 µm inner diameter, 25 cm length, 1.7 µm particle size from Ion Opticks) as separation column and an Acclaim PepMap 100 C18 column (75 µm inner diameter, 2 cm length, 3 µm particle size from Thermo Fisher Scientific) as trap column. A LC-gradient of 180 min was applied. Survey scans were carried out over a mass range from 375-1,500 m/z at a resolution of 120,000. The target value for the automatic gain control was 400,000 and the maximum fill time 60 ms. Within a cycle time of 2 s the most intense peptide ions (excluding singly charged ions) were selected for fragmentation. Peptide fragments were analyzed in the ion trap using automatic injection time mode and an automatic gain control target value of 10,000 operating in rapid mode. Already fragmented ions were excluded for fragmentation for 60 seconds. Data analysis was performed with Proteome Discoverer (version 2.4.1.15, Thermo Fisher Scientific). All RAW files were searched against the *Arabidopsis thaliana* Swissprot database (Download: 08.07.2024, 39,279 entries) and the Maxquant Contaminant database (Download: 20.02.2021), applying a precursor mass tolerance of 10 ppm and a mass tolerance of 0.6 Da for fragment spectra. Methionine oxidation, N-terminal acetylation, N-terminal methionine loss and N-terminal methionine loss combined with acetylation were considered as variable modification, carbamidomethylation as static modification as well as tryptic cleavage specificity with a maximum of two missed cleavage sites. Label-free quantification was performed using standard parameters within the predefined workflow. Post processing, proteins were filtered to 1% FDR and a minimum of 2 identified peptides per protein.

LIPID EXTRACTION

Rosettes from 5-weeks old Arabidopsis plants grown in 12h light/12h dark were harvested in liquid nitrogen. Leaves were ground to fine powder and lipids were extracted from 50 mg plant material via phase-separation using an adapted methyl-tert-butyl ether (MTBE)-based method (Matyash et al., 2008). 1 mL of MTBE:MeOH (3:1) spiked with 10 µg of the internal standard n-Dodecyl β-maltoside was added to the samples and sonicated for 15 min. Insoluble material was sedimented via centrifugation (2500 x g, 10 min). 500 µL of supernatant was transferred to a new glass tube, mixed with 500 µl MTBE:MeOH (3:1), 500 µL MTBE, and 1 mL MQ:MEOH (3:1), and vortexed. After centrifugation (2500 x g, 10 min, RT), 800 µL of the upper phase was transferred to a new glass tube, dried with a nitrogen stream, and resuspended in 250 µL of MeOH.

LC-MS ANALYSIS OF LIPIDS

Samples were analyzed using an Agilent Technologies 1290 Infinity high-performance liquid chromatography (HPLC) system, coupled to a heated electrospray ionization–mass spectrometer (Thermo Q Exactive Plus; Thermo Fisher Scientific). 5 µL was injected into an ACQUITY™ UPLC CSH C18 1.7 µm Column, 2.1 × 150 mm (Waters Chromatography Ireland Ltd) operating at 55 °C with a flow rate of 300 µL/min. Separation of the compounds was achieved by a changing gradient of eluent A (5 mM ammonium formate in water/acetonitrile 40:60, v/v) and eluent B (5 mM ammonium formate in acetonitrile/2-propanol, 10:90, v/v). The following linear gradient was applied: 1) 5% eluent B for 2.5 min, 2) a gradient from 5% to 90% eluent B over 36.5 min, 3) holding for 3 min, 4) returning to 5% eluent B in 0.5 min, 5) and holding for 8 min. The column effluent was injected directly into the Thermo Q Exactive Plus operating in positive or negative ion mode. Settings for positive mode: Spray Voltage: 3.20 |kV|, Capillary temperature: 230 °C, S-lens RF level: 50.0, sheath gas flow: 30, auxiliary gas flow: 5. Settings for negative mode: Spray Voltage: 3.20 |kV|, Capillary temperature: 230 °C, S-lens RF level: 50.0, sheath gas flow: 30, auxiliary gas flow: 20, sweep gas flow: 3, Aux gas heater temperature: 380 °C. For MS/MS the DDA method TopN (5) was used.

Spectral data constituting total ion counts were analyzed using the MacCoss Lab Software: Skyline. The following transition settings were used: Scan range: 133.4-2000 *m/z*, MS1 filtering: Orbitrap, resolving power 70,000 at *m/z* 400. MS/MS filtering: DDA, Orbitrap, resolving power: 17,500 at *m/z* 400. Total ion counts for extracted lipid species (Supplementary Table 3 - 9) were normalized for the internal standard DDM (*m/z* 509.30 $[M-H]^-$ or *m/z* 528.34 $[M+NH4]^+$).

RESULTS

TGD4 LOCALIZES TO ER-CHLOROPLAST MCSS

A proximity-dependent BiFC assay was used to confirm the localization of TGD4 at ER-chloroplasts MCSs, a putative prerequisite for its role in lipid transfer from the ER to chloroplasts. ER-chloroplasts MCSs were visualized as described in Chapter 1 and simultaneous expression of *TGD4* fused to *mCherry* assessed its *in vivo* localization. Transient expression of the respective gene cassettes was performed in tobacco leaves and transformed protoplasts were visualized.

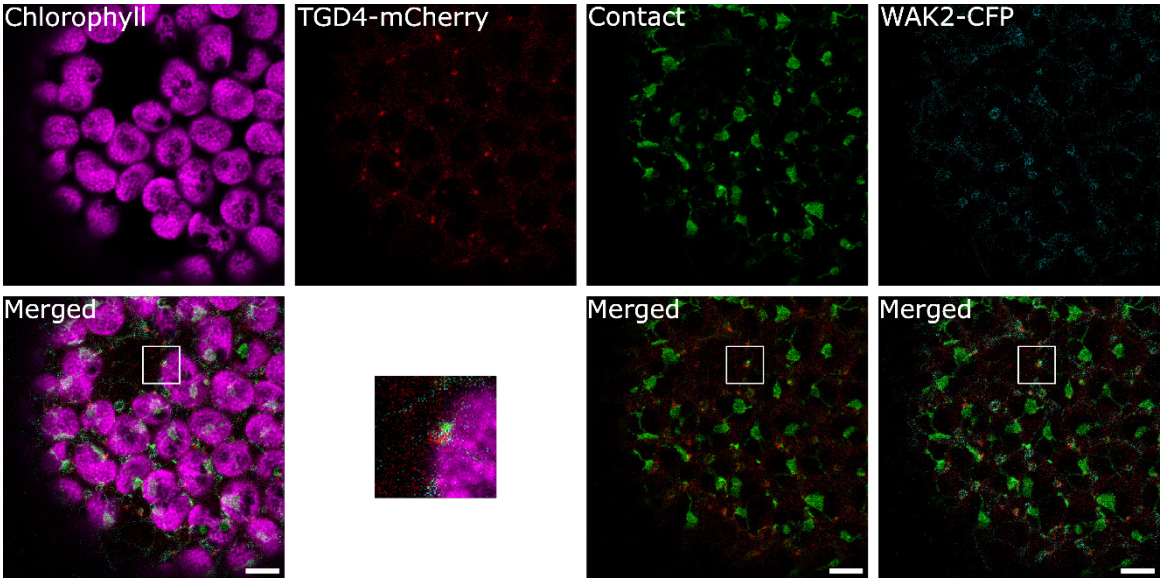

Figure 1: Transient expression reveals co-localization of TGD4 to ER-chloroplast MCSs. Simultaneous expression of a proximity-dependent BiFC assay and the TGD4-mCherry fusion protein in tobacco protoplasts showed partial co-localization (inset). In addition, some signals corresponding to either MCSs or TGD4 did not appear to co-localize. Chloroplasts were visualized by the chlorophyll autofluorescence (magenta), and ER was marked with an ER-specific marker (cyan). MCSs were detected by the BiFC (green) and TGD4 localization was indicated by mCherry fluorescence (red). Scale bar = 5 µm.

The BiFC approach reliably visualized MCSs between ER and chloroplasts as distinct punctate fluorescent signals (Figure 1, green), consistent with previously described ER-chloroplasts MCSs (Chapter 1). The mCherry fluorescence (depicted in red), corresponding to TGD4, largely co-localized with the punctate fluorescence of MCSs, indicating that a subset of TGD4 localizes to ER-chloroplast MCSs. Additional mCherry signal was observed independently of BiFC signals, suggesting the presence of TGD4 outside of these contact sites. Similarly, some BiFC-labeled MCSs did not co-localize with TGD4-mCherry, possibly representing ER-chloroplast MCSs that do not involve TGD4.

TARGETED DELETION OF TGD4'S PA-BINDING DOMAIN AFFECTS PIGMENT COMPOSITION AND LHCII PROTEIN LEVELS

Previous studies have shown that *TGD4* loss-of-function mutants are affected in lipid biosynthesis (Xu et al., 2008). To elucidate the role of the PA-binding domain of TGD4 in lipid trafficking, a mutant plant with a disruption in this domain was generated using CRISPR/Cas9. Guide RNAs targeting these PA-binding domains in the first three exons of *TGD4* were selected using CRISPR-P web tool (Lei et al., 2014).

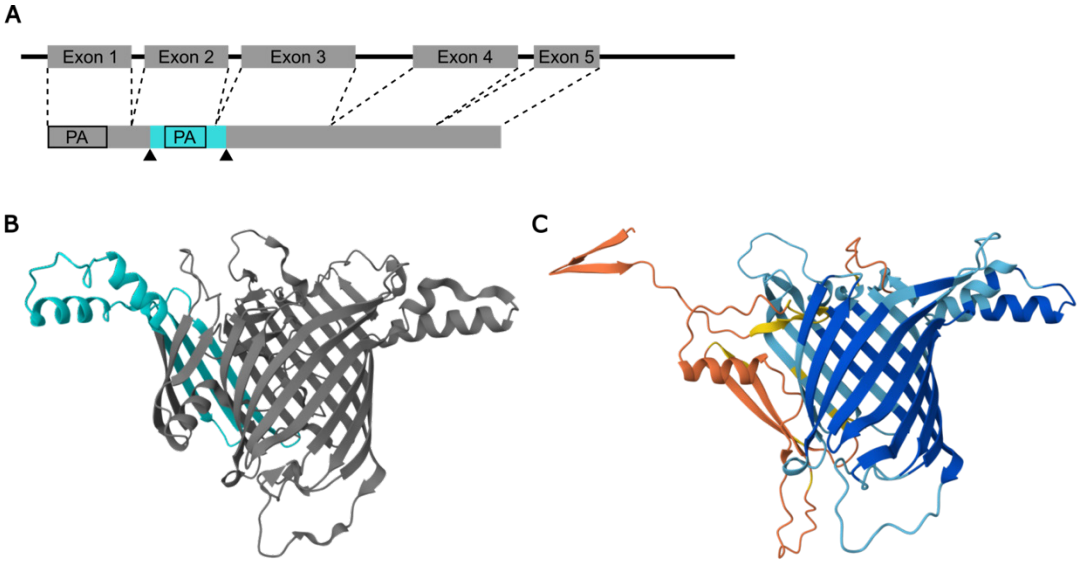

Figure 2: Schematic genomic and coding sequence of TGD4 and its secondary protein structure modeled by AlphaFold (Abramson et al., 2024). Genomic sequence contains five exons encoding the coding sequence of *TGD4* with two PA-binding domains at the N-terminal region (A). The cyan region depicts the deleted sequence. Protein structure of TGD4 modeled by AlphaFold with the deleted amino acids (cyan) of the CRISPR/Cas9 genome-edited plant – *tgd4-4* (B). Predicted structure of the truncated TGD4 protein. Structure was generated using AlphaFold3 (Abramson et al., 2024) (C).

CRISPR/Cas9-mediated mutagenesis resulted in an in-frame deletion of 255 bp, corresponding to a deletion of 85 amino acids between amino acid residue 103 - 187 and a substitution with six other amino acids (Figure 2A, Supplementary Figure 1). This region is predicted to form a cytosolic loop (Figure 2B) containing the minimum PA-binding domain of the TGD4 protein (Wang et al., 2013), and despite its deletion, the gene might still be fully expressed to generate a truncated variant. To confirm the presence of a truncated TGD4 variant in the heterozygous plants, PCR and quantitative RT-PCR (qRT-PCR) were performed.

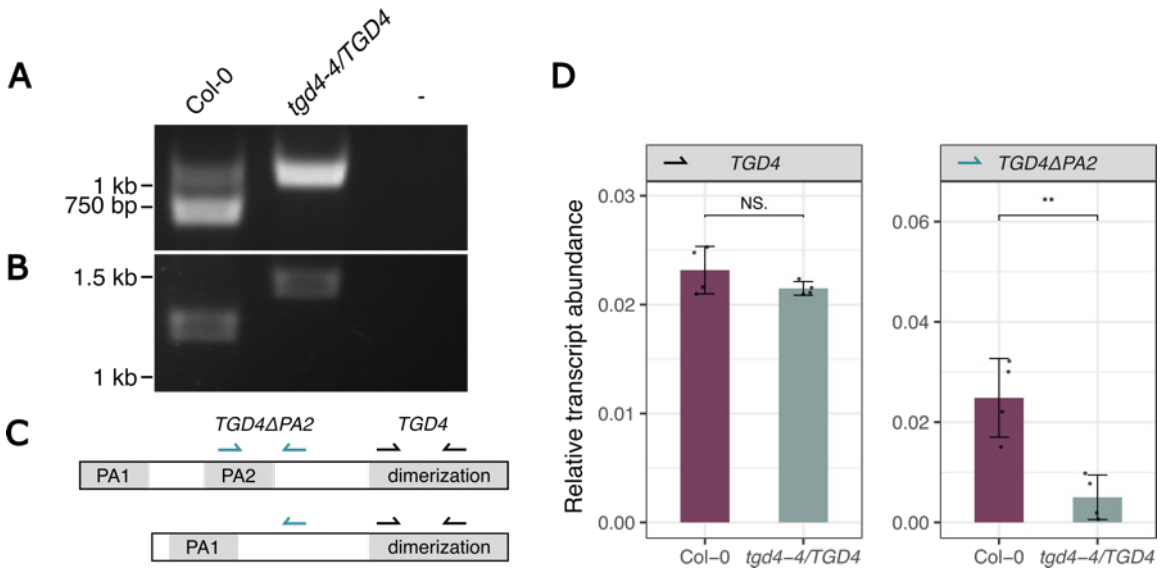

Figure 3: PCR and qRT-PCR of TGD4 gene in Col-0 and tgd4-4/TGD4 plants. Exemplary agarose gel of PCR, amplifying *TGD4* gene from genomic (A) and complementary DNA (B) of 5-weeks old Col-0 and *tgd4-4/TGD4* plants. Full-length wild-type *TGD4* gene was expected to be 1,440 bp long, whereas the in-frame deletion of the *tgd4-4* allele resulted in a 1,203 bp long product (B). For qRT-PCR, primers were selected to target the nucleotide sequence encoding for either the deleted PA-binding domain (*TGD4ΔPA2*) or the C-terminus (*TGD4*) (C). Relative transcript abundance of Col-0 and *tgd4-4/TGD4* were measured by qRT-PCR and normalized to *PP2A* reference gene (D). Data represent mean ± SD of four biological replicates. Significance was calculated by Student's t-test (** = $p < 0.01$; NS = $p > 0.05$).

Complementary DNA from 5-weeks old Col-0 and *tgd4-4/TGD4* plants were generated and used for PCR and qRT-PCR to verify the presence of a putative truncated *TGD4* transcript in *tgd4-4/TGD4* plants. Full-length transcript of the edited *TGD4* gene was shortened (Figure 3B) due to the internal deletion. Interestingly, although only one allele was affected by the deletion (Figure 3A), full-length transcript for the second allele was mostly absent (Figure 3B), indicating a dominant mutation. qRT-PCR using primer (Figure 3C), targeting the CRISPR/Cas9-targeted region, revealed a significant decrease of *TGD4* transcript (5-fold), indicating a successful deletion (Figure 3D). The transcript levels for *TGD4*, shown by targeting primers to the transcript region encoding for the C-terminus during qRT-PCR, were similar. However, the specific decrease of the amplicon, resulting from primers targeted to the region encoding the deleted PA-domain, and the presence of a shortened version of *TGD4* transcript suggests the presence of a truncated *TGD4* transcript, potentially leading to a truncated protein variant, lacking the PA-binding domain.

The resulting mutant displayed a paler leaf phenotype, a defect in growth and reduced amounts of seeds (Figure 4) possibly caused by a pollen defect, which is consistent with previous findings of *tgd4* mutants such as *tgd4-2* (Xu et al., 2008). *Tgd4-2* is a null mutant due to the presence of the T-DNA insertion within the fourth intron of the genomic *TGD4* sequence (Xu et al., 2008; Wang et al., 2012). The CRISPR/Cas9-generated mutant allele is hereafter referred to as *tgd4-4*.

Figure 4: Phenotype of tgd4 mutants. Shoots from 8-week-old mutant plants (*tgd4-4/TGD4* and *tgd4-2,* the CRISPR mutant and T-DNA insertion line, respectively,) (A) showed shorter siliques with a possible reduction in seeds number compared to Col-0 (B). 5-week-old *tgd4* mutants displayed impaired growth and a paler leaf phenotype compared to Col-0 (C). Scale bar = 1 cm

TGD4 acts as a homodimer (Wang et al., 2013), and the dominant mutation in the *tgd4-4* allele along with the phenotype of *tgd4-4/TGD4* heterozygous plants suggest that *tgd4-4* appears to have a dominant-negative effect on the plant.

The paler leaf phenotype typically indicates reduced chlorophyll content, which can be a sign of reduced chloroplast numbers or modified thylakoid membranes. This prompted further investigation of pigment- and protein content.

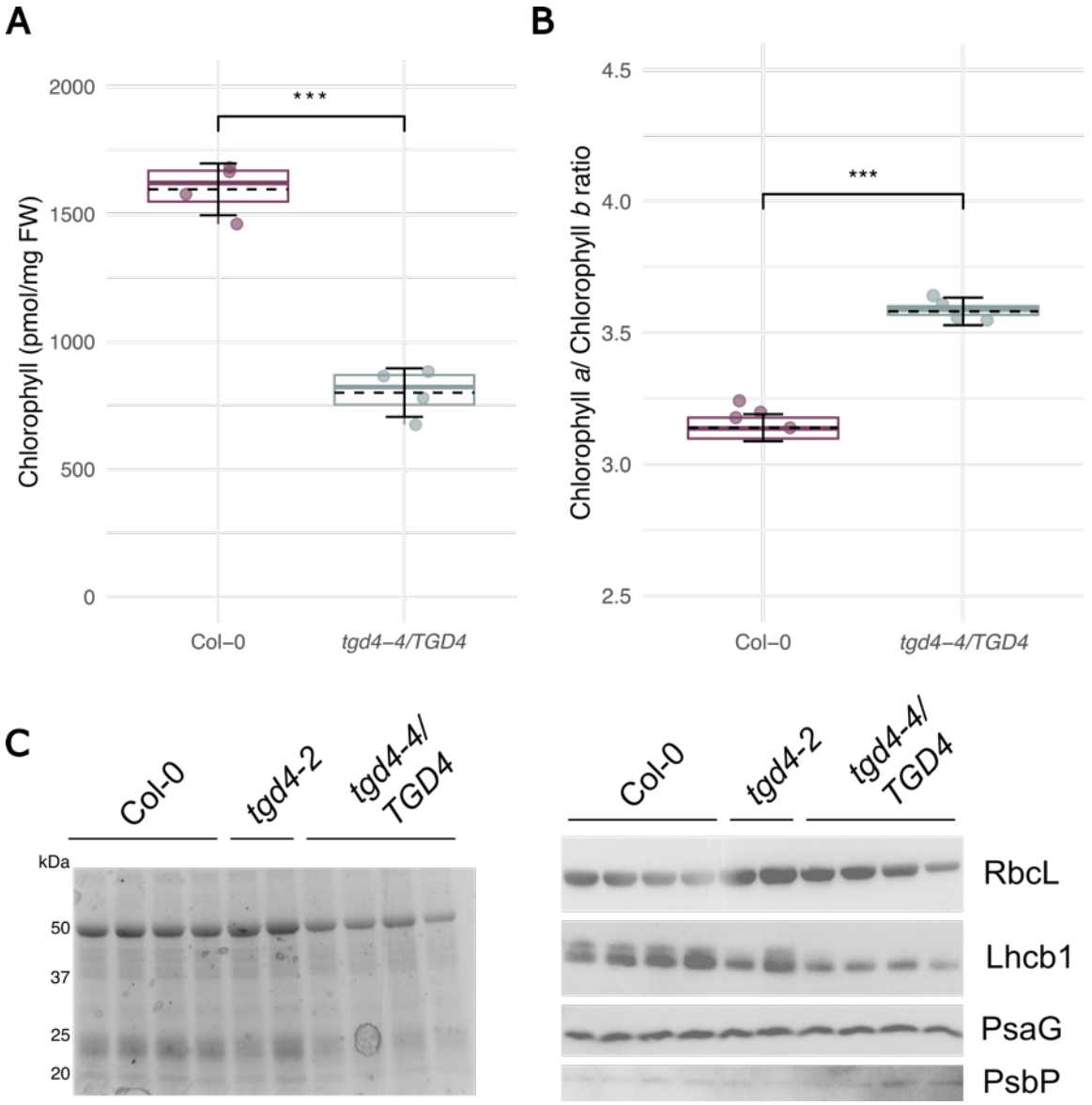

Figure 5: Chlorophyll and protein content of tgd4-4/TGD4 mutant line compared to Col-0. Tgd4-4/TGD4 mutant displays significantly reduced chlorophyll content (A) and an increased chlorophyll *a/b* ratio (B) compared to Col-0. Total chlorophyll content and chlorophyll *a/b* ratio was calculated from pigment analysis from 20 mg ground plant material harvested from 5-weeks old plants. Data are shown as mean (dashed line) ± SD (error bars) in a boxplot and whiskers, representing 4 biological replicates. Significance was calculated by Student's t-test (*** = $p < 0.001$). 50 mg of ground plant material from 5-weeks old plants was resuspended in 150 µL of SDS loading buffer, centrifuged, and 2 µL of supernatant containing total protein was separated by SDS-PAGE. RubisCO (RbcL) and proteins from the thylakoid membrane (Lhcb1, PsaG, PsbP) were detected by immunoblotting with respective antibodies (C).

Total chlorophyll content (Figure 5A) revealed significantly lower levels in *tgd4-4/TGD4* leaves compared to Col-0, but the chlorophyll *a/b* ratio (Figure 5B) increased. However, total protein extracts showed no change in the abundance of the large subunit of RubisCO (RbcL), suggesting that the mutation may primarily affect the thylakoid membranes (Figure 5C). Strikingly, other distinct protein classes visible in the SDS-PAGE showed decreased levels in *tgd4-4/TGD4* compared to Col-0. These protein classes were confirmed to belong to the light harvesting complex II by immunoblotting. In contrast, the levels of the PSI-G subunit of the photosystem I (PsaG) and the 23 kDa protein of the oxygen evolving complex (PsbP) remained unchanged. These results may indicate a selective defect in light harvesting. Future proteomic studies might provide deeper insights into further impaired thylakoid proteins.

Table 1: Pigment content of Col-0 and tgd4-4/TGD4 mutant. Pigments were extracted from 5-weeks old plants and normalized to total chlorophyll content. Normalized levels [mmol/mol chlorophyll] of antheraxanthin, β-carotene, lutein, neoxanthin, violaxanthin, chlorophyll *a* and chlorophyll *b* are listed. Data are shown as means ± SD of four biological replicates. Significance was calculated by Student's t-test (* = $p < 0.05$, ** = $p < 0.01$, *** = $p < 0.001$).

Pigments	Col-0	*tgd4-4/TGD4*	*p*-value
Chlorophyll *a*	758.36 ± 3.00	781.71 ± 2.51	***
Chlorophyll *b*	241.64 ± 3.00	218.29 ± 2.51	***
β-carotene	83.64 ± 2.56	93. 56 ± 4.11	**
Lutein	119.93 ± 1.22	148.51 ± 9.80	**
Antheraxanthin	n.d.	4.14 ± 0.96	***
Neoxanthin	36.30 ±1.02	35.69 ± 2.72	ns
Violaxanthin	23.00 ± 0.98	35.25 ± 5.05	**

The increased chlorophyll *a/b* ratio, which is due to the increase in chlorophyll *a* and decrease of chlorophyll *b* (Table 1), aligns with the observed reduction in LHCII. Pigment levels were normalized to total chlorophyll content and pigments involved in light-harvesting (chlorophylls and carotenes) and photoprotection (xanthophyll pigments) were analyzed (Table 1). Levels of the carotenoids, lutein and β-carotene, were elevated in the *tgd4-4/TGD4* mutant compared to Col-0. Violaxanthin levels were increased, possibly due to formation of a violaxanthin-isomer. Antheraxanthin showed an increase in content, but Zeaxanthin was not detected in all samples, consequently these pigments of the xanthophyll cycle were not further considered. The cause of the observed lutein increase, but no apparent alteration of pigments of the xanthophyll cycle remains inconclusive.

The altered levels of pigments and Lhcb1 protein could be the result of modified lipid composition of the thylakoid membrane. Therefore, a detailed lipid analysis was performed. The chloroplast envelope and thylakoid membranes, predominantly consist of galactolipids (LaBrant et al., 2018), which shape the environment for the light harvesting complexes and the photosynthetic apparatus. A simplified overview of galactolipid synthesis within the chloroplast is shown in Figure 6A.

Analysis of total lipids from leaves of 5-weeks old plants revealed significant alterations in galactolipid compositions in the *tgd4-4/TGD4* mutants. Overall, the galactolipid content in the *tgd4-4/TGD4* mutant was increased by only ~ 4% compared to Col-0. However, specifically the MGDG content was increased by ~ 14%, and DGDG reduced by ~ 4% (Figure 6B), leading to an increase in MGDG:DGDG ratio of 1.9 in Col-0 to 2.7 in *tgd4-4/TGD4*. Given the distinct substrate specificities of acyltransferases for the *sn-2* position, which results in the exclusive import of lipid precursors with 18C acyl-chains at the *sn-2* position (Frentzen et al., 1983), and the preservation of 16:0 acyl-chains at the *sn-1* position from desaturation in the chloroplast (Heemskerk et al., 1991), individual lipid species were classified as originating from either the eukaryotic or the prokaryotic pathway. Changes in detected lipid species in the *tgd4-4/TGD4* samples compared to Col-0 were displayed as log2 fold changes (log2FC) (Figure 6; total lipid levels are shown in Supplementary Figure 2). As the eukaryotic pathway is hypothesized to be impaired in the *tgd4-4/TGD4* mutants, lipid species derived from the prokaryotic pathway, such as MGDG 16:2-18:1, MGDG 16:2-18:2, and DGDG 16:2-18:2, showed a significant increase in abundance. Surprisingly, several lipid species derived from the eukaryotic pathway, such as MGDG 18:0-18:2, MGDG 18:1-18:1, or DGDG 18:0-18:2, also showed elevated levels. Decreased levels of lipids species revealed similar distribution. Prokaryotic (MGDG 16:3-18:3, MGDG 16:1-16:3, and DGDG 16:3-18:2) and eukaryotic (MGDG 18:2-18:3, MGDG 18:3-18:3, and DGDG 18:3-18:3) lipid species were reduced. Strikingly, these lipids were more desaturated in their acyl-chains, whereas those that increased were less desaturated (Figure 6C and D). A similar trend was observed for sulfoquinovosyl diacylglycerol (SQDG) lipids, which showed strong reduction in the polyunsaturated lipids (Figure 6E). Different plastidial FADs catalyze the desaturation steps at 18C or 16C acyl-chains. FAD5 introduces the first double bond (Figure 6A ":1"), specifically acting at 16C chains at the *sn-2* position of prokaryotic lipids. FAD6 further desaturates acyl chains to dienoic groups (Figure 6A ":2"), and FAD7 and FAD8 catalyze the third desaturation step (Figure 6A ":3"). These data suggest a reduced activity of FAD7 and FAD8 in the *tgd4-4/TGD4* mutants.

The *tgd4-4/TGD4* mutant showed the presence of TGDG (Figure 6F), as previously observed in other *tgd4* mutants (Xu et al., 2008).

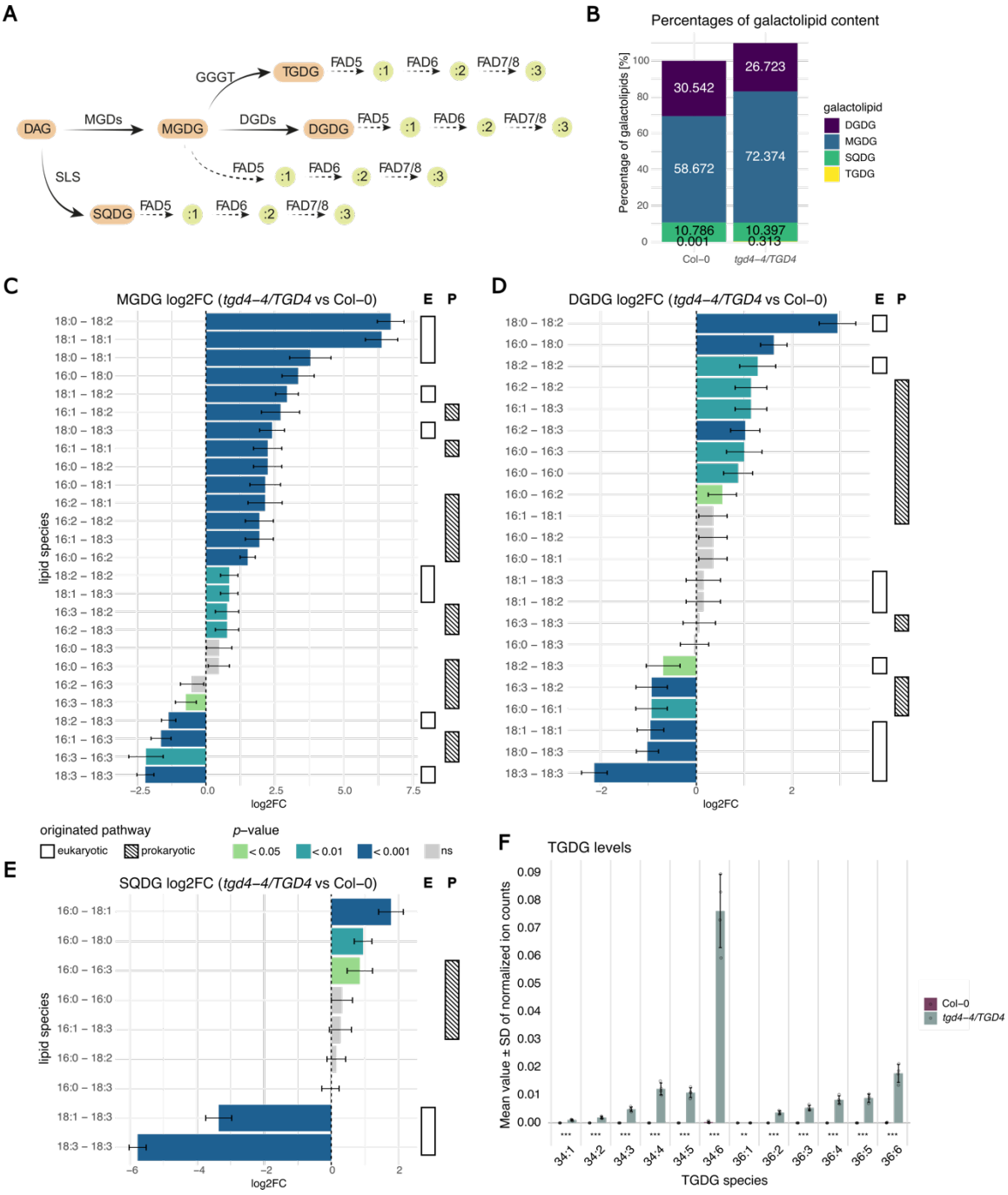

Figure 6: Lipid analyses of galactolipid in total lipid extracts of Col-0 and tgd4-4 mutants. Galactolipids, as sulfoquinovosyldiacylglycerol (SQDG) and monogalactosyldiacylglycerol (MGDG), are synthesized from a diacylglycerol (DAG) backbone. MGDG can either be processed to trigalactosyldiacylglycerol (TGDG) or digalactosyldiacylglycerol (DGDG). Fatty acid desaturases (FADs) desaturate the acyl chains at the *sn-1* and *sn-2* positions to form one (:1), two (:2), or three (:3) double bonds (A). Stacked bar plot displays the galactolipid content of Col-0 and *tgd4-4/TGD4* plants in percentages [%] (B). The data represents log2 fold changes (log_2FC) for lipid species in the lipid classes MGDG (C), DGDG (D), and SQDG (E) of *tgd4-4* mutants compared to Col-0 ± SD or the mean ± SD of normalized ion counts from TGDG lipid species (F) of 4 biological replicates. Statistical significance is color-coded (B – D) or depicted with asterisks (* = $p < 0.05$; ** = $p < 0.01$) and was calculated with Student's t-test. Pathway origin of the galactolipid species is indicated by open (eukaryotic: E) and striped (prokaryotic: P) boxes.

Besides alterations in galactolipid content, further changes were observed in other lipid classes in total lipid extracts from leaves of *tgd4-4/TGD4* mutants. TAG significantly accumulated in the *tgd4-4/TGD4* mutants, presumably, in form of lipid droplets. In addition, PC levels were elevated, whereas DAG levels remained unchanged (Table 2). While PC and DAG species with 18C acyl-chains were increased, PC and DAG species 16C acyl-chains were reduced (Supplementary Figure 3). The overall DAG levels are tightly regulated. Thus, the putative increase caused by a blockage in lipid export from the ER is likely redirected towards TAG formation (Lu et al., 2020).

Table 2: Normalized ion counts of phosphatidylcholine (PC), diacylglycerol (DAG), and triacylglycerol (TAG) in Col-0 and tgd4-4/TGD4 total lipid extracts. Data represent mean ± SD of three or four replicates. Significance was calculated by Student's t-test (* = $p < 0.05$).

Lipid	Col-0	*tgd4-4/TGD4*	*p < 0.05*
PC	86.8 ± 7.4	117.0 ± 7.2	*
DAG	3.1 ± 0.3	3.4 ± 0.2	ns
TAG	11.7 ± 0.7	47.3 ± 2.1	**

IDENTIFICATION OF TGD4 NETWORK

Lipid analyses of the *tgd4-4/TGD4* mutants revealed alterations in lipid compositions downstream of TGD4, suggesting that associated proteins might be subjected to regulatory mechanisms. To assess potential transcriptional regulation, qRT-PCR was performed (Figure 7).

Based on the lipid profiling data, several proteins acting downstream of TGD4 may be differentially regulated. For instance, the presence of TGDG lipid species suggests that the SFR2 protein is functionally active under these conditions. In contrast, the desaturases FAD7 and FAD8 may be inactivated, as levels of trienoic acyl groups were decreased across all lipid classes. qRT-PCR revealed that *SFR2* transcripts were significantly downregulated, while *FAD7* transcript abundance was significantly increased in *tgd4-4/TGD4. FAD6* transcript levels were analyzed as a control. Since lipid analyses showed no change in products of FAD6, no discernible change in the *FAD6* transcript abundance was expected, and none was detected. A defect in the PA-binding domain affects transcript abundance of proteins, acting downstream of TGD4. However, this result contradicts the observed lipid alterations.

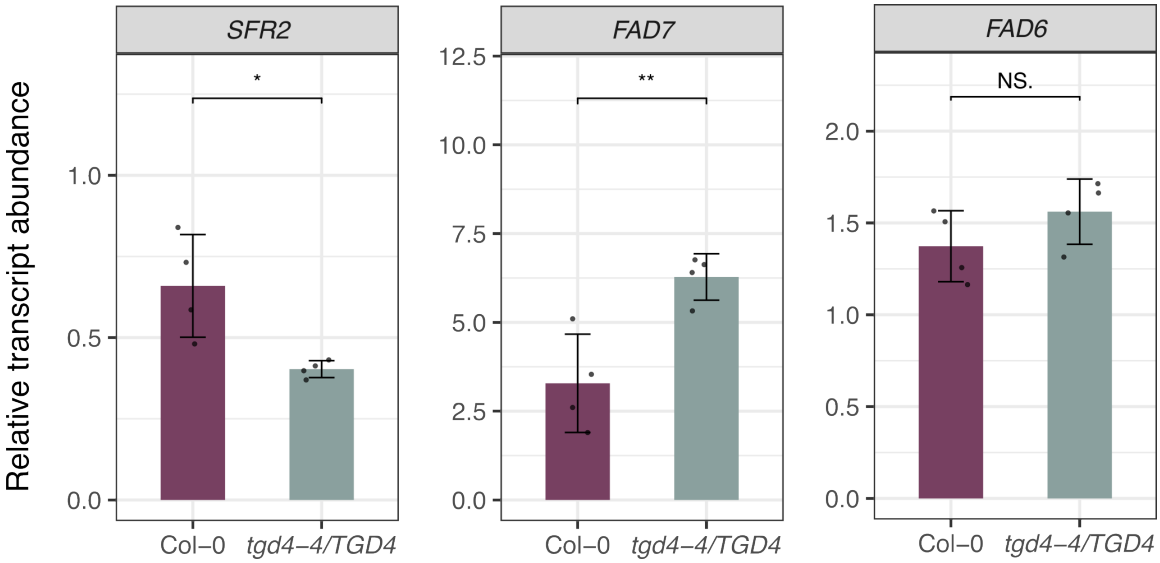

Figure 7: Relative transcript levels of 3 targets in Col-0 and tgd4-4/TGD4 by qRT-PCR. Relative transcript levels of *SFR2, FAD6, and FAD7* genes were normalized using the reference gene *PP2A* (Czechowski et al., 2005). Data represents mean ± SD of four biological replicates. Significance was calculated by Student's t-test (** = $p < 0.01$; * = $p < 0.05$; NS = $p > 0.05$).

PROXIMITY LABELING IDENTIFIES THE PHOSPHATASE PAH1 AS PUTATIVE INTERACTION PARTNER OF TGD4

Given that *tgd4-4/TGD4* plants appear to have a partially functional eukaryotic galactolipid biosynthesis pathway, despite the deletion of the PA-binding domain, it is possible that TGD4 transports a lipid other than PA to support galactolipid biosynthesis. Therefore, putative interaction partners, which possibly provide the transported lipid to TGD4, are sought to be identified to understand the functional role of TGD4 in the lipid metabolism. Proximity labeling offers a powerful approach to identify protein–protein interactions *in vivo*. This technique employs a promiscuous biotin ligase that covalently attaches a biotinoyl-group to proximal primary amines, typical lysine residues, of surrounding proteins. By fusing a biotin ligase to a protein of interest, both high- and low-affinity interactions can be captured (Choi-Rhee et al., 2004; Kim and Roux, 2016; Roux et al., 2018; Arora et al., 2020). TurboID is a biotin ligase variant with high activity and the ability to biotinylate at lower temperatures than previous variants (Branon et al., 2018; Zhang et al., 2020a).

TGD4 was fused to TurboID to direct the biotinylating to the MCSs. The resulting fusion protein, which included a GFP, was transiently expressed in tobacco leaves and transformed protoplasts were visualized by fluorescence microscopy to verify the expression and subcellular localization. Additionally, immunoblot analysis was performed to confirm the enzymatic activity of TurboID in the transformed leaves.

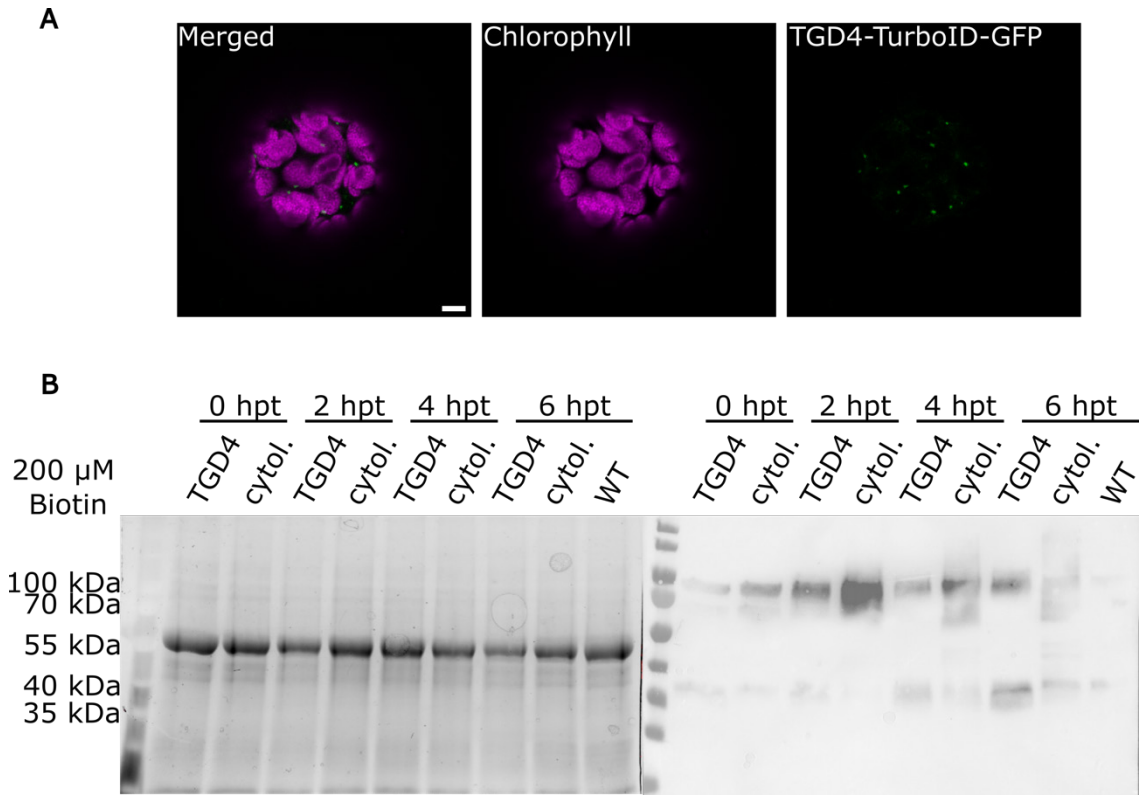

Figure 8: Verification of localization and activity of the TGD4-TurboID fusion protein. (A) Transient expression of TGD4-TurboID-GFP fusion protein in tobacco protoplasts revealed dot-like structures. Microscopy images visualize chloroplasts by their chlorophyll autofluorescence (magenta) and TGD4-TurboID localization by GFP signal (green). Scale bar = 5 µm. (B) Infiltrated tobacco leaves were harvested 0, 2, 4, or 6 hours post treatment (hpt) with 200 µM external biotin. Total protein, extracted from 50 mg harvested plant material in SDS loading buffer, was separated via SDS-PAGE and biotinylated proteins detected by immunoblotting using streptavidin-antibody.

The TGD4 localization, represented by the GFP fluorescence signal (green), appeared in a punctate pattern at chloroplasts (magenta) (Figure 8A), consistent with the previously observed localization of TGD4 at MCSs (Figure 1).

After 48 h of transient expression of the *TGD4-TurboID* gene cassette, 200 µM biotin was infiltrated into the tissue and leaf material was harvested every 2 h to determine optimal biotinylation activity. Immunoblot analysis revealed an increase of biotinylated proteins over a 6-hour period, indicating robust TurboID activity. The highest abundance of biotinylated proteins was observed at 6 h post treatment (hpt), which was therefore selected as the optimal time point for subsequent experiments. No increase in biotinylated protein levels was detected in control plants lacking *TurboID* expression.

Using the determined optimal time point for harvesting biotinylated proteins, four biological replicates expressing TGD4 fused to TurboID and a negative control expressing cytosolic TurboID were transiently expressed, treated with biotin, and harvested. Biotinylated proteins were then purified from total protein extracts using streptavidin magnetic beads, followed by protein identification via mass spectrometry.

In total, 873 proteins were identified (Supplementary Figure 4). Among these, 91 proteins were significantly enriched compared to the wild type control sample. Out of these, multiple proteins were significantly enriched in both TurboID samples, and therefore, were excluded from further analysis. Twelve proteins displayed a significant difference in the TGD4 sample compared to the wild type sample, whereas no such difference was observed in the negative control containing a cytosolic TurboID compared to the wild type. Out of these twelve proteins, eleven candidates were enriched (Table 3). As expected, TGD4 itself was among the identified proteins.

Table 3: Twelve identified proteins that revealed a significant difference in contrast to the cytosolic negative control and eleven candidates displayed further enrichment. Adj. *p*-values were calculated using Proteome Discoverer (version 2.4.1.15, Thermo Fisher Scientific) with 1% FDR (** = $p < 0.001$, *** = $p < 0.01$, ns, $p = 0.05$). Abbr.: MAPK8, mitogen-activated kinase 8; TOC132, translocase of chloroplast 132; HOP3, Hsp70-Hsp90 organizing protein 3; CYP40, Peptidyl-prolyl cis-trans isomerase CYP40; HOP2, Hsp70-Hsp90 organizing protein 2; PFD2, Prefoldin subunit 2; FKBP62, Peptidyl-prolyl cis-trans isomerase FKBP62; PAH1, Phosphatidate phosphatase PAH1; LON2, Lon protease homolog 2; CCT8, T-complex protein 1 subunit theta; PFD6, Prefoldin subunit 6; TGD4, Protein TRIGALACTOSYLDIACYLGLYCEROL 4

AGI	Abbr.	Adj. *p*-value(TGD4-TurboID/WT ratio)	Adj. *p*-value(cyt. TurboID/WT ratio)	TGD4-TurboID/ cyt. TurboID abundance ratio
At1g18150	MAPK8	**	ns	0.34
At2g16640	TOC132	**	ns	1.03
At4g12400	HOP3	***	ns	3.52
At2g15790	CYP40	***	ns	2.39
At1g62740	HOP2	**	ns	2.15
At3g22480	PFD2	***	ns	5.34
At3g25230	FKBP62	**	ns	3.14
At3g09560	PAH1	**	ns	2.54
At5g47040	LON2	**	ns	3.73
At3g03960	CCT8	**	ns	4.58
At1g29990	PFD6	**	ns	6.39
At3g06960	TGD4	**	ns	10.40

Among the 12 proteins identified, those involved in the import of nuclear-encoded pre-proteins were found, including chaperone subunits (HOP3 and HOP2) and components of the protein import machinery (TOC132). These proteins might have undergone biotinylation during the translocation of the TGD4 fusion protein to the chloroplast outer envelope.

As the TGD4 protein is hypothesized to play a role in lipid trafficking between the chloroplast and ER, proteins involved in lipid biogenesis or localized to either of these organelles were considered putative interaction partners within the TGD4-specific MCS. One such candidate is the PAH1, a soluble magnesium-dependent PA phosphatase localized to the ER membrane. PAH1 catalyzes the dephosphorylation of PA to DAG at the ER membrane (Eastmond et al., 2010). Homologs of Arabidopsis PAH1 in yeast (PAH1p) and mammals (Lipin-1) have been extensively studied. They play a role in regulatory loops controlling lipid biosynthesis via PA level modulation and provide the substrate for membrane formation and storage lipids such as TAG (Han et al., 2006; Eastmond et al., 2010). Thus, PAH1 represents a compelling candidate protein for participating in ER-derived lipid trafficking, potentially through interaction with TGD4.

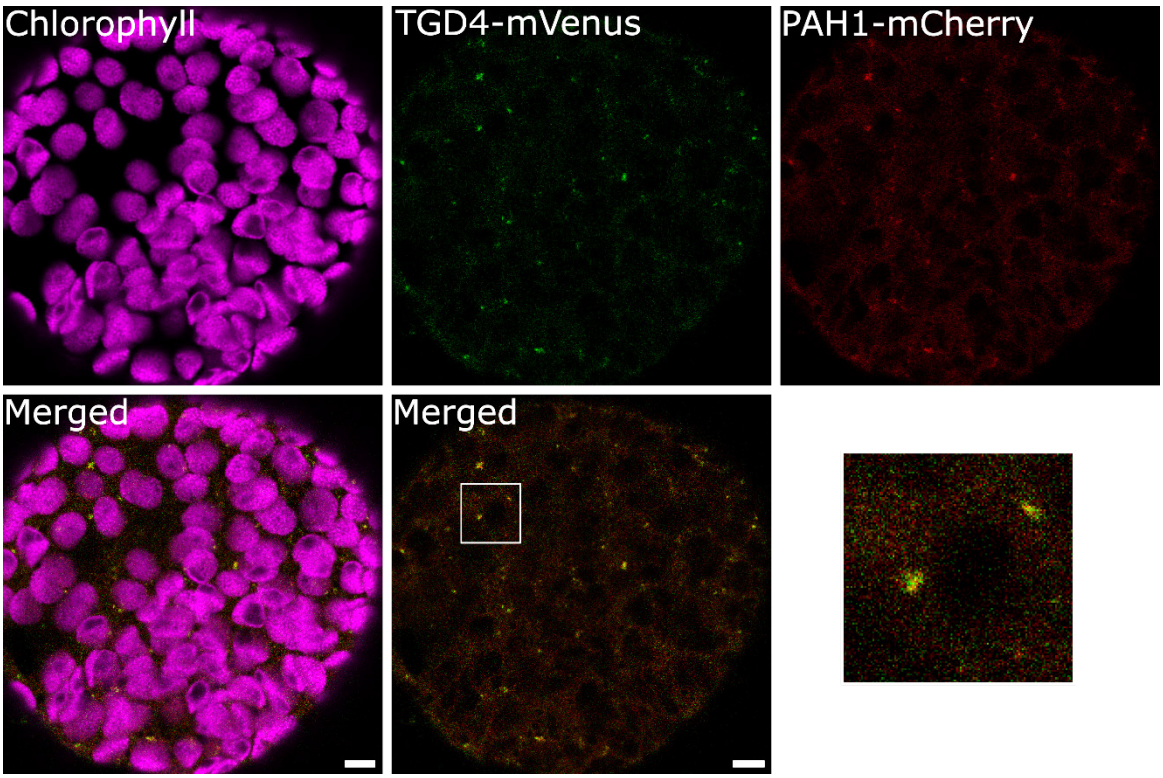

Figure 9: Simultaneous expression of TGD4-mVenus and PAH1-mCherry in tobacco protoplasts. Transient expression of TGD4-mVenus (green) and PAH1-mCherry (red) revealed co-localization at chloroplasts. Chloroplasts were visualized by chlorophyll autofluorescence (magenta). Scale bar = 5 µm.

To confirm protein-protein interaction between TGD4 and PAH1, suggested by the TurboID-based proximity labeling, co-localization studies were performed *in vivo*.

Therefore, protoplasts transiently expressing *TGD4-mVenus* and *PAH1-mCherry* fusion gene construct were visualized via confocal microscopy. Both fusion proteins displayed a distinct punctate pattern in close proximity to the autofluorescence of chloroplasts (Figure 9, Supplementary Figure 5).

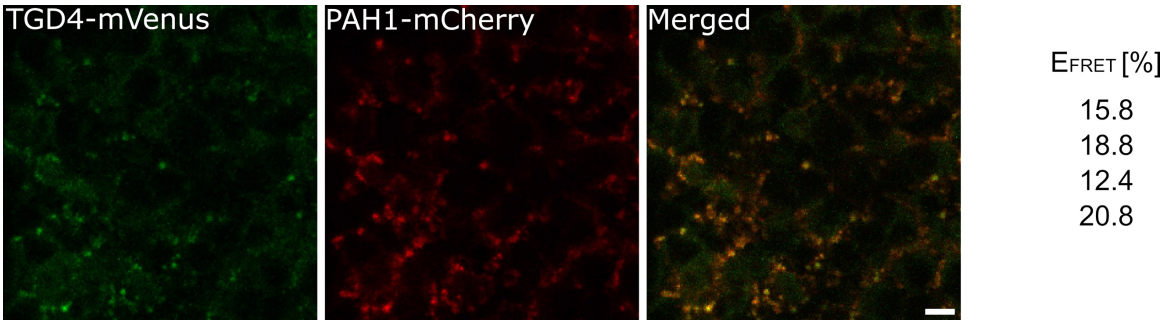

Figure 10: FRET analysis of TGD4 and PAH1. Tobacco protoplasts were isolated from infiltrated leaves and visualized. FRET analysis was carried out by measuring donor intensities before and after acceptor photo bleaching. Efficiencies (E_{FRET}) were calculated from multiple putative interaction sites. Scale bar = 5 µm.

As co-localization might lead to false positives due to overlapping signal of a 3D object in a 2D image, Förster resonance energy transfer-acceptor photo bleaching (FRET-APB) was employed to verify the protein-protein interaction of TGD4 and PAH1. FRET analysis utilizes the distance-dependent energy transfer of a donor fluorophore to the acceptor fluorophore, which occurs at a proximity of 10 nm (Förster, 1948). FRET-APB calculates the efficiency (E_{FRET}) by the increase of intensity of the donor fluorophore after photo-bleaching the acceptor fluorophore. Protoplasts, transiently expressing *TGD4-mVenus* and *PAH1-mCherry* fusion gene construct, were visualized and several putative interaction sites were subjected to acceptor photo bleaching. The increase of mVenus intensity was measured and efficiencies calculated as described in the material and methods part. The efficiencies ranging between 12% to 20% confirmed the interaction of TGD4 and PAH1 (Figure 10), supporting their potential physical association at chloroplast-ER MCSs.

DISCUSSION

The eukaryotic pathway of galactolipid biosynthesis in plants requires coordinated lipid trafficking between organelles. TGD4 is a key component of this process and is hypothesized to mediate lipid transfer from the ER to the chloroplast, potentially via MCSs. However, the exact role and mechanism of TGD4 in this trafficking pathway remains unclear. Using the established proximity-dependent BiFC approach (Chapter 1), we visualized the localization of TGD4 predominantly to ER-chloroplast MCSs (Figure 1). In addition to MCS-localized signal, TGD4 also displayed a distinct punctate localization pattern. This may reflect interactions with the inner-envelope-localized TGD1/2/3 complex and the intermembrane-space-localized TGD5 (Fan et al., 2015). These interactions may occur independently of functional ER-chloroplast MCSs, potentially indicating either an alternative function of the TGD complex within the chloroplast or possible involvement of TGD4 in MCSs with other organelles, which were not explored in this study. Furthermore, BiFC signals that did not co-localize with TGD4 suggest the existence of additional MCSs, which may be either involved in different types of lipid trafficking or serve functions unrelated to TGD4-mediated transport (Andersson et al., 2007; Zhang et al., 2020b). Overall, these findings indicate that TGD4 partially localizes to specific MCSs between the ER and chloroplasts.

As TGD4 is hypothesized to transport PA as the lipid precursor to the chloroplast for galactolipid biosynthesis, we established and analyzed a CRISPR/Cas9-generated mutant allele (*tgd4-4*), in which an in-frame deletion removed the N-terminal minimum PA-binding domain (Wang et al., 2012) (Figure 2). This mutant exhibited phenotypic traits similar to the previously described *tgd4-2* line (Xu et al., 2008), including impaired growth, infertility and a paler leaf phenotype (Figure 4). The latter, which might suggest a lower chloroplast abundance in the *tgd4-4/TGD4* mutants, was further analyzed by quantifying pigment content and composition via HPLC and protein detection via immunoblotting. This revealed a significant decrease in total chlorophyll content in *tgd4-4/TGD4* compared to Col-0. Abundances of the chloroplast marker protein RubisCO (RbcL), and marker proteins from photosystem I and II were not affected. In contrast, protein levels of LHCII were reduced, which has been previously shown in other *tgd* mutants (Li et al., 2012) (Figure 5). The elevated chlorophyll *a/b* ratio, particularly the increased levels in chlorophyll *a*, and the increased β-carotenoid content (Table 1) were in contrast to previous work (Li et al., 2012). These results suggest a defect in thylakoid membrane and light harvesting complex formation, rather than reduction in the total number of chloroplasts. Furthermore, Li and colleagues (2012) demonstrated that *tgd1* and *tgd2* mutants exhibit an impaired proton motive force, but no impact on the carbon fixation or linear electron transport. Together,

these findings point to a different, possibly more pronounced, functional consequence in *tgd4-4/TGD4* plants compared to the *tgd1* and *tgd2* mutants described by Li and colleagues (2012).

Thylakoid membranes are rich in galactolipids, which embed the photosynthetic apparatus and support light harvesting. Especially, the interaction of MGDG with LHCII is important for thylakoid structure and energy quenching of LHCII (Simidjiev et al., 2000; Tietz et al., 2020). Lipid analyses revealed significant alterations in galactolipid content in *tgd4-4/TGD4* mutant plants compared to Col-0 (Figure 6). Generally, *tgd4-4/TGD4* showed a higher galactolipid content, with an increase in MGDG and a decrease in DGDG. Contrary to the hypothesis that a defect in TGD4 would primarily impair the eukaryotic pathway, lipid species derived from both, the prokaryotic and the eukaryotic pathway, were increased. Similarly, certain lipid species independent of these pathways were decreased, especially trienoic galactolipids. These observations diverge from previous findings, which described either comparable or slightly reduced total MGDG content and mildly elevated levels of 16:3-MGDG lipid species in *tgd* mutants compared to wild type plants (Xu et al., 2008; Li et al., 2012; Fan et al., 2015). This suggests that the *tgd4-4/TGD4* may be defective in an additional regulatory mechanism within the eukaryotic pathway, rather than lipid transport per se. It is possible that the truncated TGD4 variant in the *tgd4-4/TGD4* mutant retains partial function, allowing the transport of a lipid precursor across the outer envelope to the TGD 1/2/3 complex.

Reduced levels of trienoic galactolipids hint to affected downstream lipid pathways

The prominent reduction in overall trienoic galactolipids indicate an alteration in lipid homeostasis within the chloroplast. It might be caused by an impaired activity of the fatty acid desaturases FAD7 and FAD8, which converts dienoic into trienoic acyl-chains in galactolipids. Expression of *FAD7* is known to respond to temperature stress and ABA signaling (Soria-García et al., 2019). In addition, post-translational regulation of FAD7 has been proposed to occur in a light-dependent manner by ferredoxin (Collados et al., 2006). While relative expression data (Figure 7) indicated an upregulation of *FAD7* transcripts in the *tgd4-4/TGD4* mutant compared to Col-0, the levels of trienoic galactolipids were decreased. The upregulation of the *FAD7* gene expression might suggests a cold stress- or ABA-like response by the presence of the truncated TGD4 variant. However, the observed decrease in products of the FAD7 reaction points to a different scenario. Trienoic galactolipids not only serve as structural components of thylakoid membranes, but also as precursors for jasmonic acid (JA) biosynthesis (Chaturvedi et al., 2008; Soria-García et

al., 2019). It is conceivable that these lipids were redirected toward JA production, particular since an elevated MGDG:DGDG ratio has been associated with enhanced JA biosynthesis (Yu et al., 2020). Although this hypothesis cannot be excluded, it is more likely that the reduced levels result from post-translational downregulation of FAD7 activity. FAD7 uses reduced ferredoxin as an electron donor in its desaturation reaction (Collados et al., 2006). Inhibition of desaturation of dienoic galactolipids in the *tgd4-4/TGD4* mutant may be a consequence of a decrease in available reduced ferredoxin, possibly due to a compromised electron transport caused by a lower abundance of light harvesting complexes. This aligns with the observed accumulation of mono- and dienoic galactolipids in the mutant plants.

Similarly, the oligogalactolipid TGDG was increased in the *tgd4-4/TGD4* mutant, despite reduced transcript levels of *SFR2*, which encodes the enzyme responsible for the oligogalactolipid biosynthesis (Figure 7). SFR2 is activated post-translationally under freezing conditions (Fourrier et al., 2008; Barnes et al., 2019). This activation might be caused by a defective TGD4 protein in the *tgd4-4/TGD4* mutant. These results indicate that the activities of both FAD7 and SFR2 are predominantly regulated at a post-translational level rather than through changes in transcript abundance. Future studies aim to identify the downstream regulatory network of TGD4-dependent galactolipid biosynthesis. TAG accumulation (Table 2), presumably forming lipid droplets, is possibly caused by an excess of lipids either due to an impaired export from the ER or by the accumulation of DAG as a side product of the SFR2 catalyzed oligogalactolipid biosynthesis. In future studies, possible elevated lipid droplet formation can be observed by staining with Nile Red or other dyes for neutral lipids, followed by analysis using confocal microscopy.

Putative interaction with phosphatase suggest a dual function for TGD4

Since the PA-binding domain of TGD4 was removed in the CRISPR mutant, putative transport of PA as lipid precursor has been hypothesized to be deleted. However, an increase in MGDG levels was observed, including lipid species from the eukaryotic pathway. This is in contrast to previous observed lipid compositions, indicating the transport of another lipid independent of the PA-binding domain. To assess this possibility, the interactome of TGD4 was analyzed to gain further insights into how TGD4 contributes to the formation or function of MCSs between chloroplasts and the ER. Proximity labeling has emerged as a powerful tool for identifying interaction partners by capturing transient or spatially restricted protein associations within their native cellular environment (Kim and Roux, 2016). Using TurboID-based proximity labeling, twelve candidate proteins were

found significantly enriched in the TGD4 sample compared to the negative controls. Among these candidates, we identified the magnesium-dependent phosphatase PAH1, which peripherally localizes to the ER membrane, as possible interaction partner (Table 3). Co-localization studies and FRET analysis revealed that PAH1 and TGD4 localized to distinct punctate pattern, which fully overlap, providing further support for a potential interaction.

Since the identity of the transported lipid precursor in the eukaryotic pathway remains unknown, several hypotheses can be proposed regarding how the interaction between TGD4 and PAH1 might influence galactolipid biosynthesis: *(1)* If PA is the transported lipid, both TGD4 and PAH1 would utilize the same substrate, potentially localizing to regions of PA accumulation at the ER membrane. *(2)* If the transported lipid is DAG, the product of PAH1-mediated dephosphorylation of PA, PAH1 could provide the substrate for transport into the chloroplast by TGD4. *(3)* Considering multiple aspects of the *tgd4-4/TGD4* mutant - *(a)* the potential presence of a truncated variant lacking the PA-binding domain, and that *(b)* galactolipids derived from the eukaryotic pathway were not specifically affected, however *(c)* severe changes could be observed in the overall galactolipid content - it can be proposed that TGD4 might transport two types of lipids, which might be regulated by PAH1. The absence of more severe defects in the eukaryotic pathway of the *tgd4-4/TGD4* mutant plants suggests that the lipid precursor, possibly DAG, which is the product of PAH1 reaction, could still be transported into the chloroplast. Notably, *pah1/pah2* double knockout mutants exhibit a phenotype similar to the *tgd* mutants, such as an increase in 16:3 MGDG and decrease in 18:3 MGDG lipid species, indicating a possible role of PAH1 in the eukaryotic pathway (Eastmond et al., 2010). As the *pah1/pah2* knockout mutants are not able to convert PA to DAG, this might further hint to DAG being the main lipid precursor for galactolipid biosynthesis. DAG has previously been discussed as potential lipid precursor in the eukaryotic pathway (Maréchal and Bastien, 2014). The hypothesis that DAG, rather than PA, serves as the transported lipid gains support from observations in 18:3 plants, which are fully dependent on the eukaryotic pathway to generate galactolipids, where the plastidial phosphatases working in this eukaryotic pathway appear to be absent (Nguyen and Nakamura, 2023).

The role of PAH1 has been hypothesized to be of regulatory manner, modulating phospholipid homeostasis by either indirect or direct regulation of phospholipid biosynthesis (Eastmond et al., 2010). PAH1 might influence the flux of PA towards phospholipid biosynthesis or, by converting PA to DAG, towards galactolipid biosynthesis. This may point to a regulatory mechanism of lipid homeostasis that depends on PAH1-TGD4 interaction, mediated via the PA binding domain of TGD4. Future work will include the generation of double and triple knockout plants with *tgd4-4, pah1* and *pah2*, and the

complementation of *tgd4* mutants with TGD4 proteins from 18:3 plants, as they have been shown to have a higher PA binding affinity (Wang et al., 2013) and, thus, might give further insights on the role of the PA-binding domain.

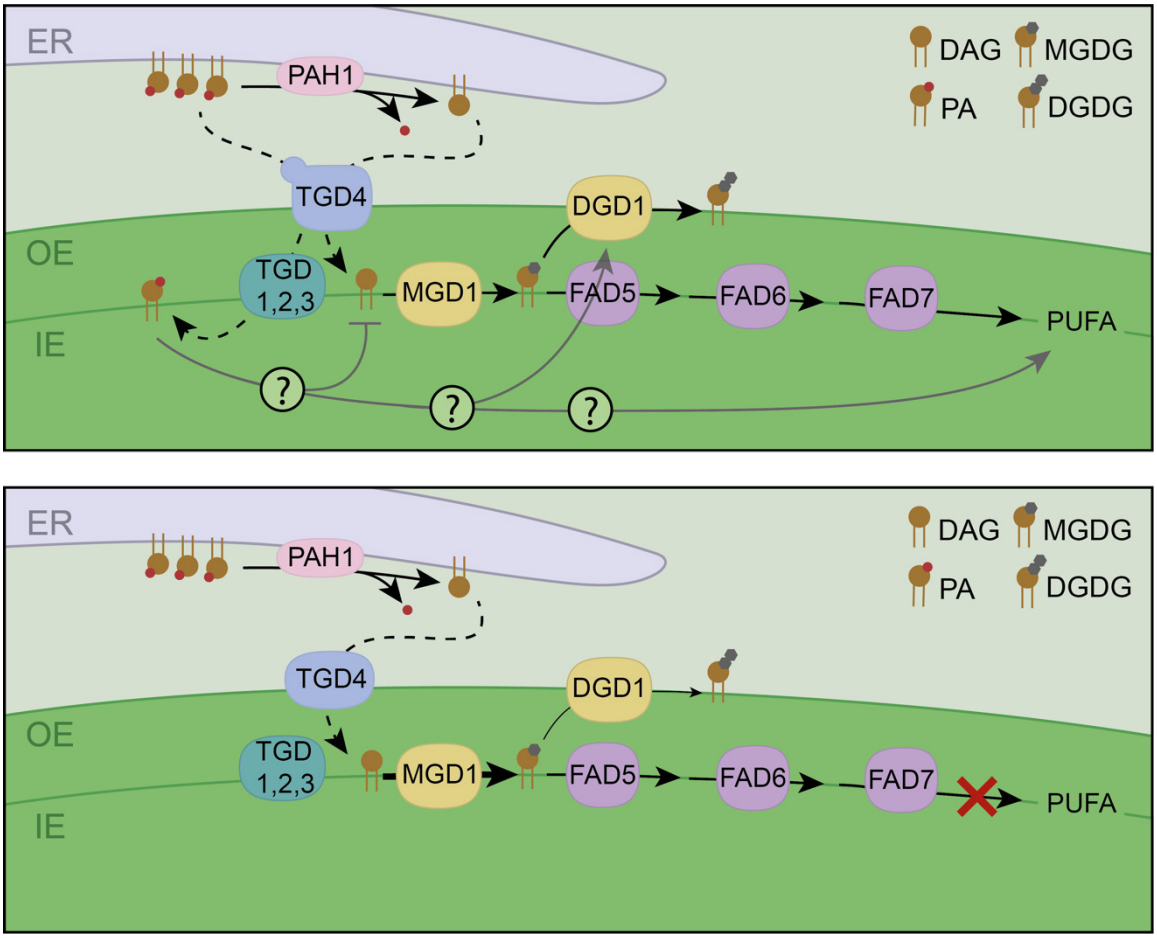

Figure 11: Novel role of TGD4 in the transport mechanism of the eukaryotic galactolipid biosynthesis pathway. Based on the data presented here, a novel role for TGD4 in cooperation with PAH1 is proposed. TGD4 may transport multiple lipid types, namely PA and DAG. DAG is suggested to serve as the core lipid precursor for the eukaryotic pathway, resulting in the formation of galactolipids such as MGDG by MGD1. In contrast, PA may play a regulatory role in the galactolipid biosynthesis, potentially influencing FAD7 activity either directly or indirectly and thereby modulating the content of polyunsaturated acyl-groups of galactolipids. The transport of either DAG or PA might be further dependent and regulated by PAH1 activity as it utilizes the PA to form DAG. The upper part illustrates the proposed model for galactolipid biosynthesis under normal conditions, while the lower part displays the situation in plants lacking the PA binding loop of the TGD4, such as in the generated CRISPR/Cas9 mutant *tgd4-4*. In the latter scenario, galactolipid biosynthesis can still occur. However, FAD7 is inactive due to the absence of PA, either as a result of inhibition or lack of activation. Abbreviation: DAG, diacylglycerol; ER, endoplasmic reticulum; FAD7, fatty acid desaturase 7; IE, inner envelope; MGD1, monogalactosyl diacylglycerol synthase 1; MGDG, monogalactosyl diacylglycerol; PA, phosphatidic acid; PAH1, phosphate phosphatase 1; PUFA, polyunsaturated fatty acid; TGD, trigalactosyl diacylglycerol proteins

Taking together, the findings of this study suggest that TGD4 might have a dual function, participating in a regulatory mechanism to modulate galactolipid biosynthesis in coordination with PAH1 (Figure 11). At ER-chloroplast MCSs, PAH1 may regulate local PA levels, which in turn regulates influx of PA and subsequently DAG to the chloroplast. PA

levels in the chloroplast envelopes modulate activity of MGD1 and DGD1, the galactolipid synthases for bulk galactolipid biosynthesis. It has been shown that MGD1 is allosterically activated by PA and its active site faces the stroma. The supply of PA derives from both the prokaryotic and eukaryotic pathway. Under influx of DAG, PA levels in chloroplast increase by PAP feedback inhibition and in turn further activate MGD1 (Dubots et al., 2010; Maréchal and Bastien, 2014). The elevated MGDG levels in the *tgd4-4/TGD4* mutant might be the result of the DAG influx, and possibly further elevated by the defect in PA import by TGD4, thus, unable to regulate DAG transport. The influx in DAG might lead to enhanced MGDG synthesis by MGD1 to normalize DAG levels in the chloroplast envelopes. DGD1 requires the presence of PA for the transport of MGDG from the inner envelope to the outer envelope for DGDG synthesis (Kelly et al., 2016). As DGD1 is localized to the outer envelope (Froehlich et al., 2001), the PA level might derive predominantly from the eukaryotic pathway, in contrast to PA levels in thylakoid membranes (Fritz et al., 2007) and possibly the inner envelope. Thus, the lack of eukaryotic PA prevents the DGDG synthesis to a certain level. The elevated MGDG:DGDG ratio, mainly due to an increase in MGDG levels, which was not previously reported for any *tgd* mutants, might on the one hand effect the thylakoid membrane integrity, and potentially compromising light harvesting complexes, and on the other hand increase JA biosynthesis, consuming 16:3 and 18:3 acyl-chains from MGDG. The defect in light harvesting complexes might lead to diminished levels of reduced ferredoxin, the electron donor for FAD7, inhibiting its desaturase activity. JA biosynthesis utilizes trienoic acyl-chains further reducing polyunsaturated MGDG.

In summary, TGD4 may transport DAG as lipid precursor for the eukaryotic pathway of galactolipid biosynthesis and uses PA as a regulatory factor. TGD4 function appears to be regulated by PAH1 and influences the desaturation levels of galactolipids in the chloroplasts. This working model raises several important new questions and urges to unravel standing questions, such as the precise identity of the transported lipid(s), the mechanism on how PAH1 is regulated upstream, and the nature of the feedback mechanisms that maintain galactolipid biosynthesis for membrane homeostasis, particular at thylakoid membranes.

REFERENCES

Abramson, J., Adler, J., Dunger, J., Evans, R., Green, T., Pritzel, A., Ronneberger, O., Willmore, L., Ballard, A.J., Bambrick, J., et al., (2024). Accurate structure prediction of biomolecular interactions with AlphaFold 3. Nature. 2024:**630**(8016):493–500. https://doi.org/10.1038/s41586-024-07487-w

Aliaga-Franco, N., Zhang, C., Presa, S., Srivastava, A.K., Granell, A., Alabadí, D., Sadanandom, A., Blázquez, M.A., and Minguet, E.G., (2019). Identification of Transgene-Free CRISPR-Edited Plants of Rice, Tomato, and Arabidopsis by Monitoring DsRED Fluorescence in Dry Seeds. Front Plant Sci. 2019:**10**. https://doi.org/10.3389/fpls.2019.01150

Andersson, M.X., Goksör, M., and Sandelius, A.S., (2007). Membrane contact sites: Physical attachment between chloroplasts and endoplasmic reticulum revealed by optical manipulation. Plant Signal Behav. 2007:**2**(3):185–187. https://doi.org/10.4161/psb.2.3.3973

Arora, D., Abel, N.B., Liu, C., van Damme, P., Yperman, K., Eeckhout, D., Vu, L.D., Wang, J., Tornkvist, A., Impens, F., et al., (2020). Establishment of proximity-dependent biotinylation approaches in different plant model systems. Plant Cell. 2020:**32**(11):3388–3407. https://doi.org/10.1105/TPC.20.00235

Barnes, A.C., Elowsky, C.G., and Roston, R.L., (2019). An Arabidopsis protoplast isolation method reduces cytosolic acidification and activation of the chloroplast stress sensor SENSITIVE TO FREEZING 2. Plant Signal Behav. 2019:**14**(9). https://doi.org/10.1080/15592324.2019.1629270

van Besouw, A., and Wintermans, J.F.G.M., (1978). Galactolipid formation in chloroplast envelopes. Biochimica et Biophysica Acta (BBA) - Lipids and Lipid Metabolism. 1978:**529**(1):44–53. https://doi.org/10.1016/0005-2760(78)90102-9

Biemans-Oldehinkel, E., (2003). On the role of the two extracytoplasmic substrate-binding domains in the ABC transporter OpuA. EMBO J. 2003:**22**(22):5983–5993. https://doi.org/10.1093/emboj/cdg581

Block, M.A., Dorne, A.J., Joyard, J., and Douce, R., (1983). Preparation and characterization of membrane fractions enriched in outer and inner envelope membranes from spinach chloroplasts. II. Biochemical characterization. Journal of Biological Chemistry. 1983:**258**(21):13281–13286. https://doi.org/10.1016/s0021-9258(17)44113-5

Branon, T.C., Bosch, J.A., Sanchez, A.D., Udeshi, N.D., Svinkina, T., Carr, S.A., Feldman, J.L., Perrimon, N., and Ting, A.Y., (2018). Efficient proximity labeling in

living cells and organisms with TurboID. Nat Biotechnol. 2018:**36**(9):880–898. https://doi.org/10.1038/nbt.4201

Cabantous, S., Terwilliger, T.C., and Waldo, G.S., (2005). Protein tagging and detection with engineered self-assembling fragments of green fluorescent protein. Nat Biotechnol. 2005:**23**(1):102–107. https://doi.org/10.1038/nbt1044

Chang, C.L., Hsieh, T.S., Yang, T.T., Rothberg, K.G., Azizoglu, D.B., Volk, E., Liao, J.C., and Liou, J., (2013). Feedback regulation of receptor-induced ca2+ signaling mediated by e-syt1 and nir2 at endoplasmic reticulum-plasma membrane junctions. Cell Rep. 2013:**5**(3):813–825. https://doi.org/10.1016/j.celrep.2013.09.038

Chaturvedi, R., Krothapalli, K., Makandar, R., Nandi, A., Sparks, A.A., Roth, M.R., Welti, R., and Shah, J., (2008). Plastid ω3-fatty acid desaturase-dependent accumulation of a systemic acquired resistance inducing activity in petiole exudates of Arabidopsis thaliana is independent of jasmonic acid. Plant Journal. 2008:**54**(1):106–117. https://doi.org/10.1111/j.1365-313X.2007.03400.x

Choi-Rhee, E., Schulman, H., and Cronan, J.E., (2004). Promiscuous protein biotinylation by Escherichia coli biotin protein ligase. Protein Science. 2004:**13**(11):3043–3050. https://doi.org/10.1110/ps.04911804

Clough, S.J., and Bent, A.F., (1998). Floral dip: A simplified method for Agrobacterium-mediated transformation of Arabidopsis thaliana. Plant Journal. 1998:**16**(6):735–743. https://doi.org/10.1046/j.1365-313X.1998.00343.x

Collados, R., Andreu, V., Picorel, R., and Alfonso, M., (2006). A light-sensitive mechanism differently regulates transcription and transcript stability of ω3 fatty-acid desaturases (FAD3, FAD7 and FAD8) in soybean photosynthetic cell suspensions. FEBS Lett. 2006:**580**(20):4934–4940. https://doi.org/10.1016/j.febslet.2006.07.087

Cook, R., Froehlich, J.E., Yang, Y., Korkmaz, I., Kramer, D.M., and Benning, C., (2024). Chloroplast phosphatases LPPγ and LPPϵ1 facilitate conversion of extraplastidic phospholipids to galactolipids. Plant Physiol. 2024:**195**(2):1506–1520. https://doi.org/10.1093/plphys/kiae100

Czechowski, T., Stitt, M., Altmann, T., Udvardi, M.K., and Scheible, W.R., (2005). Genome-wide identification and testing of superior reference genes for transcript normalization in arabidopsis. Plant Physiol. 2005:**139**(1):5–17. https://doi.org/10.1104/pp.105.063743

Douce, R., (1974). Site of Biosynthesis of Galactolipids in Spinach Chloroplasts. Science (1979). 1974:**183**(4127):852–853. https://doi.org/10.1126/science.183.4127.852

Dubots, E., Audry, M., Yamaryo, Y., Bastien, O., Ohta, H., Breton, C., Maréchal, E., and Block, M.A., (2010). Activation of the chloroplast monogalactosyldiacylglycerol

synthase MGD1 by phosphatidic acid and phosphatidylglycerol. Journal of Biological Chemistry. 2010:**285**(9):6003–6011. https://doi.org/10.1074/jbc.M109.071928

Eastmond, P.J., Quettier, A.L., Kroon, J.T.M., Craddock, C., Adams, N., and Slabas, A.R., (2010). PHOSPHATIDIC ACID PHOSPHOHYDROLASE1 and 2 regulate phospholipid synthesis at the endoplasmic reticulum in Arabidopsis. Plant Cell. 2010:**22**(8):2796–2811. https://doi.org/10.1105/tpc.109.071423

Eisenberg-Bord, M., Shai, N., Schuldiner, M., and Bohnert, M., (2016). A Tether Is a Tether Is a Tether: Tethering at Membrane Contact Sites. Dev Cell. 2016:**39**(4):395–409. https://doi.org/10.1016/j.devcel.2016.10.022

Engler, C., Youles, M., Gruetzner, R., Ehnert, T.M., Werner, S., Jones, J.D.G., Patron, N.J., and Marillonnet, S., (2014). A Golden Gate modular cloning toolbox for plants. ACS Synth Biol. 2014:**3**(11):839–843. https://doi.org/10.1021/sb4001504

Fan, J., Zhai, Z., Yan, C., and Xu, C., (2015). Arabidopsis TRIGALACTOSYLDIACYLGLYCEROL5 interacts with TGD1, TGD2, and TGD4 to facilitate lipid transfer from the endoplasmic reticulum to plastids. Plant Cell. 2015:**27**(10):2941–2955. https://doi.org/10.1105/tpc.15.00394

Farber, A., Young, A.J., Ruban, A. V., Horton, P., and Jahns, P., (1997). Dynamics of Xanthophyll-Cycle Activity in Different Antenna Subcomplexes in the Photosynthetic Membranes of Higher Plants (The Relationship between Zeaxanthin Conversion and Nonphotochemical Fluorescence Quenching). Plant Physiol. 1997:**115**(4):1609–1618. https://doi.org/10.1104/pp.115.4.1609

Förster, T., (1948). Zwischenmolekulare Energiewanderung und Fluoreszenz. Ann Phys. 1948:**437**(1–2):55–75. https://doi.org/10.1002/andp.19484370105

Fourrier, N., Bédard, J., Lopez-Juez, E., Barbrook, A., Bowyer, J., Jarvis, P., Warren, G., and Thorlby, G., (2008). A role for SENSITIVE to FREEZING2 in protecting chloroplasts against freeze-induced damage in Arabidopsis. Plant Journal. 2008:**55**(5):734–745. https://doi.org/10.1111/j.1365-313X.2008.03549.x

Frentzen, M., Heinz, E., McKeon, T.A., and Stumpf, P.K., (1983). Specificities and Selectivities of Glycerol-3-Phosphate Acyltransferase and Monoacylglycerol-3-Phosphate Acyltransferase from Pea and Spinach Chloroplasts. Eur J Biochem. 1983:**129**(3):629–636. https://doi.org/10.1111/j.1432-1033.1983.tb07096.x

Fritz, M., Lokstein, H., Hackenberg, D., Welti, R., Roth, M., Zähringer, U., Fulda, M., Hellmeyer, W., Ott, C., Wolter, F.P., et al., (2007). Channeling of eukaryotic diacylglycerol into the biosynthesis of plastidial phosphatidylglycerol. Journal of Biological Chemistry. 2007:**282**(7):4613–4625. https://doi.org/10.1074/jbc.M606295200

Froehlich, J.E., Benning, C., and Dörmann, P., (2001). The Digalactosyldiacylglycerol (DGDG) Synthase DGD1 Is Inserted into the Outer Envelope Membrane of Chloroplasts in a Manner Independent of the General Import Pathway and Does Not Depend on Direct Interaction with Monogalactosyldiacylglycerol Synthase for DGDG Biosynthesis. Journal of Biological Chemistry. 2001:**276**(34):31806–31812. https://doi.org/10.1074/jbc.M104652200

Gallie, D.R., Sleat, D.E., Watts, J.W., Tumer, P.C., Michael, T., and Wilson, A., (1987). The 5'-leader sequence of tobacco mosaic virus RNA enhances the expression of foreign gene transcripts in vitro and in vivo.

Grefen, C., Donald, N., Hashimoto, K., Kudla, J., Schumacher, K., and Blatt, M.R., (2010). A ubiquitin-10 promoter-based vector set for fluorescent protein tagging facilitates temporal stability and native protein distribution in transient and stable expression studies. Plant Journal. 2010:**64**(2):355–365. https://doi.org/10.1111/j.1365-313X.2010.04322.x

Grossmann, D., Berenguer-Escuder, C., Bellet, M.E., Scheibner, D., Bohler, J., Massart, F., Rapaport, D., Skupin, A., Fouquier D'Hérouël, A., Sharma, M., et al., (2019). Mutations in RHOT1 Disrupt Endoplasmic Reticulum-Mitochondria Contact Sites Interfering with Calcium Homeostasis and Mitochondrial Dynamics in Parkinson's Disease. Antioxid Redox Signal. 2019:**31**(16):1213–1234. https://doi.org/10.1089/ars.2018.7718

Han, G.-S., Wu, W.-I., and Carman, G.M., (2006). The Saccharomyces cerevisiae Lipin Homolog Is a Mg2+-dependent Phosphatidate Phosphatase Enzyme*. Journal of Biological Chemistry. 2006:**281**(14):9210–9218. https://doi.org/10.1074/jbc.M600425200

Heemskerk, J.W.M., Schmidt, H., Hammer, U., and Heinz, E., (1991). Biosynthesis and Desaturation of Prokaryotic Galactolipids in Leaves and Isolated Chloroplasts from Spinach1.

Hurlock, A.K., Roston, R.L., Wang, K., and Benning, C., (2014). Lipid trafficking in plant cells. Traffic. 2014:**15**(9):915–932. https://doi.org/10.1111/tra.12187

Jinek, M., Chylinski, K., Fonfara, I., Hauer, M., Doudna, J.A., and Charpentier, E., (2012). A Programmable Dual-RNA–Guided DNA Endonuclease in Adaptive Bacterial Immunity. Science (1979). 2012:**337**(6096):816–821. https://doi.org/10.1126/science.1225829

Kelly, A.A., Kalisch, B., Hölzl, G., Schulze, S., Thiele, J., Melzer, M., Roston, R.L., Benning, C., and Dörmann, P., (2016). Synthesis and transfer of galactolipids in the chloroplast envelope membranes of Arabidopsis thaliana. Proc Natl Acad Sci U S A. 2016:**113**(38):10714–10719. https://doi.org/10.1073/pnas.1609184113

Kim, D.I., and Roux, K.J., (2016). Filling the Void: Proximity-Based Labeling of Proteins in Living Cells. Trends Cell Biol. 2016:**26**(11):804–817. https://doi.org/10.1016/j.tcb.2016.09.004

LaBrant, E., Barnes, A.C., and Roston, R.L., (2018). Lipid transport required to make lipids of photosynthetic membranes. Photosynth Res. 2018:**138**(3):345–360. https://doi.org/10.1007/s11120-018-0545-5

Langridge, W.H.R., Fitzgerald, K.J., Konczt, C., Schellt, J., and Szalay, A.A., (1989). Dual promoter of Agrobacterium tumefaciens mannopine synthase genes is regulated by plant growth hormones (auxin/cytokinin-regulated promoters of opine synthase genes/bacterial luciferase/video imaging).

Lee, J.H., Won, H.J., Oh, E.S., Oh, M.H., and Jung, J.H., (2020). Golden Gate Cloning-Compatible DNA Replicon/2A-Mediated Polycistronic Vectors for Plants. Front Plant Sci. 2020:**11**. https://doi.org/10.3389/fpls.2020.559365

Lei, Y., Lu, L., Liu, H.Y., Li, S., Xing, F., and Chen, L.L., (2014). CRISPR-P: A web tool for synthetic single-guide RNA design of CRISPR-system in plants. Mol Plant. 2014:**7**(9):1494–1496. https://doi.org/10.1093/mp/ssu044

Li, Z., Gao, J., Benning, C., and Sharkey, T.D., (2012). Characterization of photosynthesis in Arabidopsis ER-to-plastid lipid trafficking mutants. Photosynth Res. 2012:**112**(1):49–61. https://doi.org/10.1007/s11120-012-9734-9

Lin, H.Y., Chen, J.C., and Fang, S.C., (2018). A protoplast transient expression system to enable molecular, cellular, and functional studies in phalaenopsis orchids. Front Plant Sci. 2018:**9**(June):1–13. https://doi.org/10.3389/fpls.2018.00843

Lu, B., and Benning, C., (2009). A 25-amino acid sequence of the Arabidopsis TGD2 protein is sufficient for specific binding of phosphatidic acid. Journal of Biological Chemistry. 2009:**284**(26):17420–17427. https://doi.org/10.1074/jbc.M109.016014

Lu, B., Xu, C., Awai, K., Jones, A.D., and Benning, C., (2007). A small ATPase protein of Arabidopsis, TGD3, involved in chloroplast lipid import. Journal of Biological Chemistry. 2007:**282**(49):35945–35953. https://doi.org/10.1074/jbc.M704063200

Lu, J., Xu, Y., Wang, J., Singer, S.D., and Chen, G., (2020). The role of triacylglycerol in plant stress response. Plants. 2020:**9**(4). https://doi.org/10.3390/plants9040472

Maréchal, E., and Bastien, O., (2014). Modeling of regulatory loops controlling galactolipid biosynthesis in the inner envelope membrane of chloroplasts. J Theor Biol. 2014:**361**:1–13. https://doi.org/10.1016/j.jtbi.2014.07.013

Matyash, V., Liebisch, G., Kurzchalia, T. V., Shevchenko, A., and Schwudke, D., (2008). Lipid extraction by methyl-terf-butyl ether for high-throughput lipidomics. In Journal of Lipid Research, pp. 1137–1146. https://doi.org/10.1194/jlr.D700041-JLR200

Michel, A.H., and Kornmann, B., (2012). The ERMES complex and ER-mitochondria connections. Biochem Soc Trans. 2012:**40**(2):445–450. https://doi.org/10.1042/BST20110758

Mongrand, S., Bessoule, J.-J., Cabantous, F., and Cassagne, C., (1998). The C16:3\C18:3 fatty acid balance in photosynthetic tissues from 468 plant species. Phytochemistry. 1998:**49**(4):1049–1064. https://doi.org/10.1016/S0031-9422(98)00243-X

Moreau, F., Dupont, J., and Lance, C., (1974). Phospholipid and fatty acid composition of outer and inner membranes of plant mitochondria. BBA - Biomembranes. 1974:**345**(3):294–304. https://doi.org/10.1016/0005-2736(74)90191-6

Nakamura, Y., Koizumi, R., Shui, G., Shimojima, M., Wenk, M.R., Ito, T., and Ohtad, H., (2009). Arabidopsis lipins mediate eukaryotic pathway of lipid metabolism and cope critically with phosphate starvation. Proc Natl Acad Sci U S A. 2009:**106**(49):20978–20983. https://doi.org/10.1073/pnas.0907173106

Nakamura, Y., Tsuchiya, M., and Ohta, H., (2007). Plastidic phosphatidic acid phosphatases identified in a distinct subfamily of lipid phosphate phosphatases with prokaryotic origin. Journal of Biological Chemistry. 2007:**282**(39):29013–29021. https://doi.org/10.1074/jbc.M704385200

Nguyen, V.C., and Nakamura, Y., (2023). Distinctly localized lipid phosphate phosphatases mediate endoplasmic reticulum glycerolipid metabolism in Arabidopsis. Plant Cell. 2023:**35**(5):1548–1571. https://doi.org/10.1093/plcell/koad021

Ongun, A., and Mudd, J.B., (1968). Biosynthesis of galactolipids in plants. Journal of Biological Chemistry. 1968:**243**(7):1558–1566. https://doi.org/10.1016/s0021-9258(18)93578-7

Paradis, S., Villasuso, A.L., Aguayo, S.S., Maldiney, R., Habricot, Y., Zalejski, C., Machado, E., Sotta, B., Miginiac, E., and Jeannette, E., (2011). Arabidopsis thaliana lipid phosphate phosphatase 2 is involved in abscisic acid signalling in leaves. Plant Physiology and Biochemistry. 2011:**49**(3):357–362. https://doi.org/10.1016/j.plaphy.2011.01.010

Roston, R.L., Gao, J., Murcha, M.W., Whelan, J., and Benning, C., (2012). TGD1, -2, and -3 proteins involved in lipid trafficking form ATP-binding cassette (ABC) transporter with multiple substrate-binding proteins. Journal of Biological Chemistry. 2012:**287**(25):21406–21415. https://doi.org/10.1074/jbc.M112.370213

Roston, R.L., Wang, K., Kuhn, L.A., and Benning, C., (2014). Structural determinants allowing transferase activity in sensitive to freezing 2, classified as a family i lycosyl

hydrolase. Journal of Biological Chemistry. 2014:**289**(38):26089–26106. https://doi.org/10.1074/jbc.M114.576694

Roux, K.J., Kim, D.I., Burke, B., and May, D.G., (2018). BioID: A Screen for Protein-Protein Interactions. Curr Protoc Protein Sci. 2018:**91**(1):19.23.1-19.23.15. https://doi.org/10.1002/cpps.51

Schindelin, J., Arganda-Carreras, I., Frise, E., Kaynig, V., Longair, M., Pietzsch, T., Preibisch, S., Rueden, C., Saalfeld, S., Schmid, B., et al., (2012). Fiji: An open-source platform for biological-image analysis. Nat Methods. 2012:**9**(7):676–682. https://doi.org/10.1038/nmeth.2019

Shi, L., Marti Ferrando, T., Landeo Villanueva, S., Joosten, M.H.A.J., Vleeshouwers, V.G.A.A., and Bachem, C.W.B., (2023). Protocol to identify protein-protein interaction networks in Solanum tuberosum using transient TurboID-based proximity labeling. STAR Protoc. 2023:**4**(4):102577. https://doi.org/10.1016/j.xpro.2023.102577

Simidjiev, I., Stoylova, S., Amenitsch, H., Já vorfi, T., szló Mustá rdy, L., Laggner, P., and Holzenburg, A., (2000). Self-assembly of large, ordered lamellae from non-bilayer lipids and integral membrane proteins in vitro.

Soria-García, Á., Rubio, M.C., Lagunas, B., López-Gomollón, S., De Los Ángeles Luján, M., Díaz-Guerra, R., Picorel, R., and Alfonso, M., (2019). Tissue distribution and specific contribution of Arabidopsis FAD7 and FAD8 plastid desaturases to the JA- And ABA-mediated cold stress or defense responses. Plant Cell Physiol. 2019:**60**(5):1025–1040. https://doi.org/10.1093/pcp/pcz017

Tietz, S., Leuenberger, M., Höhner, R., Olson, A.H., Fleming, G.R., and Kirchhoff, H., (2020). A proteoliposome-based system reveals how lipids control photosynthetic light harvesting. Journal of Biological Chemistry. 2020:**295**(7):1857–1866. https://doi.org/10.1074/jbc.RA119.011707

Tsugama, D., Liu, S., and Takano, T., (2011). A rapid chemical method for lysing Arabidopsis cells for protein analysis. Plant Methods. 2011:**7**(1):1–7. https://doi.org/10.1186/1746-4811-7-22

Wang, Z., Anderson, N.S., and Benning, C., (2013). The phosphatidic acid binding site of the arabidopsis trigalactosyldiacylglycerol 4 (TGD4) protein required for lipid import into chloroplasts. Journal of Biological Chemistry. 2013:**288**(7):4763–4771. https://doi.org/10.1074/jbc.M112.438986

Wang, Z., Xu, C., and Benning, C., (2012). TGD4 involved in endoplasmic reticulum-to-chloroplast lipid trafficking is a phosphatidic acid binding protein. Plant Journal. 2012:**70**(4):614–623. https://doi.org/10.1111/j.1365-313X.2012.04900.x

Wang, Z.P., Xing, H.L., Dong, L., Zhang, H.Y., Han, C.Y., Wang, X.C., and Chen, Q.J., (2015). Egg cell-specific promoter-controlled CRISPR/Cas9 efficiently generates homozygous mutants for multiple target genes in Arabidopsis in a single generation. Genome Biol. 2015:**16**(1). https://doi.org/10.1186/s13059-015-0715-0

Xie, K., Minkenberg, B., and Yang, Y., (2015). Boosting CRISPR/Cas9 multiplex editing capability with the endogenous tRNA-processing system. Proc Natl Acad Sci U S A. 2015:**112**(11):3570–3575. https://doi.org/10.1073/pnas.1420294112

Xu, C., Fan, J., Cornish, A.J., and Benning, C., (2008). Lipid trafficking between the endoplasmic reticulum and the plastid in Arabidopsis requires the extraplastidic TGD4 protein. Plant Cell. 2008:**20**(8):2190–2204. https://doi.org/10.1105/tpc.108.061176

Xu, C., Fan, J., Froehlich, J.E., Awai, K., and Benning, C., (2005). Mutation of the TGD1 chloroplast envelope protein affects phosphatidate metabolism in Arabidopsis. Plant Cell. 2005:**17**(11):3094–3110. https://doi.org/10.1105/tpc.105.035592

Xu, C., Fan, J., Riekhof, W., Froehlich, J.E., and Benning, C., (2003). A permease-like protein involved in ER to thylakoid lipid transfer in Arabidopsis. 2003:**22**(10). https://doi.org/10.1093/emboj/cdg234

Yu, C.W., Lin, Y.T., and Li, H. min, (2020). Increased ratio of galactolipid MGDG : DGDG induces jasmonic acid overproduction and changes chloroplast shape. New Phytologist. 2020:**228**(4):1327–1335. https://doi.org/10.1111/nph.16766

Zhang, Y., Li, Y., Yang, X., Wen, Z., Nagalakshmi, U., and Dinesh-Kumar, S.P., (2020a). TurboID-Based Proximity Labeling for In Planta Identification of Protein-Protein Interaction Networks. Journal of Visualized Experiments. 2020:**176**(159):139–148. https://doi.org/10.3791/60728

Zhang, Y., Sampathkumar, A., Kerber, S.M.-L., Swart, C., Hille, C., Seerangan, K., Graf, A., Sweetlove, L., and Fernie, A.R., (2020b). A moonlighting role for enzymes of glycolysis in the co-localization of mitochondria and chloroplasts. Nat Commun. 2020:**11**(1). https://doi.org/10.1038/s41467-020-18234-w

Zhang, Y., Song, G., Lal, N.K., Nagalakshmi, U., Li, Y., Zheng, W., Huang, P. jui, Branon, T.C., Ting, A.Y., Walley, J.W., et al., (2019). TurboID-based proximity labeling reveals that UBR7 is a regulator of N NLR immune receptor-mediated immunity. Nat Commun. 2019:**10**(1). https://doi.org/10.1038/s41467-019-11202-z

SUPPLEMENTARY DATA

Supplementary Figure 1: Chromatogram of tgd4-4 compared to Col-0. Nucleotide sequence (Nuc. Seq.) of Col-0 and *tgd4-4*, depicting the in-frame deletion 85 amino acids that leads to the resulting amino acid sequence (Aa. Seq.) in *tgd4-4* mutants.

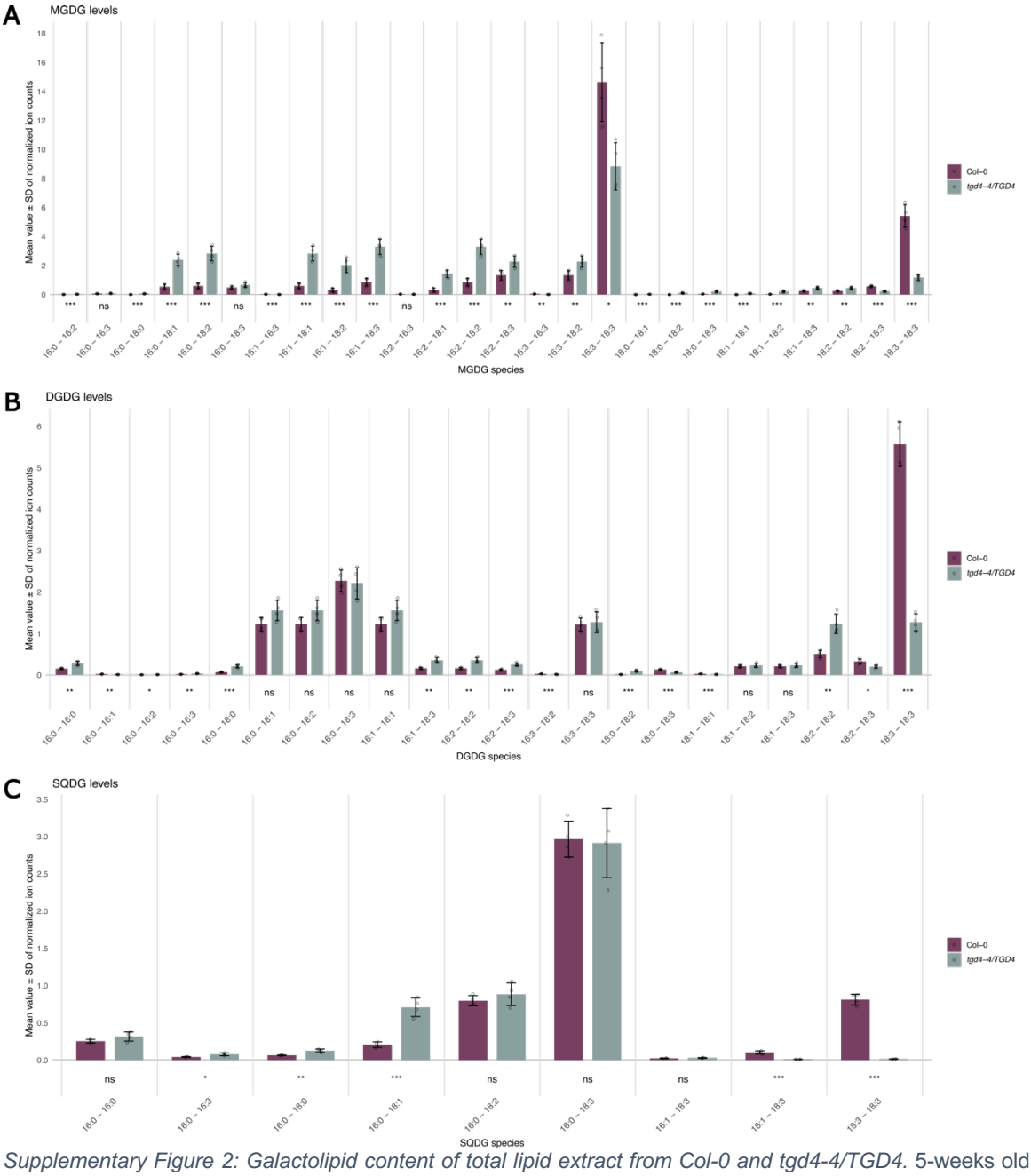

Supplementary Figure 2: Galactolipid content of total lipid extract from Col-0 and tgd4-4/TGD4. 5-weeks old plants were harvested and plant material used for lipid extraction. Content of detected lipid species of MGDG (A), DGDG (B) and SQDG (C) are shown as mean value ± SD of normalized ion counts from 4 biological replicates of Col-0 and *tgd4-4/TGD4*. Significance was calculated via Student's t-test (ns = *p*-value > 0.05; * = *p*-value < 0.05; ** = *p*-value < 0.01; *** = *p*-value < 0.001).

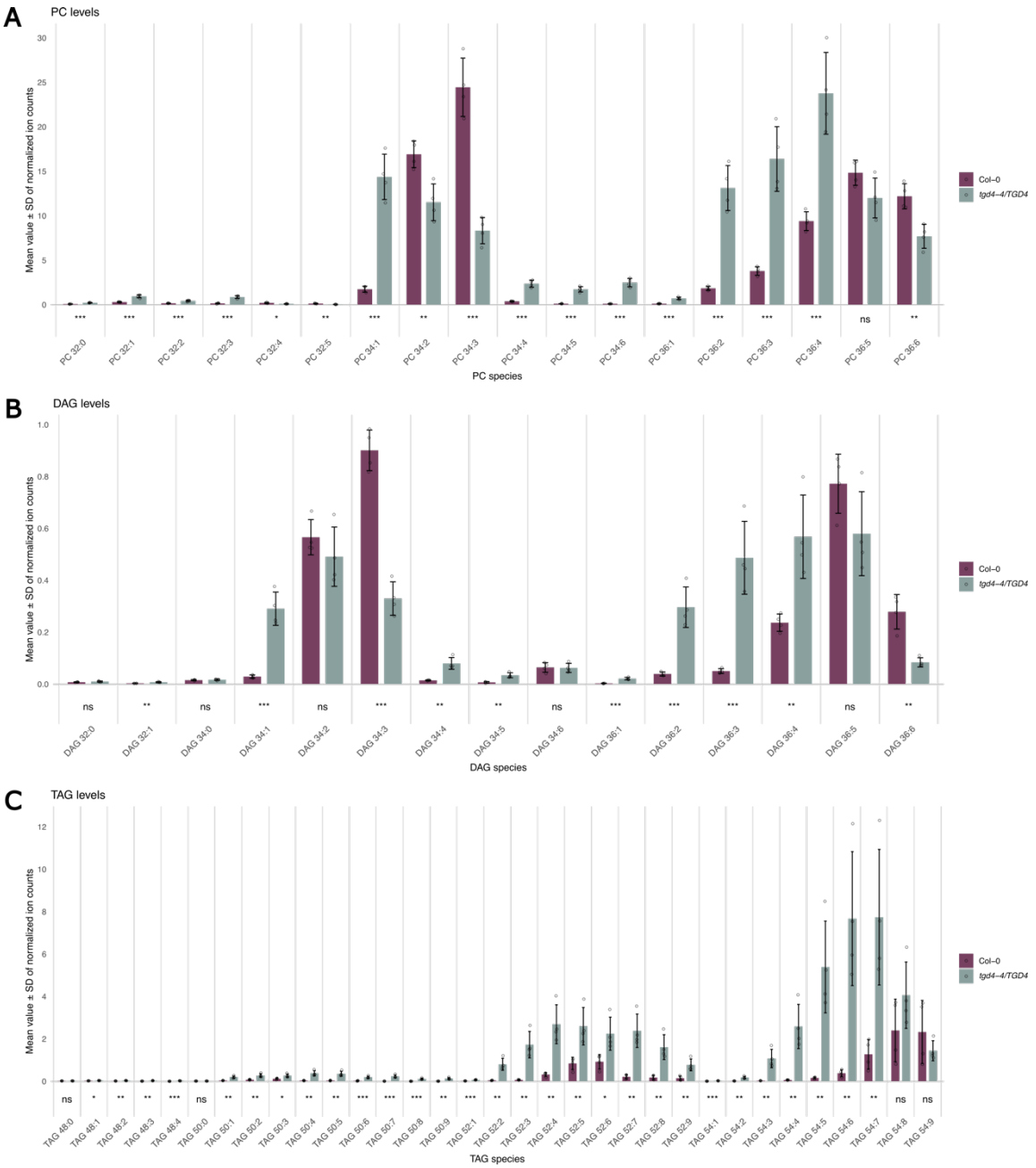

Supplementary Figure 3: Phosphatidylcholine (PC), diacylglycerol (DAG) and triacylglycerol (TAG) content of total lipid extract from Col-0 and tgd4-4/TGD4. 5-weeks old plants were harvested and plant material used for lipid extraction. Content of detected lipid species of PC (A), DAG (B), and TAG (C) are shown as mean value ± SD of normalized ion counts from 4 biological replicates of Col-0 and *tgd4-4/TGD4*. Significance was calculated via Student's t-test (ns = *p*-value > 0.05; * = *p*-value < 0.05; ** = *p*-value < 0.01; *** = *p*-value < 0.001).

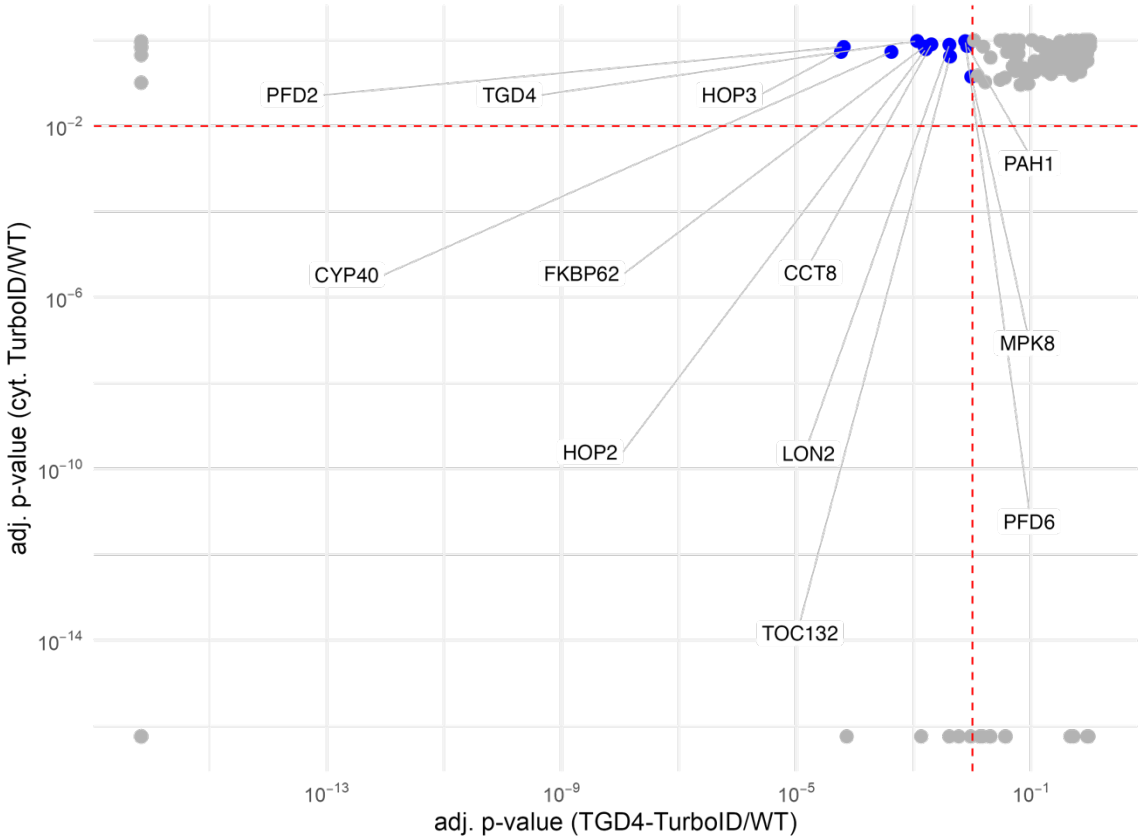

Supplementary Figure 4: Scatterplot of detected proteins by the proximity labeling approach with TGD4 bait protein. Adjusted *p*-values for proteins detected in samples of TGD4-TurboID or cytosolic TurboID, relative to the control, are presented on a logarithmic scale (log10). The red dashed line indicates the 0.01 threshold for adj. *p*-values. Biological relevant proteins are highlighted in blue and labeled with their respective abbreviations. Adj. *p*-values were calculated using Proteome Discoverer (version 2.4.1.15, Thermo Fisher Scientific) with 1% FDR. Abbr.: MAPK8, mitogen-activated kinase 8; TOC132, translocase of chloroplast 132; HOP3, Hsp70-Hsp90 organizing protein 3; CYP40, Peptidyl-prolyl cis-trans isomerase CYP40; HOP2, Hsp70-Hsp90 organizing protein 2; PFD2, Prefoldin subunit 2; FKBP62, Peptidyl-prolyl cis-trans isomerase FKBP62; PAH1, Phosphatidate phosphatase PAH1; LON2, Lon protease homolog 2; CCT8, T-complex protein 1 subunit theta; PFD6, Prefoldin subunit 6; TGD4, Protein TRIGALACTOSYLDIACYLGLYCEROL 4

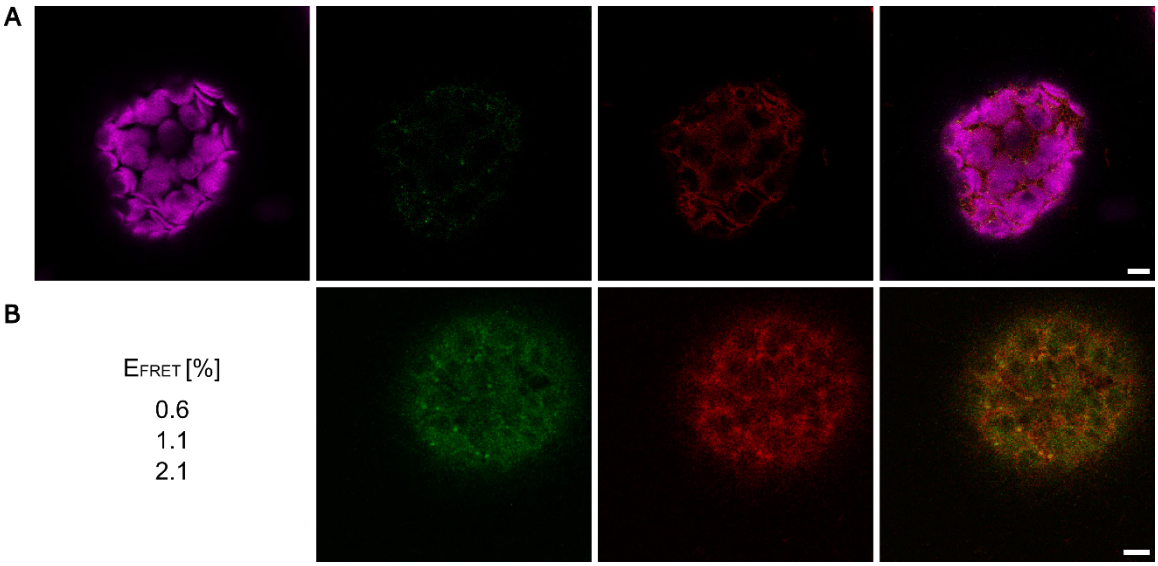

Supplementary Figure 5: Visualization of TGD4-Venus and cytosolic mCherry as control for the cleavable peptide P2A and FRET analysis. Tobacco protoplasts transiently expressing the gene cassette *TGD4-mVenus::P2A::mCherry* showed dot-like TGD4-mVenus fluorescent signal (green) and mCherry fluorescence (red) was visualized in the cytosol (A). Chloroplasts were visualized by their chlorophyll autofluorescence (magenta). FRET efficiencies (E_{FRET}) were measured and calculated as described in material and methods (B). Scale bar = 5 µm.

Supplementary Table 1: Expression constructs used in this study. The constructs listed here were generated by Golden Gate cloning (Engler et al., 2014).

Expression construct	Backbone	Purpose
35Sp::KAO2::GFP1-10 + UBQ10p::OEP7.1::2xGFP11 + MASp::mCherry::Linker 5::TGD4	pAGM4723	Co-localization of TGD4 with ER-chloroplast MCSs
NapinA::GFP + EC1.2p::Cas9 + U6-26p::polycistronic tRNA-gRNA + 2S3p::GFP	pAGM4723	Expression of egg cell-specific Cas9 for genome editing of the *TGD4* gene with four guides targeting the first three exons: - TCAACTCCGGTGACGCTCGA - CGATGTTCAGAGATTCGTAA - TCTGCTGTCAGATTGTGAAG - CGAATCTCTGAACATCGAAT Based on Xie et al., (2015)
35Sp::GFP::TurboID::TGD4	pICH86966	Proximity labeling
35Sp::TurboID::TGD4	pICH86966	
35Sp::TurboID::GFP	pICH86966	
35Sp::mVenus::TGD4::P2A::PAH1:: mCherry	pICH86966	Co-localization/FRET
35Sp::mVenus::TGD4::P2A::mCherry	pICH86966	

Supplementary Table 2: Primer sequences used in this study for cloning and qRT-PCR (qPCR). Primer sequences are compatible for Golden Gate and were used to introduce genes and parts into the MoClo tool kit *(Engler et al., 2014)*. qPCR primers were designed by Primer3 and tested for efficiency.

Primer name	Primer sequence (5' → 3')	Purpose
TGD4_1.fwd	TTGAAGACAATTCGATGAACAGAATGAGATGGG	Cloning of TGD4 into Level 0 backbone
TGD4_1.rev	TTGAAGACAAGAGTCCTAGAGGAAGAGGATCG	
TGD4_2.fwd	TTGAAGACAAACTCTCTAGAGGCACTCGT	
TGD4_2.rev	TTGAAGACAACGATGACCCTCGACCAAAAGC	
TGD4_3.fwd	TTGAAGACAAATCGTCTACAGTAGCTTCT	
TGD4_3.rev	TTGAAGACAAGAAAACATCATAGGGCTTGCA	
TGD4_4.fwd	TTGAAGACAATTTCCTCAGTAGTCCTCA	
TGD4_4.rev	TTGAAGACAAAAGCCTATGTCTCAAAGAAACGAA	

Continued on the next page

Supplementary Table 2 (continued)

At_TGD4_gR1-F	TAGGTCTCCGGTGACGCTCGAGTTTTAGAGCTAGAA	Cloning of CRISPR guides into Level 0 backbone
At_TGD4_gR1-R	ATGGTCTCACACCGGAGTTGATGCACCAGCCGGGAA	
At_TGD4_gR2-F	TAGGTCTCCAGAGATTCGTAAGTTTTAGAGCTAGAA	
At_TGD4_gR2-R	ATGGTCTCACTCTGAACATCGTGCACCAGCCGGGAA	
At_TGD4_gR3-F	TAGGTCTCCCAGATTGTGAAGGTTTTAGAGCTAGAA	
At_TGD4_gR3-R	ATGGTCTCATCTGACAGCAGATGCACCAGCCGGGAA	
At_TGD4_gR4-F	TAGGTCTCCTGAACATCGAATGTTTTAGAGCTAGAA	
At_TGD4_gR4-R	ATGGTCTCATTCAGAGATTCGTGCACCAGCCGGGAA	
TurboID_AGGT.fwd	TTGAAGACAAAGGTAAAGACAATACTGTGCCTCTG	Cloning of TurboID coding
TurboID_AATG.fwd	TTGAAGACATAATGAAAGACAATACTGTGCCTCTG	
TurboID_TTCG.fwd	TTGAAGACAATTCGAAAGACAATACTGTGCCTCTG	
TurboID_TTCG.rev	TTGAAGACAACGAACCTCCAGATGCGTAATCCGGTACATCG	
TurboID_GCTT.rev	TTGAAGACAAAAGCTTATGCGTAATCCGGTACATCG	
TurboID_AGGT.rev	TTGAAGACAAACCTGATGATCCTGCGTAATCCGGTACATCG	
P2A.fwd	TTGAAGACAAAGGTGCTACTAATTTTTCTCTTCTTAA	Cloning of cleavable (P2A) and non-cleavable peptide (P2A*; by site-directed mutagenesis) in pAGM1299
P2A.rev	TTGAAGACAACGAACCGCCCGAG	
P2A*.fwd	AAATCCTGGAGCGTCGGGCGG	
P2A*.fwd	TCTTCAACATCTCCAGCTTGC	
mCherry-pAGM1301.fwd	TTGAAGACAATTCGATGGTGAGCAAGGGC	Cloning of mCherry in pAGM1301
mCherry-pAGM1301.rev	TTGAAGACAAAAGCTCACTTGTACAGCTCGTCCATGC	
TGD4_mVenus.fwd	TTGAAGACAATTCTATGAACAGAATGAGATGGGT	Cloning of TGD4 with mVenus
TGD4_mVenus.rev	TTGAAGACAAACCTGATGTCTCAAAGAAACGAAGCT	
PAH-mCherry.fwd	TTGGTCTCAGGATCAGGATCAATGGTGAGCAAGGGC	Cloning of PAH1 with mCherry
PAH-mCherry.rev	TTGGTCTCAACAAAAGCTCATGATCCCTTGTACAGCTC	
mVenus_C.fwd	AAGGTCTCAACATGGATCAGGATCAATGGTGAGCAAGGGCGAGG	Cloning of mVenus in pAGM1311 with overlap to the gene and pICH41258
mVenus_N.fwd	TTGGTCTCAACATAATGGTGAGCAAGGGCGAGG	
mVenus_C.rev	TTTGGTCTCAACAAACCTGACTTGTACAGCTCGTCCATGCC	
mVenus_N.rev	TTGGTCTCAACAAAGAACCACTACCCTTGTACAGCTCGTCCATGCC	

Continued on the next page

Supplementary Table 2 (continued)

GFP_N.fwd	TTGGTCTCAACATAATGTCTAAGGGCGAAGAG	Cloning of GFP in pAGM1311 with overlap to the gene and pICH41258
GFP_C.rev	TTTGGTCTCAACAAACCTGACGTGATGCCAGCTGC	
GFP_C.fwd	AAGGTCTCAACATGGATCAGGATCAATGTCTAAGG GCGAAGAG	
GFP_N.rev	TTGGTCTCAACAAAGAACCACTACCCGTGATGCCA GCTGC	
mCherry_N.fwd	TTGGTCTCAACATTTCGATGGTGAGCAAGGGC	Cloning of mCherry in pAGM1311 with overlap to the gene and pAGM1301
mCherry_N.rev	TTGGTCTCAACAAAGAACCACTACCCTTGTACAGC TC	
mCherry_C.fwd	AAGGTCTCAACATGGATCAGGATCAATGGTGAGCA AGGGC	
mCherry_C.rev	TTTGGTCTCAACAAAAGCTCATGATCCCTTGTACAG CTC	
TGD4_qPCR.fwd	GAACGGAGCTAACCCTGTGA	qPCR on *TGD4* transcript
TGD4_qPCR.rev	AACAGCCTTGGCAGAAAGAA	
PAH1_qPCR.fwd	GCCATCGTTCAGGCATATCT	qPCR on *PAH1* transcript
PAH1_qPCR.rev	AGGCCATCTGGTGAAATGAC	
SFR2_qPCR.fwd	ATTAAGGTCGCCGGACTTTT	qPCR on *SFR2* transcript
SFR2_qPCR.rev	TCGATTGGAGAGCGAAACTT	
TGD4ΔPA2_qPCR.fwd	ATCACGAGTTTCCGCTTCAC	qPCR on *TGD4* transcript
TGD4ΔPA2_qPCR.rev	GGCACATCCCAATATTCACC	
TGD4_T-DNA_qPCR.fwd	CGGCAGCCTAGTTTAGAAGC	
TGD4_T-DNA_qPCR.rev	CGATCTCAATTCCAGACTCCA	
qFAD7_F	CTCTCCAACAACAACAAATTCAGAC	*FAD7* transcript primer by Soria-García et al., (2019)
qFAD7_R	CCAAAAGACAGAGGAGATGATGAT	
FAD6_qPCR.fwd	ATCACCCGTGATGAGAAAGG	qPCR on *FAD6* transcript
FAD6_qPCR.rev	GAAGTGCCAGTTCACCCAGT	
TGD4_short.rev	ttGAAGACaaGAAAACATCATAGGGCTTGCA	Verification of *tgd4-4* (Genotyping and semi-qPCR)
TGD4.fwd	ATCGGTCGACATGAACAGAATGAGATGGG	
TGD4.rev	GCTAACTAGTCTATGTCTCAAAGAAACGAA	
SAIL_760_F05 RP	TCGCAGTATCTGGGATTATCG	Genotyping of *tgd4-2* T-DNA insertion
SAIL_760_F05 LP	ATGCGGCCGCTGTCTCAAAGAAACGAAG	

Supplementary Table 3: Precursor mass for MGDG lipid species.

MGDG	Molecular formula	Precursor adduct	Precursor mass (m/z)
16:0_18:3	C43H76O10	$[M+HCOO^-]^-$	797.54
16:1_18:3	C43H74O10	$[M+HCOO^-]^-$	795.53
16:2_18:3	C43H72O10	$[M+HCOO^-]^-$	793.51
16:3_18:3	C43H70O10	$[M+HCOO^-]^-$	791.50
18:0_18:3	C45H80O10	$[M+HCOO^-]^-$	825.57
18:1_18:3	C45H78O10	$[M+HCOO^-]^-$	823.56
18:2_18:3	C45H76O10	$[M+HCOO^-]^-$	821.54
18:3_18:3	C45H74O10	$[M+HCOO^-]^-$	819.53
16:0_18:2	C43H78O10	$[M+HCOO^-]^-$	799.56
16:1_18:2	C43H76O10	$[M+HCOO^-]^-$	797.54
16:2_18:2	C43H74O10	$[M+HCOO^-]^-$	795.53
16:3_18:2	C43H72O10	$[M+HCOO^-]^-$	793.51
18:0_18:2	C45H82O10	$[M+HCOO^-]^-$	827.59
18:1_18:2	C45H80O10	$[M+HCOO^-]^-$	825.57
18:2_18:2	C45H78O10	$[M+HCOO^-]^-$	823.56
16:0_18:1	C43H80O10	$[M+HCOO^-]^-$	801.57
16:1_18:1	C43H78O10	$[M+HCOO^-]^-$	799.56
16:2_18:1	C43H76O10	$[M+HCOO^-]^-$	797.54
18:0_18:1	C45H84O10	$[M+HCOO^-]^-$	829.60
18:1_18:1	C45H82O10	$[M+HCOO^-]^-$	827.59
16:0_18:0	C43H82O10	$[M+HCOO^-]^-$	803.59
16:0_16:3	C41H72O10	$[M+HCOO^-]^-$	769.51
16:1_16:3	C41H70O10	$[M+HCOO^-]^-$	767.50
16:2_16:3	C41H68O10	$[M+HCOO^-]^-$	765.48
16:3_16:3	C41H66O10	$[M+HCOO^-]^-$	763.46
16:0_16:2	C41H74O10	$[M+HCOO^-]^-$	771.53

Supplementary Table 4: Precursor mass for DGDG lipid species.

DGDG	Molecular formula	Precursor adduct	Precursor mass (m/z)
16:0_18:3	C49H86O15	$[M+HCOO^-]^-$	959.59
16:1_18:3	C49H84O15	$[M+HCOO^-]^-$	957.58
16:2_18:3	C49H82O15	$[M+HCOO^-]^-$	955.56
16:3_18:3	C49H80O15	$[M+HCOO^-]^-$	953.55

Continued on the next page

Supplementary Table 4 (continued)

18:0_18:3	C51H90O15	$[M+HCOO^-]^-$	987.63
18:1_18:3	C51H88O15	$[M+HCOO^-]^-$	985.61
18:2_18:3	C51H86O15	$[M+HCOO^-]^-$	983.59
18:3_18:3	C51H84O15	$[M+HCOO^-]^-$	981.58
16:0_18:2	C49H88O15	$[M+HCOO^-]^-$	961.61
16:2_18:2	C49H84O15	$[M+HCOO^-]^-$	957.58
16:3_18:2	C49H82O15	$[M+HCOO^-]^-$	955.56
18:0_18:2	C51H92O15	$[M+HCOO^-]^-$	989.64
18:1_18:2	C51H90O15	$[M+HCOO^-]^-$	987.63
18:2_18:2	C51H88O15	$[M+HCOO^-]^-$	985.61
16:0_18:1	C49H90O15	$[M+HCOO^-]^-$	963.63
16:1_18:1	C49H88O15	$[M+HCOO^-]^-$	961.61
18:1_18:1	C51H92O15	$[M+HCOO^-]^-$	989.64
16:0_18:0	C49H92O15	$[M+HCOO^-]^-$	965.64
16:0_16:3	C47H82O15	$[M+HCOO^-]^-$	931.56
16:0_16:2	C47H84O15	$[M+HCOO^-]^-$	933.58
16:0_16:1	C47H86O15	$[M+HCOO^-]^-$	935.59
16:0_16:0	C47H88O15	$[M+HCOO^-]^-$	937.61

Supplementary Table 5: Precursor mass for SQDG lipid species.

SQDG	**Molecular formula**	**Precursor adduct**	**Precursor mass (m/z)**
16:0_18:3	C43H76O12S	$[M-H]^-$	815.50
16:1_18:3	C43H74O12S	$[M-H]^-$	813.48
18:1_18:3	C45H78O12S	$[M-H]^-$	841.51
18:3_18:3	C45H74O12S	$[M-H]^-$	837.48
16:0_18:2	C43H78O12S	$[M-H]^-$	817.51
16:0_18:1	C43H80O12S	$[M-H]^-$	819.53
16:0_18:0	C43H82O12S	$[M-H]^-$	821.55
16:0_16:3	C41H72O12S	$[M-H]^-$	787.47
16:0_16:0	C41H78O12S	$[M-H]^-$	793.51

Supplementary Table 6: Precursor mass for TGDG lipid species.

TGDG*	Molecular formula	Precursor adduct	Precursor mass (m/z)
34:1	C55H100O20	$[M+HCOO^-]^-$	1125.68
34:2	C55H98O20	$[M+HCOO^-]^-$	1123.67
34:3	C55H96O20	$[M+HCOO^-]^-$	1121.65
34:4	C55H94O20	$[M+HCOO^-]^-$	1119.63
34:5	C55H92O20	$[M+HCOO^-]^-$	1117.62
34:6	C55H90O20	$[M+HCOO^-]^-$	1115.60
36:1	C57H104O20	$[M+HCOO^-]^-$	1153.71
36:2	C57H102O20	$[M+HCOO^-]^-$	1151.70
36:3	C57H100O20	$[M+HCOO^-]^-$	1149.68
36:4	C57H98O20	$[M+HCOO^-]^-$	1147.66
36:5	C57H96O20	$[M+HCOO^-]^-$	1145.65
36:6	C57H94O20	$[M+HCOO^-]^-$	1143.63

*Due to low levels, reliable fragmentation data was not available for TGDG species.

Supplementary Table 7: Precursor mass for TAG lipid species.

TAG	Molecular formula	Precursor adduct	Precursor mass (m/z)
48:0	C51H98O6	$[M+NH4^+]^+$	824.77
48:1	C51H96O6	$[M+NH4^+]^+$	822.75
48:2	C51H94O6	$[M+NH4^+]^+$	820.74
48:3	C51H92O6	$[M+NH4^+]^+$	818.72
48:4	C51H90O6	$[M+NH4^+]^+$	816.71
50:0	C53H102O6	$[M+NH4^+]^+$	852.80
50:1	C53H100O6	$[M+NH4^+]^+$	850.79
50:2	C53H98O6	$[M+NH4^+]^+$	848.77
50:3	C53H96O6	$[M+NH4^+]^+$	846.75
50:4	C53H94O6	$[M+NH4^+]^+$	844.74
50:5	C53H92O6	$[M+NH4^+]^+$	842.72
50:6	C53H90O6	$[M+NH4^+]^+$	840.71
50:7	C53H88O6	$[M+NH4^+]^+$	838.69
50:8	C53H86O6	$[M+NH4^+]^+$	836.68
50:9	C53H84O6	$[M+NH4^+]^+$	834.66
52:1	C55H104O6	$[M+NH4^+]^+$	878.82
52:2	C55H102O6	$[M+NH4^+]^+$	876.80

Continued on the next page

Supplementary Table 7 (continued)

52:3	C55H100O6	$[M+NH4^+]^+$	874.79
52:4	C55H98O6	$[M+NH4^+]^+$	872.77
52:5	C55H96O6	$[M+NH4^+]^+$	870.75
52:6	C55H94O6	$[M+NH4^+]^+$	868.74
52:7	C55H92O6	$[M+NH4^+]^+$	866.72
52:8	C55H90O6	$[M+NH4^+]^+$	864.71
52:9	C55H88O6	$[M+NH4^+]^+$	862.69
54:1	C57H108O6	$[M+NH4^+]^+$	906.85
54:2	C57H106O6	$[M+NH4^+]^+$	904.83
54:3	C57H104O6	$[M+NH4^+]^+$	902.82
54:4	C57H102O6	$[M+NH4^+]^+$	900.80
54:5	C57H100O6	$[M+NH4^+]^+$	898.79
54:6	C57H98O6	$[M+NH4^+]^+$	896.77
54:7	C57H96O6	$[M+NH4^+]^+$	894.75
54:8	C57H94O6	$[M+NH4^+]^+$	892.74
54:9	C57H92O6	$[M+NH4^+]^+$	890.72

Supplementary Table 8: Precursor mass for DAG lipid species.

DAG	**Molecular formula**	**Precursor adduct**	**Precursor mass (m/z)**
32:0	C35H68O5	$[M+NH4^+]^+$	586.54
32:1	C35H66O5	$[M+NH4^+]^+$	584.52
34:0	C37H72O5	$[M+NH4^+]^+$	614.57
34:1	C37H70O5	$[M+NH4^+]^+$	612.56
34:2	C37H68O5	$[M+NH4^+]^+$	610.54
34:3	C37H66O5	$[M+NH4^+]^+$	608.52
34:4	C37H64O5	$[M+NH4^+]^+$	606.51
34:5	C37H62O5	$[M+NH4^+]^+$	604.49
34:6	C37H60O5	$[M+NH4^+]^+$	602.48
36:1	C39H74O5	$[M+NH4^+]^+$	640.59
36:2	C39H72O5	$[M+NH4^+]^+$	638.57
36:3	C39H70O5	$[M+NH4^+]^+$	636.56
36:4	C39H68O5	$[M+NH4^+]^+$	634.54
36:5	C39H66O5	$[M+NH4^+]^+$	632.52
36:6	C39H64O5	$[M+NH4^+]^+$	630.51

Supplementary Table 9: Precursor mass for PC lipid species.

PC	Molecular formula	Precursor adduct	Precursor mass (m/z)
32:0	C40H80NO8P	$[M+H]^+$	734.57
32:1	C40H78NO8P	$[M+H]^+$	732.55
32:2	C40H76NO8P	$[M+H]^+$	730.54
32:3	C40H74NO8P	$[M+H]^+$	728.52
32:4	C40H72NO8P	$[M+H]^+$	726.51
32:5	C40H70NO8P	$[M+H]^+$	724.49
34:1	C42H82NO8P	$[M+H]^+$	760.59
34:2	C42H80NO8P	$[M+H]^+$	758.57
34:3	C42H78NO8P	$[M+H]^+$	756.55
34:4	C42H76NO8P	$[M+H]^+$	754.54
34:5	C42H74NO8P	$[M+H]^+$	752.52
34:6	C42H72NO8P	$[M+H]^+$	750.51
36:1	C44H86NO8P	$[M+H]^+$	788.62
36:2	C44H84NO8P	$[M+H]^+$	786.60
36:3	C44H82NO8P	$[M+H]^+$	784.59
36:4	C44H80NO8P	$[M+H]^+$	782.57
36:5	C44H78NO8P	$[M+H]^+$	780.55
36:6	C44H76NO8P	$[M+H]^+$	778.54

All precursor masses were identified within an error of 4 ppm.

Chapter III:

Immunopurification of intact chloroplasts: A gateway for rapid identification of proteins at membrane contact sites

Vanessa Valencia[1], Franziska Kuhnert[1]†, Danielle Glatter[1], Anja Stefanski[2], Kai Stühler[2], Andreas P.M. Weber[1]

[1] Institute of Plant Biochemistry, SFB1208, Heinrich Heine University, Universitätsstrasse 1, 40225 Düsseldorf, Germany
[2] Molecular Proteomics Laboratory (MPL), Biologisch-Medizinisches Forschungszentrum (BMFZ), Heinrich Heine University, Universitätsstrasse 1, 40225 Düsseldorf, Germany
† Plant Energy Biology, University of Western Australia; Crawley, 6009, Australia

Author contribution: VV performed plant selection, cloning, developed immunopurification method, performed immunoblots, prepared protein samples for mass spectrometry, performed proteomic analyses; DG assisted with cell-type specific promoter studies; AS and KS supervised and performed mass spectrometric analyses of protein samples; FK performed cloning, generation of transgenic Arabidopsis lines and conceptualized the project; APMW designed and supervised the research and the experiments.

ABSTRACT

Plants contain various plastid types across tissues, each serving distinct functions in development and environmental responses. For instance, the chloroplasts – the most extensively studied type of plastids - are found in green tissues and house the photosynthetic machinery. Understanding the functional and molecular roles of plastids requires effective isolation techniques, particularly for studying subdomains, such as plastid-associated membranes (PLAMs), which are hypothesized to facilitate processes like lipid trafficking but remain poorly understood. Traditional chloroplast isolation methods are time-consuming and require large amounts of plant material. In this study, we established a rapid and reliable isolation method for isolating intact chloroplasts from Arabidopsis rosettes using a single epitope-tag targeted to the chloroplast outer envelope. Additionally, chloroplast envelopes were separated using osmotic pressure, allowing for the enrichment of envelope proteins potentially involved in PLAMs and other membrane contact sites. The system is adaptable for cell-type specific studies by modulating expression with promoters such as *SULTR2;2* for bundle sheath-specific expression. In summary, the use of one epitope-tag targeted to the chloroplast outer envelope allowed efficient isolation of chloroplasts, which will broaden the understanding of molecular mechanisms in chloroplasts and help to unravel the molecular basis of plastid associated membranes.

INTRODUCTION

Plastids govern multiple functions in plant cells. Depending on the tissue and cell-types, different plastid types develop and facilitate distinct functions. Proplastids, found in meristems, represent the undifferentiated state of plastids. From this state, leucoplasts form in non-green tissues. They include starch-enriched amyloplasts, protein-enriched proteinoplasts or lipid-enriched elaioplasts. In green-tissue, chloroplasts house well-characterized pathways such as oxygenic photosynthesis including the carbon fixation reaction, and a part of the photorespiratory cycle. Chromoplasts, which accumulate carotenoids and contribute to pigmentation, are typically found in reproductive tissues. Gerontoplasts are senescing chloroplasts, which are characterized by the accumulation of plastoglobuli and degradation of thylakoid membranes, in preparation to recycle nutrients within the plant cell (Choi et al., 2021). Among plastids, chloroplasts are the most extensively studied type. However, their functions vary between different cell-types. For instance, the electron transport chain in guard cell chloroplasts supplies energy for stomatal function (Lawson, 2009), epidermal plastids play a role in defense mechanisms against pathogens (Irieda and Takano, 2021), and mesophyll cells contain large chloroplasts, which are the primary sites of photosynthesis within the plant. In C_4-plants, mesophyll and bundle sheath cells contain functionally distinct chloroplasts to enable spatial separation of carbon fixation. In addition, in C_3-plants like Arabidopsis, chloroplasts differ between cell types in terms of amino acid metabolism or signaling (Gowik and Westhoff, 2011; Lundquist et al., 2014). Even within a cell type, differences might be present. For instance, the mesophyll is divided in palisade and spongy parenchyma with differences on RNA level (Kim et al., 2021), suggesting differences in functions and regulations in these cells, and possibly extend to their chloroplasts. Many of these differences remain poorly understood at the molecular level.

Multiple functions of chloroplasts are in a dynamic interaction with other organelles. For example, galactolipid biosynthesis is subdivided across the endoplasmic reticulum (ER) and chloroplast, while photorespiration involves chloroplasts, mitochondria and peroxisomes (LaBrant et al., 2018; Eisenhut et al., 2019). Such inter-organelle interactions and communication processes might be facilitated by membrane contact sites (MCSs) - regions of close proximity between interacting membranes. Plastid associated ER membrane patches (PLAMs) have been observed during chloroplast isolation procedures. They exhibit a strong affinity towards the chloroplast surface, resembling those of protein-protein interactions (Andersson et al., 2007). Since chloroplasts also interact with other organelles via MCSs (Zhang et al., 2020), some membrane patches from other organelles

may remain attached to isolated chloroplasts. The precise nature of PLAMs and other MCS-like structures remain unclear.

Traditional plastid isolation procedures include differential centrifugation followed by Percoll density gradient purification (Joy and Mills, 1987). These methods yield a high amount of intact plastids, and were previously used to advance research on the plastids' proteome in *Arabidopsis thaliana* (Arabidopsis) (Kleffmann et al., 2004), tomato (Tamburino et al., 2017), cassava (Chang et al., 2019), and wheat (Zhu et al., 2021), on functional dynamics such as protein import in pea (Chu and Li, 2015) and Arabidopsis (Aronsson and Jarvis, 2002), and on photosynthesis in Arabidopsis (Seigneurin-Berny et al., 2008). However, these methods are time-consuming, often rely on high amounts of plant material (Satori et al., 2012), and typically isolate plastids without resolving cell-type specificity. An alternative strategy based on immunopurification uses anti-YFP antibody, but requires the isolation of protoplasts prior to chloroplast purification (Truernit and Hibberd, 2007). Recently, a new isolation method, called IPTACT (Isolation of Plastids TAgged in specific Cell Types), using biotinylated chloroplasts was developed (Boussardon and Keech, 2023). Similar to the immunopurification method, IPTACT relies on the generation of transgenic plants, which express a biotin ligase. However, the use of BirA requires the expression of the biotin ligase recognition peptide targeted to the chloroplast outer envelope, further expanding the size of the T-DNA construct. Thereby, the biotin ligase biotinylates the surface of the chloroplast, enabling affinity purification via streptavidin. Additionally, plants contain endogenous biotinylated proteins such as carboxylases, which might get enriched during purification (Boussardon and Keech, 2023). In previous work, mitochondria were successfully isolated using the triple hemagglutinin epitope-tag targeted to the surface of the mitochondria, followed by immunopurification with anti-hemagglutinin magnetic beads. The immunopurified mitochondria have been subjected to proteomic analysis, respiratory measurements, and enzyme assays, proving their intactness and activity of intrinsic enzymes (Kuhnert et al., 2020).

Building on these studies and previous work by Kuhnert et al., (2020), this project aims to increase the understanding of plastids and their communication with the intracellular environment by establishing a rapid isolation method for plastids based on a small, single-gene-encoded epitope-tag, targeted to the chloroplast outer envelope. Intact epitope-tagged chloroplasts are immunopurified with antibody-coated beads and subjected to proteomic analysis, confirming their intactness and highlighting their potential to identify PLAM- and MCS-associated proteins.

MATERIAL AND METHODS

ARABIDOPSIS THALIANA GROWTH CONDITIONS

Arabidopsis thaliana (Arabidopsis) Col-0 was used in this study. Seeds were sterilized by washing twice with 70% ethanol supplemented with 1% (v/v) Triton X-100, followed by washing twice with 100% ethanol. Seeds were germinated on 0.5-strength Murashige and Skoog (MS) medium supplemented with 0.8% (w/v) agar under 12 h light/12 h dark cycle (22 °C/18 °C). Seeds carrying a kanamycin resistance cassette were germinated on agar plates supplemented with 50 µg/mL kanamycin. 14 days old seedlings were transferred to soil and grown under the conditions stated above. For root cultures, sterilized seeds were germinated on sterile filter paper soaked with 0.5-strength MS medium supplemented with 3% (w/v) sucrose for three days. Seedlings were transferred to sterile glass vessels filled with 0.5-strength MS medium supplemented with 3% (w/v) sucrose and grown in the dark at 30 °C and 140 rpm for two weeks.

MOLECULAR CLONING AND GENERATION OF TRANSGENIC ARABIDOPSIS LINES

The coding sequence of *OEP7* was amplified from Arabidopsis cDNA without its stop codon. The coding sequence of *sfGFP* without its start and stop codons but including a GSGSGSG linker peptide at the 5' and a GGSG linker peptide at the 3' end, was amplified from the Gateway binary vector pGWB4 (GenBank accession AB289767). Starting from the 5' end to the 3' end, the amplified *OEP7*, *sfGFP* and *FLAG* epitope-tag (DYKDHDGDYK-DHDIDYKDDDDK) were cloned into the pUTKan vector (Krebs et al., 2012) using Gibson cloning. Expression of the gene cassette was driven by different promoters. Promoters were changed by restriction digestion using *Bam*HI and *Kpn*I and ligation into the vectors containing the expression cassette. Respective promoter regions were chosen from literature according to their expression pattern. All expression constructs and oligonucleotides used in this study are listed in Supplementary Table 1 and Supplementary Table 2. *Agrobacterium tumefaciens* GV3101 strains containing the expression construct was used to introduce the transcriptional unit into Arabidopsis Col-0 via floral-dip (Clough and Bent, 1998). Plants were propagated and chloroplast isolations were performed on the T3 generation.

PLASTID IMMUNOPURIFICATION

Plastids were isolated from 5 g of plant material, harvested from rosettes in the beginning of the light period, or two-weeks old root cultures. Plant material was homogenized in ice-cold extraction buffer (0.3 M D-sorbitol, 5 mM $MgCl_2$, 5 mM EGTA, 5 mM EDTA, 20 mM HEPES pH 8.0, 10 mM $NaHCO_3$; after Aronsson and Jarvis, (2002)) using a Waring blender by 4 rounds of 4 sec of homogenization and 4 sec of break. The extract was filtrated through one layer of pre-soaked Mira cloth, followed by centrifugation for 8 min at 500 x g at 4 °C. The pellet, containing crude plastids, was carefully resuspended in 1 mL washing buffer (0.3 M D-sorbitol, 3 mM $MgSO_4$, 50 mM HEPES pH 7.6; Aronsson and Jarvis, (2002)), filled to 30 mL with washing buffer, and centrifuged for 6 min at 3,800 x g at 4 °C. In case of the filtered extract from root cultures, the suspension was centrifuged for 5 min at 4,000 x g at 4 °C. The chloroplast or root plastid pellet was carefully resuspended in 1 mL washing buffer. The crude fractions were incubated with magnetic anti-FLAG beads for 20 minutes at 4 °C. Bound plastids were collected using a magnetic stand and washed three times with washing buffer. For purification of envelopes the beads were washed once with a washing buffer without D-sorbitol. After the final washing step, plastids or envelopes were collected, resuspended in 200 µL washing buffer and stored at -20 °C.

MICROSCOPY

Microscopy images were acquired using Axio Imager M2m (Zeiss) and SP8 confocal microscope (Leica). The following excitation/emission settings were used: GFP fluorescence (488 nm/498–550 nm), Chlorophyll fluorescence (autofluorescence) was observed at 640 to 710 nm. For the Axio Imager M2m, filters for GFP (450-490 nm/500-550 nm) and for chlorophyll (460-500 nm/from 600 nm on) fluorescence were used. Images were analyzed using Fiji (Schindelin et al., 2012) and InkScape (version 1.4.1).

CHLOROPHYLL MEASUREMENTS

Chlorophyll measurements were performed based on Porra, (2002). 10 µL of extract or isolated chloroplasts were diluted in 1 mL 100% methanol, vortexed and centrifuged for 1 min at 16,100 x g. Absorbance of the supernatant was measured at OD_{652} and OD_{665}, and chlorophyll concentration calculated.

SDS-PAGE AND IMMUNOBLOT ANALYSIS

20 µg of total protein extract or 10 µg of purified plastids were incubated in SDS-PAGE loading buffer for 10 min at 95 °C. Proteins were separated onto a 12% stain-free SDS-PAGE (Bio-RAD) and subsequently transferred onto 0.45 µm nitrocellulose membrane using the Trans-Blot Turbo Transfer system (Bio-RAD). Membranes were blocked using 5% (w/v) milk fat powder solubilized in Tris-buffered saline containing 0.1% (v/v) Tween-20 (TBS-T) for 30 min, washed with TBS for 10 min, and subsequently incubated with either the primary- or a single-step antibody for 1 hour at room temperature or over-night at 4 °C. Membranes were washed twice for 10 min with TBS, and incubated with the secondary antibody for 1 hour. Phosphate-buffered saline was used instead of TBS when using Anti-Catalase antibody. Proteins were detected by chemiluminescence detection method (Immobilon Western HRP Substrate, Merck). The following antibodies were used: Anti-FLAG-HRP (Miltenyi; 130-101-572) 1:5,000; Anti-RbcL (Agrisera; AS03037) 1:7,500; Anti-TOC75 (Agrisera; AS06150) 1:2,500; Anti-TIC40 (Agrisera; AS10709) 1:2,500; Anti-D1 (Agrisera; AS05084) 1:10,000; Anti-VDAC1 (Agrisera; AS07212) 1:5,000; Anti-Histone H3 (Agrisera; AS10710) 1:5,000; Anti-Catalase (Agrisera; AS09501) 1:1,000; Anti-BiP2 (Agrisera; AS09481) 1:2,000; Anti-Rabbit-HRP (Millipore; 12-348) 1:2,000.

PROTEOMICS

Protein samples were loaded onto a SDS-PAGE, concentrated in the stacking gel and silver stained according to MS-compatible protocol. Proteins were reduced, alkylated and digested with trypsin. Peptides were extracted from the gel with 0.1% trifluoroacetic acid and subjected to liquid chromatography.

For the LC-MS acquisition an Orbitrap Fusion Lumos Tribrid Mass Spectrometer (Thermo Fisher Scientific) coupled to an Ultimate 3000 Rapid Separation liquid chromatography system (Thermo Fisher Scientific, Idstein, Germany) equipped with an Aurora Ultimate C18 column (75 µm inner diameter, 25 cm length, 1.7 µm particle size from Ion Opticks) as separation column and an Acclaim PepMap 100 C18 column (75 µm inner diameter, 2 cm length, 3 µm particle size from Thermo Fisher Scientific) as trap column was used. A LC-gradient of 180 min was applied. Within a cycle time of 2 s the most intense peptide ions (excluding singly charged ions) were selected for fragmentation. Peptide fragments were analyzed in the ion trap using automatic injection time mode. Already fragmented ions were excluded for fragmentation for 60 seconds.

Data analysis was performed with Proteome Discoverer (version 2.4.1.15, Thermo Fisher Scientific). All RAW files were searched against the *Arabidopsis thaliana* Swissprot database (Download: 08.07.2024, 39,279 entries) and the Maxquant Contaminant

database (Download: 20.02.2021). Variable modification as methionine oxidation, N-terminal acetylation, N-terminal methionine loss and N-terminal methionine loss combined with acetylation were considered. Further, consideration represented carbamidomethylation as static modification as well as tryptic cleavage specificity with a maximum of two missed cleavage sites. Labelfree quantification was performed using standard parameters within the predefined workflow. Proteins were filtered to 1% FDR and a minimum of 2 identified peptides per protein.

DATA ANALYSIS

Cellular localization of proteins was assessed by SUBA5 (https://suba.live; Hooper et al., (2017)) and PPDB (http://ppdb.tc.cornell.edu; Sun et al., (2009)). GO term enrichment was performed by g:Profiler (https://biit.cs.ut.ee/gprofiler/gost; Kolberg et al., (2023)) and Revigo (http://revigo.irb.hr; Supek et al., (2011)). Data were further processed and visualized using R (R version 4.2.3) and R packages listed in Table 1. Cell-type specificity with promoters were assessed with the single-cell RNAseq Atlas (https://www.zmbp-resources.uni-tuebingen.de/timmermans/PSCB3_leaf/; Ma, Denyer & Timmermans (2020); Kim et al. (2021)).

Table 1: R packages used in this study.

R package	Reference
readxl version 1.4.3	Wickham and Bryan, (2023)
ggplot2	Wickham, (2016)
tidyverse	Wickham et al., (2019)
dplyr version 1.4.4	Wickham et al., (2023)
ggrepel version 0.9.6	Slowikowski, (2024)
scales version 1.2.1	Wickham and Seidel, (2022)

RESULTS

IDENTIFICATION OF A SUITABLE ARABIDOPSIS LINE WITH TAGGED CHLOROPLASTS

For efficient purification, chloroplasts must be uniformly covered with an epitope-tag that allows optimal binding to affinity beads. The FLAG-tag, first described by Hopp et al., (1988), is a commonly used epitope tag. In this study a 3xFLAG-tag, compromising 22 amino acids (DYKDHDG-DYKDHDI-DYKDDDDK) was used and is referred to as the FLAG-tag hereafter. The FLAG-tag was targeted to the outer envelope of chloroplasts using the well-characterized membrane protein OEP7.1, hereafter referred to as OEP7. OEP7 has been characterized to localize reliably to the outer envelope (Lee et al., 2001). It contains a transmembrane domain at its N-terminus, with the C-terminus facing the cytosol. Therefore, the FLAG-tag was fused to the cytosol-facing C-terminus. To verify correct localization of the fusion protein to the chloroplast outer envelope, a superfolder green fluorescent protein (sfGFP) was fused between the OEP7 and the FLAG-tag. The entire fusion construct – *OEP7-sfGFP-FLAG* – was expressed under the control of the constitutive UBIQUITIN10 promoter to ensure strong expression across all cell types. This construct is hereafter referred to as Chloro-tag.

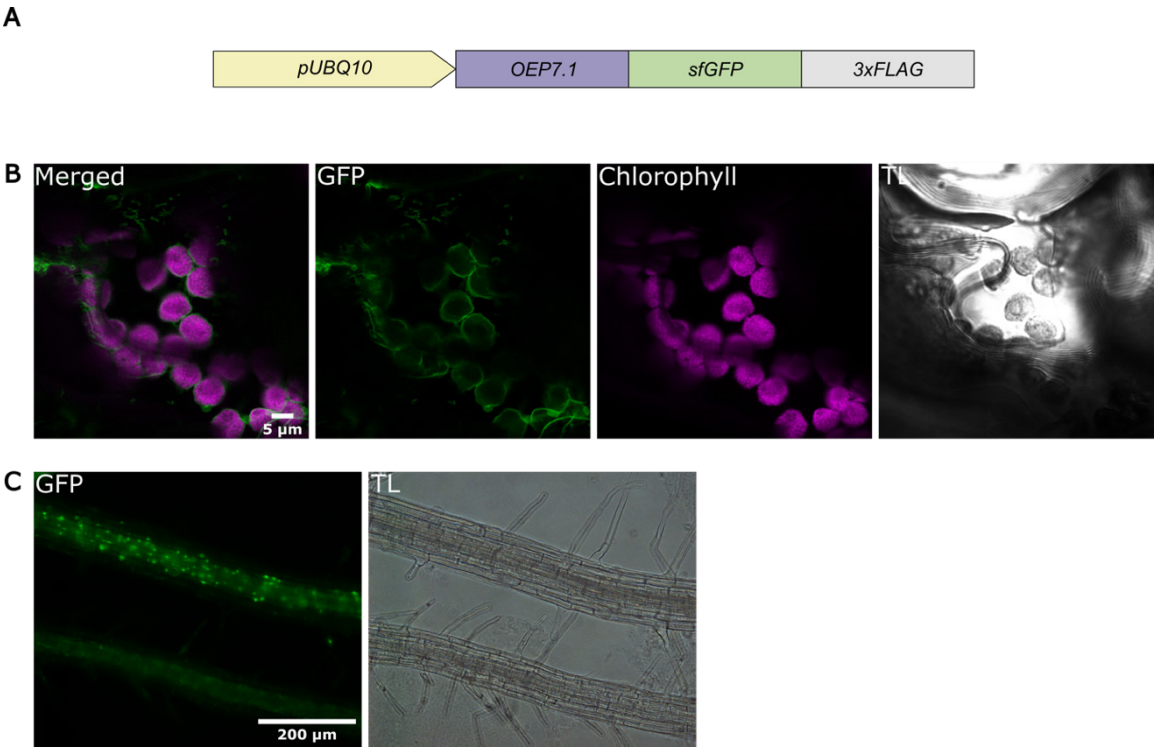

Figure 1: Localization of the Chloro-tag in Arabidopsis leaf and root tissue. Schematic depiction of the transcriptional unit for the fusion protein *pUBQ10::OEP7.1-sfGFP-FLAG*, which was cloned into the pUTKan backbone that contains a plant kanamycin resistance cassette (A). Localization of the fusion construct to chloroplasts in rosettes (B) and in roots (C) of a stable Arabidopsis line. GFP (green) was detected at plastids in rosettes and roots. Chloroplasts were visualized by the chlorophyll autofluorescence (magenta).

The gene cassette carrying the Chloro-tag (Figure 1 A) was introduced into Arabidopsis Col-0 via floral dipping. Positive T1 transformants were identified using confocal microscopy. The GFP fluorescence of the Chloro-tag was evenly distributed and surrounded the chloroplasts in leaf tissue, visualized by their chlorophyll autofluorescence (magenta), suggesting the correct localization to the chloroplast outer envelope (Figure 1 B). The Chloro-tag also showed a punctate GFP signal, resembling the structures of root plastids (Kato et al., 2008) (Figure 1 C).

PURIFICATION OF PLASTIDS FROM DIFFERENT TISSUES

Plastids were purified by homogenizing plant material and filtrating the suspension through Mira cloth. A crude chloroplast fraction was obtained after two rounds of differential centrifugation and incubated with magnetic beads. Unbound cellular material was removed by washing and plastids were collected using a magnetic stand (Figure 2).

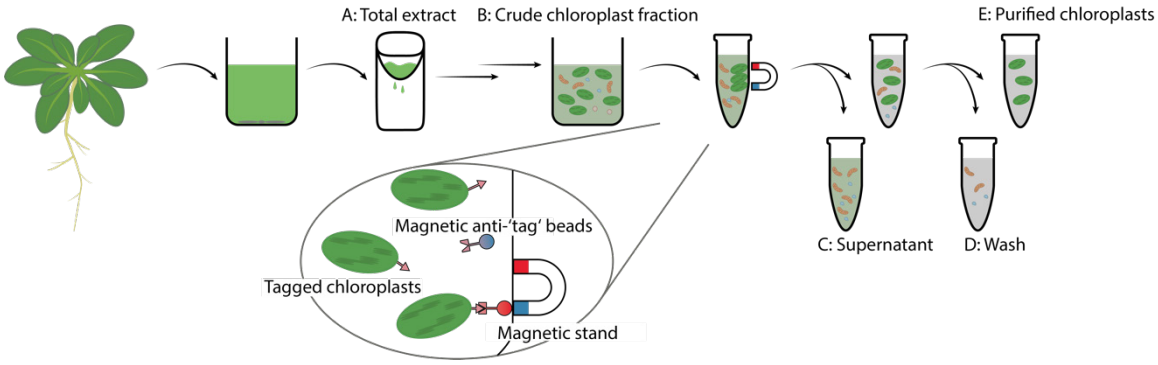

Figure 2: Schematic overview of plastid purification from Chloro-tagged lines using anti-FLAG beads. Plant material was homogenized, filtered obtaining the total extract (A), which was subsequently centrifuged. The obtained crude chloroplast fraction (B) was incubated with magnetic anti-FLAG beads. Unbound material, referred to as supernatant (C), was discarded and bound plastids were washed three times. The wash fractions (D) were discarded and purified chloroplasts were captured using a magnetic stand (E).

Chloroplasts bound to the magnetic beads were visualized under the microscope. Enrichment of chloroplasts was specifically observed in Chloro-tagged lines expressing the *OEP7-sfGFP-FLAG* fusion gene compared to Col-0 wild type plants (Figure 3A & B). GFP fluorescence localized specifically to the magnetic beads, indicating successful binding of the fusion proteins via FLAG-epitope recognition. Additionally, chloroplasts were observed not directly attached to the beads. This may be due to partial release of the fusion protein from the chloroplast envelope, possibly caused by shearing forces introduced during preparation of microscopy samples.

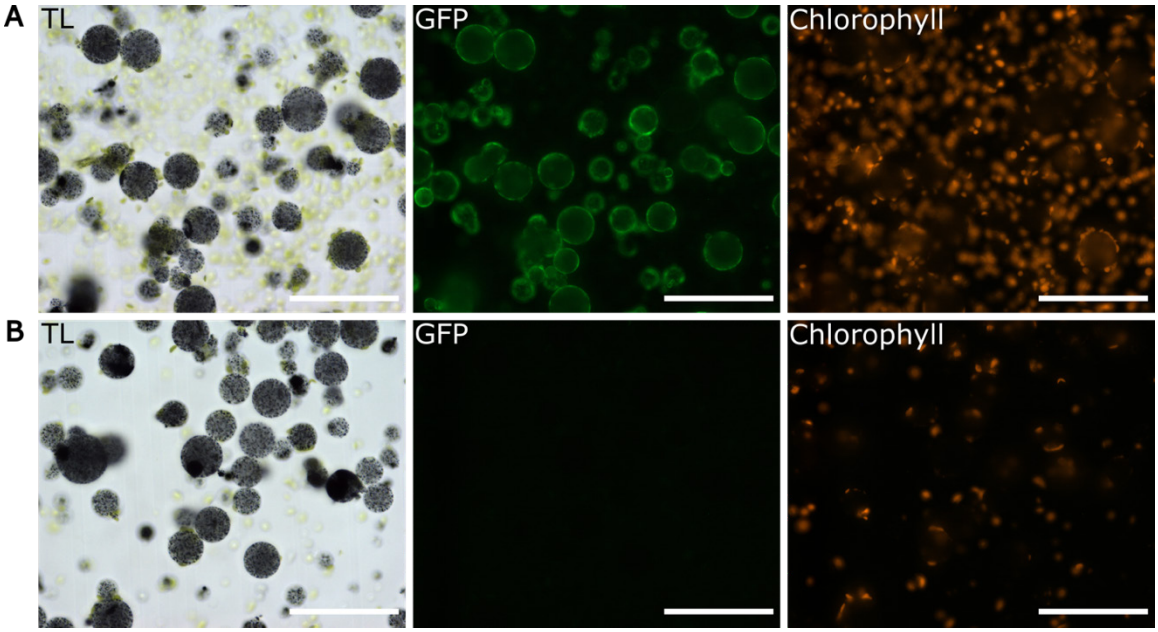

Figure 3: Microscopy of purified chloroplasts bound to magnetic anti-FLAG beads. Purified chloroplasts from Chloro-tagged Arabidopsis lines expressing the *OEP7-sfGFP-FLAG* fusion construct (A) and wild type Col-0 (B) were visualized after the immunopurification. Green color represents detected GFP signal. Chloroplasts were visualized by chlorophyll autofluorescence (orange). Respective bright field images are shown on the left side (TL). Scale bar = 100 µm

Total chlorophyll amounts were calculated by measuring absorbance of chlorophyll *a* and chlorophyll *b* in the fractions along the purification process (Figure 4A). The crude chloroplast fraction showed a strong enrichment compared to the total extract in both Arabidopsis lines. Total chlorophyll content was reduced in both purified chloroplast samples, suggesting a substantial loss of chloroplasts during the immunopurification procedure. An almost 3-fold enrichment was observed when comparing the chlorophyll content of the purified chloroplasts from the Col-0 sample with samples from the Chloro-tagged line, indicating enrichment of chloroplasts in the Chloro-tagged line.

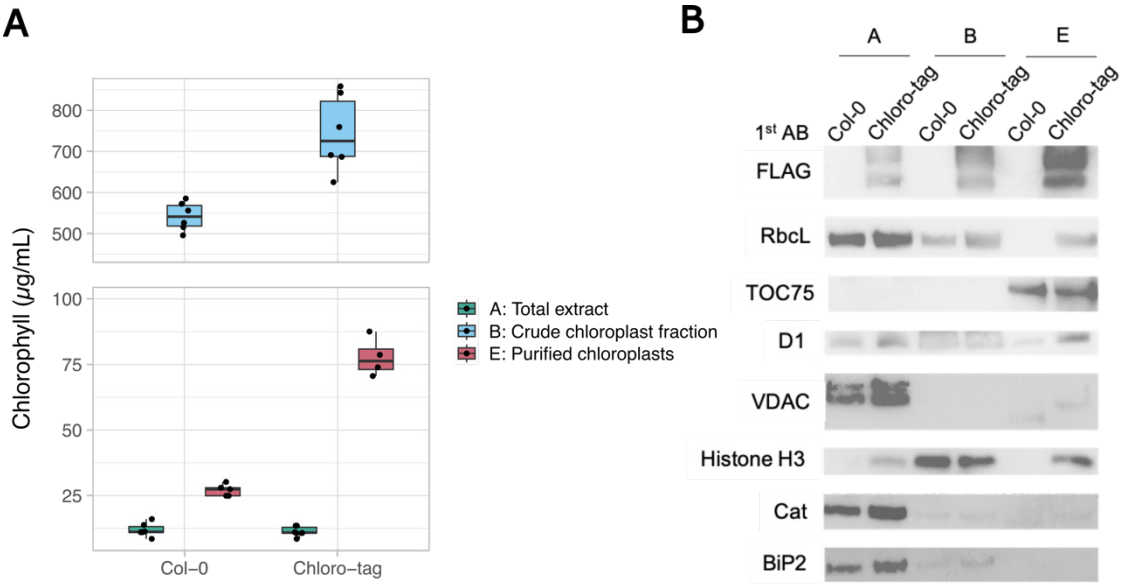

Figure 4: Analyses of purified chloroplasts. Chlorophyll content of total chlorophyll extract, crude chloroplast fraction, and purified chloroplasts from Col-0 and the Chloro-tagged line overexpressing the *OEP7.1-sfGFP-FLAG* fusion construct (A). Chlorophyll content in purified chloroplasts from the Chloro-tag line compared to Col-0 is significantly enriched ($p < 0.001$). Significance was calculated with Student's t-test. Chlorophyll content is shown as box and whiskers (min to max) from three biological replicates. Assessment of the enrichment of chloroplasts and the contaminations in the total chlorophyll extract, crude chloroplast fraction, and purified chloroplasts via immunoblotting (B). 20 µg for total extract and crude chloroplast fraction and 10 µg of purified chloroplasts were separated on a SDS-PAGE and analyzed via immunoblotting. The following protein marker for the respective organelles and subfractions were used: RbcL, stroma of chloroplasts; TOC75, chloroplast outer envelope; D1, thylakoids; VDAC, mitochondria; histone H3, nucleus; Cat, peroxisomes; BiP2, ER.

Enrichment of chloroplasts and possible contaminations along the purification procedure was assessed by immunoblots using antibodies against marker proteins of different organelles (Figure 4B). The anti-FLAG antibody served as control. Chloroplasts were successfully isolated from the Chloro-tag line, verified by immunoblot analyses with antibodies directed against the FLAG epitope-tag and different chloroplasts marker proteins, including the large subunit of RubisCO (RbcL, stromal marker), Translocase of the Outer membrane of Chloroplasts 75 (TOC75, outer envelope), and D1 protein of photosystem II (D1, thylakoid membrane). In the wild type, immunoblot analyses showed a signal for the thylakoid and envelope marker, D1 and TOC75, respectively, suggesting an unspecific binding of membrane fractions to the magnetic beads. The enrichment of the

stromal marker RbcL in the Chloro-tagged line compared to the wild type suggest a successful isolation of intact chloroplasts. The purified chloroplast fraction in the Chloro-tag line showed almost no contamination with mitochondria (VDAC), peroxisomes (Cat), and the ER (BiP2). Minor contaminations with the nucleus (Histone H3) were observed.

Proteomic analysis of immunopurified plastids

To assess the quality of the isolated chloroplasts and gain insights to their proteome, immunopurified chloroplasts were identified and quantified by mass spectrometry from four biological replicates.

In total, around 3,500 proteins were detected in the chloroplast enriched samples. 87% of the quantified abundances of all detected proteins in the samples were plastid proteins, 3% were mitochondrial proteins, 3% localized to the ER, 3% were cytosolic proteins, and the remaining 4% were proteins associated with the Golgi apparatus, vacuole, nucleus, or plasma membrane (Figure 5). In contrast, only 10% of total protein abundance in the purified root plastid fraction was attributed to plastids (Supplementary Figure 1). Hence, further analyses of root plastids were not pursued.

Among the plastid proteins from rosettes, 39% localized to the thylakoids, 32% to the plastid stroma, and 4% to the plastid envelopes (Figure 5). These results indicate high purity of the isolated plastid fraction, which was comparable to previous reported intact chloroplast isolations (Bouchnak et al., 2019).

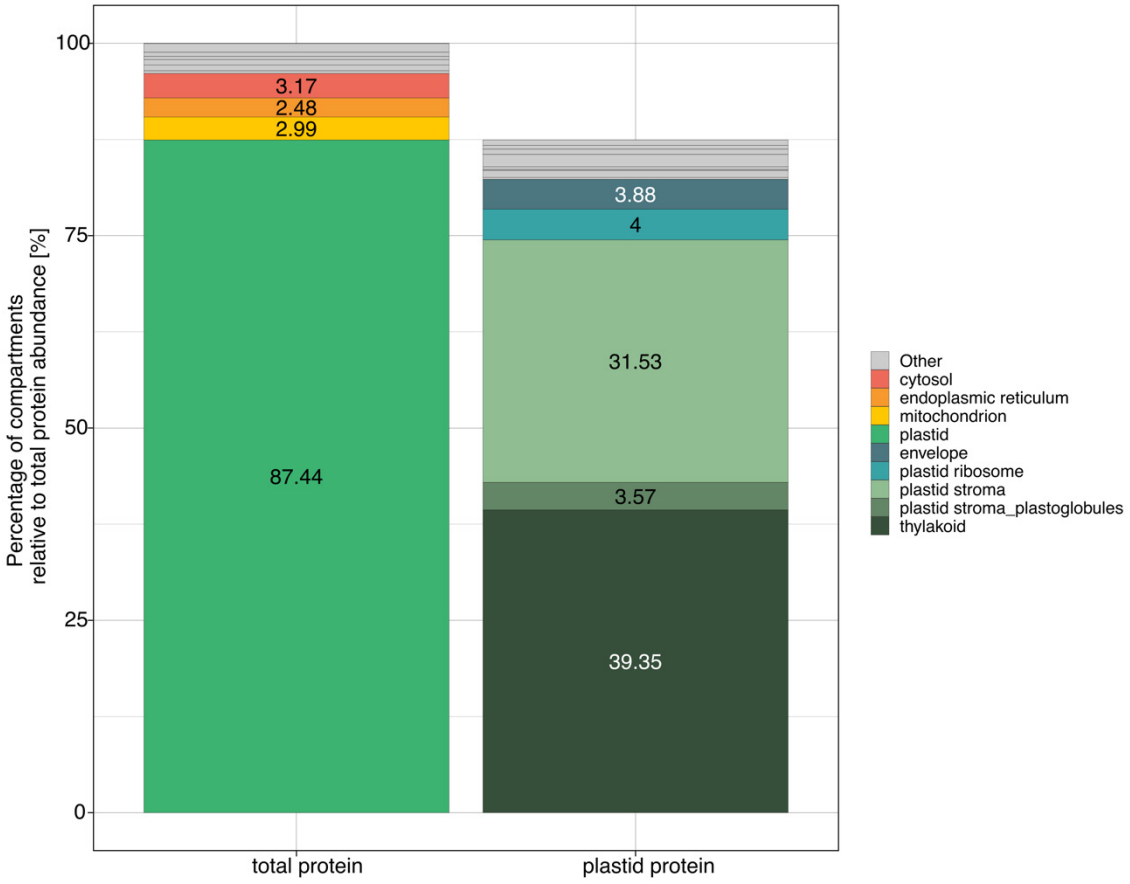

Figure 5: Percentage of protein abundances for organelle localization and plastid sub-localization. Protein abundances of total proteins grouped by organellar localization (left side) and protein abundances of plastid proteins grouped by their localization within the plastid in percentage [%] (right side). Other localizations include the Golgi apparatus and vacuole among others for total protein, and ambiguous localization for plastid proteins. Localization of total proteins were determined by SUBA5 and localization within the plastid of plastid proteins were identified by PPDB (Van Wijk, 2004).

The total isolation procedure of intact chloroplasts via an epitope-tag decorating the chloroplast outer envelope from harvesting of the tissue to obtaining the intact chloroplast was approximately 45 minutes. This is significantly faster than conventional chloroplast isolation methods via Percoll gradient centrifugation (Aronsson and Jarvis, 2002), and still yields a comparable isolation depth.

Proteins were mapped to Gene Ontology terms (GO terms) using g:Profiler. The obtained GO terms were visualized with Revigo, forming clusters of semantically similar GO terms. Among the 13% of total protein abundances, which localized to other compartments and representing 1556 distinct proteins, 184 proteins were enriched in purified chloroplasts from the Chloro-tag line. These proteins formed multiple clusters associated with GO terms such as localization, nitrogen compound transport, and endoplasmic reticulum organization, which includes the term cellular component organization in its cluster (Figure 6). These biological processes can be associated with MCSs. Proteins in these clusters were therefore selected for further analysis. One protein

candidate that was found in the cluster organelle dynamics and was enriched in the purified chloroplast fraction is the peroxisomal membrane protein peroxisome biogenesis factor 14 (PEX14). PEX14 has been implicated to function in MCSs between the ER, mitochondria and peroxisomes in yeast and mammals (Liu et al., 2019; Cho et al., 2020).

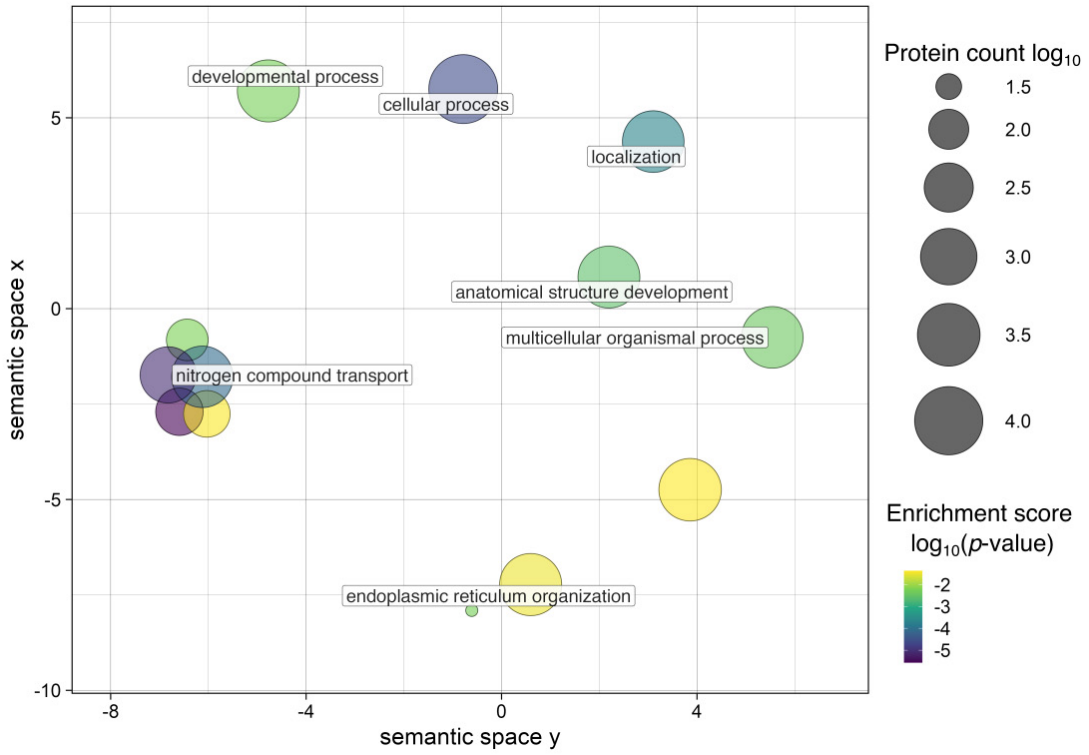

Figure 6: Scatterplot of GO term enrichment of non-plastid proteins found in the purified chloroplast fraction of the immunopurification. Scatterplot depicts the clusters and representative GO terms after analysis via Revigo (Supek et al., 2011) from the detected and enriched non-plastid proteins. GO term and adj. *p*-value for each protein compared to the Gene Ontology Annotation database from EBI were assigned and calculated by g:Profiler. The enrichment is color-coded and the size of bubbles represents the frequency of the GO term in the Gene Ontology Annotation database based on the linked proteins. The semantic space of each cluster is derived by applying a multidimensional scaling for semantic similarities across the GO terms (Supek et al., 2011).

Another MCS-associated protein identified within the cluster of cellular component organization or biogenesis was the mitochondrial Rho GTPase 2. It was characterized to form a MCS between the ER and mitochondria regulating mitochondrial dynamics (White et al., 2020).

Within the GO term ER organization, four proteins were enriched: the 25.3 kDa vesicle transport protein SEC22-1, the Reticulon-Like Protein B3 (RTNLB3), the proteins GuidedEntry of Tail-anchored membrane protein 1 and -4.

The prominent cluster nitrogen compound transport also includes GO terms such as macromolecule localization and cellular localization. One protein included and enriched in this cluster was the putative calcium-dependent lipid-binding family protein (AT1G48090). It contains a calcium binding domain (C2 domain) found in proteins such as

synaptotagmins, and a vacuolar protein sorting-associated protein 13 (VPS13) C- and N-terminal domain characterized for their role in lipid binding and transfer (Chang et al., 2013; Leonzino et al., 2021).

PURIFICATION OF PLASTID MEMBRANES

Rapid purification of plastid membranes was achieved by applying osmotic pressure during the first wash step, causing rupture of the chloroplasts. Subsequent washing steps removed stromal and thylakoid components, leaving enriched membrane fractions (Figure 7).

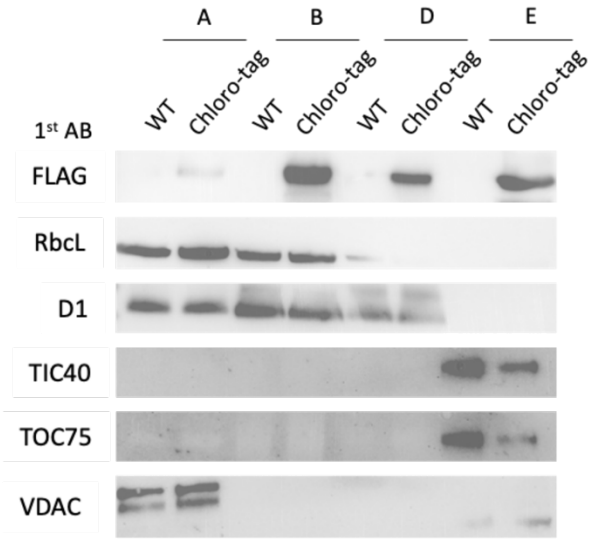

Figure 7: Protein detection of purified chloroplast envelopes via immunoblot. Proteins were separated with a SDS-PAGE and enrichment as well as contaminations were detected by immunoblotting, as described in the material and methods part. The following protein marker for the respective organelles and subfractions were used: RbcL, stroma of chloroplasts; D1, thylakoids; TIC40, chloroplast inner envelope; TOC75, chloroplast outer envelope; VDAC, mitochondria. A: Total extract; B: Crude chloroplast fraction; D: Supernatant after osmotic pressure; E: purified chloroplast envelopes.

While the intact chloroplast purification yielded approximately 5% envelope-localized plastidial proteins, the membrane purification increased this to approximately 8%, indicating improved enrichment, although, fewer individual proteins were detected overall. Two plastid envelope proteins enriched in the envelope fraction compared to intact chloroplasts were the Phosphoenolpyruvate/Phosphate Translocator 1 (PPT1) and Acclimation of Photosynthesis to Environment 2 (APE2). Both proteins belong to the plastid phosphate translocator family (Bockwoldt et al., 2019).

In total, 67 non-plastid proteins were enriched in tagged chloroplast envelopes compared to un-tagged chloroplast envelopes. A prominent cluster of these proteins were annotated with the GO term ADP transport, which also includes GO terms as mitochondrial transport, establishment of localization, and monoatomic anion transport. Additional

enrichment was observed in GO terms generation of precursor metabolites and energy derivation by oxidation of organic compounds (Figure 8). Within this cluster, the Voltage Dependent Anion Channel (VDAC) 1 and -3 were enriched. They were previously characterized to be involved in a MCSs between mitochondria and chloroplasts (Zhang et al., 2020). Notably, they were not enriched in the purification of intact chloroplasts.

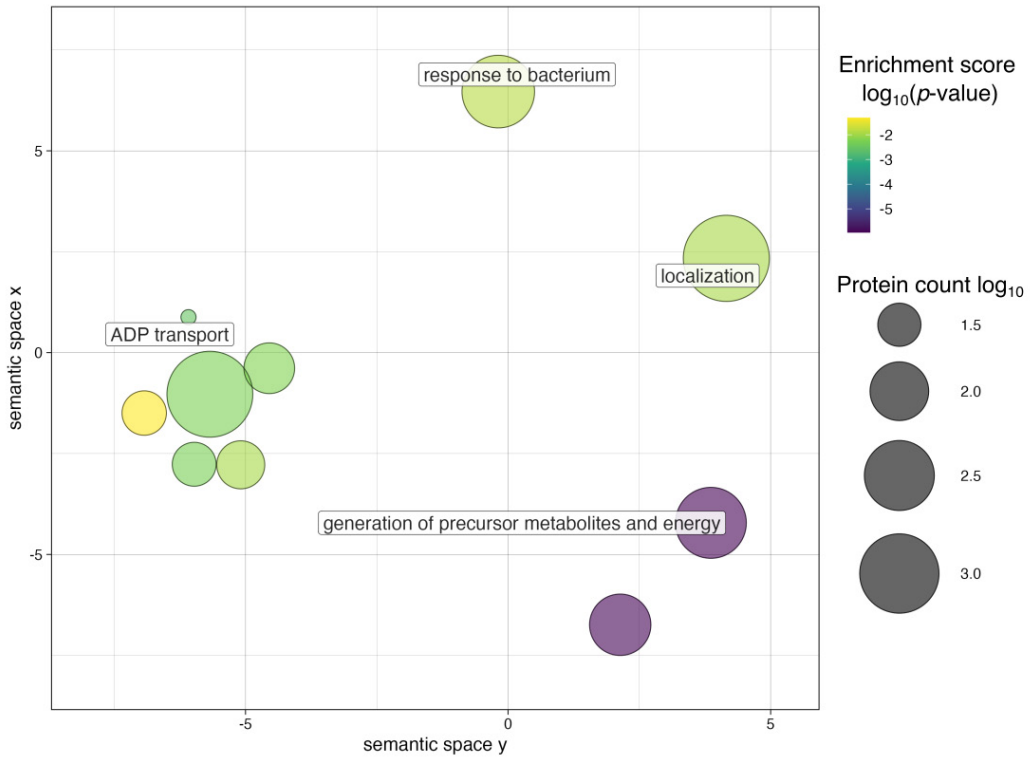

Figure 8: Scatterplot of GO terms of enriched non-plastid proteins in purified chloroplast envelopes compared to intact chloroplasts. Scatterplot depicts the GO terms in clusters that were represented in the purified chloroplast envelope samples after GO term enrichment and semantic similarity reduction via g:Profiler and Revigo (Supek et al., 2011). Enrichment score is color-coded and displays the $\log_{10}$(*p*-value of GO term enrichment via g:Profiler). The gene count is represented as the bubble size and visualizes the frequency of the GO term in the Gene Ontology Annotation database. The semantic space of each cluster originates by applying a multidimensional scaling for semantic similarities across the GO terms (Supek et al., 2011).

The ER membrane protein RTNLB3 was also enriched as observed previously in the intact chloroplast fraction. Strikingly, 33 of the 67 enriched non-plastid proteins were mitochondrial proteins (63% of enriched non-plastid protein abundances), of which 30 proteins were membrane-localized.

DISCUSSION

Traditional chloroplast isolation methods have yielded good results and provided valuable insights into chloroplast metabolism and molecular mechanisms. However, these methods typically require large amounts of plant material and are time-consuming. In recent years, protocols for immunopurification of chloroplasts have emerged. Although they yield intact chloroplasts, the methods still require additional steps such as the isolation of protoplasts prior to chloroplast purification. This study aimed to establish an immunopurification protocol for chloroplasts using a single epitope tag localized to the chloroplast outer envelope.

The gene expression cassette *OEP7-sfGFP-FLAG* was stably expressed in Arabidopsis, and the fusion protein correctly localized to the chloroplast outer envelope. This resulted in a successful single epitope-based immunopurification of intact chloroplasts from leaves.

Chlorophyll measurements of the purified chloroplasts showed a higher number of isolated chloroplasts in the Chloro-tagged line compared to Col-0. However, comparison with the chlorophyll content in the crude chloroplast fraction and the quantity of FLAG-tagged protein detected in the wash fraction (Supplementary Figure 2), suggests that the binding capacity of the beads may have been reached, potentially resulting in the loss of a significant number of chloroplasts. Another factor that might influence the binding capacity is the density of the chloroplasts in the crude chloroplast fraction. Future work will include optimizing the bead to chloroplast ratio by either diluting the crude chloroplast fraction to possibly improve yield, thereby, reducing bead saturation, or by decreasing the amount of plant material used for the immunopurification. The reduction of plant material might be especially helpful with plastid analyses of mutant plants severely impaired in growth. Optimizing chloroplast recovery will be essential for downstream applications that require a high yield of intact chloroplasts, such as physiological assays.

Nevertheless, the purified chloroplasts yielded a sufficient amount of protein for mass spectrometric analyses and showed strong enrichment of chloroplast-localized proteins with minimal contamination. Protein abundances across different subplastidial compartments, such as envelope, stroma, or thylakoid, aligned with expectations based on literature, suggesting the integrity of the organelles was preserved (Bouchnak et al., 2019). The functional integrity of chloroplasts can be further assessed by protein import assays or the Hill reaction (Walker et al., 1987; Aronsson and Jarvis, 2002)

Approximately 13% of the identified proteins did not show a predicted localization to plastids. Among those, numerous proteins involved in transport processes or organelle organization – functions commonly associated with MCSs (Prinz et al., 2020) – were found, such as MIRO2, PEX14, RTNLB3, and AT1G48090. This indicates that instead of being false positive hits, these proteins might present components of MCSs, which remained attached to the chloroplast surface.

For instance, the detection of PEX14 supports findings from other organisms, where this protein is involved pexophagy (Li et al., 2015; Liu et al., 2019; Cho et al., 2020), although its exact localization to MCS remains unknown. MIRO2 is a mitochondrial membrane protein (White et al., 2020) and PEX14 a peroxisomal membrane protein (Hayashi, 2000), both facilitating MCSs with the ER. However, as MIRO2 and PEX14 both localize neither to the ER nor to the chloroplasts, their role in MCSs at chloroplasts remain speculative for a tri-organellar MCS or a moonlighting function for these proteins, facilitating MCSs between mitochondria or peroxisomes with chloroplasts. Additionally, reticulon proteins have been found in ER-mitochondria MCSs, possibly controlling ER shape at MCSs (Reali et al., 2015; Cho et al., 2017). RTNLB3 has been shown to predominantly localize to plasmodesmata, forming a contact site with the desmotubule, but also localize to the cortical ER (Knox et al., 2015). This suggests that RTNLB3 might be involved in controlling ER shape at ER-chloroplasts MCSs. Another enriched protein was AT1G48090, an unknown protein, which contains calcium-binding motifs and a VPS13 domain. The VPS13 protein from yeast and mammalian cells acts as tether and is recruited to many MCSs, participating in glycerolipid transport as lipid transport proteins, autophagy and organelle dynamics (Bean et al., 2018; Munõz-Braceras et al., 2019; Yeshaw et al., 2019; Leonzino et al., 2021). Reviewing non-plastid-localized proteins of purified chloroplasts might help to further evaluate and find suitable candidate proteins in uncharacterized MCSs in plants.

The analysis of the detected proteins from the immunopurification of chloroplast envelopes revealed a reduction in detected total protein and only a slight increase in envelope proteins compared to intact chloroplasts. Nevertheless, comparison of plastid envelope proteins between purified envelopes and intact chloroplasts revealed an enrichment of PPT1 and APE2, an isoform of triose phosphate/phosphate translocator (TPT), which are both part of the phosphate translocator family of the chloroplast envelopes. PPT1 imports phosphoenolpyruvate, a substrate for the shikimate pathway, into plastids (Knappe et al., 2003; Hilgers et al., 2018), while APE2 may similarly to TPT

catalyze the export of triose phosphates from chloroplasts during the day (Hilgers et al., 2018). Previously, TPT was identified in a MCS between the chloroplast and the mitochondria via a complex containing three glycolytic enzymes and the mitochondrial outer membrane proteins VDAC1 and VDAC3 (Zhang et al., 2020). Given TPT's role in such MCSs, its isoform APE2 and PPT1 might also participate in MCSs to facilitate a targeted transport across membranes. The enrichment of VDAC1 and VDAC3 in the purified envelope fraction, supports the suitability of this method to isolate MCSs between the chloroplast and other cellular compartments. However, not all detected non-plastid proteins are necessarily components of MCSs. Therefore, careful selection and evaluation of candidate proteins for further characterization are required. This immunopurification offers a first insight into potential MCS-involved proteins. Future refinements may include the use of a crosslinking molecule to stabilize protein-protein interactions during or after purification. Attached organellar membranes by MCSs are most likely tethered by protein interactions, which can be crosslinked and labeled. For example, 3,3′-dithiobis(sulfosuccinimidyl propionate) (DTSSP) is a membrane-impermeable, cleavable crosslinker that contains two reactive N-hydroxysulfosuccinimide ester, which form bonds with primary amines found in lysine residues. The disulfide bond is cleavable upon reducing agents and enables labeling of proteins (Boleij et al., 2011). DTSSP therefore serves as a suitable crosslinker to label neighboring proteins and help identify MCSs component on the surface of chloroplasts via mass spectrometry.

POTENTIAL FOR PROMOTER-SPECIFIC CHLOROPLAST IMMUNOPURIFICATIONS

Due to ubiquitously expression of the Chloro-tag across tissues, we tested the potential of immunopurifying root plastids. However, only approx. 10% of the recovered proteins were plastid-localized. A similar amount was found for mitochondria (Supplementary Figure 1), indicating simultaneous purification due to similar sizes, additional mistargeting of the Chloro-tag to mitochondria, or possible association of these two organelles. Other cellular compartments showed even higher abundances, highlighting the need for further optimization of the protocol in root tissue. As the root plastids are smaller than chloroplasts (Chu and Li, 2015), the plastids may be washed more rigorously to reduce contamination.

Cell-type specific immunopurification of plastids using cell-type specific expression of the Chloro-tag has the potential to broaden our understanding of chloroplast diversity. Several cell-type specific promoters were chosen (Supplementary Table 5) upon literature research and their cell specificity shown (Supplementary Figure 3) in the single cell RNAseq Leaf Atlas (Ma et al., 2020; Kim et al., 2021). The successful targeting of the Chloro-tag to bundle sheath cells using the *SULTR2;2* promoter serves as a promising

proof of concept (Supplementary Figure 4) and creates a novel opportunity for research on different plastid proteomes and their roles in cellular metabolism. Further refinement might include the use of different membrane proteins to immunopurify different cellular compartments and subcompartments. For instance, changing the OEP7 chloroplast anchor to a thylakoid membrane protein might allow for rapid immunopurification of thylakoids. A potential candidate is the FtsH Interacting Protein (FIP). FIP is a thylakoid membrane protein involved in the response to abiotic stresses. Overexpression of FIP has no phenotypic effect under control conditions. Furthermore, its topology is well defined: the N-terminus contains a transit peptide and a hydrophobic domain for targeting to the thylakoid membrane, whereas the C-terminus includes zinc-finger domains facing the stroma (Lopes et al., 2018). Immunopurification of thylakoids could further expand the knowledge on the thylakoid proteome and its response to environmental cues, since the isolation process is significantly faster compared to traditional methods. Furthermore, the rapid isolation of such compartments and subcompartments can support topological studies of membrane proteins using proteases. Immunopurified chloroplasts or thylakoids can be subjected to trypsin and thermolysin digestion to distinguish between peripheral and integral membrane proteins, and characterize membrane protein topology in general (Minai et al., 1996).

Future application may also include immunopurification of other cell compartments, such as peroxisomes, using appropriate membrane anchors. With the use of distinct epitope-tags for different compartments, multiplexed organelle purification from a single plant line might be feasible, offering versatile system for rapid and specific isolation of multiple organelles.

In conclusion, this study presents a rapid immunopurification protocol for chloroplasts that yields intact organelles suitable for proteomic studies. The method provides comparable depth to traditional chloroplast isolation techniques and enables the study of the dynamic proteome of chloroplasts. In addition, the targeted isolation of intact chloroplasts and chloroplast envelopes enables characterization of PLAMs and proteins involved in membrane contact sites.

REFERENCES

Andersson, M.X., Goksör, M., and Sandelius, A.S., (2007). Optical manipulation reveals strong attracting forces at membrane contact sites between endoplasmic reticulum and chloroplasts. Journal of Biological Chemistry. 2007:**282**(2):1170–1174. https://doi.org/10.1074/jbc.M608124200

Aronsson, H., and Jarvis, P., (2002). A simple method for isolating import-competent Arabidopsis chloroplasts. FEBS Lett. 2002:**529**(2–3):215–220. https://doi.org/10.1016/S0014-5793(02)03342-2

Bean, B.D.M., Dziurdzik, S.K., Kolehmainen, K.L., Fowler, C.M.S., Kwong, W.K., Grad, L.I., Davey, M., Schluter, C., and Conibear, E., (2018). Competitive organelle-specific adaptors recruit Vps13 to membrane contact sites. Journal of Cell Biology. 2018:**217**(10):3593–3607. https://doi.org/10.1083/JCB.201804111

Bockwoldt, M., Heiland, I., and Fischer, K., (2019). The evolution of the plastid phosphate translocator family. Planta. 2019:**250**(1):245–261. https://doi.org/10.1007/s00425-019-03161-y

Boleij, A., Laarakkers, C.M., Gloerich, J., Swinkels, D.W., and Tjalsma, H., (2011). Surface-affinity profiling to identify host-pathogen interactions. Infect Immun. 2011:**79**(12):4777–4783. https://doi.org/10.1128/IAI.05572-11

Bouchnak, I., Brugière, S., Moyet, L., Le Gall, S., Salvi, D., Kuntz, M., Tardif, M., and Rolland, N., (2019). Unraveling hidden components of the chloroplast envelope proteome: Opportunities and limits of better MS sensitivity. Molecular and Cellular Proteomics. 2019:**18**(7):1285–1306. https://doi.org/10.1074/mcp.RA118.000988

Boussardon, C., and Keech, O., (2023). Tissue-Specific Isolation of Tagged Arabidopsis Plastids. Curr Protoc. 2023:**3**(2):1–20. https://doi.org/10.1002/cpz1.673

Chae, K., and Lord, E.M., (2011). Pollen tube growth and guidance: Roles of small, secreted proteins. Ann Bot. 2011:**108**(4):627–636. https://doi.org/10.1093/aob/mcr015

Chang, C.L., Hsieh, T.S., Yang, T.T., Rothberg, K.G., Azizoglu, D.B., Volk, E., Liao, J.C., and Liou, J., (2013). Feedback regulation of receptor-induced ca2+ signaling mediated by e-syt1 and nir2 at endoplasmic reticulum-plasma membrane junctions. Cell Rep. 2013:**5**(3):813–825. https://doi.org/10.1016/j.celrep.2013.09.038

Chang, L., Wang, L., Peng, C., Tong, Z., Wang, D., Ding, G., Xiao, J., Guo, A., and Wang, X., (2019). The chloroplast proteome response to drought stress in cassava leaves. Plant Physiology and Biochemistry. 2019:**142**:351–362. https://doi.org/10.1016/j.plaphy.2019.07.025

Cho, I.T., Adelmant, G., Lim, Y., Marto, J.A., Cho, G., and Golden, J.A., (2017). Ascorbate peroxidase proximity labeling coupled with biochemical fractionation identifies promoters of endoplasmic reticulum–mitochondrial contacts. Journal of Biological Chemistry. 2017:**292**(39):16382–16392. https://doi.org/10.1074/jbc.M117.795286

Cho, K.F., Branon, T.C., Rajeev, S., Svinkina, T., Udeshi, N.D., Thoudam, T., Kwak, C., Rhee, H.W., Lee, I.K., Carr, S.A., et al., (2020). Split-TurboID enables contact-dependent proximity labeling in cells. Proc Natl Acad Sci U S A. 2020:**117**(22). https://doi.org/10.1073/pnas.1919528117

Choi, H., Yi, T., and Ha, S.H., (2021). Diversity of Plastid Types and Their Interconversions. Front Plant Sci. 2021:**12**(June):1–14. https://doi.org/10.3389/fpls.2021.692024

Chu, C.-C., and Li, H., (2015). Protein import into isolated pea root leucoplasts. Front Plant Sci. 2015:**6**. https://doi.org/10.3389/fpls.2015.00690

Clough, S.J., and Bent, A.F., (1998). Floral dip: A simplified method for Agrobacterium-mediated transformation of Arabidopsis thaliana. Plant Journal. 1998:**16**(6):735–743. https://doi.org/10.1046/j.1365-313X.1998.00343.x

Cui, H., Kong, D., Liu, X., and Hao, Y., (2014). SCARECROW, SCR-LIKE 23 and SHORT-ROOT control bundle sheath cell fate and function in Arabidopsis thaliana. Plant Journal. 2014:**78**(2):319–327. https://doi.org/10.1111/tpj.12470

Dickinson, P.J., Kneřová, J., Szecówka, M., Stevenson, S.R., Burgess, S.J., Mulvey, H., Bågman, A.M., Gaudinier, A., Brady, S.M., and Hibberd, J.M., (2020). A bipartite transcription factor module controlling expression in the bundle sheath of Arabidopsis thaliana. Nat Plants. 2020:**6**(12):1468–1479. https://doi.org/10.1038/s41477-020-00805-w

Eisenhut, M., Roell, M.S., and Weber, A.P.M., (2019). Mechanistic understanding of photorespiration paves the way to a new green revolution. New Phytologist. 2019:**223**(4):1762–1769. https://doi.org/10.1111/nph.15872

Engel, N., Ewald, R., Gupta, K.J., Zrenner, R., Hagemann, M., and Bauwe, H., (2011). The presequence of arabidopsis serine hydroxymethyltransferase SHM2 selectively prevents import into mesophyll mitochondria. Plant Physiol. 2011:**157**(4):1711–1720. https://doi.org/10.1104/pp.111.184564

Gowik, U., and Westhoff, P., (2011). The Path from C3 to C4 photosynthesis. Plant Physiol. 2011:**155**(1):56–63. https://doi.org/10.1104/pp.110.165308

Grefen, C., Donald, N., Hashimoto, K., Kudla, J., Schumacher, K., and Blatt, M.R., (2010). A ubiquitin-10 promoter-based vector set for fluorescent protein tagging facilitates temporal stability and native protein distribution in transient and stable

expression studies. Plant Journal. 2010:**64**(2):355–365. https://doi.org/10.1111/j.1365-313X.2010.04322.x

Hayashi, M., (2000). AtPex14p maintains peroxisomal functions by determining protein targeting to three kinds of plant peroxisomes. EMBO J. 2000:**19**(21):5701–5710. https://doi.org/10.1093/emboj/19.21.5701

Hilgers, E.J.A., Staehr, P., Flügge, U.I., and Häusler, R.E., (2018). The xylulose 5-phosphate/phosphate translocator supports triose phosphate, but not phosphoenolpyruvate transport across the inner envelope membrane of plastids in arabidopsis thaliana mutant plants. Front Plant Sci. 2018:**871**. https://doi.org/10.3389/fpls.2018.01461

Hooper, C.M., Castleden, I.R., Tanz, S.K., Aryamanesh, N., and Millar, A.H., (2017). SUBA4: The interactive data analysis centre for Arabidopsis subcellular protein locations. Nucleic Acids Res. 2017:**45**(D1):D1064–D1074. https://doi.org/10.1093/nar/gkw1041

Hopp, T.P., Prickett, K.S., Price, V.L., Libby, R.T., March, C.J., Pat Cerretti, D., Urdal, D.L., and Conlon, P.J., (1988). A Short Polypeptide Marker Sequence Useful for Recombinant Protein Identification and Purification. Bio/Technology. 1988:**6**(10):1204–1210. https://doi.org/10.1038/nbt1088-1204

Irieda, H., and Takano, Y., (2021). Epidermal chloroplasts are defense-related motile organelles equipped with plant immune components. Nat Commun. 2021:**12**(1). https://doi.org/10.1038/s41467-021-22977-5

Joy, K.W., and Mills, W.R., (1987). [17] Purification of chloroplasts using silica sols. In , pp. 179–188. https://doi.org/10.1016/0076-6879(87)48019-1

Kato, N., Reynolds, D., Brown, M.L., Boisdore, M., Fujikawa, Y., Morales, A., and Meisel, L.A., (2008). Multidimensional fluorescence microscopy of multiple organelles in Arabidopsis seedlings. Plant Methods. 2008:**4**(1). https://doi.org/10.1186/1746-4811-4-9

Kim, J.-Y., Symeonidi, E., Pang, T.Y., Denyer, T., Weidauer, D., Bezrutczyk, M., Miras, M., Zöllner, N., Hartwig, T., Wudick, M.M., et al., (2021). Distinct identities of leaf phloem cells revealed by single cell transcriptomics. Plant Cell. 2021:**33**(3):511–530. https://doi.org/10.1093/plcell/koaa060

Kirschner, S., Woodfield, H., Prusko, K., Koczor, M., Gowik, U., Hibberd, J.M., and Westhoff, P., (2018). Expression of SULTR2;2, encoding a low-affinity sulphur transporter, in the Arabidopsis bundle sheath and vein cells is mediated by a positive regulator. J Exp Bot. 2018:**69**(20):4897–4906. https://doi.org/10.1093/jxb/ery263

Kleffmann, T., Russenberger, D., Von Zychlinski, A., Christopher, W., Sjölander, K., Gruissem, W., and Baginsky, S., (2004). The Arabidopsis thaliana chloroplast

proteome reveals pathway abundance and novel protein functions. Current Biology. 2004:**14**(5):354–362. https://doi.org/10.1016/j.cub.2004.02.039

Knappe, S., Löttgert, T., Schneider, A., Voll, L., Flügge, U.I., and Fischer, K., (2003). Characterization of two functional phosphoenolpyruvate/phosphate translocator (PPT) genes in Arabidopsis - AtPPT1 may be involved in the provision of signals for correct mesophyll development. Plant Journal. 2003:**36**(3):411–420. https://doi.org/10.1046/j.1365-313X.2003.01888.x

Knox, K., Wang, P., Kriechbaumer, V., Tilsner, J., Frigerio, L., Sparkes, I., Hawes, C., and Oparka, K., (2015). Putting the squeeze on plasmodesmata: A role for reticulons in primary plasmodesmata formation. Plant Physiol. 2015:**168**(4):1563–1572. https://doi.org/10.1104/pp.15.00668

Kolberg, L., Raudvere, U., Kuzmin, I., Adler, P., Vilo, J., and Peterson, H., (2023). G:Profiler-interoperable web service for functional enrichment analysis and gene identifier mapping (2023 update). Nucleic Acids Res. 2023:**51**(W1):W207–W212. https://doi.org/10.1093/nar/gkad347

Krebs, M., Held, K., Binder, A., Hashimoto, K., Den Herder, G., Parniske, M., Kudla, J., and Schumacher, K., (2012). FRET-based genetically encoded sensors allow high-resolution live cell imaging of Ca2+ dynamics. The Plant Journal. 2012:**69**(1):181–192. https://doi.org/10.1111/j.1365-313X.2011.04780.x

Kuhnert, F., Stefanski, A., Overbeck, N., Drews, L., Reichert, A.S., Stühler, K., and Weber, A.P.M., (2020). Rapid Single-Step Affinity Purification of HA-Tagged Plant Mitochondria. Plant Physiol. 2020:**182**(2):692–706. https://doi.org/10.1104/pp.19.00732

LaBrant, E., Barnes, A.C., and Roston, R.L., (2018). Lipid transport required to make lipids of photosynthetic membranes. Photosynth Res. 2018:**138**(3):345–360. https://doi.org/10.1007/s11120-018-0545-5

Lawson, T., (2009). Guard cell photosynthesis and stomatal function. New Phytologist. 2009:**181**(1):13–34. https://doi.org/10.1111/j.1469-8137.2008.02685.x

Lee, Y.J., Kim, D.H., Kim, Y.-W., and Hwang, I., (2001). Identification of a Signal That Distinguishes between the Chloroplast Outer Envelope Membrane and the Endomembrane System in Vivo. Plant Cell. 2001:**13**(10):2175–2190. https://doi.org/10.1105/tpc.010232

Leonzino, M., Reinisch, K.M., and De Camilli, P., (2021). Insights into VPS13 properties and function reveal a new mechanism of eukaryotic lipid transport. Biochim Biophys Acta Mol Cell Biol Lipids. 2021:**1866**(10). https://doi.org/10.1016/j.bbalip.2021.159003

Li, F., Chung, T., Pennington, J.G., Federico, M.L., Kaeppler, H.F., Kaeppler, S.M., and Otegui, M.S., (2015). Autophagic recycling plays a central role in maize nitrogen remobilization. Plant Cell. 2015:**27**(5):1389–1408. https://doi.org/10.1105/tpc.15.00158

Liu, X., Wen, X., and Klionsky, D.J., (2019). Endoplasmic Reticulum–Mitochondria Contacts Are Required for Pexophagy in Saccharomyces cerevisiae . Contact. 2019:**2**:251525641882158. https://doi.org/10.1177/2515256418821584

Lopes, K.L., Rodrigues, R.A.O., Silva, M.C., Braga, W.G.S., and Silva-Filho, M.C., (2018). The Zinc-finger thylakoid-membrane protein FIP is involved with abiotic stress response in arabidopsis thaliana. Front Plant Sci. 2018:**9**. https://doi.org/10.3389/fpls.2018.00504

Lu, R., Zhang, J., Wu, Y.W., Wang, Y., Zhang, J., Zheng, Y., Li, Y., and Li, X.B., (2021). bHLH transcription factors LP1 and LP2 regulate longitudinal cell elongation. Plant Physiol. 2021:**187**(4):2577–2591. https://doi.org/10.1093/plphys/kiab387

Lundquist, P.K., Rosar, C., Bräutigam, A., and Weber, A.P.M., (2014). Plastid signals and the bundle sheath: Mesophyll development in reticulate mutants. Mol Plant. 2014:**7**(1):14–29. https://doi.org/10.1093/mp/sst133

Ma, X., Denyer, T., and Timmermans, M.C.P., (2020). PscB: A Browser to Explore Plant Single Cell RNA-Sequencing Data Sets. Plant Physiol. 2020:**183**(2):464–467. https://doi.org/10.1104/pp.20.00250

Minai, L., Cohen, Y., Chitnist, P.R., and Nechushtai, R., (1996). The precursor of PsaD assembles into the photosystem I complex in two steps (thylakoids/peripheral membrane proteins/protein folding).

Munõz-Braceras, S., Tornero-Écija, A.R., Vincent, O., and Escalante, R., (2019). VPS13A is closely associated with mitochondria and is required for efficient lysosomal degradation. DMM Disease Models and Mechanisms. 2019:**12**(2). https://doi.org/10.1242/DMM.036681

Porra, R.J., (2002). The chequered history of the development and use of simultaneous equations for the accurate determination of chlorophylls a and b. Photosynth Res. 2002:**73**:149–156. https://doi.org/10.1023/A:1020470224740

Prinz, W.A., Toulmay, A., and Balla, T., (2020). The functional universe of membrane contact sites. Nat Rev Mol Cell Biol. 2020:**21**(1):7–24. https://doi.org/10.1038/s41580-019-0180-9

Reali, V., Mehdawy, B., Nardacci, R., Filomeni, G., Risuglia, A., Rossin, F., Antonioli, M., Marsella, C., Fimia, G.M., Piacentini, M., et al., (2015). Reticulon protein-1C is a key component of MAMs. Biochim Biophys Acta Mol Cell Res. 2015:**1853**(3):733–745. https://doi.org/10.1016/j.bbamcr.2014.12.031

Satori, C.P., Kostal, V., and Arriaga, E.A., (2012). Review on recent advances in the analysis of isolated organelles. Anal Chim Acta. 2012:**753**:8–18. https://doi.org/10.1016/j.aca.2012.09.041

Schindelin, J., Arganda-Carreras, I., Frise, E., Kaynig, V., Longair, M., Pietzsch, T., Preibisch, S., Rueden, C., Saalfeld, S., Schmid, B., et al., (2012). Fiji: An open-source platform for biological-image analysis. Nat Methods. 2012:**9**(7):676–682. https://doi.org/10.1038/nmeth.2019

Seigneurin-Berny, D., Salvi, D., Dorne, A.J., Joyard, J., and Rolland, N., (2008). Percoll-purified and photosynthetically active chloroplasts from Arabidopsis thaliana leaves. Plant Physiology and Biochemistry. 2008:**46**(11):951–955. https://doi.org/10.1016/j.plaphy.2008.06.009

Slowikowski, K., (2024). ggrepel: Automatically Position Non-Overlapping Text Labels with "ggplot2." 2024.

Sun, Q., Zybailov, B., Majeran, W., Friso, G., Olinares, P.D.B., and van Wijk, K.J., (2009). PPDB, the Plant Proteomics Database at Cornell. Nucleic Acids Res. 2009:**37**(SUPPL. 1). https://doi.org/10.1093/nar/gkn654

Supek, F., Bošnjak, M., Škunca, N., and Šmuc, T., (2011). Revigo summarizes and visualizes long lists of gene ontology terms. PLoS One. 2011:**6**(7). https://doi.org/10.1371/journal.pone.0021800

Susek, R.E., Ausubel, F.M., and Chory', J., (1993). Signal Transduction Mutants of Arabidopsis Uncouple Nuclear CAB and RBCS Gene Expression from Chloroplast Development.

Tamburino, R., Vitale, M., Ruggiero, A., Sassi, M., Sannino, L., Arena, S., Costa, A., Batelli, G., Zambrano, N., Scaloni, A., et al., (2017). Chloroplast proteome response to drought stress and recovery in tomato (Solanum lycopersicum L.). BMC Plant Biol. 2017:**17**(1). https://doi.org/10.1186/s12870-017-0971-0

Truernit, E., and Hibberd, J.M., (2007). Immunogenic tagging of chloroplasts allows their isolation from defined cell types. Plant Journal. 2007:**50**(5):926–932. https://doi.org/10.1111/j.1365-313X.2007.03113.x

Walker, D.A., Cerovic, Z.G., and Robinson, S.P., (1987). Isolation of Intact Chloroplasts: General Principles and Criteria of Integrity. 1987:**148**(1979):145–157.

White, R.R., Lin, C., Leaves, I., Castro, I.G., Metz, J., Bateman, B.C., Botchway, S.W., Ward, A.D., Ashwin, P., and Sparkes, I., (2020). Miro2 tethers the ER to mitochondria to promote mitochondrial fusion in tobacco leaf epidermal cells. Commun Biol. 2020:**3**(1):1–8. https://doi.org/10.1038/s42003-020-0872-x

Wickham, H., (2016). ggplot2: Elegant Graphics for Data Analysis (Springer-Verlag New York).

Wickham, H., Averick, M., Bryan, J., Chang, W., McGowan, L., François, R., Grolemund, G., Hayes, A., Henry, L., Hester, J., et al., (2019). Welcome to the Tidyverse. J Open Source Softw. 2019:**4**(43):1686. https://doi.org/10.21105/joss.01686

Wickham, H., and Bryan, J., (2023). readxl: Read Excel Files. 2023.

Wickham, H., François, R., Henry, L., Müller, K., and Vaughan, D., (2023). dplyr: A Grammar of Data Manipulation. 2023.

Wickham, H., and Seidel, D., (2022). scales: Scale Functions for Visualization. 2022.

Van Wijk, K.J., (2004). Plastid proteomics. Plant Physiology and Biochemistry. 2004:**42**(12):963–977. https://doi.org/10.1016/j.plaphy.2004.10.015

Yeshaw, W.M., van der Zwaag, M., Pinto, F., Lahaye, L.L., Faber, A.I., Gómez-Sánchez, R., Dolga, A.M., Poland, C., Monaco, A.P., van IJzendoorn, S.C., et al., (2019). Human VPS13A is associated with multiple organelles and influences mitochondrial morphology and lipid droplet motility. Elife. 2019:**8**. https://doi.org/10.7554/eLife.43561

Zhang, Y., Sampathkumar, A., Kerber, S.M.-L., Swart, C., Hille, C., Seerangan, K., Graf, A., Sweetlove, L., and Fernie, A.R., (2020). A moonlighting role for enzymes of glycolysis in the co-localization of mitochondria and chloroplasts. Nat Commun. 2020:**11**(1). https://doi.org/10.1038/s41467-020-18234-w

Zhu, D., Luo, F., Zou, R., Liu, J., and Yan, Y., (2021). Integrated physiological and chloroplast proteome analysis of wheat seedling leaves under salt and osmotic stresses. J Proteomics. 2021:**234**. https://doi.org/10.1016/j.jprot.2020.104097

SUPPLEMENTARY DATA

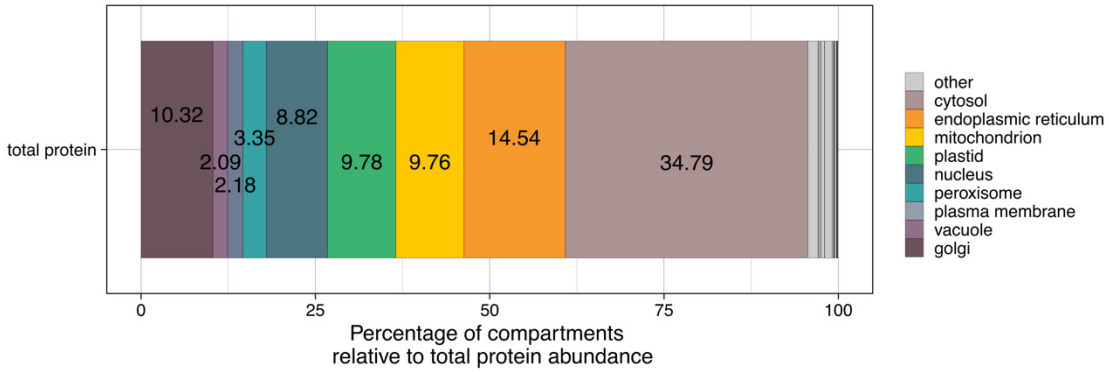

Supplementary Figure 1: Percentage of protein abundances for organelle localization of proteins detected in the immunopurification of root plastids. Protein abundances of total proteins grouped by organellar localization in percentage [%]. Other localizations include mostly ambiguous localization for plastid proteins. Localization of total proteins were determined by SUBA5 (Hooper et al., 2017).

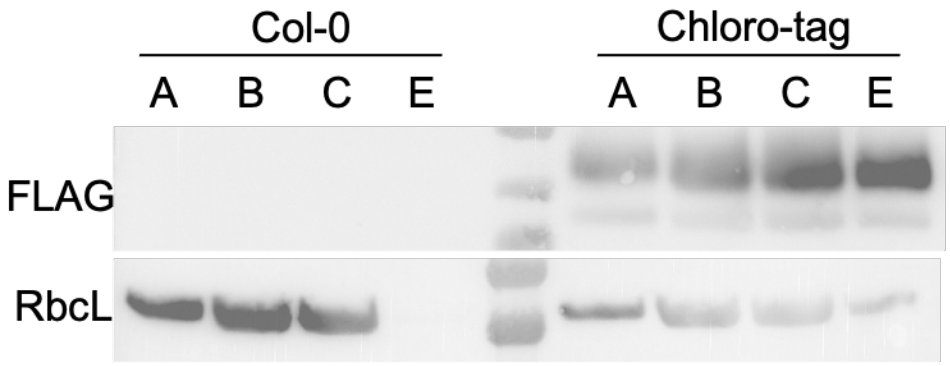

Supplementary Figure 2: Immunoblot of chloroplast immunopurification of wild type Col-0 plants and Col-0 plants expressing the Chloro-tag. Anti-FLAG antibody detected proteins in the expression lines and the anti-RbcL antibody served as chloroplast marker. The enrichment of chloroplasts was revealed by detecting the RbcL protein in the purified chloroplast fraction (E) in the Chloro-tag line. The supernatant (C) is the unbound fraction after capturing chloroplast via magnetic beads. It still contained a high level of FLAG-tagged proteins and chloroplast fractions marked by the anti-RbcL antibody, indicating that the initial concentration of chloroplasts might be too high for the amount of beads used for the immunopurification. This suggests that the plant material used for the immunopurification can possibly be reduced even further.

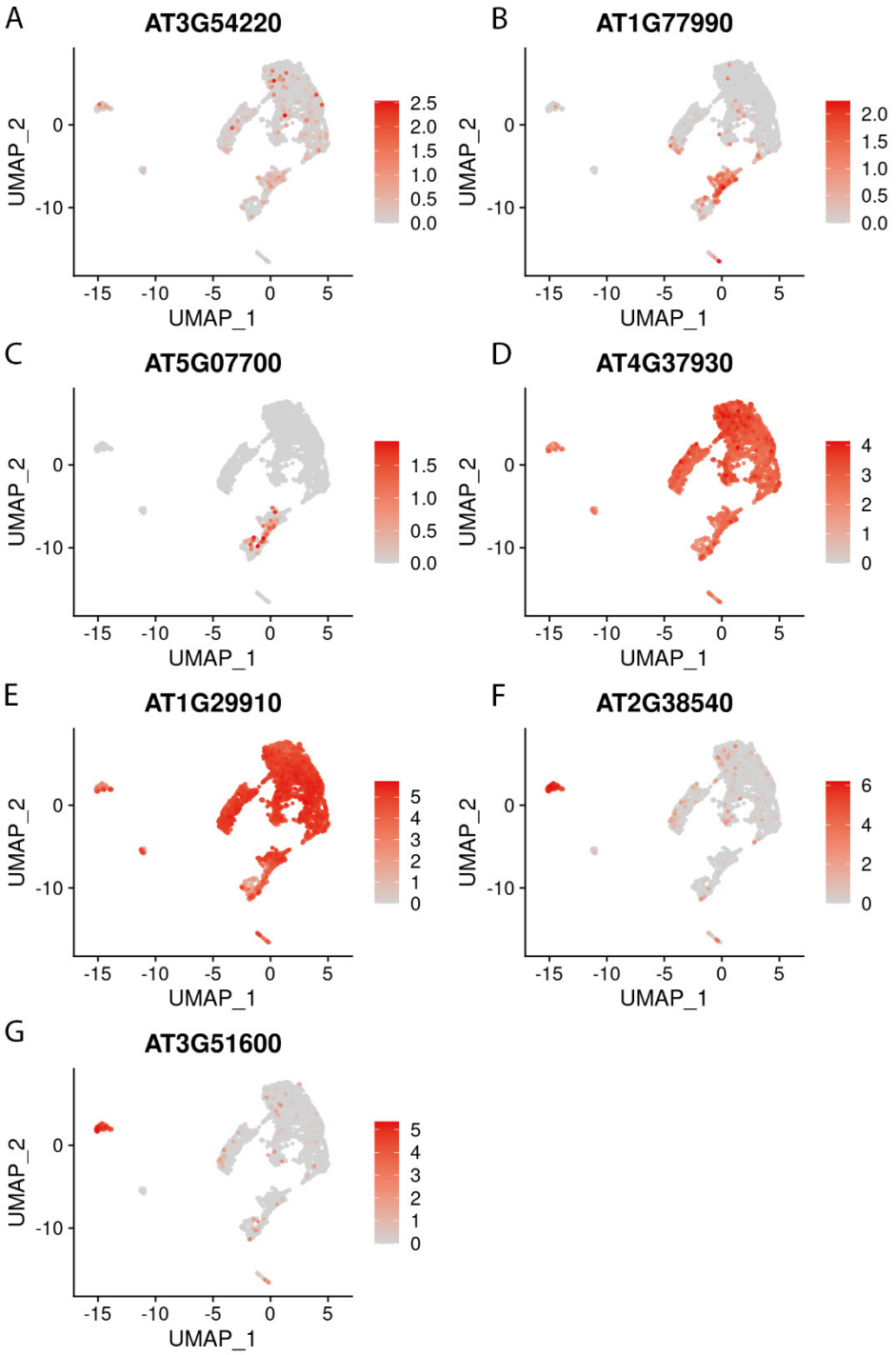

Supplementary Figure 3: Uniform Manifold Approximation and Projection plots to visualize expression levels of SCR (AT3G54220), SULTR2;2 (AT1G77990), MYB76 (AT5G07700), SHM1 (AT4G37930), CAB3 (AT1G29910), LTP1 (AT2G38540), and LTP5 (AT3G51600) on a single cell level, representing cell-type specificity. Dimensional reduction projection of 5230 leaf cells separated into different clusters. SCR (A), SULTR2;2 (B) and MYB76 (C) revealed a bundle sheath cell expression, although SCR showed a low expression level. SHM1 (D) and CAB3 (E) showed a broad expression pattern with their highest expression in the mesophyll cluster. LTP1 (F) and LTP5 (G) displayed an epidermal expression pattern. Single cell data and visualization were provided and designed by the webtool scRNA-seq Leaf Atlas (Ma et al., 2020; Kim et al., 2021).

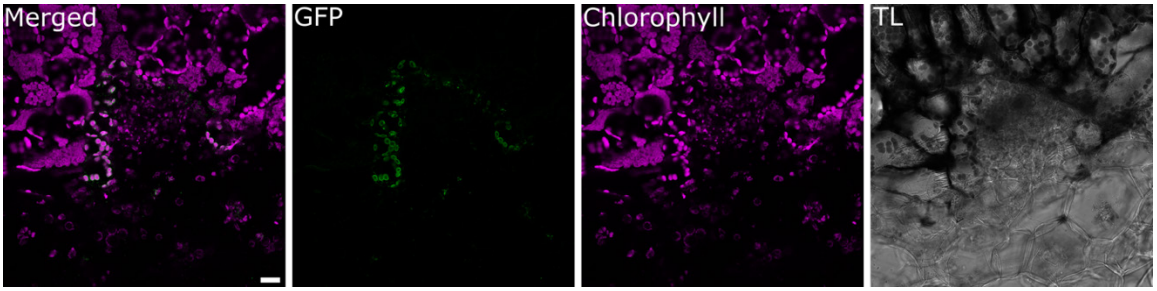

Supplementary Figure 4: Verification of cell-type specificity of the Chloro-tag driven by the SULTR2;2 promoter in a T1 plant. Confocal microscopy revealed the bundle sheath cell specific expression of the Chloro-tag driven by the SULTR2;2 in leaf sections of 5-week-old plants. GFP localization (green) was verified to surround the chloroplasts (magenta) in the bundles sheath cells. Scale bar = 20 µm.

Supplementary Table 1: Expression constructs of this study. Expression constructs were prepared by restriction ligation as described in material and methods. The UBQ10 and SULTR2;2 driven Chloro-tag were characterized in plants. The other listed constructs were generated, but not yet completely characterized in plants. BSC: bundle sheath cells; MC: mesophyll cells

Expression construct	Backbone	Purpose
UBQ10::OEP7.1::sfGFP::FLAG	pUTKan	Ubiquitously expressed Chloro-tag
SULTR2;2::OEP7.1::sfGFP::FLAG	pUTKan	BSC expression of Chloro-tag
SCR::OEP7.1::sfGFP::FLAG	pUTKan	BSC expressed Chloro-tag
SHM1::OEP7.1::sfGFP::FLAG	pUTKan	MC expressed Chloro-tag
CAB3::OEP7.1::sfGFP::FLAG	pUTKan	MC expressed Chloro-tag
2xMYB76-35s::OEP7.1::sfGFP::FLAG	pUTKan	BC expressed Chloro-tag
MYB76-35s::OEP7.1::sfGFP::FLAG	pUTKan	BC expressed Chloro-tag

Supplementary Table 2: Primer used in this study.

Primer name	Primer sequence (5' → 3')	Purpose
OEP7.fwd	TCCGCGGAGATCTACGCGTGATGGGAAAAACTTCGGGAG	Cloning of the Chloro-tag
OEP7.rev	TCCGGAGCCTGAACCAGATCCCAAACCCTCTTTGGATGTG	
sfGFP.fwd	GGATCTGGTTCAGGCTCCGGAGTGAGCAAGGGCGAGGAG	
sfGFP-3xFLAG.rev	AACTAGTTGGATATCTCGAGTTACTTATCATCATCATCCTTATAATCAATATCATGATCCTTATAATCTCCATCATGATCCTTATAATCTCCACTACCTCCCTTGTACAGCTCGTCCATG	
SULTR.fwd	ATGGTACCATGCATCCAAAACATGG	Cloning of different promoters into the pUTKan backbone, driving the expression of the Chloro-tag

Continued on the next page

Supplementary Table 2 (Continued)

SULTR.rev	ATGGATCCTCAGCTCTCTCTC TAGATAT	
SHM1p.fwd	ATGGATCCTTTTCGCTAAACCT CTCTCT	
SHM1p.rev	ATGGTACCCAGCCTGAACATT CCGATTA	
CAB3.fwd	ATGGTACCTTCACCCCAAAGC TTAG	
CAB3.rev	ATGGATCCTGAAACTTTTTGTG TTTTTTTTTTTTTT	
SCRp.rev	TAGGATCCGAGATTGAAGGGT TGTTGGTCG	
SCRp.fwd	TAGGTACCCCAAACAGATATTT GCATTTGGGC	
Gibson_2xMYB76-35s.fwd	TACGAATTCGAGCTCGGTACC CCTTCACCGATGATAA	
Gibson_MYB76-35s.fwd	TACGAATTCGAGCTCGGTACG ATGATAACACCTGAATTTAATG	
Gibson_2xMYB76-35s.rev	CTCCGCGGACGTCCCGGGCC TGTTATATCTCCTTGGATCC	
SULTR_gen.fwd	CCTATAATTCCCTATGTCTCGG	Genotyping of plants with SULTR2;2p driven gene cassette
SULTR_gen.rev	GCCTGAACCAGATCCCAA	
rbcs term	cacagttcgatagcgaaaacc	Genotyping of plants with UBQ10p driven gene cassette
pUBQ10 prom	TTTCGTTCGATCCCAATTTC	

Supplementary Table 3: Significantly enriched non-plastid proteins from intact chloroplasts purified form Chloro-tag line relative to samples from the un-tagged Col-0 control. Localization of proteins were determined by SUBA5. Significantly enriched non-plastid proteins present putative candidate proteins, localizing to membrane patches attached to the chloroplast envelope.

Protein name	**AGI**	**Protein name**	**AGI**	**Protein name**	**AGI**
Cytosol		**ER**		**Mitochondrion**	
NAD(P)-binding Rossmann-fold superfamily protein	AT1G01800	Sterol 14-demethylase	AT1G11680	MICOS complex subunit Mic10-like protein (DUF543)	AT1G22520
Ran-binding protein 1 homolog a	AT1G07140	25.3 kDa vesicle transport protein SEC22-1	AT1G11890	FAD/NAD(P)-binding oxidoreductase family protein	AT1G24340
mRNA-decapping enzyme-like protein	AT1G08370	Reticulon-like protein B3	AT1G64090	HISTIDINE TRIAD NUCLEOTIDE-BINDING 2	AT1G31160
Glutathione S-transferase U17	AT1G10370	Signal peptide peptidase	AT2G03120	K+-H+ exchange-like protein	AT1G53760
Heat shock protein 70 (Hsp 70) family protein	AT1G11660	Alpha/beta-Hydrolases superfamily protein	AT2G36290	AT1G56000 protein	AT1G56000
Cinnamoyl-CoA reductase 1	AT1G15950	Protein DEFECTIVE IN EXINE FORMATION 1	AT3G09090	S-adenosyl-L-methionine-dependent tRNA 4-demethylwyosine synthase	AT1G75200
UPF0725 protein At1g23960	AT1G23960	AT3g14620/MIE1_12	AT3G14620	Mitochondrial uncoupling protein 5	AT2G22500

Continued on the next page

Supplementary Table 3 (Continued)

Protein name	AGI	Protein name	AGI	Protein name	AGI
Cytosol		**ER**		**Mitochondrion**	
ARM repeat superfamily protein	AT1G65220	Transmembrane emp24 domain-containing protein p24beta3	AT3G22845	Glutamate dehydrogenase 2	AT5G07440
Probable protein phosphatase 2C 28	AT2G34740	Cytochrome P450 71B19	AT3G26170	Protein SCO1 homolog 1, mitochondrial	AT3G08950
SNF1-related protein kinase catalytic subunit alpha KIN10	AT3G01090	Cytochrome P450 71B34	AT3G26300	AT3g27930/K24A2_2	AT3G27930
Cyclin-dependent kinase A-1	AT3G48750	Bifunctional dihydrocamalexate synthase/camalexin synthase	AT3G26830	peptidyl-tRNA hydrolase	AT4G32900
Eukaryotic translation initiation factor 6-2	AT3G55620	At3g57220	AT3G57220	Dynamin-related protein 3A	AT4G33650
At3g60450	AT3G60450	AT4g14420/dl3250c	AT4G14420	2'-phosphotransferase	AT5G23600
ABC transporter E family member 2	AT4G19210	Monooxygenase 1	At4g15760	GTPase activator protein of Rab-like small GTPases-like protein	AT5G41940
Putative L-ascorbate peroxidase 6	AT4G32320	Protein GET1	AT4G16444	Mitochondrial import receptor subunit TOM9-2	AT5G43970
Eukaryotic translation initiation factor 3 subunit K	AT4G33250	Derlin-1	AT4G29330	Cytochrome b	AtMg00220
Folylpolyglutamate synthase	AT5G05980	NADPH--cytochrome P450 reductase	AT4G30210	Arginine--tRNA ligase, cytoplasmic	AT1G66530
Cytokinin riboside 5'-monophosphate phosphoribohydrolase LOG8	AT5G11950	Squalene synthase 1	AT4G34640	Aminomethyltransferase	AT1G11860
Molybdopterin biosynthesis protein CNX1	AT5G20990	Probable prolyl 4-hydroxylase 4	AT5G18900	Peptidyl-prolyl cis-trans isomerase	AT1G26550
Chaperone protein dnaJ 2	AT5G22060	Ubiquitin-conjugating enzyme E2 8	AT5G41700	Mitochondrial Rho GTPase 2	AT3G63150
Eukaryotic translation initiation factor isoform 4E	AT5G35620	Acyl-CoA-binding domain-containing protein 2	AT4G27780	Pentatricopeptide repeat-containing protein At1g26460, mitochondrial	AT1G26460
Translation initiation factor eIF2B subunit delta	AT5G38640	Dihomomethionine N-hydroxylase	AT1G16410	Cytochrome c-1	AT1G22840
Ras-related protein RABA1f	AT5G60860	**ER,Golgi**		Aconitate hydratase 3, mitochondrial	AT2G05710
Protein GET4	AT5G63220	Protein transport protein SEC23 A	AT4G01810	Succinate--CoA ligase [ADP-forming] subunit alpha, mitochondrial	AT5G23250
Nucleoside diphosphate kinase 1	AT4G09320	**Extracellular**		**Peroxisome**	
Defective in cullin neddylation protein	AT3G12760	Phosphorylase superfamily protein	AT4G24350	Stress-response A/B barrel domain-containing protein UP3	AT2G31670
Serine hydroxymethyltransferase 4	AT4G13930	Expansin	AT1G20190	Probable mitochondrial adenine nucleotide transporter BTL1	AT3G20240
Cysteine synthase 1	AT4G14880	Subtilisin-like protease SBT1.6	AT4G34980	Peptidase C78, ubiquitin fold modifier-specific peptidase 1/ 2	AT3G48380
Glutathione S-transferase U20	AT1G78370	Leucine-rich repeat (LRR) family protein	AT3G19320	Probable acyl-activating enzyme 5, peroxisomal	AT5G16370
Protein METHYLENE BLUE SENSITIVITY 2	AT5G16470	Polygalacturonase inhibitor 2	AT5G06870	Nudix hydrolase 19, chloroplastic	AT5G20070

Continued on the next page

Supplementary Table 3 (Continued)

Protein name	AGI	Protein name	AGI	Protein name	AGI
Cytosol		**Extracellular**		**Peroxisome**	
Glutaredoxin-C1	AT5G63030	Glutathione hydrolase 1	AT4G39640	Peroxisomal membrane protein PEX14	AT5G62810
TBCC domain-containing protein 1	AT2G42230	Subtilisin-like protease SBT1.2	AT1G04110	Serine--glyoxylate aminotransferase	AT2G13360
Cytosol, nucleus		Germin-like protein subfamily 3 member 1	AT1G72610	**Plasma membrane**	
Cryptochrome-2	AT1G04400	Germin-like protein subfamily 2 member 1	AT1G09560	Glycosyltransferase	AT1G01420
ARM repeat superfamily protein	AT2G26780	glucose-6-phosphate 1-epimerase	AT4G25900	Wall-associated receptor kinase 1	AT1G21250
Protein transport protein SEC13 homolog A	AT3G01340	Pectin acetylesterase 7	AT4G19410	Vacuolar protein sorting-associated protein 45 homolog	AT1G77140
U-box domain-containing protein 13	AT3G46510	Beta-galactosidase 6	AT5G63800	At1g78490	AT1G78490
Vacuolar protein sorting-associated protein 25	AT4G19003	Berberine bridge enzyme-like 26	AT5G44400	Guanylate-binding family protein	AT2G38840
26S proteasome regulatory particle chain RPT6-like protein	AT5G53540	At1g49750	AT1G49750	Clathrin interactor EPSIN 2	AT2G43160
Nuclear transport factor 2A	AT1G27310	**Golgi**		EH domain-containing protein 1	AT3G20290
Nucleus		Sucrose nonfermenting 4-like protein	AT1G09020	Cyclopropane-fatty-acyl-phospholipid synthase	AT3G23510
Scarecrow-like 5	AT1G50600	Serine decarboxylase	AT1G43710	Cytochrome P450, family 71, subfamily B, polypeptide 26	AT3G26290
Protein PAT1 homolog	AT1G79090	Calcium-dependent lipid-binding family protein	AT1G48090	UPF0496 protein At3g28270	AT3G28270
At1g80930/F23A5_23	AT1G80930	Protein SWEETIE	AT1G67140	Probable glycerol-3-phosphate acyltransferase 8	AT4G00400
DNA-directed RNA polymerases II, IV and V subunit 3	AT2G15430	At1g71070/F23N20_6	AT1G71070	Monocopper oxidase-like protein SKU5	AT4G12420
Polyadenylate-binding protein-interacting protein 7	AT2G26280	SCY1-like protein 2 B	AT1G71410	Root phototropism protein 3	AT5G64330
Choline-phosphate cytidylyltransferase 1	AT2G32260	Transmembrane 9 superfamily member 3	AT2G01970	AT5G66420 protein	AT5G66420
Pre-mRNA-processing factor 19 homolog 2	AT2G33340	BAT2 domain protein	AT2G15860	G-type lectin S-receptor-like serine/threonine-protein kinase SD3-1	AT2G41890
KH domain-containing protein At2g38610	AT2G38610	AP-1 complex subunit sigma-1	AT2G17380	Probable aquaporin PIP2-6	AT2G39010
DEAD-box ATP-dependent RNA helicase 14	AT3G01540	CLIP-associated protein	AT2G20190	**Vacuole**	
At3g06670/T8E24.10	AT3G06670	Transmembrane protein	AT2G22795	Protein STRICTOSIDINE SYNTHASE-LIKE 4	AT3G51420
B3 domain-containing transcription factor VRN1	AT3G18990	PRA1 family protein B4	AT2G38360		
Histone H2B.7	AT3G46030	Kinase family with ARM repeat domain-containing protein	AT2G40730		
Actin-related protein 7	AT3G60830	PLAC8 family protein	AT2G45010		
At5g18940	AT5G18940	Apyrase 1	AT3G04080		
RabGAP/TBC domain-containing protein	AT5G52580	Syntaxin-43	AT3G05710		

Continued on the next page

Supplementary Table 3 (Continued)

Protein name	AGI	Protein name	AGI	Protein name	AGI
Nucleus		**Golgi**			
Polypyrimidine tract-binding protein homolog 2	AT5G53180	Leucine-rich repeat (LRR) family protein	AT3G15410		
Histone acetyltransferase type B catalytic subunit	AT5G56740	AT3g17900/MEB5_12	AT3G17900		
AT2G21270 protein	AT2G21270	Syntaxin-32	AT3G24350		
Protein EXPORTIN 1A	AT5G17020	Probable prolyl 4-hydroxylase 7	AT3G28480		
Polyadenylate-binding protein RBP45B	AT1G11650	Vacuolar-sorting receptor 1	AT3G52850		
Phytochrome B	AT2G18790	Peptidyl-prolyl cis-trans isomerase CYP21-2	AT3G55920		
Histone deacetylase HDT2	AT5G22650	AT3g56820/T8M16_150	AT3G56820		
Serine/threonine-protein kinase STY17	AT4G35780	Bet1-like SNARE 1-1	AT3G58170		
Importin subunit alpha-1	AT3G06720	GPN-loop GTPase 3	AT4G12790		
Golgi, vacuole		Putative MO25-like protein At4g17270	AT4G17270		
Transmembrane/coiled-coil protein (DUF726)	AT4G36210	Vacuolar protein sorting-associated protein 54	AT4G19490		
		At4g37190	AT4G37190		
		Transmembrane 9 superfamily member 8	AT5G10840		
		Beta-adaptin-like protein	AT5G11490		
		Conserved oligomeric Golgi complex subunit 1	AT5G16300		
		ARM repeat superfamily protein	AT5G27970		
		Transmembrane protein	AT5G58100		
		Trafficking protein particle complex subunit-like protein	AT5G65950		

Supplementary Table 4: Significantly enriched non-plastid proteins from chloroplast envelopes purified form Chloro-tag line relative to samples from the un-tagged Col-0 control. Localization of proteins were determined by SUBA5. Significantly enriched non-plastid proteins present putative candidate proteins, localizing to membrane patches attached to the chloroplast envelope.

Protein name	AGI	Protein name	AGI	Protein name	AGI
Cytosol		**Mitochondrion**			
Eukaryotic initiation factor 4A-2	AT1G54270	Prohibitin-2, mitochondrial	AT1G03860	AT5G37510 protein	AT5G37510
Probable protein phosphatase 2C 20	AT2G20630	Mitochondrial outer membrane import complex protein METAXIN	AT2G19080	NADH dehydrogenase [ubiquinone] 1 beta subcomplex subunit 9	AT4G34700
Villin-2	AT2G41740	Hexokinase-2	AT2G19860	Cytochrome b-c1 complex subunit 8-2, mitochondrial	AT5G05370
Delta-1-pyrroline-5-carboxylate synthase B	AT3G55610	Alanine-tRNA ligase	AT2G45060	**Nucleus**	
Eukaryotic initiation factor 4A-1	AT3G13920	Glycerol-3-phosphate dehydrogenase SDP6, mitochondrial	AT3G10370	Nuclear transport factor 2B	AT1G27970
GTP-binding nuclear protein Ran-1	AT5G20010	Mitochondrial adenine nucleotide transporter ADNT1	AT4G01100	OBP3-responsive protein 4 (ORG4)	AT2G06010
Adenylyl cyclase-associated protein	AT4G34490	AT4g29480/F17A13_300	AT4G29480	ABC transporter F family member 4	AT3G54540
14-3-3-like protein GF14 chi	AT4G09000	Cytochrome b-c1 complex subunit Rieske-1, mitochondrial	AT5G13430	Protein BTR1	AT5G04430
Polyubiquitin 8	AT3G09790	ADP,ATP carrier protein 2, mitochondrial	AT5G13490	**Peroxisome**	
Cytosol, nucleus		Alpha/beta-Hydrolases superfamily protein	AT5G20060	Long chain acyl-CoA synthetase 6, peroxisomal	AT3G05970
Eukaryotic translation initiation factor 3 subunit A	AT4G11420	NADH dehydrogenase [ubiquinone] 1 alpha subcomplex subunit 2	AT5G47890	Ubiquitin-conjugating enzyme E2 7	AT5G59300
ER		Succinate dehydrogenase subunit 7B, mitochondrial	AT5G62575	AT3G48140 protein	AT3G48140
Prolyl 4-hydroxylase 5	AT2G17720	Mitochondrial carnitine/acylcarnitine carrier-like protein	AT5G46800	Peroxisomal membrane protein 11D	AT2G45740
Cytochrome b5 isoform E	AT5G53560	Mitochondrial outer membrane protein porin 2	AT5G67500	At1g64850/F13O11_15	AT1G64850
Dolichyl-diphosphooligosaccharide--protein glycosyltransferase 48 kDa subunit	AT5G66680	Mitochondrial phosphate carrier protein 3, mitochondrial	AT5G14040	Glutathione S-transferase T1	AT5G41210
Cytochrome P450 98A3	AT2G40890	Prohibitin-3, mitochondrial	AT5G40770	**Plasma membrane**	
Calnexin homolog 1	AT5G61790	Mitochondrial import receptor subunit TOM9-2	AT5G43970	UPF0496 protein At3g28270	AT3G28270
ER, cytosol		Mitochondrial dicarboxylate/tricarboxylate transporter DTC	AT5G19760	Reticulon-like protein B1	AT4G23630
Small COPII coat GTPase SAR1B	AT1G56330	ADP,ATP carrier protein 1, mitochondrial	AT3G08580	**Vacuole**	
Extracellular		Succinate dehydrogenase subunit 6, mitochondrial	AT1G08480	Protein STRICTOSIDINE SYNTHASE-LIKE 4	AT3G51420
Leucine-rich repeat (LRR) family protein	AT1G33600	NADH dehydrogenase [ubiquinone] flavoprotein 1, mitochondrial	AT5G08530	Ankyrin repeat-containing protein 2	AT4G35450
Golgi		NADH dehydrogenase [ubiquinone] flavoprotein 2, mitochondrial	AT4G02580		
GEM-like protein 1	AT1G28200	NADH dehydrogenase [ubiquinone] 1 alpha subcomplex subunit 9, mitochondrial	AT2G20360		

Continued on the next page

Supplementary Table 3 (Continued)

Protein name	AGI	Protein name	AGI	Protein name	AGI
Golgi		**Mitochondrion**			
Coatomer subunit alpha-1	AT1G62020	Mitochondrial outer membrane protein porin 4	AT5G57490		
At2g44060	AT2G44060	Probable mitochondrial-processing peptidase subunit alpha-1, mitochondrial	AT1G51980		
		Mitochondrial outer membrane protein porin 1	AT3G01280		
		Cytochrome b-c1 complex subunit 10, mitochondrial	AT2G40765		
		Probable mitochondrial-processing peptidase subunit beta, mitochondrial	AT3G02090		
		ATP synthase protein MI25	AtMg00640		
		Mitochondrial outer membrane protein porin 3	AT5G15090		

Supplementary Table 5: Summary of utilized promoters. Promoter regions were chosen from literature and the single cell RNAseq Atlas (*Supplementary Figure 3*). Constructs were generated as described in material and methods. Promoters UBQ10 and SULTR2;2 were verified for their activity, targeting the Chloro-tag to the chloroplasts in expected cell types.

Promoter	Cell type	AGI	Reference
UBQ10	ubiquitous	AT4G05320	Grefen et al., (2010)
SCR	Bundle sheath cells	AT3G54220	Cui et al., (2014)
SULTR2;2		AT1G77990	Kirschner et al., (2018)
MYB76-35S		AT5G07700	Dickinson et al., (2020)
2xMYB76-35S			Dickinson et al., (2020)
SHM1	Mesophyll	AT4G37930	Engel et al., (2011)
CAB3		AT1G29910	Susek et al., (1993)
LTP1	Epidermis	AT2G38540	Lu et al., (2021)
LTP5		AT3G51600	Chae and Lord, (2011)

Chapter IV:

Investigating the plant organellar contactome with a proximity-dependent and dual split-protein technique

Vanessa Valencia[1], Elisa S. Großmann[1], Anja Stefanski[2], Kai Stühler[2], Franziska Kuhnert[1]†, Andreas P.M. Weber[1]

[1] Institute of Plant Biochemistry, SFB1208, Heinrich Heine University, Universitätsstrasse 1, 40225 Düsseldorf, Germany

[2] Molecular Proteomics Laboratory, Biologisch-Medizinisches Forschungszentrum für Synthetische Lebenswissenschaften, Heinrich Heine University, Universitätsstrasse 1, 40225 Düsseldorf, Germany

† Plant Energy Biology, University of Western Australia; Crawley, 6009, Australia

Author contribution: VV designed the experiments, performed cloning, transient expressions, confocal microscopy, protein purification, and data analysis; ESG assisted with the cloning, transient expression and performed immunoblots; AS and KS performed the mass spectrometry, and proteomic analysis, FK and APMW conceptualized the research and supervised the experiments

ABSTRACT

The organellar contactome enables direct communication and molecular exchange between organelles at specific membrane contact sites. In recent years, unraveling the molecular compositions of these sites has become a major research focus, with proximity labeling emerging as a powerful technique to identify novel interaction partners. This method was further refined by Cho and colleagues (2020) through the development of split-TurboID, a system in which the enzymatic activity is spatially restricted to the interaction site of its two fragments, thereby increasing labeling specificity. In this study, we adapted the split-TurboID system for the use in plants by integrating it into the modular Golden Gate cloning toolkit. The availability of the split-GFP system in this toolkit allowed the simultaneous use of both split proteins in a single assay. Expression of a combined split-GFP/split-TurboID construct targeting two organellar membranes enabled visualization of membrane contact sites, while simultaneously facilitating the specific biotinylation of proteins putatively localized at these interfaces. Mass spectrometry analysis of the biotinylated proteins revealed a set of novel candidate proteins potentially associated with membrane contact sites in plant cells.

INTRODUCTION

In addition to vesicular trafficking, intracellular transport can occur via direct contact between membranes – referred to as membrane contact sites (MCSs). In plants, our understanding of the molecular mechanisms underpinning MCSs remains limited. One approach addressing this gap is through proteomic identification of MCS-associated proteins. Once such proteins are known, techniques like co-immunopurification and pull-down assays can be used to identify direct interaction partners. However, these methods are limited: They require robust protein-protein interactions (PPIs) and rely on the temporally restricted presence of the interaction. Especially, transient interactions with low affinities cannot be captured using such methods (Titeca et al., 2019).

In recent years, proximity labeling gained increasing attention as an *in vivo* labeling technique to map the interaction network of a bait protein. It employs enzymes, which produce molecules that covalently bind to proximal proteins of the bait protein. The added group can then be used for purification and identification of the labeled proximal proteins via mass spectrometry (Kim and Roux, 2016). BioID is one of the first promiscuous biotin ligases utilized for proximity labeling. It is a truncated variant of the BirA from *E. coli*, and labels proximal proteins via biotinylation. BioID generates a reactive biotin group that binds to lysine residues of a neighboring protein and thus biotinylates possible interacting proteins (Roux et al., 2018). It was successfully used to identify novel substrates for enzymes such as the E3 ubiquitin ligase (Coyaud et al., 2015), interaction partners such as for the human lamin A (Mehus et al., 2016), or to characterize nuclear pore architecture (Kim et al., 2014). Proximity labeling based on APEX, an ascorbate peroxidase, which was originally used for generating electron-dense regions for electron microscopy, labels proximal proteins by utilizing biotin phenol radicals in the presence of hydrogen peroxide (Han et al., 2019). Both enzymes, BioID and APEX, have their limitations: BioID is active at 37 °C and may not be suitable for temperature-sensitive approaches, while APEX, functions at 30 °C, but requires the presence of hydrogen peroxide, which can be cytotoxic. To overcome these limitations, Branon and colleagues (2018) developed the TurboID, a faster and more efficient biotin ligase containing 15 mutations in comparison to BirA. TurboID operates optimally at 30 °C (Branon et al., 2018) and has been successfully applied in a range of organisms, including mammalian cells (Ahmed et al., 2024), Drosophila (Feizy et al., 2024), *C. elegans* (Nikonorova et al., 2025), yeast (Kovacs et al., 2023), and plants (Kim et al., 2023). However, TurboID can cause background biotinylation due to the presence of endogenous biotin. Strategies to mitigate this include the use of an inducible expression system, inducible activation of the protein (Lee et al., 2023), or split variants of the proteins. In split systems, the protein is divided into fragments that are

inactive on their own, but become functional upon reassembly – similar to bimolecular fluorescence complementation (BiFC). This enhances the specificity temporally and spatially towards the interaction of both fragments.

Split-APEX was developed to have inactive split fragments with a PPI-dependent labeling and was used to label soluble PPI, and protein-RNA- and membrane-membrane interactions, specifically at ER-mitochondria MCSs (Han et al., 2019). The labeling generates a higher contrast for electron microscopy and, thus, MCSs can be visualized with higher resolution. Similarly, split-BioID was shown to reliably label proteins at specific PPIs (Schopp et al., 2017). Cho and colleagues (2020) developed split-TurboID, which consists of two fragments based on full length TurboID. Two split-TurboID variants with different affinities were generated: a low-affinity pair cleaved at amino acid 73/74, and a high-affinity pair cleaved at 78/79. While the high-affinity fragments could spontaneously reconstitute, the low-affinity pair required an enforced interaction for activation, offering higher specificity but lower overall activity. Using split-TurboID, Cho and colleagues (2020) successfully labeled the proteome of an ER-mitochondria MCSs in mammalian cells (Cho et al., 2020).

Split-biotin ligase variants are in particular suitable for labeling proteins specifically at interaction sites. Interaction requires proximity of two proteins or, in case of MCSs, two membranes. At MCSs, membranes come as close together as 10 nm (Giacomello and Pellegrini, 2016), which resembles PPIs. Additionally, it was shown that MCSs mirror the interaction forces seen in PPIs, such as those at plastid associated membranes (PLAMs) (Andersson et al., 2007). PLAMs are defined as endoplasmic reticulum (ER) membrane patches attached to the chloroplast envelopes and, with their now characterized attracting forces similar to PPIs, they might function as MCSs. PLAMs might include proteins involved in lipid trafficking between the ER and chloroplast (Hurlock et al., 2014; Block and Jouhet, 2015), or stress response (Liu and Li, 2019). Additionally, chloroplasts interact with other cellular compartments such as mitochondria (Jouhet et al., 2004; Zhang et al., 2020), indicating that many MCSs in plants remain to be discovered.

This project aims to characterize the proteome of MCSs and to provide an initial set of candidate proteins to unravel new MCSs in plants. To this end, the TurboID and split-TurboID were implemented into the GoldenGate-compatible MoClo toolkit for efficient cloning and expression in plants. With a proximity-dependent BiFC, MCSs between ER-mitochondria, ER-chloroplasts and chloroplasts-mitochondria (Chapter 1) have been visualized, offering a broad overview of potential MCSs in plants. Since the BiFC is also available for GoldenGate system, both techniques can be used in combination. This dual approach allows simultaneous visualization and proximity labeling of MCSs in plant cells. A similar strategy was recently applied in yeast to visualize and characterize ER-

mitochondria MCSs (Fujimoto et al., 2023). Here, ER-chloroplast and ER-mitochondria MCSs from plants are visualized and simultaneously labeled by biotinylation for the identification of the plant contactome.

MATERIAL & METHODS

PLASMID DESIGN AND CONSTRUCTION

TurboID was split in the fragment pair, N-TbID and C-TbID, at amino acids 73/74 according to Cho et al., (2020). N-TbID and C-TbID were implemented into the Golden Gate Cloning method (Engler et al., 2014). Both fragments were amplified with and without a stop codon and ligated into multiple Level 0 backbones to allow for efficient modular design. The modular design with Golden Gate allows for utilizing previous established BiFC modules (Chapter 1). In brief, self-assembling superfolder green fluorescent protein (sfGFP) parts, linker and spacers, as well as established membrane anchors to reliably target reporter systems to the outer membrane of organelles were established and are incorporable with the split-TurboID approach. Between each module, a four amino acid GS linker was included. Gene cassettes were ligated into the expression vector pAGM4723 (Addgene #48015) for plant expression, containing the transcriptional unit for tether 1, including the split-protein fragments fused to a membrane anchor under the control of the 35S promoter (Gallie et al., 1987), the transcriptional unit for tether 2, including the complementary split-protein fragments and another membrane anchor under the control of the UBQ10 promoter (Grefen et al., 2010), and a kanamycin resistance cassette under the control of the nos promoter (Gynheung, 1986).

TRANSIENT EXPRESSION IN *NICOTIANA BENTHAMIANA*

Leaves of 4- to 5-week-old *Nicotiana benthamiana* (tobacco) plants were infiltrated with bacterial suspension at the abaxial side. The bacterial suspension harbors *Agrobacterium tumefaciens* GV3101 strains containing the expression constructs at an OD_{600} of 0.5 resuspended in infiltration buffer (10 mM MES-KOH pH 5.7, 10 mM $MgCl_2$, 200 µM Acetosyringone) or, for co-infiltration, the bacterial suspension contained two *Agrobacterium tumefaciens* GV3101 strains each at OD_{600} of 0.4. After infiltration, the plants were kept at 22 °C and transient gene expression was ensured for 2 days.

PROTOPLAST PREPARATION

Infiltrated leaves were cut into small pieces and vacuum-infiltrated with digestion buffer (0.4 M Mannitol, 20 mM MES-KOH pH 5.7, 20 mM KCl, 10 mM $CaCl_2$) containing freshly added 1.5% (w/v) Cellulase R-10, 0.4% (w/v) Macerozyme R-10 and 0.1% (w/v) BSA. The solution was kept at 30 °C for 2 hours. Protoplasts in the solution were extracted and washed with washing buffer (0.7 M mannitol, 15 mM $MgCl_2$, 4 mM MES-KOH pH 5.7).

CONFOCAL MICROSCOPY

Confocal images were acquired with the Leica SP8 confocal microscope with the following excitation and emission settings: GFP fluorescence (488 nm/498–550 nm), MitoTracker (561nm/582 –615 nm), and WAK2-CFP ER marker (458 nm/465-500 nm). Chlorophyll fluorescence (autofluorescence) was observed at 640 to 710 nm. Crosstalk was minimized by using frame-sequential scanning mode. Fiji (Schindelin et al., 2012) and InkScape (version 1.4.1) were used for image preparation.

PROTEIN PURIFICATION

Biotinylated proteins were purified as described by Shi et al., (2023). Briefly, 5 g of infiltrated leaf material was ground in liquid nitrogen and resuspended in 10 mL of RIPA buffer (150 mM NaCl, 1.0% (v/v) NP-40, 1.0% (w/v) sodium deoxycholate, 0.1% (w/v) SDS, 25 mM Tris-HCl pH 7.6) supplemented with protease inhibitor cocktail (EDTA-free cOmplete tablets, Merck). The suspension was centrifuged at 4,500 x g for 30 minutes at 4 °C. The supernatant was transferred onto PD10 desalting columns to remove free biotin. Proteins were collected and incubated with magnetic streptavidin beads for 1 hour at 4 °C. Biotinylated proteins bound to streptavidin beads were collected with a magnetic stand and washed three times with NP40-free RIPA. Afterwards, they were stored in 100 µL NP40-free RIPA at -20 °C.

SDS-PAGE & IMMUNOBLOT

50 mg infiltrated leaf material was prepared in 150 µL SDS sample buffer (Tsugama et al., 2011), heated at 95 °C for 10 minutes and centrifuged at 16,100 x g for 1 minute. 10 µL of the supernatant was loaded onto a 12% stain-free SDS-PAGE (Bio-RAD) (Laemmli, 1970), the proteins were separated and subsequently transferred to a 0.45 µm nitrocellulose membrane (Cytiva) using the Trans-Blot Turbo Transfer system (Bio-RAD). Membranes were blocked in Tris-buffered saline containing 0.1% (v/v) Tween-20 (TBS-T) and 5% (w/v) milk powder for 30 minutes at room temperature and afterwards incubated with the streptavidin antibody solution (1:1,000, Thermo Fisher) for 1 hour with gentle agitation. The membranes were washed three times with TBS-T for 10 minutes and subsequently visualized using chemiluminescence detection method (Immobilon Western HRP Substrate, Merck).

PROTEOMICS

Protein samples were loaded on a SDS polyacrylamide gel, concentrated in the stacking gel, silver stained according to MS-compatible protocol, reduced, alkylated and digested with trypsin. Peptides were extracted from the gel with 0.1% trifluoroacetic acid and subjected to liquid chromatography. For the LC-MS acquisition an Orbitrap Fusion Lumos Tribrid Mass Spectrometer (Thermo Fisher Scientific) coupled to an Ultimate 3000 Rapid Separation liquid chromatography system (Thermo Fisher Scientific, Idstein, Germany) equipped with an Aurora Ultimate C18 column (75 µm inner diameter, 25 cm length, 1.7 µm particle size from Ion Opticks) as separation column and an Acclaim PepMap 100 C18 column (75 µm inner diameter, 2 cm length, 3 µm particle size from Thermo Fisher Scientific) as trap column. A LC-gradient of 180 min was applied. Survey scans were carried out over a mass range from 375-1,500 m/z at a resolution of 120,000. The target value for the automatic gain control was 400,000 and the maximum fill time 60 ms. Within a cycle time of 2 s the most intense peptide ions (excluding singly charged ions) were selected for fragmentation. Peptide fragments were analyzed in the ion trap using automatic injection time mode and an automatic gain control target value of 10,000 operating in rapid mode. Already fragmented ions were excluded for fragmentation for 60 seconds. Data analysis was performed with Proteome Discoverer (version 2.4.1.15, Thermo Fisher Scientific). All RAW files were searched against the *Arabidopsis thaliana* Swissprot database (Download: 08.07.2024, 39,279 entries) and the Maxquant Contaminant database (Download: 20.02.2021), applying a precursor mass tolerance of 10 ppm and a mass tolerance of 0.6 Da for fragment spectra. Methionine oxidation, N-terminal acetylation, N-terminal methionine loss and N-terminal methionine loss combined with acetylation were considered as variable modification, carbamidomethylation as static modification as well as tryptic cleavage specificity with a maximum of two missed cleavage sites. Label-free quantification was performed using standard parameters within the predefined workflow. Post processing, proteins were filtered to 1% FDR and a minimum of 2 identified peptides per protein.

DATA ANALYSIS

Proteomic data was analyzed by using ID mapping webtool from UniProt (https://www.uniprot.org/id-mapping; Bateman et al., (2025)), SUBA5 to assess cellular localization (https://suba.live; Hooper et al., (2017)). The data was visualized in a volcano plot using R (R version 4.2.3).

RESULTS

MODULAR CLONING STRATEGY FOR COMBINED VISUALIZATION AND PROXIMITY LABELING OF MEMBRANE CONTACT SITES

The split-TurboID was implemented into the modular Golden Gate system (Engler et al., 2014) to rapidly and efficiently identify proteins involved in MCSs. TurboID was split between the 73/74 amino acids into two fragments (referred to as N-TbID and C-TbID), following the design of Cho et al., (2020). Both fragments were integrated as Level 0 modules into the Golden Gate toolkit (Figure 1).

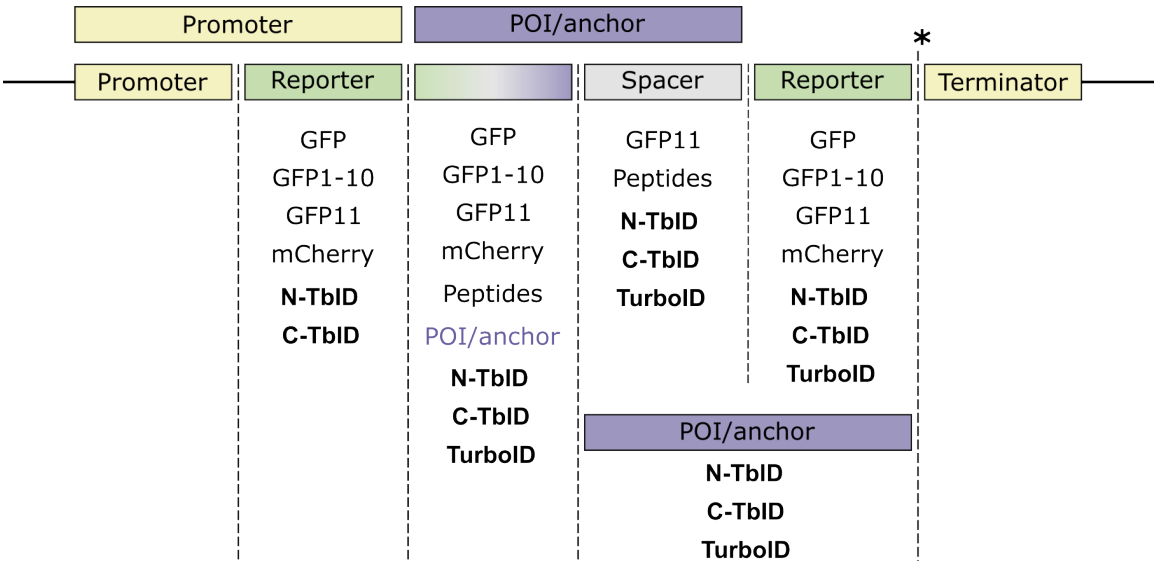

Figure 1: Schematic overview of level 0 modules with their respective position in a transcriptional unit. Modules containing promoters and terminators are depicted in yellow and flank the coding sequences. Reporter genes are depicted in green and include full-length fluorescent proteins, the split-GFP fragments (GFP1-10 and GFP11), the newly implemented (bold) full-length TurboID, and its split-TurboID fragments (N-TbID and C-TbID, corresponding to the N-terminal and C-terminal part of TurboID, split between amino acids 73/74, respectively). Protein of interest (POI) or membrane anchors are depicted in purple and spacers containing peptides of various length are depicted in grey. The principle to generate a transcriptional unit is to assemble these modules seamlessly from promoter to terminator. The asterisk marks the stop codon included in these modules.

Combining proximity labeling with the flexibility of Golden Gate cloning enables the fast and efficient design of constructs to identify proteins within a protein complex or MCSs. The two split-TurboID fragments, N-TbID and C-TbID, can be fused to proteins either hypothesized to participate in multi protein complexes or deliberately targeted to opposing membranes at a MCS.

Instead of relying on direct protein-protein interactions to reconstitute split-TurboID activity, the proximity of membranes at MCSs was used to drive the reassembly and identify candidate proteins of novel MCSs. Accordingly, membrane-anchored proteins were used to target each split-TurboID fragment to the outer membrane of a designated organelle. The chosen membrane anchor for chloroplasts, mitochondria and ER were

OEP7 (Lee et al., 2001), TOM20 (Horie et al., 2003) and KAO2 (Helliwell et al., 2001), respectively, and they were previously shown to reliably target reporter systems to their destination compartments.

In Chapter 1, these proteins successfully targeted the self-assembling split-GFP fragments, GFP1-10 and GFP11, to the outer membranes, enabling BiFC visualization of MCSs *in planta*. Since these components have been implemented into the Golden Gate system, the new toolkit now supports a combined approach: split-GFP for visualization and split-TurboID for proximity labeling. This dual system allows for simultaneous visualization and proteomic characterization of MCSs, further identifying the contactome in plants (Figure 2).

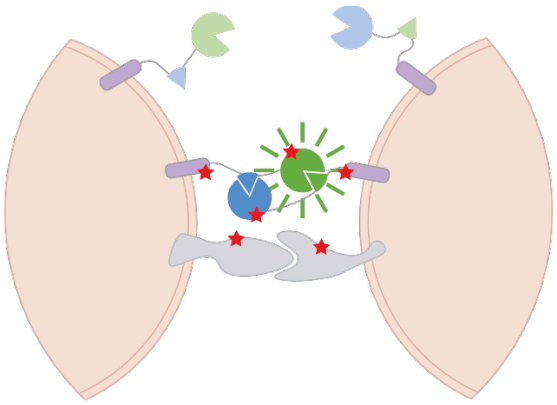

Figure 2: Scheme of the simultaneous approach to synthetically tether endogenous MCSs with split-GFP and split-TurboID. The order of the split fragments of the two proteins were chosen to result in the least increase of tether length to reduce false positives. The split-GFP fragments are depicted in green and the split-TurboID fragments in blue. Biotinylation activity is represented by red stars at proximal proteins, including the synthetic and endogenous tethers.

The order and orientation of the two split protein fragments within the tethers were chosen to minimize the effect on tether length expansion, thereby reducing the risk of false positives.

SIMULTANEOUS VISUALIZATION AND FUNCTIONAL VALIDATION OF SPLIT CONSTRUCTS

To verify the system's functionality in this simultaneous approach, the MCSs were visualized using the self-assembling GFP fragments. The constructs were transiently expressed in tobacco leaves, and transformed protoplasts were isolated and imaged by confocal microscopy.

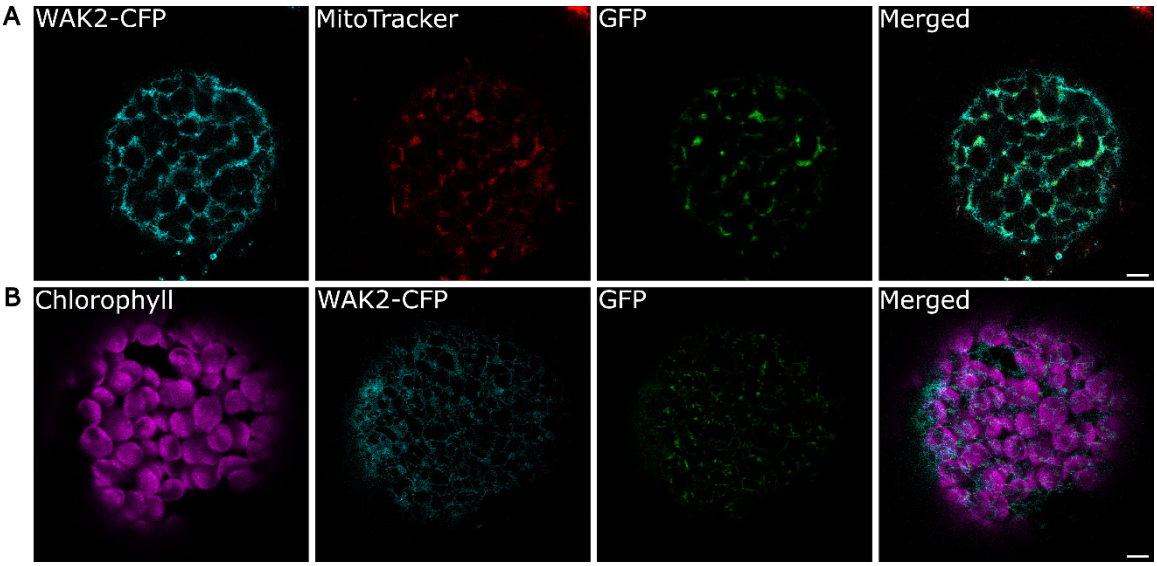

Figure 3: Visualization of split-GFP/split-TurboID approach targeting different MCSs in tobacco protoplasts. The expression constructs were transiently expressed in tobacco protoplasts and visualized by confocal microscopy. ER-mitochondria (A) and ER-chloroplasts (B) MCSs were visualized by their assembled GFP fluorescence (green). Mitochondria were stained using Mito Tracker Red CMXRos (red), the ER was visualized by the ER marker (WAK2-CFP; ***Nelson et al., (2007)***), and chlorophyll autofluorescence represent the chloroplasts (magenta). Scale bar = 5 µm

MCSs between the ER and mitochondria (Figure 3A), and the ER and chloroplasts (Figure 3B) were visualized at respective interfaces of organellar membranes, indicating correct and specific localization of reassembled fragments at MCSs. However, visualized regions of ER-mitochondria MCSs seem to surround the mitochondria entirely, suggesting false positive signals.

The activity of the split-TurboID was assessed via immunoblotting using streptavidin antibody to detect biotinylated proteins. Therefore, *Agrobacterium tumefaciens* carrying the respective expression constructs for ER-chloroplast or ER-mitochondria MCS were infiltrated into tobacco leaves. Total protein was isolated from transformed leaves transiently expressing the gene cassettes and biotinylated proteins were detected via immunoblotting.

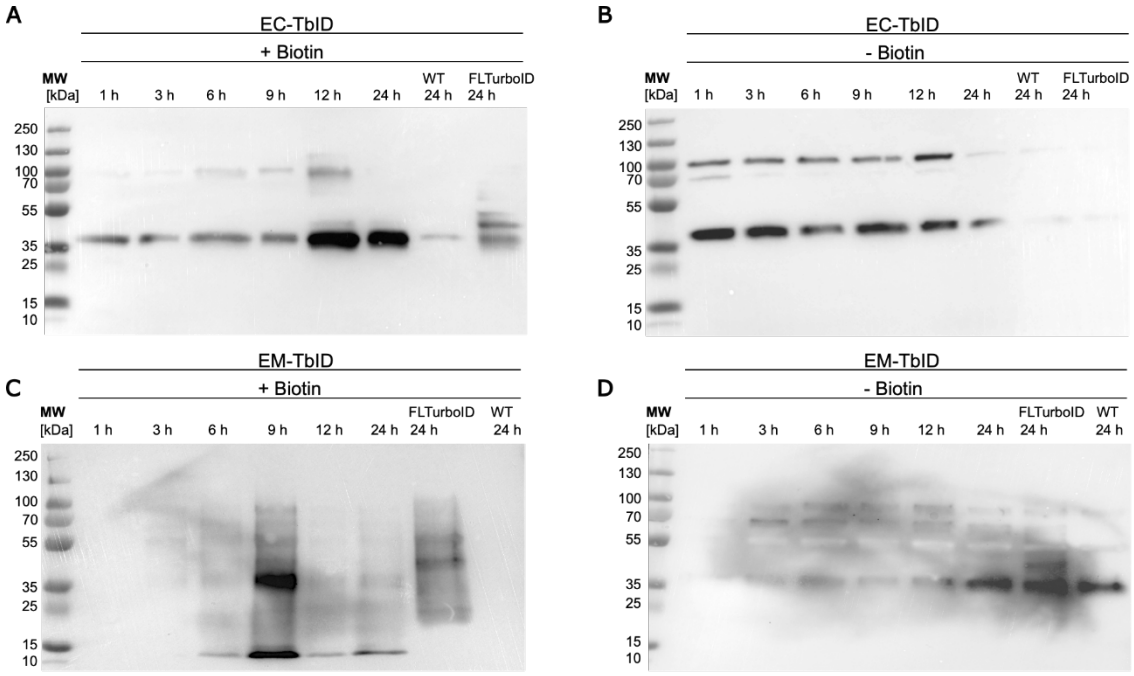

Figure 4: Total protein extracts from plants either expressing ER-chloroplast (A & B) or ER-mitochondria (C & D) split-TurboID constructs subjected to immunoblotting. The plants were treated with 200 µM biotin 48 h after infiltration with *Agrobacterium tumefaciens* carrying the expression constructs. Infiltrated leaves were harvested 1 h, 3 h, 6 h, 9 h, 12 h, and 24 h after treatment with external biotin. As control a mock-treated wild type control and a plant transiently expressing the full-length TurboID (FLTurboID) were harvested after 24 h (A & C). Similarly, leaves from un-treated plants were harvested (B & D). 50 mg of plant material was resuspended in 150 µL of SDS loading buffer and prepared for SDS-PAGE as described in material and methods. Biotinylated proteins were detected by streptavidin antibody.

A time-course experiment with plants transiently expressing ER-chloroplasts (EC-TbID) or ER-mitochondria split-TurboID (EM-TbID) was conducted. Biotinylation levels increased after addition of 200 µM external biotin, indicating split-TurboID activity. EC-TbID samples showed the highest biotinylation at 12 h post treatment (hpt), while EM-TbID samples peaked at 9 hpt. Interestingly, after these time points, the levels of biotinylated proteins declined, suggesting protein degradation. The optimal time points, showing the highest level of biotinylated proteins, were chosen for downstream proteomic analyses.

SPLIT-TURBOID REVEALS DISTINCT PROTEOMES OF ER-MITOCHONDRIA AND ER-CHLOROPLASTS MCS

For the identification of MCS-resident proteins, proximity labeling using the previously implemented split-TurboID constructs was performed. Tobacco leaves were infiltrated with *Agrobacterium tumefaciens* strains carrying the constructs and treated with 200 µM biotin 48 h after infiltration. Leaves were harvested at the previously determined optimal time points (EC-TbID: 12 hpt, EM-TbID: 9 hpt), and 5 g of plant material per sample was processed as described in material and methods. Biotinylated proteins were purified and analyzed via mass spectrometry in four biological replicates for EC-TbID and EM-TbID.

Additionally, the cytosolic full-length TurboID control was prepared and analyzed by mass spectrometry.

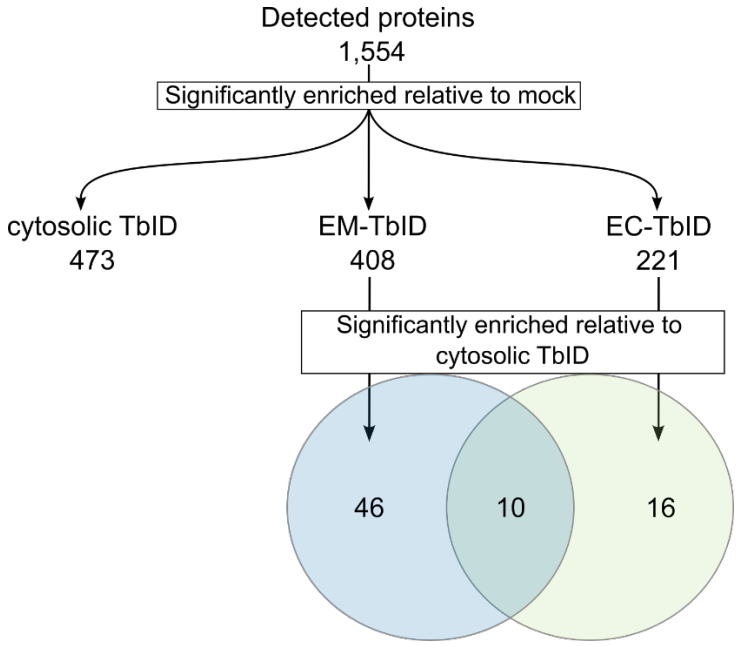

Figure 5: Schematic workflow for filtering proteomic data. The detected proteins (1,554) were filtered for significant enrichment relative to the mock control (*p*-value < 0.05), containing background proteins and endogenous biotinylated proteins. The enriched proteins were further filtered for significant enrichment relative to the cytosolic TurboID (cytosolic TbID) control (*p*-value < 0.05). 56 and 26 proteins were enriched in EM-TbID samples and EC-TbID, respectively. 10 proteins were enriched in both samples relative to the cytosolic TbID.

A total of 1,554 proteins were detected. Of these, 473, 408, and 221 proteins were significantly enriched in the cytosolic TurboID, EM-TbID, and EC-TbID samples, respectively, relative to the un-treated mock control. Proteins were further filtered by their significant enrichment of abundances from identified proteins in EM-TbID or EC-TbID samples relative to the ones quantified in the cytosolic TurboID control. This yielded in 56 and 26 enriched proteins in EM-TbID and EC-TbID, respectively. Of these, 10 proteins were shared by both split-TurboID samples, indicating enrichment of these proteins in both MCSs (Supplementary Table 1). This resulted in 46 proteins enriched exclusively in ER-mitochondria and 16 in ER-chloroplasts MCSs. Among the 10 shared proteins, KAO2, the membrane anchors used for targeting the ER in both constructs, was enriched. Other proteins found in the list of shared enriched proteins were, for instance, proteins involved in the transport ways of the endomembrane system, such as Ras-related proteins, methyltransferases, which were previously suggested to be found in PLAMs, and the fatty acid desaturase 2 (FAD2). Ras-related proteins contribute to the coordination of vesicular trafficking and MCSs within the endomembrane system in different organisms (Borchers et al., 2021) and might possess a similar role in plants. Cycloartenol-C-24-methyltransferase (SMT1) and 24-methylenesterol C-methyltransferase 3 (SMT3) are

involved in the sterol biosynthesis (Diener et al., 2000). This is a known MCS function and might present SMTs as putative candidates for sterol biosynthesis at MCSs. FAD2 is localized to the ER membrane and catalyzes the desaturation of monounsaturated C16 and C18 fatty acids (Okuley et al., 1994; Covello and Reed, 1996). For instance, the resulting 18:2/18:X lipid precursor is exported to both the mitochondria (Caiveau et al., 2001) and the chloroplasts, where it is utilized subsequently for galactolipid biosynthesis. Especially, lipids containing 18:2 acyl-chains are known to be transported from the ER to the chloroplasts (Xu et al., 2010). FAD2 is thereby a suitable candidate for a MCSs involved in lipid trafficking towards the mitochondria and the chloroplasts, providing the transported lipid precursor.

PUTATIVE PROTEINS OF ER-MITOCHONDRIA MCSS

To identify candidate proteins involved in ER-mitochondria MCSs, the 56 significantly enriched proteins in the EM-TbID dataset were analyzed for their subcellular localization using SUBA5 (Figure 6). The 46 proteins specifically enriched in the EM-TbID dataset (Supplementary Table 2) are described in more detail below.

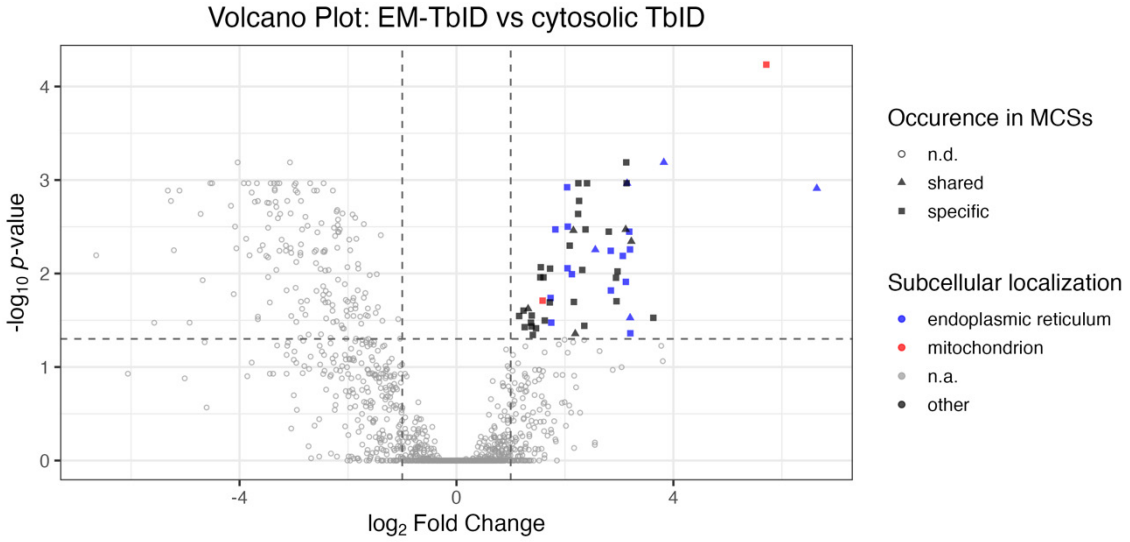

Figure 6: Volcano plot of detected proteins in the EM-TbID dataset. Protein abundances from the EM-TbID dataset relative to the cytosolic TurboID (TbID) were calculated and the *p*-value determined using one-way ANOVA as described in materials and methods. The negative logarithmic ($-\log_{10}$) *p*-value of each detected protein was plotted against the corresponding $\log_2$ fold change. Localization of significantly enriched proteins were assessed using SUBA5, and proteins localized at the ER (blue) or mitochondria (red) were highlighted. Proteins from other subcellular compartments, such as the Golgi or cytosol, were summarized in "other" (black). Proteins specifically enriched in the EM-TbID compared to the EC-TbID dataset are marked with a rectangle, while shared proteins enriched in both datasets are depicted with a triangle. Proteins, which were not significantly enriched are visualized in grey circles. Significant enrichment was set as: $\log_2$ fold change > 1 and *p*-value < 0.05. These thresholds are displayed as dark grey dashed lines.

Previously characterized proteins of ER-mitochondria MCSs, such as MIRO2 or VAP11 (Wang et al., 2014; White et al., 2020), were not detected. Several of the enriched proteins

in the EM-TbID dataset are associated with vesicle trafficking within the endomembrane system, which may reflect an experimental artefact, as visualized previously (Figure 3). However, in mammalian cells, components of the vesicular trafficking machinery such as the SNARE complex have been shown to contribute to MCS formation (Hewlett et al., 2021). In the following, proteins localized to the ER or mitochondria were analyzed in more detail. Only two mitochondrial proteins were enriched in the EM-TbID samples, namely the TOM20, which served as the mitochondrial membrane anchor for this assay, and prohibitin (PHB) 2, a mitochondrial membrane protein. PHBs form a multimeric complex and have been shown to regulate cell homeostasis in various organisms through processes such as mitophagy (Wei et al., 2017), stress response (Chang et al., 2021), and plant development in *Arabidopsis thaliana* (Huang et al., 2019). These are putative functions mediated by MCSs and might suggest a possible role for PHB2 in ER-mitochondria MCSs. Another MCS candidate, At4g24330, is an uncharacterized protein containing a domain of unknown function 1682. It was assigned the GO term for ER calcium ion homeostasis – another known function of ER-mitochondria MCSs.

Putative proteins of ER-chloroplasts MCSs

For assessing proteins associated with ER-chloroplasts MCSs, the 26 significantly enriched proteins in the EC-TbID dataset relative to the cytosolic TurboID were further analyzed, and their localization was assessed using SUBA5 (Figure 7). They were further filtered for their specific enrichment in the EC-TbID samples compared to the EM-TbID samples, leading to 16 specifically enriched proteins in the EC-TbID dataset (Supplementary Table 3). Among these, the plastidial membrane anchors, OEP7, which was used for the assay to target the split TurboID fragment to the chloroplast envelope, was found significantly enriched.

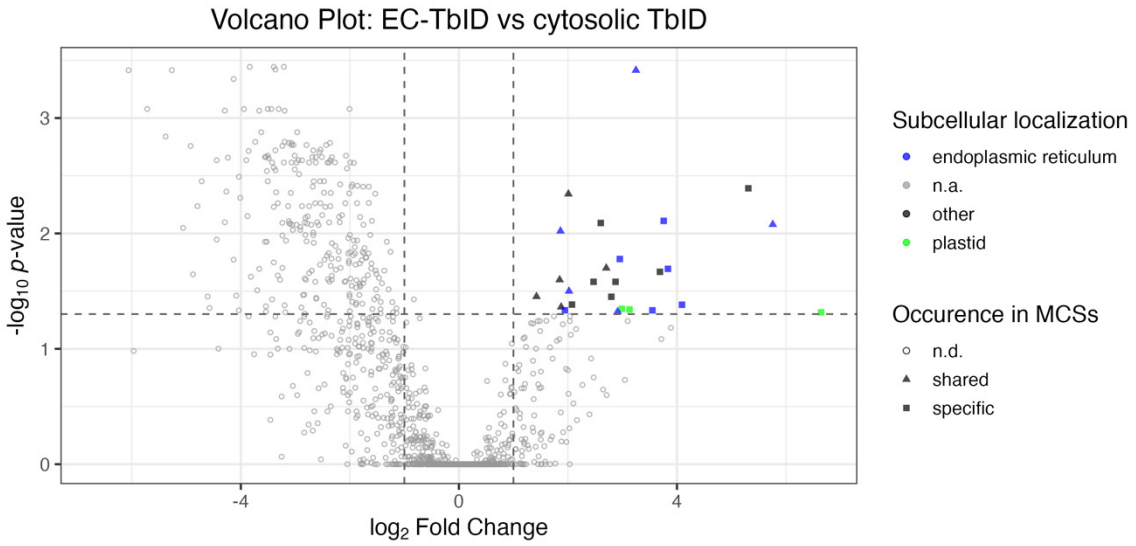

Figure 7: Volcano plot of detected proteins in the EC-TbID dataset. Protein abundances from the EC-TbID dataset relative to the cytosolic TurboID (TbID) were calculated and the *p*-value determined using one-way ANOVA as described in materials and methods. The negative logarithmic ($-\log_{10}$) *p*-value of each detected protein was plotted against the corresponding $\log_2$ fold change. Localization of significantly enriched proteins were assessed using SUBA5, and proteins localized at the ER (blue) or plastid (green) were highlighted. Proteins from other cell compartments were summarized in "other" (black). Proteins specifically enriched in the EC-TbID compared to the EM-TbID dataset are marked with a rectangle, while shared proteins enriched in both datasets are depicted with a triangle. Non-enriched proteins were not further analyzed for either their occurrence in MCSs (n.d.) or subcellular localization (n.a.). Significant enrichment was set as: $\log_2$ fold change > 1 and *p*-value < 0.05. These thresholds are displayed as dark grey dashed lines.

Other enriched proteins, for instance, were the PHB3, cytochrome b5 isoform E (CYTB5-E) and the Sensitive to Freezing 2 (SFR2). PHB3, similar to the PHB2, is a mitochondrial membrane protein (Huang et al., 2019) and might function in tandem to the previously described PHB2. PHB3 has been shown to have multiple roles in the cell's development (Christians and Larsen, 2007; Huang et al., 2019). Given its mitochondrial localization, the presence of PHB3 in the EC-TbID dataset might hint to a tri-organelle MCSs. CYTB5-E is an ER-associated heme-binding protein, which provides electrons for the ER-localized fatty acid desaturases FAD2 and FAD3 (Napier et al., 1997; Kumar et al., 2012). Although, it has been shown that CYTB5-E preferentially provides electrons for FAD3, it is still able to supply electrons to FAD2 for introducing the second double bond to acyl-chains of lipids. FAD2 was previously found to be enriched in both MCSs by the split-TurboID assay and might co-localize with CYTB5-E at specific regions of the ER membrane, efficiently providing the lipid precursor for lipid trafficking at MCSs. SFR2 is a galactolipid:galactolipid galactosyltransferase, which is localized to the chloroplast outer envelope and generates oligogalactolipids upon freezing stress to maintain membrane stability (Fourrier et al., 2008). These proteins contain functions similar to those known for MCSs, and therefore, might represent candidate proteins for ER-chloroplast MCSs.

DISCUSSION

TurboID-based proximity labeling has emerged in recent years as a versatile tool to map the proteome of a bait protein and identify high- and low-affinity PPI *in vivo*. To improve the specificity towards the desired interaction, split variants of reporter proteins have been developed. Cho and colleagues (2020) introduced split-TurboID, a proximity-dependent labeling system based on this principle. While this system has been successfully used in mammalian cells (Cho et al., 2020) and was later implemented for yeast (Fujimoto et al., 2023), it had not been implemented in plant system until now. In this study, we successfully established split-TurboID for the use in plant systems using tobacco as a model. To facilitate ease of the use and broad applicability, the system was implemented into the modular Golden Gate toolkit. This enabled the generation of a membrane-membrane interaction-dependent labeling approach, using organellar membrane proteins as membrane anchors for the split-TurboID fragments.

Designed as a complementary system to the previously established BiFC approach using split-GFP, the split-TurboID can be applied either independently or in combination with split-GFP. This enables a dual approach that allows for simultaneous visualization of MCSs and characterization of their proteome. Similar dual functionality was demonstrated in yeast (Fujimoto et al., 2023). In this study, dual assays for ER-chloroplasts and ER-mitochondria MCSs in plants visualized regions at the interface of the organelles. In parallel, we confirmed the biotinylation activity of the split-TurboID system, and identified optimal harvesting time points for MCS-specific labeling. Interestingly, optimal biotinylation of ER-chloroplasts MCSs required longer treatment (12 hpt) than that of ER-mitochondria MCSs (9 hpt), based on biotinylated protein levels detected by immunoblot (Figure 4). This difference may reflect more extensive or less specific labeling in the ER-mitochondria MCSs, potentially due to enlarged or misregulated MCSs, as suggested by the extensive GFP signal surrounding the mitochondria entirely (Figure 3A). Simultaneous visualization of MCSs in parallel to the proximity labeling served as a control to support the specificity of the labeling, as there is currently no independent method available to verify that the split-TurboID specifically labels MCSs. However, the use of split-GFP might have increased the length of the tethering construct, potentially resulting in false positives. The modular nature of the Golden Gate toolkit allows for flexible assembly of split-TurboID constructs with or without split-GFP, enabling adjustments of the tether length and reducing nonspecific interactions. Chloroplasts-mitochondria MCSs were additionally visualized as dot-like structures and can serve as target in future proteomic studies (Supplementary Figure 1).

To identify novel MCS-associated proteins, we applied split-TurboID-based labeling and analyzed biotinylated proteins presumed to be in proximity to membrane-membrane interactions by mass spectrometry. Proteomic analyses revealed a number of putative candidate proteins potentially involved in MCSs between the ER and mitochondria, and the ER and chloroplasts.

Targeting MCSs between the ER, mitochondria, and chloroplasts was achieved by the membrane anchors KAO2, TOM20, and OEP7, respectively. These anchors were enriched in the proteomic datasets, indicating successful biotinylation and specific enrichment of biotinylated proteins. However, bona fide proteins, localizing to MCSs such as MIRO2 or VAP11, were not found with this approach. This might have multiple reasons. As different MCSs differ in their intermembrane distances between two membranes, shown by split-GFP in Chapter 1 and previous works (Giacomello and Pellegrini, 2016), the here targeted MCSs were not facilitated by such bona fide proteins and hence, were not successfully biotinylated. Alternatively, the chosen membrane anchors were explicitly excluded from certain MCSs, as these structures are strictly regulated and have defined protein compositions (Scorrano et al., 2019). The modular design of the Golden Gate toolkit provides a valuable platform to address these challenges. For example, membrane anchors can be easily replaced alternatives that may localize to different MCSs or spacers and peptides of varying lengths can be included to adjust the tether and better match the intermembrane distance of specific MCSs.

Table 1: Proposed putative proteins for ER-mitochondria and ER-chloroplasts MCSs. The proposed proteins are listed according to their detection in the split-TurboID assay to a respective MCSs. Mentioned candidate proteins that were significantly enriched in both MCSs are displayed in an italic's font. Abbr.: PHB2, prohibitin 2; PHB 3, prohibitin 3; CYTB5-E, cytochrome b5 isoform E; SFR2, sensitive to freezing 2; SMT1, sterol methyltransferase 1; SMT3, sterol methyltransferase 3; FAD2, fatty acid desaturase 2

ER-mitochondria MCS		ER-chloroplasts MCS	
Protein	Function	Protein	Function
PHB2	Cell homeostasis	PHB3	Cell homeostasis
At4g24330 (DUF1682)	Ca^{2+} homeostasis	CYTB5-E	Electron donor
		SFR2	Stress response
SMT3	*Sterol biosynthesis*	*SMT3*	*Sterol biosynthesis*
SMT1	*Sterol biosynthesis*	*SMT1*	*Sterol biosynthesis*
FAD2	*Lipid biosynthesis*	*FAD2*	*Lipid biosynthesis*

Putative proteins involved in MCSs were selected based on their known or predicted roles in cellular functions commonly associated with MCSs, such as sterol biosynthesis, Ca^{2+} homeostasis, and cellular homeostasis, and a set of putative proteins is listed in Table 1.

Among them, an uncharacterized protein containing a domain of unknown function 1682 is predicted to be a membrane protein, localizing to the endomembrane system, possibly the ER based on the presence of transmembrane domains. This protein has been proposed to be involved in ER Ca^{2+} homeostasis. However, due to the limited information available, its exact function and relevance to MCSs remains to be determined.

Two sterol methyltransferases (SMT1 and SMT3) were significantly enriched in both split-TurboID datasets compared to the cytosolic TurboID control. Notably, a sterol methyltransferase was previously detected in proteomic data (Data not shown), where it localized to plastid associated membranes, which are ER membrane patches associated with the chloroplast envelope. Similarly, SFR2, another protein proposed to localize to plastid associated membranes, was enriched in the EC-TbID samples. These findings suggest that SMTs and SFR2 may represent promising candidates for MCS-localized proteins. Additionally, proteins such as SFR2, FAD2 and CYTB5-E function in lipid biosynthesis, which is a well-established function of MCSs between the ER and mitochondria, and the ER and chloroplasts (Pérez-Sancho et al., 2016; Prinz et al., 2020). The PHB3 enriched in the EC-TbID dataset, PHB2 and 25.3 kDa vesicle transport protein SEC22-1 in the EM-TbID dataset were also found enriched via the chloroplast immunopurification of intact chloroplasts and chloroplast envelopes (Chapter 3). In mammalian cells, SEC22b, a component of the SNARE complex, was found in ER-mitochondria MCSs (Kwak et al., 2020; Bonaud et al., 2023). Since SEC22-1, PHB2, and PHB3, which were previously described, were enriched in two independent biochemical approaches, they present possible candidate proteins associated with MCSs.

Due to the surrounding GFP fluorescence of the EM-TbID, this dataset needs to be handled with caution. To support the data, the split-TurboID approach for ER-mitochondria MCSs should be repeated using constructs that exclude the split-GFP fragments. This would shorten the tether and likely improve specificity. Comparing the resulting proteomic dataset with existing ones may refine the list of candidate proteins of MCSs.

Future work will include *in vivo* localization studies to validate candidate proteins and their association with MCSs. The split-TurboID approach can be further refined to suit the diversity of MCS types, which vary in intermembrane distances (Giacomello and Pellegrini, 2016; Cieri et al., 2018) and respond dynamically to different environmental and developmental cues (Calì et al., 2025). The Golden Gate-based modular method and the transient expression system support such adaptations, for instance, by adjusting tether lengths with spacer modules, by enabling expression of constructs under specific conditions, such as abiotic stress, simulated by heat or cold treatment during the

expression of the constructs in plants, or by expressing the construct in different tissue types or developmental stages of the plant.

In conclusion, the established split-TurboID-based proximity labeling for plants offers a flexible and robust platform for identifying candidate proteins at organellar contact sites, possibly under various physiological conditions. This approach holds great potential for uncovering the dynamic and transient nature of MCSs and will be a powerful tool to map the plant contactome at organellar interfaces.

REFERENCES

Ahmed, N., Preisinger, C., Wilhelm, T., and Huber, M., (2024). TurboID-Based IRE1 Interactome Reveals Participants of the Endoplasmic Reticulum-Associated Protein Degradation Machinery in the Human Mast Cell Leukemia Cell Line HMC-1.2. Cells. 2024:**13**(9). https://doi.org/10.3390/cells13090747

Andersson, M.X., Goksör, M., and Sandelius, A.S., (2007). Optical manipulation reveals strong attracting forces at membrane contact sites between endoplasmic reticulum and chloroplasts. Journal of Biological Chemistry. 2007:**282**(2):1170–1174. https://doi.org/10.1074/jbc.M608124200

Bateman, A., Martin, M.-J., Orchard, S., Magrane, M., Adesina, A., Ahmad, S., Bowler-Barnett, E.H., Bye-A-Jee, H., Carpentier, D., Denny, P., et al., (2025). UniProt: the Universal Protein Knowledgebase in 2025. Nucleic Acids Res. 2025:**53**(D1):D609–D617. https://doi.org/10.1093/nar/gkae1010

Block, M.A., and Jouhet, J., (2015). Lipid trafficking at endoplasmic reticulum-chloroplast membrane contact sites. Curr Opin Cell Biol. 2015:**35**:21–29. https://doi.org/10.1016/j.ceb.2015.03.004

Bonaud, A., Gargowitsch, L., Gilbert, S.M., Rajan, E., Canales-Herrerias, P., Stockholm, D., Rahman, N.F., Collins, M.O., Taskiran, H., Hill, D.L., et al., (2023). Sec22b is a critical and nonredundant regulator of plasma cell maintenance. Proc Natl Acad Sci U S A. 2023:**120**(2). https://doi.org/10.1073/pnas.2213056120

Borchers, A.C., Langemeyer, L., and Ungermann, C., (2021). Who's in control? Principles of rab gtpase activation in endolysosomal membrane trafficking and beyond. Journal of Cell Biology. 2021:**220**(9). https://doi.org/10.1083/jcb.202105120

Branon, T.C., Bosch, J.A., Sanchez, A.D., Udeshi, N.D., Svinkina, T., Carr, S.A., Feldman, J.L., Perrimon, N., and Ting, A.Y., (2018). Efficient proximity labeling in living cells and organisms with TurboID. Nat Biotechnol. 2018:**36**(9):880–898. https://doi.org/10.1038/nbt.4201

Caiveau, O., Fortune, D., Cantrel, C., Zachowski, A., and Moreau, F., (2001). Consequences of ω-6-Oleate Desaturase Deficiency on Lipid Dynamics and Functional Properties of Mitochondrial Membranes of Arabidopsis thaliana. Journal of Biological Chemistry. 2001:**276**(8):5788–5794. https://doi.org/10.1074/jbc.M006231200

Calì, T., Bayer, E.M., Eden, E.R., Hajnóczky, G., Kornmann, B., Lackner, L., Liou, J., Reinisch, K., Rhee, H.-W., Rizzuto, R., et al., (2025). Key challenges and recommendations for defining organelle membrane contact sites. Nat Rev Mol Cell Biol. 2025. https://doi.org/10.1038/s41580-025-00864-x

Chang, X., Zhu, G., Chen, S., Sun, D., He, H., Li, G., Xu, Y., Ren, Z., Xu, C., and Jin, S., (2021). AtPHB2 regulates salt stress response in Arabidopsis thaliana. Plant Growth Regul. 2021:**94**(1):23–32. https://doi.org/10.1007/s10725-021-00692-x

Cho, K.F., Branon, T.C., Rajeev, S., Svinkina, T., Udeshi, N.D., Thoudam, T., Kwak, C., Rhee, H.W., Lee, I.K., Carr, S.A., et al., (2020). Split-TurboID enables contact-dependent proximity labeling in cells. Proc Natl Acad Sci U S A. 2020:**117**(22). https://doi.org/10.1073/pnas.1919528117

Christians, M.J., and Larsen, P.B., (2007). Mutational loss of the prohibitin AtPHB3 results in an extreme constitutive ethylene response phenotype coupled with partial loss of ethylene-inducible gene expression in Arabidopsis seedlings. J Exp Bot. 2007:**58**(8):2237–2248. https://doi.org/10.1093/jxb/erm086

Cieri, D., Vicario, M., Giacomello, M., Vallese, F., Filadi, R., Wagner, T., Pozzan, T., Pizzo, P., Scorrano, L., Brini, M., et al., (2018). SPLICS: A split green fluorescent protein-based contact site sensor for narrow and wide heterotypic organelle juxtaposition. Cell Death Differ. 2018:**25**(6):1131–1145. https://doi.org/10.1038/s41418-017-0033-z

Covello, P.S., and Reed, D.W., (1996). Functional Expression of the Extraplastidial Arabidopsis thaliana Oleate Desaturase Gene (FAD2) in Saccharomyces cerevisiae. Plant Physiol. 1996:**111**(1):223–226. https://doi.org/10.1104/pp.111.1.223

Coyaud, E., Mis, M., Laurent, E.M.N., Dunham, W.H., Couzens, A.L., Robitaille, M., Gingras, A.C., Angers, S., and Raught, B., (2015). BioID-based identification of skp cullin F-box (SCF)β-TrCP1/2 E3 ligase substrates. Molecular and Cellular Proteomics. 2015:**14**(7):1781–1795. https://doi.org/10.1074/mcp.M114.045658

Diener, A.C., Li, H., Zhou, W.-X., Whoriskey, W.J., David Nes, W., and Fink, G.R., (2000). STEROL METHYLTRANSFERASE 1 Controls the Level of Cholesterol in Plants.

Engler, C., Youles, M., Gruetzner, R., Ehnert, T.M., Werner, S., Jones, J.D.G., Patron, N.J., and Marillonnet, S., (2014). A Golden Gate modular cloning toolbox for plants. ACS Synth Biol. 2014:**3**(11):839–843. https://doi.org/10.1021/sb4001504

Feizy, N., Leuchtenberg, S.F., Steiner, C., Würtz, B., Fliegner, L., and Huber, A., (2024). In vivo identification of Drosophila rhodopsin interaction partners by biotin proximity labeling. Sci Rep. 2024:**14**(1). https://doi.org/10.1038/s41598-024-52041-3

Fourrier, N., Bédard, J., Lopez-Juez, E., Barbrook, A., Bowyer, J., Jarvis, P., Warren, G., and Thorlby, G., (2008). A role for SENSITIVE to FREEZING2 in protecting chloroplasts against freeze-induced damage in Arabidopsis. Plant Journal. 2008:**55**(5):734–745. https://doi.org/10.1111/j.1365-313X.2008.03549.x

Fujimoto, S., Tashiro, S., and Tamura, Y., (2023). Complementation Assay Using Fusion of Split-GFP and TurboID (CsFiND) Enables Simultaneous Visualization and Proximity Labeling of Organelle Contact Sites in Yeast. Contact. 2023:**6**. https://doi.org/10.1177/25152564231153621

Gallie, D.R., Sleat, D.E., Watts, J.W., Tumer, P.C., Michael, T., and Wilson, A., (1987). The 5'-leader sequence of tobacco mosaic virus RNA enhances the expression of foreign gene transcripts in vitro and in vivo.

Giacomello, M., and Pellegrini, L., (2016). The coming of age of the mitochondria-ER contact: A matter of thickness. Cell Death Differ. 2016:**23**(9):1417–1427. https://doi.org/10.1038/cdd.2016.52

Grefen, C., Donald, N., Hashimoto, K., Kudla, J., Schumacher, K., and Blatt, M.R., (2010). A ubiquitin-10 promoter-based vector set for fluorescent protein tagging facilitates temporal stability and native protein distribution in transient and stable expression studies. Plant Journal. 2010:**64**(2):355–365. https://doi.org/10.1111/j.1365-313X.2010.04322.x

Gynheung, A.N., (1986). Development of Plant Promoter Expression Vectors and Their Use for Analysis of Differential Activity of Nopaline Synthase Promoter in Transformed Tobacco Cells'.

Han, Y., Branon, T.C., Martell, J.D., Boassa, D., Shechner, D., Ellisman, M.H., and Ting, A., (2019). Directed Evolution of Split APEX2 Peroxidase. ACS Chem Biol. 2019:**14**(4):619–635. https://doi.org/10.1021/acschembio.8b00919

Helliwell, C.A., Sullivan, J.A., Mould, R.M., Gray, J.C., Peacock, W.J., and Dennis, E.S., (2001). A plastid envelope location of Arabidopsis ent-kaurene oxidase links the plastid and endoplasmic reticulum steps of the gibberellin biosynthesis pathway. The Plant Journal. 2001:**28**(2):201–208. https://doi.org/10.1046/j.1365-313X.2001.01150.x

Hewlett, B., Singh, N.P., Vannier, C., and Galli, T., (2021). ER-PM Contact Sites – SNARING Actors in Emerging Functions. Front Cell Dev Biol. 2021:**9**. https://doi.org/10.3389/fcell.2021.635518

Hooper, C.M., Castleden, I.R., Tanz, S.K., Aryamanesh, N., and Millar, A.H., (2017). SUBA4: The interactive data analysis centre for Arabidopsis subcellular protein locations. Nucleic Acids Res. 2017:**45**(D1):D1064–D1074. https://doi.org/10.1093/nar/gkw1041

Horie, C., Suzuki, H., Sakaguchi, M., and Mihara, K., (2003). Targeting and Assembly of Mitochondrial Tail-anchored Protein Tom5 to the TOM Complex Depend on a Signal Distinct from That of Tail-anchored Proteins Dispersed in the Membrane. Journal of

Biological Chemistry. 2003:**278**(42):41462–41471. https://doi.org/10.1074/jbc.M307047200

Huang, R., Yang, C., and Zhang, S., (2019). The Arabidopsis PHB3 is a pleiotropic regulator for plant development. Plant Signal Behav. 2019:**14**(11). https://doi.org/10.1080/15592324.2019.1656036

Hurlock, A.K., Roston, R.L., Wang, K., and Benning, C., (2014). Lipid trafficking in plant cells. Traffic. 2014:**15**(9):915–932. https://doi.org/10.1111/tra.12187

Jouhet, J., Maréchal, E., Baldan, B., Bligny, R., Joyard, J., and Block, M.A., (2004). Phosphate deprivation induces transfer of DGDG galactolipid from chloroplast to mitochondria. Journal of Cell Biology. 2004:**167**(5):863–874. https://doi.org/10.1083/jcb.200407022

Kim, D.I., Birendra, K.C., Zhu, W., Motamedchaboki, K., Doye, V., and Roux, K.J., (2014). Probing nuclear pore complex architecture with proximity-dependent biotinylation. Proc Natl Acad Sci U S A. 2014:**111**(24). https://doi.org/10.1073/pnas.1406459111

Kim, D.I., and Roux, K.J., (2016). Filling the Void: Proximity-Based Labeling of Proteins in Living Cells. Trends Cell Biol. 2016:**26**(11):804–817. https://doi.org/10.1016/j.tcb.2016.09.004

Kim, T.W., Park, C.H., Hsu, C.C., Kim, Y.W., Ko, Y.W., Zhang, Z., Zhu, J.Y., Hsiao, Y.C., Branon, T., Kaasik, K., et al., (2023). Mapping the signaling network of BIN2 kinase using TurboID-mediated biotin labeling and phosphoproteomics. Plant Cell. 2023:**35**(3):975–993. https://doi.org/10.1093/plcell/koad013

Kovacs, M., Geltinger, F., Schartel, L., Pöschl, S., Briza, P., Paschinger, M., Boros, K., Felder, T.K., Wimmer, H., Duschl, J., et al., (2023). Ola1p trafficking indicates an interaction network between mitochondria, lipid droplets, and stress granules in times of stress. J Lipid Res. 2023:**64**(12). https://doi.org/10.1016/j.jlr.2023.100473

Kumar, R., Tran, L.S.P., Neelakandan, A.K., and Nguyen, H.T., (2012). Higher plant cytochrome b5 polypeptides modulate fatty acid desaturation. PLoS One. 2012:**7**(2). https://doi.org/10.1371/journal.pone.0031370

Kwak, C., Shin, S., Park, J., Jung, M., Thi, T., Nhung, M., Kang, M., Kwon, T., Park, S.K., Mun, J.Y., et al., (2020). Correction for Kwak et al., Contact-ID, a tool for profiling organelle contact sites, reveals regulatory proteins of mitochondrial-associated membrane formation. Proceedings of the National Academy of Sciences. 2020:**117**(32):19605–19605. https://doi.org/10.1073/pnas.2014254117

Laemmli, U.K., (1970). Cleavage of Structural Proteins during the Assembly of the Head of Bacteriophage T4. Nature. 1970:**227**:680–685.

Lee, S.Y., Cheah, J.S., Zhao, B., Xu, C., Roh, H., Kim, C.K., Cho, K.F., Udeshi, N.D., Carr, S.A., and Ting, A.Y., (2023). Engineered allostery in light-regulated LOV-Turbo enables precise spatiotemporal control of proximity labeling in living cells. Nat Methods. 2023:**20**(6):908–917. https://doi.org/10.1038/s41592-023-01880-5

Lee, Y.J., Kim, D.H., Kim, Y.-W., and Hwang, I., (2001). Identification of a Signal That Distinguishes between the Chloroplast Outer Envelope Membrane and the Endomembrane System in Vivo. Plant Cell. 2001:**13**(10):2175–2190. https://doi.org/10.1105/tpc.010232

Liu, L., and Li, J., (2019). Communications between the endoplasmic reticulum and other organelles during abiotic stress response in plants. Front Plant Sci. 2019:**10**. https://doi.org/10.3389/fpls.2019.00749

Mehus, A.A., Anderson, R.H., and Roux, K.J., (2016). BioID Identification of Lamin-Associated Proteins. In Methods in Enzymology (Academic Press Inc.), pp. 3–22. https://doi.org/10.1016/bs.mie.2015.08.008

Nakamura, Y., Tsuchiya, M., and Ohta, H., (2007). Plastidic phosphatidic acid phosphatases identified in a distinct subfamily of lipid phosphate phosphatases with prokaryotic origin. Journal of Biological Chemistry. 2007:**282**(39):29013–29021. https://doi.org/10.1074/jbc.M704385200

Napier, J.A., Sayanova, O., Stobart, A.K., and Shewry, P.R., (1997). A new class of cytochrome b5 fusion proteins. Biochem J. 1997:**328 (Pt 2)**(Pt 2):717–8.

Nelson, B.K., Cai, X., and Nebenführ, A., (2007). A multicolored set of in vivo organelle markers for co-localization studies in Arabidopsis and other plants. Plant Journal. 2007:**51**(6):1126–1136. https://doi.org/10.1111/j.1365-313X.2007.03212.x

Nikonorova, I.A., desRanleau, E., Jacobs, K.C., Saul, J., Walsh, J.D., Wang, J., and Barr, M.M., (2025). Polycystins recruit cargo to distinct ciliary extracellular vesicle subtypes in C. elegans. Nat Commun. 2025:**16**(1):2899. https://doi.org/10.1038/s41467-025-57512-3

Okuley, J., Lightner, J., Feldmann, K., Yadav, N., Lark, E., and Browseai', J., (1994). Arabidopsis FAD2 Gene Encodes the Enzyme That 1s Essential for Polyunsaturated Lipid Synthesis.

Pérez-Sancho, J., Tilsner, J., Samuels, A.L., Botella, M.A., Bayer, E.M., and Rosado, A., (2016). Stitching Organelles: Organization and Function of Specialized Membrane Contact Sites in Plants. Trends Cell Biol. 2016:**26**(9):705–717. https://doi.org/10.1016/j.tcb.2016.05.007

Prinz, W.A., Toulmay, A., and Balla, T., (2020). The functional universe of membrane contact sites. Nat Rev Mol Cell Biol. 2020:**21**(1):7–24. https://doi.org/10.1038/s41580-019-0180-9

Roux, K.J., Kim, D.I., Burke, B., and May, D.G., (2018). BioID: A Screen for Protein-Protein Interactions. Curr Protoc Protein Sci. 2018:**91**(1):19.23.1-19.23.15. https://doi.org/10.1002/cpps.51

Schindelin, J., Arganda-Carreras, I., Frise, E., Kaynig, V., Longair, M., Pietzsch, T., Preibisch, S., Rueden, C., Saalfeld, S., Schmid, B., et al., (2012). Fiji: An open-source platform for biological-image analysis. Nat Methods. 2012:**9**(7):676–682. https://doi.org/10.1038/nmeth.2019

Schopp, I.M., Amaya Ramirez, C.C., Debeljak, J., Kreibich, E., Skribbe, M., Wild, K., and Béthune, J., (2017). Split-BioID a conditional proteomics approach to monitor the composition of spatiotemporally defined protein complexes. Nat Commun. 2017:**8**. https://doi.org/10.1038/ncomms15690

Scorrano, L., De Matteis, M.A., Emr, S., Giordano, F., Hajnóczky, G., Kornmann, B., Lackner, L.L., Levine, T.P., Pellegrini, L., Reinisch, K., et al., (2019). Coming together to define membrane contact sites. Nat Commun. 2019:**10**(1):1–11. https://doi.org/10.1038/s41467-019-09253-3

Shi, L., Marti Ferrando, T., Landeo Villanueva, S., Joosten, M.H.A.J., Vleeshouwers, V.G.A.A., and Bachem, C.W.B., (2023). Protocol to identify protein-protein interaction networks in Solanum tuberosum using transient TurboID-based proximity labeling. STAR Protoc. 2023:**4**(4):102577. https://doi.org/10.1016/j.xpro.2023.102577

Titeca, K., Lemmens, I., Tavernier, J., and Eyckerman, S., (2019). Discovering cellular protein-protein interactions: Technological strategies and opportunities. Mass Spectrom Rev. 2019:**38**(1):79–111. https://doi.org/10.1002/mas.21574

Tsugama, D., Liu, S., and Takano, T., (2011). A rapid chemical method for lysing Arabidopsis cells for protein analysis. Plant Methods. 2011:**7**(1):1–7. https://doi.org/10.1186/1746-4811-7-22

Wang, P., Hawkins, T.J., Richardson, C., Cummins, I., Deeks, M.J., Sparkes, I., Hawes, C., and Hussey, P.J., (2014). The plant cytoskeleton, NET3C, and VAP27 mediate the link between the plasma membrane and endoplasmic reticulum. Current Biology. 2014:**24**(12):1397–1405. https://doi.org/10.1016/j.cub.2014.05.003

Wei, Y., Chiang, W.-C., Sumpter, R., Mishra, P., and Levine, B., (2017). Prohibitin 2 Is an Inner Mitochondrial Membrane Mitophagy Receptor. Cell. 2017:**168**(1–2):224-238.e10. https://doi.org/10.1016/j.cell.2016.11.042

White, R.R., Lin, C., Leaves, I., Castro, I.G., Metz, J., Bateman, B.C., Botchway, S.W., Ward, A.D., Ashwin, P., and Sparkes, I., (2020). Miro2 tethers the ER to mitochondria to promote mitochondrial fusion in tobacco leaf epidermal cells. Commun Biol. 2020:**3**(1):1–8. https://doi.org/10.1038/s42003-020-0872-x

Xu, C., Moellering, E.R., Muthan, B., Fan, J., and Benning, C., (2010). Lipid transport mediated by arabidopsis TGD proteins is unidirectional from the endoplasmic reticulum to the plastid. Plant Cell Physiol. 2010:**51**(6):1019–1028. https://doi.org/10.1093/pcp/pcq053

Zhang, Y., Sampathkumar, A., Kerber, S.M.-L., Swart, C., Hille, C., Seerangan, K., Graf, A., Sweetlove, L., and Fernie, A.R., (2020). A moonlighting role for enzymes of glycolysis in the co-localization of mitochondria and chloroplasts. Nat Commun. 2020:**11**(1). https://doi.org/10.1038/s41467-020-18234-w

SUPPLEMENTARY DATA

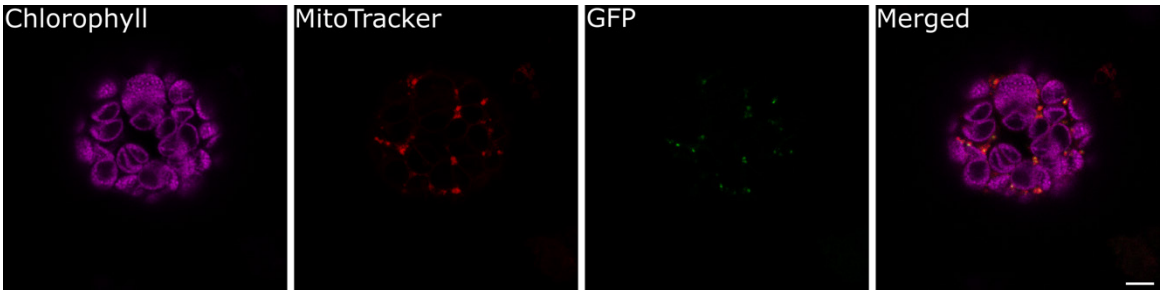

Supplementary Figure 1: Visualization of split-TurboID assay of MCSs between chloroplasts and mitochondria. Expression constructs containing the two tethers targeting the chloroplast envelope and mitochondrial membrane with respective split-GFP and split-TurboID fragments were transiently expressed in tobacco protoplasts. GFP fluorescence (green) indicate reassembled GFP fragments at MCSs. Mitochondria were visualized by MitoTracker Red CMXRos (red) and chloroplasts were represented by their chlorophyll autofluorescence (magenta). Scale bar = 5 µm.

Supplementary Table 1: The 10 significantly enriched proteins of both MCS samples (EM-TbID and EC-TbID) relative to the cytosolic TurboID control. Proteins with a $\log_2$ fold change of above 1 and *p*-value below 0.05 in both datasets relative to the cytosolic TurboID were considered significantly enriched. Their localization was assessed by SUBA5.

Accession	Protein name	AGI	Localization
P19892	Ras-related protein RABA5e	At1g05810	cytosol
F4HTM3	Mannosyl-oligosaccharide glucosidase GCS1	At1g67490	endoplasmic reticulum
Q94JS4	24-methylenesterol C-methyltransferase 3	At1g76090	endoplasmic reticulum
Q9ZQ34	Uncharacterized protein At2g24330	At2g24330	nucleus
P92994	Trans-cinnamate 4-monooxygenase	At2g30490	endoplasmic reticulum
Q9C5Y2	Ent-kaurenoic acid oxidase 2	At2g32440	endoplasmic reticulum
B3H636	NAC domain containing protein 41	At2g33480	nucleus
P46313	Delta(12)-fatty-acid desaturase	At3g12120	endoplasmic reticulum
Q96283	Ras-related protein RABA2c	At3g46830	golgi
Q9LM02	Cycloartenol-C-24-methyltransferase	At5g13710	golgi

Supplementary Table 2: Specifically enriched proteins in the EM-TbID dataset. Proteins, which were significantly enriched (log_2 fold change > 1 and *p*-value < 0.05) relative to the cytosolic TurboID control in the EM-TbID dataset, but not in the EC-TbID samples, are listed here. Their localization was determined by SUBA5.

Accession	Protein name	AGI	Localization
Q9ZNT7	Prohibitin-2, mitochondrial	AT1G03860	mitochondrion
P28185	Ras-related protein RABA1a	AT1G06400	golgi
A0A1P8AST0	3-ketoacyl-CoA synthase	AT1G07720	extracellular
O04486	Ras-related protein RABA2a OS=Arabidopsis thaliana OX=3702 GN=RABA2A PE=2 SV=1	AT1G09630	plasma membrane, cytosol
Q94AU2	25.3 kDa vesicle transport protein SEC22-1	AT1G11890	endoplasmic reticulum
Q9LNB6	Hsp70-Hsp90 organizing protein 1	AT1G12270	nucleus
Q9M9E1	ABC transporter G family member 40	AT1G15520	plasma membrane
P82873	Mitochondrial import receptor subunit TOM20-2	AT1G27390	mitochondrion
A0A1P8AM79	alpha-1,2-Mannosidase	AT1G30000	golgi
Q94BQ9	Integral membrane HRF1 family protein	AT1G30890	endoplasmic reticulum
P59277	Syntaxin-81	AT1G51740	endoplasmic reticulum
C0LGH2	Probable LRR receptor-like serine/threonine-protein kinase At1g56130	AT1G56130	plasma membrane
Q9CAL3	Cysteine-rich receptor-like protein kinase 2	AT1G70520	plasma membrane
Q9C7H2	Threonylcarbamoyladenosine tRNA methylthiotransferase	AT1G72090	endoplasmic reticulum
Q9FRK5	Uncharacterized membrane protein At1g75140	AT1G75140	endoplasmic reticulum
F4IRC0	Sucrose transporter 2	AT2G02860	golgi
Q9SL48	SEC1 family transport protein SLY1	AT2G17980	plasma membrane
Q9ZQH3	Protein transport protein SEC23 D	AT2G27460	golgi, endoplasmic reticulum
F4ISU2	Early endosome antigen	AT2G32240	endoplasmic reticulum
Q9ZR72	ABC transporter B family member 1	AT2G36910	plasma membrane
Q9SRI1	Protein transport protein SEC13 homolog A	AT3G01340	nucleus, cytosol
Q9M8T0	Probable inactive receptor kinase At3g02880	AT3G02880	plasma membrane
Q9SS37	Reticulon-like protein B8	AT3G10260	vacuole
Q9LSX7	Peroxisome biogenesis protein 22	AT3G21865	nucleus
Q9LSJ5	ABC transporter B family member 18	AT3G28390	plasma membrane
Q8L776	ATP-dependent helicase/deoxyribonuclease subunit B	AT3G51610	vacuole, endoplasmic reticulum
B3H4I6	UDP-glucuronate decarboxylase	AT3G53520	golgi
A0A1I9LT70	Ras-related small GTP-binding family protein	AT3G54840	golgi
Q9M2R0	FT-interacting protein 3	AT3G57880	endoplasmic reticulum
F4J110	Transducin family protein / WD-40 repeat family protein	AT3G63460	golgi
Q93ZN5	AT4g00090/F6N15_8	AT4G00090	endoplasmic reticulum
Q9STW1	At4g24330	AT4G24330	endoplasmic reticulum

Continued on the next page

Supplementary Table 2 (continued)

Q9SB48	NADPH--cytochrome P450 reductase 1	AT4G24520	endoplasmic reticulum
Q9M0A0	AT4g30600/F17I23_60	AT4G30600	endoplasmic reticulum
Q9SB75	Probable xyloglucan glycosyltransferase 5	AT4G31590	plasma membrane
F4JN35	Protein NTM1-like 9	AT4G35580	nucleus
O22476	Protein BRASSINOSTEROID INSENSITIVE 1	AT4G39400	plasma membrane
Q6NLA5	Lipid phosphate phosphatase gamma	AT5G03080	*plastid* (Nakamura et al., 2007)
Q9S814	Ethylene-insensitive protein 2	AT5G03280	endoplasmic reticulum
Q9LZ83	At5g04420	AT5G04420	golgi
Q93ZY3	Dolichyl-diphosphooligosaccharide--protein glycosyltransferase subunit STT3A	AT5G19690	endoplasmic reticulum
Q9LT02	Probable manganese-transporting ATPase PDR2	AT5G23630	endoplasmic reticulum
A0A1P8B9J9	Chloride channel protein	AT5G26240	golgi
Q84WI4	Protein transport protein SEC23 G	AT5G43670	golgi, endoplasmic reticulum
A0A1P8B9X0	Protein transport protein sec16	AT5G47490	nucleus
Q9FLH0	Protein CROWDED NUCLEI 4	AT5G65770	nucleus

Supplementary Table 3: Enriched proteins of EC-TbID samples relative to EM-TbID. Proteins of EC-TbID samples that were enriched relative to the cytosolic TurboID samples were further filtered for their enrichment relative to MCS-enriched proteins detected in EM-TbID (log_2 fold change > 1). These proteins were further filtered for their localization to the ER and plastids, leading to 17 proteins.

Accession	Protein name	AGI	Localization
Q940J9	Probable methyltransferase PMT8	AT1G04430	golgi
A0A1P8AZZ4	Uncharacterized protein	AT2G10455	unknown
Q8GW96	AAA-ATPase At2g18193	AT2G18193	endoplasmic reticulum
Q9ZVI9	Ethanolamine-phosphate cytidylyltransferase	AT2G38670	mitochondrion
Q93Y07	Galactolipid galactosyltransferase SFR2, chloroplastic	AT3G06510	plastid
Q9ZRE2	Ras-related protein RABD1	AT3G11730	golgi
Q9FYC2	Pheophorbide a oxygenase, chloroplastic	AT3G44880	plastid
Q9SVC4	Outer envelope membrane protein 7	AT3G52420	plastid
P59233	Ubiquitin-ribosomal protein eS31x fusion protein	AT3G62250	cytosol
F4IYB7	Late embryogenesis abundant protein (LEA) family protein	AT3G62580	endoplasmic reticulum
Q8H1F4	Coatomer subunit zeta-3	AT4G08520	endoplasmic reticulum
Q9STX5	Endoplasmin homolog	AT4G24190	endoplasmic reticulum
Q8W4S4	V-type proton ATPase subunit a3	AT4G39080	vacuole
O04331	Prohibitin-3, mitochondrial	AT5G40770	mitochondrion
Q42342	Cytochrome b5 isoform E	AT5G53560	endoplasmic reticulum
A0A1P8BAU5	Glucosidase II subunit alpha	AT5G63840	endoplasmic reticulum

CONCLUDING REMARKS

The understanding of MCSs in plants remains limited compared to other eukaryotic organisms such as yeast and mammals (Pérez-Sancho et al., 2016). This knowledge gap in both molecular mechanisms and physiological functions underscores the need for molecular screening methods tailored to plant systems. Insights from model organisms have guided the development of such tools (Calì et al., 2025), and adapting them for use in plants presents unique opportunities.

This thesis introduced several methodological innovations that significantly advanced the capacity to visualize and characterize plant MCSs. A modular BiFC system based on split-GFP was established to detect MCSs *in planta* in a reliable and fast way between two organelles, providing information on their spatial architecture, such as intermembrane distances of MCSs between two interacting membranes (Chapter 1). This assay can be extended to additional organelle combinations and subdomains, enabling broader surveys of the organellar contactome. Future adaptations such as trimolecular fluorescence complementation (Koraïchi et al., 2018) may help resolve even more complex interactions involving three membrane structures. The irreversible nature of the BiFC also offers the potential for stable fixation and subsequent biochemical isolation of MCSs via affinity-based purification, allowing unbiased identification of MCS-associated proteins.

Two complementary biochemical approaches for isolating MCS-associated candidate proteins were also developed. First, a method for isolating intact chloroplasts and chloroplast envelopes, including PLAMs, was refined (Chapter 3). These membrane regions are likely MCSs and represent a promising entry point for proteomic discovery, particular for plastid-MCS-associated proteins (Andersson et al., 2007b, 2007a). The integration of this method with a chemical crosslinker will enable the identification of interacting protein complexes within PLAMs using mass spectrometry.

Second, proximity labeling using split-TurboID (Cho et al., 2020) was adapted for use in transient plant expression systems (Chapter 4). This tool permits spatially restricted labeling of proteins at membrane interfaces, allowing the discovery of MCS components without prior knowledge of specific bait proteins. Combined with environmental perturbations such as heat stress, which is known to stimulate lipid biosynthesis via the eukaryotic galactolipid biosynthesis pathway, suggesting the activation or increase of ER-chloroplasts MCSs (Barrero-Sicilia et al., 2017; Lu et al., 2020), this technique presents various opportunities for dynamic studies of MCS mechanisms and functions.

Applying these tools, this thesis identified the candidate protein TGD4, a known player in lipid trafficking (Xu et al., 2008; Wang et al., 2012), as a component of ER-

chloroplasts MCSs. TDG4 was shown to localize to these contact sites using the established BiFC system and to interact with the phosphatase PAH1, supported by proximity labeling and FRET analysis (Chapter 2). Together, this newly identified regulatory relationship suggests a coordinated mechanism through which ER-chloroplasts MCSs balance overall lipid biosynthesis in plant cells. The functional interconnection and underlying molecular mechanisms are objectives of future work, which will be addressed by genetic and molecular advances.

In summary, this thesis provides a versatile toolkit for investigating the plant organellar contactome and offers new insights into the molecular components and functions. The establishment of methods for spatial visualization, biochemical isolation, and proximity-based labeling of MCSs lays the groundwork for comprehensive and fundamental studies of membrane interactions *in planta.* In the past decade, the research on MCSs revealed that organelles form multiple dynamic MCSs. This intracellular communication mechanism influences cellular signaling and metabolic networks. Future research, building on the methods established in this thesis, will help to understand the plasticity of MCSs by visualizing two-way or even three-way MCSs under various conditions, and identifying the mediators of such dynamic remodeling by proximity-dependent biochemical approaches. In the next decade, identification of molecular players at individual MCSs will clarify how the cell flexibly integrates its contactome to adapt to external and internal stimuli. The characterization of TGD4 as a dual-function regulator in lipid homeostasis highlights the importance for understanding the dynamics of these contact sites in the cellular context. The evolving research on MCSs in various organisms, including plants, will provide insights into the evolutionary trajectory and adaptations of contact sites during eukaryogenesis and the acquisition of plastids billion years ago, which may reveal new principles unique to the plant kingdom, reshaping our understanding of plant physiology.

Andersson, M.X., Goksör, M., and Sandelius, A.S., (2007a). Membrane contact sites: Physical attachment between chloroplasts and endoplasmic reticulum revealed by optical manipulation. Plant Signal Behav. 2007:**2**(3):185–187. https://doi.org/10.4161/psb.2.3.3973

Andersson, M.X., Goksör, M., and Sandelius, A.S., (2007b). Optical manipulation reveals strong attracting forces at membrane contact sites between endoplasmic reticulum and chloroplasts. Journal of Biological Chemistry. 2007:**282**(2):1170–1174. https://doi.org/10.1074/jbc.M608124200

Barrero-Sicilia, C., Silvestre, S., Haslam, R.P., and Michaelson, L. V., (2017). Lipid remodelling: Unravelling the response to cold stress in Arabidopsis and its extremophile relative Eutrema salsugineum. Plant Science. 2017:**263**:194–200. https://doi.org/10.1016/j.plantsci.2017.07.017

Calì, T., Bayer, E.M., Eden, E.R., Hajnóczky, G., Kornmann, B., Lackner, L., Liou, J., Reinisch, K., Rhee, H.-W., Rizzuto, R., et al., (2025). Key challenges and recommendations for defining organelle membrane contact sites. Nat Rev Mol Cell Biol. 2025. https://doi.org/10.1038/s41580-025-00864-x

Cho, K.F., Branon, T.C., Rajeev, S., Svinkina, T., Udeshi, N.D., Thoudam, T., Kwak, C., Rhee, H.W., Lee, I.K., Carr, S.A., et al., (2020). Split-TurboID enables contact-dependent proximity labeling in cells. Proc Natl Acad Sci U S A. 2020:**117**(22). https://doi.org/10.1073/pnas.1919528117

Koraïchi, F., Gence, R., Bouchenot, C., Grosjean, S., Lajoie-Mazenc, I., Favre, G., and Cabantous, S., (2018). High-content tripartite split-GFP cell-based assays to screen for modulators of small GTPase activation. J Cell Sci. 2018:**131**(1). https://doi.org/10.1242/jcs.210419

Lu, J., Xu, Y., Wang, J., Singer, S.D., and Chen, G., (2020). The role of triacylglycerol in plant stress response. Plants. 2020:**9**(4). https://doi.org/10.3390/plants9040472

Pérez-Sancho, J., Tilsner, J., Samuels, A.L., Botella, M.A., Bayer, E.M., and Rosado, A., (2016). Stitching Organelles: Organization and Function of Specialized Membrane Contact Sites in Plants. Trends Cell Biol. 2016:**26**(9):705–717. https://doi.org/10.1016/j.tcb.2016.05.007

Wang, Z., Xu, C., and Benning, C., (2012). TGD4 involved in endoplasmic reticulum-to-chloroplast lipid trafficking is a phosphatidic acid binding protein. Plant Journal. 2012:**70**(4):614–623. https://doi.org/10.1111/j.1365-313X.2012.04900.x

Xu, C., Fan, J., Cornish, A.J., and Benning, C., (2008). Lipid trafficking between the endoplasmic reticulum and the plastid in Arabidopsis requires the extraplastidic TGD4 protein. Plant Cell. 2008:**20**(8):2190–2204. https://doi.org/10.1105/tpc.108.061176

ACKNOWLEDGEMENTS

First and foremost, I want to thank **Prof. Dr. Andreas P.M. Weber** for his guidance and support throughout the last years. I highly appreciate the opportunity to not only work on this fascinating project, but bring in my own ideas to shape the outcome, and present the results in various conference. This allowed me to connect with many different people and creating my own network around the world.

Further, I want to thank my mentor, **Prof. Dr. Matias Zurbriggen,** and **Prof. Dr. Alexej Kedrov** for the fruitful discussions and scientific input during the yearly committee meetings and their support beyond these meetings.

I am sincerely grateful to **Dr. Franziska Kuhnert** for her advice, encouragement and feedback from the beginning of my PhD journey to proofreading this thesis. Also, many thanks to **apl. Prof. Nicole Linka** for her input and discussions throughout the last years.
I have been incredible lucky to work in an immensely supporting and welcoming Weber Lab group. Thanks to **Karo**, **Hannah**, **Hanna**, **Jana**, **Sebastian**, **Moritz**, **Laia**, **Lucas, Patrick** and all others for creating this amazing atmosphere. Special thanks to **Jan** for his constant patience, solving tons of R questions and proofreading the thesis.

I want to express my gratitude towards multiple people that supported me along the way.
I appreciate the opportunity to do the Fast Track promotion within the CRC1208 graduate school, and want to thank all the amazing people I was able to meet, especially **Dr. Cordula Kruse** for welcoming me to this grad school and for all her help in non-scientific matters.
I want to thank **Dr. Anja Stefanski** for patiently answering all my questions regarding the proteomic data for all of my projects.
And thanks to my students, **Lisa**, **Danielle, Sven** and **Elisa**, as well as the student helpers, **Elena** and **Eve**, for their help on different parts of the projects.

Finally, I would like to thank my family and friends for being my constant support-system and the balance I needed besides the work.

Thanks to you, I could continue and finish this journey.